Process Analysis of Asymmetric Hollow Fiber Permeators, Unsteady State Permeation and Membrane-Amine Hybrid Systems for Gas Separations

by

Prodip Kundu

A thesis
presented to the University of Waterloo
in fulfillment of the
thesis requirement for the degree of
Doctor of Philosophy
in
Chemical Engineering

Waterloo, Ontario, Canada, 2013

Author’s Declaration

I hereby declare that I am the sole author of this thesis. This is a true copy of the thesis, including any required final revisions, as accepted by my examiners.

I understand that my thesis may be made electronically available to the public.

Abstract

The global market for membrane separation technologies is forecast to reach $16 billion by the year 2017 due to wide adoption of the membrane technology across various end-use markets. With the growth in demand for high quality products, stringent regulations, environmental concerns, and exhausting natural resources, membrane separation technologies are forecast to witness significant growth over the long term (Global Industry Analysts Inc., 2011). The future of membrane technology promises to be equally exciting as new membrane materials, processes and innovations make their way to the marketplace. The current trend in membrane gas separation industry is, however, to develop robust membranes, which exhibit superior separation performance, and are reliable and durable for particular applications. Process simulation allows the investigation of operating and design variables in the process, and in new process configurations. An optimal operating condition and/or process configuration could possibly yield a better separation performance as well as cost savings. Moreover, with the development of new process concepts, new membrane applications will emerge.

The thesis addresses developing models that can be used to help in the design and operation of CO_2 capture processes. A mathematical model for the dynamic performance of gas separation with high flux, asymmetric hollow fiber membranes was developed considering the permeate pressure build-up inside the fiber bore and cross flow pattern with respect to the membrane skin. The solution technique is advantageous since it requires minimal computational effort and provides improved solution stability. The model predictions and the robustness of the numerical technique were validated with experimental data for several membrane systems with different flow configurations. The model and solution technique were applied to investigate the performance of several membrane module configurations for air separation and methane recovery from biogas (landfill gas or digester gas). Recycle ratio plays a crucial role, and optimum recycle ratios vital for the retentate recycle to permeate and permeate recycle to feed operation were found. From the concept of two recycle operations, complexities involved in the design and operation of continuous membrane column were simplified. Membrane permselectivity required for a targeted separation to produce pipeline quality natural gas by methane-selective or nitrogen-selective membranes was calculated. The study demonstrates that the new

solution technique can conveniently handle the high-flux hollow fiber membrane problems with different module configurations.

A section of the study was aimed at rectifying some commonly believed perceptions about pressure build-up in hollow fiber membranes. It is a general intuition that operating at higher pressures permeates more gases, and therefore sometimes the membrane module is tested or characterized at lower pressures to save gas consumption. It is also perceived that higher pressure build-up occurs at higher feed pressures, and membrane performance deteriorates at higher feed pressures. The apparent and intrinsic permeances of H_2 and N_2 for asymmetric cellulose acetate-based hollow fiber membranes were evaluated from pure gas permeation experiments and numerical analysis, respectively. It was shown that though the pressure build-up increases as feed pressure increases, the effect of pressure build-up on membrane performance is actually minimized at higher feed pressures. Membrane performs close to its actual separation properties if it is operated at high feed pressures, under which conditions the effect of pressure build-up on the membrane performance is minimized. The pressure build-up effect was further investigated by calculating the average loss and percentage loss in the driving force due to pressure build-up, and it was found that percentage loss in driving force is less at high feed pressures than that at low feed pressures.

It is true that unsteady state cyclic permeation process can potentially compete with the most selective polymers available to date, both in terms selectivity and productivity. A novel process mode of gas separation by means of cyclic pressure-vacuum swings for feed pressurization and permeate evacuation using a single pump was evaluated for CO_2 separation from flue gas. Unlike transient permeation processes reported in the literature which were based on the differences in sorption uptake rates or desorption falloff rates, this process was based on the selective permeability of the membrane for separations. The process was analyzed to elucidate the working principle, and a parametric study was carried out to evaluate the effects of design and operating parameters on the separation performance. It was shown that improved separation efficiency (i.e., product purity and

throughput) better than that of conventional steady-state permeation could be obtained by means of pressure-vacuum swing permeation.

The effectiveness of membrane processes and feasibility of hybrid processes combining membrane permeation and conventional amine absorption process were investigated for post-combustion CO_2 capture. Traditional MEA process uses a substantial amount of energy at the stripper reboiler when CO_2 concentration increases. Several single stage and multi-stage membrane process configurations were simulated for a target design specification aiming at possible application in enhanced oil recovery. It was shown that membrane processes offer the lowest energy penalty for post-combustion CO_2 capture and likely to expand as more and more CO_2 selective membranes are developed. Membrane processes can save up to 20~45% energy compared to the stand-alone MEA capture processes. A comparison of energy perspective for the CO_2 capture processes studied was drawn, and it was shown that the energy requirements of the hybrid processes are less than conventional MEA processes. The total energy penalty of the hybrid processes decreases as more and more CO_2 is removed by the membranes.

Acknowledgements

I would like to begin by sincerely thanking my advisors Dr. Xianshe Feng and Dr. Amit Chakma for their constant support, guidance and mentorship over the last four years. I had always pestered Dr. Feng with tons of silly questions and doubts, and it was very kind of him to have answered all my questions patiently. Whenever I was bereft of ideas, my discussions with him and his insights always helped me to get back on the right track. I am grateful to him and will ever remain. Special thanks to Dr. Chakma, whose success stories are inspiration to the thousands of my fellow people and I am very proud to have him as my advisor. I would also like to thank my thesis committee members Dr. Ali Elkamel, Dr. Zhongwei Chen and Dr. Sigrid Peldszus for being my mentors and for their valuable suggestions.

I would like to take this opportunity to thank all my colleagues and friends for their encouragement and friendship.

Lastly, I am thankful to my parents, my sister and my wife Keya for their unceasing love, understanding and encouragements.

Financial support as the Ontario Graduate Scholarship (OGS) and Research support from Natural Sciences and Engineering Research Council of Canada (NSERC) is gratefully acknowledged.

Dedication

To

My Parents

Table of Contents

Table of Contents

Table of Contents

Table of Contents

Table of Contents

List of Figures

List of Figures

List of Figures

List of Figures

List of Figures

List of Figures

List of Tables

List of Tables

List of Abbreviations

BDF	Backward Differential Formula
BTU	British Thermal Unit
BVP	Boundary Value Problem
CCS	Carbon Capture and Sequestration
CMC	Continuous Membrane Column
DEA	Diethanolamine
ECBM	Enhanced Coal Bed Methane
EOR	Enhanced Oil Recovery
GHG	Green House Gas
GPU	Gas Permeation Unit
IMSL	International Mathematical and Statistical Library
ISP	Internally Staged Permeator
IVP	Initial Value Problem
LFG	Landfill Gas
MEA	Monoethanolamine
MSW	Municipal Solid Waste
MW	Megawatt
ODE	Ordinary Differential Equation
PSA	Pressure Swing Adsorption
PSP	Pressure Swing Permeation
VOC	Volatile Organic Compound

List of Symbols

Chapter 2

C	[mol/m^3]	Concentration of a species
D	[m^2/s]	Diffusion coefficient
F	[m^3/(m^2.s)]]	Flux of a gas across the membrane
p	[Pa]	Partial pressure
P	[mol.m/(m^2.s.Pa)]	Permeability
S	[mol/(m^3.Pa)]	Sorption coefficient
T_g	[K]	Glass transition temperature

Greek symbols

α	[-]	Selectivity

Chapter 3

A	[m^2]	Effective membrane area
C_P	[J/mol.K]	Heat capacity at constant pressure
C_V	[J/mol.K]	Heat capacity at constant volume
D_i	[m]	Inside diameter of hollow fibers
D_o	[m]	Outer diameter of hollow fibers
J	[mol/s]	Permeation rate of gas component
K_1, K_2, K_{1M}	[-]	Dimensionless constant
l_E	[m]	Module length
N_T	[-]	Number of fibers in module
P_F	[kPa]	Feed pressure at any membrane location
P_P	[kPa]	Permeate pressure at any membrane location
P_{PO}	[kPa]	Permeate outlet pressure
P_{Fi}	[kPa]	Feed inlet pressure
Q	[mol/Pa.m^2.s]	Permeance of gas component

List of Symbols

R	[J/mol.K]	Ideal gas constant
T	[K]	Temperature
U	[mol/s]	Molar flow rate at feed side at any membrane location
U^*	[-]	Normalized flow rate (dimensionless)
V	[mol/s]	Molar flow rate at permeate side at any membrane location
V^*	[-]	Normalized permeate flow rate (dimensionless)
x	[mol frac]	Feed mole fraction
y	[mol frac]	Mole fraction on permeate side
y'	[mol frac]	Local permeate mole fraction
z	[m]	Axial coordinate
z^*	[-]	Dimensionless axial coordinate

Greek symbols

α	[-]	Selectivity
β	[-]	Feed side pressure to inlet feed pressure ratio
θ	[-]	Stage cut
γ	[-]	Permeate to inlet feed pressure ratio
γ_o	[-]	Permeate outlet to inlet feed pressure
μ	[Pa.s]	Viscosity of gas

Subscripts

A	Faster permeating component
B	Slower permeating component
F	Feed side
R	Residue end

Chapter 4

A	[m^2]	Membrane area
D_i	[m]	Inside diameter of hollow fibers
D_o	[m]	Outer diameter of hollow fibers
J_i	[mol/m^2.s.Pa]	Permeance of component *i*
J_{Ref}	[mol/m^2.s.Pa]	Permeance of reference component
K_1, K_2	[-]	Dimensionless constant
L	[m]	Length of hollow fiber membrane
N	[-]	Number of hollow fibers in module
P_F	[Pa]	Gas pressure on retentate side
P_{Fi}	[Pa]	Feed inlet pressure
P_P	[Pa]	Gas pressure on permeate side
P_{PO}	[Pa]	Permeate outlet pressure
R	[J/mol.K]	Ideal gas constant
R_b	[-]	Retentate recycle ratio
R_p	[-]	Permeate recycle ratio
T	[K]	Temperature
U	[mol/s]	Gas flow rate on retentate side
U_F	[mol/s]	Gas flow rate on feed inlet
U^*	[-]	Normalized gas flow rate on retentate side (U/U_F)
V	[mol/s]	Gas flow rate on permeate side
V^*	[-]	Normalized gas flow rate on permeate side (V/U_F)

x_i	[-]	Mole fraction of component *i* on retentate side
y_i	[-]	Mole fraction of component *i* on permeate side
y_i'	[-]	Local permeate concentration of component *i* substrate
z	[m]	Axial coordinate
z^*	[-]	Dimensionless axial coordinate (z/L)

Greek symbols

α	[-]	Selectivity (J_i/J_{Ref})
γ	[-]	Permeate to inlet feed pressure ratio (P_P/P_F)
γ_o	[-]	Permeate outlet to inlet feed pressure (P_{PO}/P_F)
μ	[Pa.s]	Viscosity of gas

Subscripts

i	Component *i*
F	Feed
P	Permeate
PR	Permeate recycle
R	Retentate
RR	Retentate recycle
Ref	Reference component

Chapter 5

A	[m^2]	Effective membrane area
D_i	[m]	Inner diameter
D_o	[m]	Outer diameter
l	[m]	Membrane thickness
l_a	[m]	Active fiber length
l_p	[m]	Potted length
N	[-]	Number of fibers in module
P_F	[Pa]	Feed pressure
P_P	[Pa]	Permeate pressure
Δp	[Pa]	Pressure difference across the membrane
J	[mol/m^2.Pa.s]	Gas permeance
R	[J/mol.K]	Ideal gas constant
T	[K]	Temperature
Q	[mol/s]	Permeate flow rate
z	[m]	Axial coordinate

Greek symbol

μ	[Pa. s]	Viscosity of gas

Chapter 6

A	[m^2]	Membrane area
D	[m^2/s]	Diffusivity coefficient
J	[mol/m^2.s.Pa]	Permeance
L	[m]	Membrane thickness
p	[kPa]	Permeate side pressure
p_V	[kPa]	Permeate pressure when the permeate side is evacuated
P	[kPa]	Feed side pressure
Q	[mol]	Quantity of permeate
Q_P	[mol]	Quantity of permeate withdrawn and collected
R	[J/mol.K]	Ideal gas constant
t	[s]	Permeation time
T	[K]	Temperature
V_F	[m^3]	Volume occupied by feed
V_M	[m^3]	Volume occupied by permeate
X	[-]	Mole fraction of the most permeable component in retentate
Y_P	[-]	Local permeate mole fraction
Y_M	[-]	Bulk permeate mole fraction

Greek symbols

θ	[s]	Time lag

Subscripts

1~5	Different Steps
A	Component A
B	Component B
F	Feed side
O	Initial condition

Chapter 1

Introduction

1.1 Background

Membrane technology has become very lucrative these days and has been widely accepted by industries due to its vast potential in resolving a critical problem. Gas separation via membranes is one of the most exciting and significant new unit processes that have appeared in recent years. Membrane-based gas separation technology mainly expanded during the last few decades and has led to significant innovations in both processes and products. Though the first commercially significant gas separation membrane was introduced only in late 1979, this technology found its way into a wide range of industries and applications within a span of ten years. In the US, the combined market for membranes used in all applications was estimated to be worth $5 billion in 2005. The market was rising at an average annual growth rate of 6.6%, and expected to reach $6.9 billion in 2009 according to a report by Business Communications Co. (Membrane Technology, 2005). The US market for membrane modules used in liquid and gas separation was worth an estimated $2.1 billion in 2008, and is forecast to increase to $3.3 billion by 2013 (with a compound annual growth rate of 7.8%) according to a technical market research report (Membrane Technology, 2009). Global Industry Analysts Inc. reports that due to wide adoption of the membrane technology across various end-use markets, the global market for membrane separation technologies is forecast to reach $16 billion by the year 2017. With the growth in demand for high quality products, stringent regulations, environmental concerns, and exhausting natural resources, membrane separation technologies are forecast to witness significant growth over the long term (Global Industry Analysts Inc., 2011).

Membrane gas separation is based on preferential permeation of one or more components of a gas mixture through a membrane. Mechanical or chemical processes are absent in this technology, which makes the membrane process relatively simple and easy to operate/scale-up. Membrane processes generally consume less energy than conventional

separation processes and can be easily combined with other separation processes. The process is environmentally friendly due to the absence of harmful chemical additives during the separation. Membrane based gas separation is well consolidated today and can often outperform conventional processes in terms of economics, safety, and environmental and technical aspects. The future of membrane technology promises to be equally exciting as new membrane materials, processes and innovations make their way to the marketplace.

Over the years, a great variety of membranes have been developed and reported. The current trend in membrane gas separation industry is, however, to develop robust membranes with superior separation performance that are reliable and durable for particular applications. The economic viability of gas membrane systems can be significantly affected by the process design. In most applications, mathematical models are required to predict the performance of gas separation modules for process design and optimization. Process simulation allows the investigation of operating and design variables in the process, and in new process configurations. An optimized operating condition and/or process configuration will likely yield a better separation performance as well as cost savings. Moreover, with the development of new process concepts, new membrane applications will emerge.

1.2 Motivation

Since membrane technology has radiant prospect, more applications in chemical industry are expected to come in the near future. However, there exists substantial confusions and sometimes debates about the preferential use of membranes over alternative processes. Since membrane technology is one of the newest additions, the confusion is sometimes aggravated by the fact that the technology is not well understood by many of the potential benefactors (i.e., industry and personnel). The study here is a contribution to the exploration of new and existing technologies where membranes offer significant potential and where there still remain considerable obstacles. The study focuses on better understanding of membrane processes to facilitate reasoning on the preferential use of membranes over alternative technology. The study also rectifies some general intuitions

and perceptions, which are prevalent in case of pressure build-up in hollow fiber membranes.

Though membrane gas separations already have widely penetrated in the markets, there are still many opportunities to extend new markets. Even though a great deal of new and improved materials has been developed lately in this field, the current trend in membrane gas separation industry is to develop robust membranes that exhibit both higher selectivity and permeability. Nevertheless, in some cases, membrane configurations and process designs are inadequate to fully exploit the membrane potential. Through the analysis of new process concepts, new membrane applications may also emerge. Therefore, process analysis such as modeling, simulation and optimization (operating/design stages) are deemed essential to membrane professionals for decision making. Moreover, successful membrane modeling and simulation can provide valuable information for the design, optimization and economics of the overall separation process with minimal costs and efforts.

Membrane gas separations under transient state conditions are rather unexplored compared to steady-state operations. Transient and, in particular, steady cyclic operation of the membrane can be used to alter the separation performance. Since very little is known about unsteady-state permeation, an investigation of the extent of separation achievable for gas separation of industrial importance through transient permeation could potentially infiltrate new process concepts.

Amine absorption has been regarded as one of the most promising methods to capture CO_2 from flue gas. However, it uses a substantial amount of energy at the stripper reboiler as the CO_2 concentration increases. Membranes, on the other hand, appear to be most effective at high CO_2 concentrations. Questions are sometimes raised if the membranes can compete with amine absorption for post-combustion CO_2 capture. Although both processes have their own advantages, can a hybrid process for post-combustion CO_2 capture be yielded combining membranes and amine absorption with cost/performance advantages that neither process could achieve individually? The potential

of hybrid separation processes for flue gas separation on industrial scale is not fully exploited because of the lack of general design methodologies and detailed process know-how.

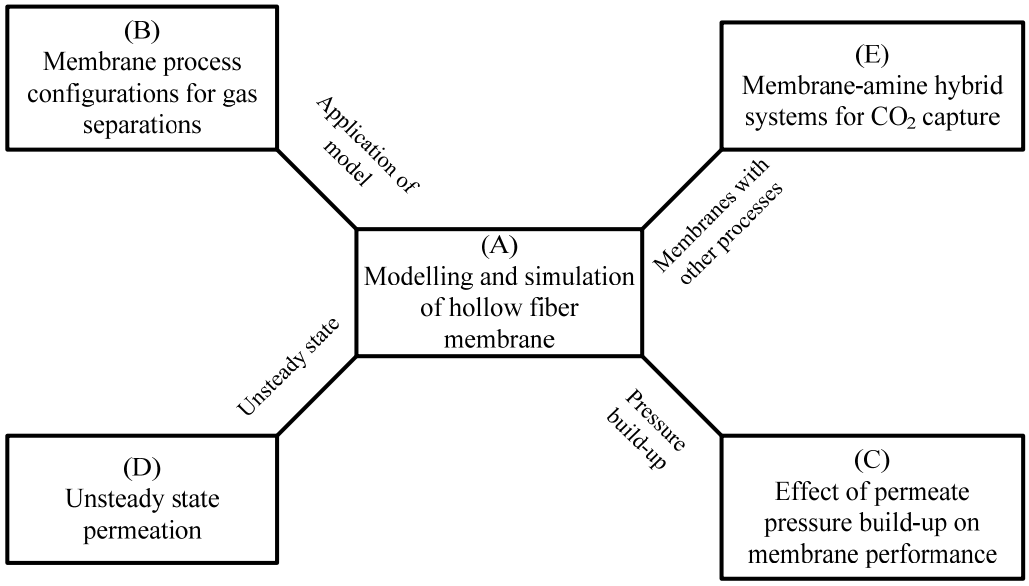

Fig. 1.1: Schematic of research objectives and scope.

1.3 Research objectives

The overall objective of the study is to develop models that can be used to help in the design and operation of CO_2 capture processes. This work targets several case studies in membrane gas separations, and five important aspects have been targeted as shown A, B, C, D & E, respectively, in Figure 1.1. The thesis revolves around modeling and simulation of hollow fiber membranes. Firstly, to develop a detailed and rigorous mathematical model for simulation of asymmetric hollow fiber membranes (A). Secondly, application of the developed membrane model in different flow and process configurations of gas separations (B). Thirdly, analysis of the effect of permeate pressure build-up and membrane asymmetry on membrane performance to rectify some commonly believed perceptions about pressure build-up in hollow fiber membranes (C). Along with the steady state process, the extent of separation achievable in unsteady state permeation process was also investigated (D).

Finally, the effectiveness of membrane processes for post combustion CO_2 capture and feasibility of building a hybrid of membrane process with amine absorption process for carbon capture (E).

The following specific objectives have been derived in consideration of the above:

- Develop mathematical model for simulation of binary/multicomponent gas separation in asymmetric hollow fiber membranes considering the asymmetric structure of the membrane, and develop a robust and reliable numerical technique for solving the associated equations.
- Apply the developed numerical model and solution technique to investigate the performance of several membrane process configurations for nitrogen- and oxygen-enriched air production, and methane recovery from biogas (landfill gas or digester gas) using representative membranes.
- Rectify some common perceptions of pressure build-up in hollow fiber membranes. Clarify the effect of permeate pressure build-up on the intrinsic separation performance of hollow fiber membranes.
- Analyze a pressure-vacuum swing permeation process and study the effects of design and operating parameters on the performance for CO_2 separation from flue gas.
- Effectiveness of membrane processes for CO_2 capture from flue gas to meet the selected design specifications. Simulate conventional MEA process for the aforementioned design specifications. Explore the feasibility of membrane-amine hybrid systems for post-combustion CO_2 capture.

1.4 Outline of the thesis

The thesis consists of eight chapters as follows:

- Chapter 1 presents the background, motivations and specific objectives.

- Chapter 2 presents an overview of membrane gas separations. The chapter addresses a brief history of membrane based gas separation, mechanism of transport through membranes, and a review of different polymeric membranes used for gas separation. The chapter provides a discussion on basic features of hollow fiber membranes, hollow fiber permeator modeling, membrane process and cascade configurations, unsteady-state permeation and hybrid membrane systems. The chapter also briefly discusses industrial applications of membrane gas separations.
- Chapter 3 presents the modeling and simulation of binary gas separation in asymmetric hollow fiber membranes, and application of the developed model for a case study in air separation to produce nitrogen- and oxygen-enriched air using representative membranes with different configurations.
- Chapter 4 provides a modeling and simulation study of multicomponent gas separation in asymmetric hollow fiber membranes, and application of the membrane technology for methane enrichment from biogases. Current scenario of Canadian landfills and potential renewable methane generation from municipal solid wastes in Canada is presented in Chapter 4.
- Chapter 5 discusses the effect of permeate pressure build-up on the intrinsic separation performance of hollow fiber membranes. Common perceptions about pressure build-up in hollow fiber membrane are rectified in this Chapter through experimental and theoretical analysis.
- Chapter 6 presents CO_2 separation from flue gas using pressure-vacuum swing permeation, and the feasibility and effectiveness of the process is evaluated.
- Chapter 7 presents effectiveness of membrane processes for post combustion CO_2 capture, and a comparison with conventional MEA process in terms of energy perspective. The Chapter also presents feasibility of building a membrane-amine hybrid systems for post combustion CO_2 capture from flue gases. The study targets CO_2 capture for potential application in enhance oil recovery (EOR).
- Chapter 8 summarizes the general conclusions, contributions to research and knowledge, and recommendations for future work.

Chapter 2

Features of hollow fiber membranes, unsteady state permeation and membrane hybrid systems for gas separations

2.1 Introduction

Membrane technology is an effective tool to implement the process intensification, thereby reducing production costs, equipment size, energy utilization, and waste generation (Dautzenberg and Mukherjee, 2001). An ideal membrane has the ability to selectively allow a certain component of a gas mixture to pass through it while rejecting others in a continuous manner, which makes the process extremely appealing. Membrane process is an attractive alternative to conventional technologies for gas separations due to its simplicity in operation, low maintenance and reliable performance. Unlike conventional separation unit operations (e.g., cryogenic distillation and adsorption processes), membrane gas separation does not involve a phase change. Moreover, the absence of moving parts makes membrane systems particularly suited for uses where operator attendance is critical. In addition, the small footprint makes the process very attractive for remote applications such as offshore gas processing (Bernardo et al., 2009). It is also environmentally sustainable, as no harmful chemical additives are required during the separation. However, despite its apparent advantages, numerous factors must be considered for successful application and commercialization of membrane technology. The optimum process design and operating conditions play an important role in successful and economic application of membranes for gas separations.

Membrane gas separation is a pressure-driven process with numerous industrial applications, but these applications represent only a small fraction of the potential ground in refineries and chemical industries though prospect could be endless. The use of membranes in separation processes is growing at a steady rate (Baker, 2002). It is estimated that the market of membrane gas separation technology in year 2020 would be five times of that of year 2000 (Baker, 2002). It is expected that membrane gas separation will play an increasingly important role in reducing the environmental impact and costs of industrial

processes, particularly in the present scenario when energy cost is volatile and the global hydrocarbon reservoirs are destined to reduce dramatically during this century (Koros, 2007). Opportunities to extend the markets for membrane gas separation are limitless. However, in some cases, the membrane materials, membrane configuration, process designs are inadequate to meet all industrial needs. A broad range of materials was investigated and many improvements were achieved lately in this field. Today, much of the research work is being addressed to the investigation of new materials and to the development of new membrane structures that exhibit both a high selectivity and permeability to specific gases (Bernardo et al., 2009). However, modeling and simulation of the membrane process is a viable means to provide valuable information to the design, operating and economics of the separation process with minimal cost.

This chapter briefly addresses the history of membrane based gas separation, the mechanism of transport through membranes and the different polymeric membranes used for gas separation. The chapter also intends to provide a discussion on basic features of hollow fiber membranes, flow patterns, hollow fiber permeator modeling and numerical solution techniques. Advantages of membrane modular configurations, performance improvement through recycle/purge/multi-stage operations, enhancing separation efficiency beyond transient permeation through novel designs of unsteady state and cyclic operations will be also discussed. Hybrid processes combining membrane gas separation with other traditional gas separation processes (i.e., amine, cryogenic, PSA) and their cost/performance advantages will be presented. A brief review of industrial applications of membrane gas separation will be presented too.

2.2 Membrane-based gas separation: A brief history

It was Graham who in 1829 initiated and pioneered the foundation of membrane gas separation by performing permeation tests for some of the known gases that time (Graham, 1866; Kesting and Fritzsche, 1993). Graham introduced the concept of solution-diffusion mechanism for the first time to explain the selective permeation of gases (Baker, 2004). Graham's theory has contributed considerably to the knowledge of gas diffusion

phenomena together with Fick's law, which quantitatively defines concentration gradient driven mass transport. However, it was Loeb and Sourirajan who in 1961 invented an integrally asymmetric high-flux reverse osmosis membrane for desalination, and transformed membrane from concept to industrial application (Baker, 2004). With the introduction of a large surface area in compact modules through hollow fiber membranes in the 1970's, the industry further boosted and gained considerable interest. Monsanto company further refined the membranes for gas separation applications and launched its first composite polysulfone Prism® membrane in the 1980's for hydrogen separation application (Koros and Fleming, 1993). Briefly after that, many giants in gas separation industry extended the application of membrane processes for carbon dioxide removal from natural gas (e.g., Cynara, Saparex, and Grace). The progress was further accelerated in the 1980's with the innovation and development of highly selective synthetic polymeric materials. Specifically, the improved selectivity of oxygen/nitrogen in polymeric membranes has expanded its application to air separation to produce nitrogen- and oxygen-enriched air. Among many commercial plants producing nitrogen- and oxygen-enriched air, Praxair is one of the largest, and one of Praxair's plants in Belgium (began operation in 1996) has a nitrogen production capacity of nearly 24 ton/hr (Maier, 1998). Applications in other industries gradually advanced and widely penetrated the market.

2.3 Gas transport mechanism

Gas transport in the membrane is a function of membrane properties (physical and chemical structure), the nature of the permeant species (size, shape and polarity), and the interaction between the membrane and the permeant. The mechanism of gas transport across membranes varies with the types of membranes involved. Convective flow, Knudsen diffusion, and molecular sieving are the three accepted mechanisms for porous membranes. The most widely accepted mechanism for gas transport in dense membranes is the solution-diffusion mechanism. Figure 2.1 provides a schematic of gas transport mechanisms for porous and dense membranes. The transport mechanism in porous membranes is governed by the relative pore sizes of the membranes and the mean free path of the gas molecules. If the pores are relatively large (from 0.1 to 10 μm), gases permeate

through the membrane pores by convective (vicous) flow described by the Poiseuille's law, and no separation occurs. If the pore size is similar to or smaller than the mean free path of the gas molecules, gas permeation is governed by the Knudsen diffusion. The gas molecules in Knudsen diffusion collide more frequently with the pore walls than colliding with other gas molecules on the go, which make them to move independent of each other (Pandey and Chauhan, 2001). The transport rate of a gas across the membrane by Knudsen diffusion is inversely proportional to the square root of its molecular weight. When the membrane pores are extremely small (of the order of 5-20 Å), e.g., in between the size of smaller and larger molecules, the gases are separated by molecular sieving. Transport through this type of membrane is complex and includes both diffusion in the gas phase and diffusion of adsorbed species on the surface of the pores (surface diffusion). This types of membranes has not been used on a large scale. However, ceramic and ultra-microporous glassy membranes with extraordinary high selectivities for similar molecules have been prepared in the laboratory (Baker, 2004). Details of the transport models related with porous membranes can be found elsewhere (Matsuura, 1994; Mulder, 1996).

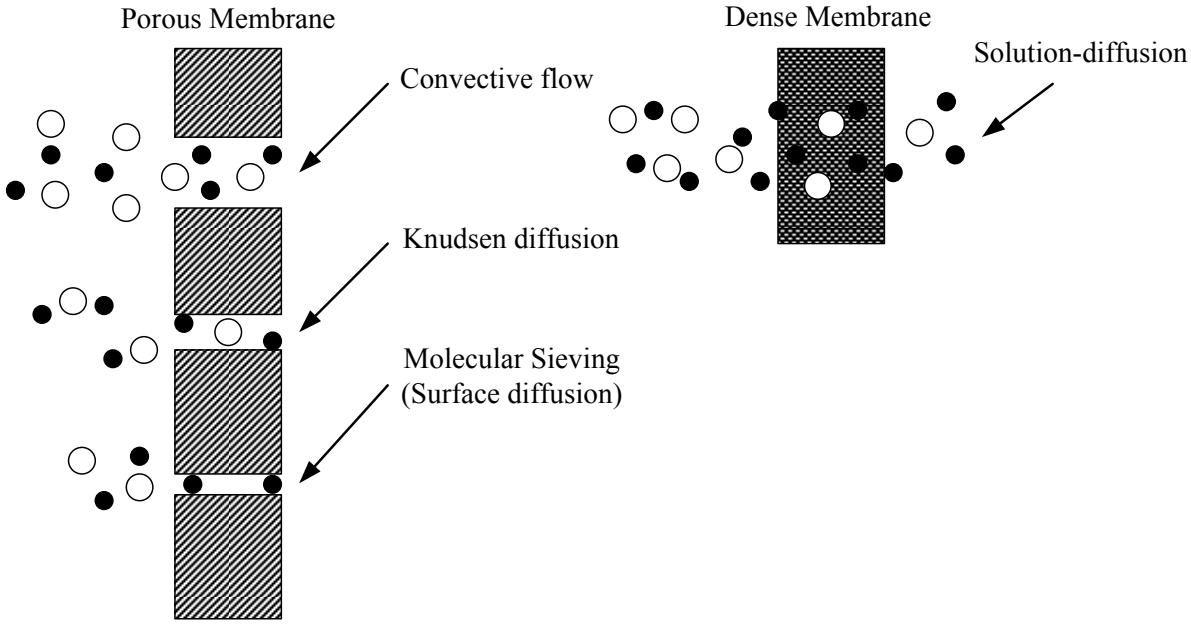

Fig. 2.1: Schematic of main mechanisms for gas permeation through membranes (Baker, 2004).

Chapter 2

Although microporous membranes are topics of considerable research interest, all current membranes for commercial separations are based on dense polymer membranes. Separation through dense polymer films occurs by a solution-diffusion mechanism, which was initially proposed by Graham. The gas transport through dense polymer films occur fundamentally in three steps according to Graham, as shown schematically in Figure 2.2. In this model it is assumed that the gas at the high pressure side of the membrane dissolves in the polymer, diffuses down to the low pressure side, and finally desorbs and releases at the low pressure end. It is further assumed that the sorption and desorption at the interfaces are fast compared to the diffusion rate in the polymer. The gas phases on both sides of the membrane are in equilibrium with the polymer interfaces. The permeants are separated from each other due to the difference in their solubility and diffusivity in the polymer matrix (Wijmans and Baker, 1995).

Diffusion is the process by which matter is transported from one part of a system to another by a concentration gradient. The gas transport flux across the membrane can be described by the Fick's law:

$$F = -D\frac{dC}{dx} \tag{2.1}$$

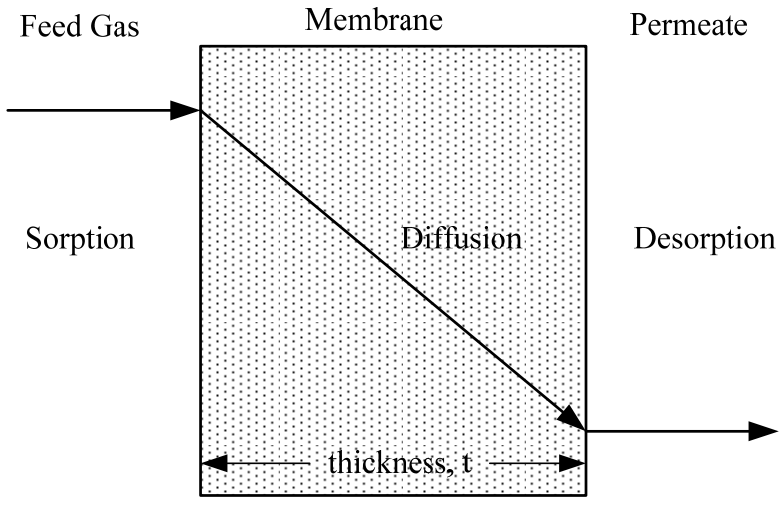

Fig. 2.2: Schematic of solution-diffusion model.

The concentration of a component at the feed interface of the membrane can be written by the Henry's law:

$$C = Sp \tag{2.2}$$

Combining Eqs. (2.1) and (2.2) and integration lead to the expression of gas transport flux across the membrane:

$$F = -SD\frac{\Delta p}{t} \tag{2.3}$$

The product *SD* can be written as *P*, which is called the membrane permeability. It is a measure of the ability of the membrane to permeate gases. Rewriting Eq. (2.3):

$$F = -P\frac{\Delta p}{t} \tag{2.4}$$

The measure of the ability of a membrane to separate a pair of gases *i* and *j* is the ratio of their permeabilities α_{ij}, called the membrane selectivity:

$$\alpha_{ij} = \frac{P_i}{P_j} = \left[\frac{D_i}{D_j}\right]\left[\frac{S_i}{S_j}\right] \tag{2.5}$$

The ratio of diffusion coefficients (D_i/D_j) can be viewed as the mobility selectivity, reflecting the different sizes of the permeating molecules, while the ratio of the sorption coefficients (S_i/S_j) can be viewed as the solubility selectivity, reflecting the relative condensabilities of the two gases. In general, the diffusivity coefficient decreases with increasing molecular size. However, the magnitude of diffusivity selectivity often depends on whether the membrane is at a glassy or rubbery state. Glassy polymers refer to polymeric materials below their glass transition temperatures, while a rubbery polymer results when the polymer is at a temperature above the glass transition temperature. The polymer chains are rigid below the glass transition temperature. On the other hand, the polymer gains sufficient thermal energy above the glass transition temperature and allows some rotation around the chain backbone, which causes the polymer to become rubbery. The mobility selectivity of gases is relatively higher in glassy polymers than that of the rubbery polymers (Baker, 2004; Zakaria, 2006). The solubility selectivity generally increases with molecular sizes of the permeant. In glassy polymers, the mobility term is usually more dominant, which causes small molecules to permeate faster. Contrarily, in

rubbery polymers, the solubility term often predominates, and larger molecules permeate preferentially through the membrane (Baker, 2004). Reviews on the relationships between polymer structure and transport properties of gases can be found in Baker (2004) and Freeman (1999).

2.4 Membrane materials

The selection of a membrane material for gas separation applications is based on specific physical and chemical properties. Membrane materials need to be tailored in an advanced way to separate particular gas mixtures. Moreover, robust (i.e., long term and stable) materials are required to find potential applications in membrane gas separation processes. The separation performance of membranes depends upon:

- membrane material (permeability, selectivity),
- membrane structure and thickness (permeance),
- membrane configurations (e.g., flat, hollow fiber) and
- module and system designs

Membrane permeability and selectivity determine the economics of membrane gas separation processes. A large number of polymeric materials have been developed for gas separation applications. However, polymers cannot withstand very high temperatures and aggressive chemical environments. Moreover, in petrochemical plants, refineries and natural gas treatment, the presence of heavy hydrocarbons in the feed streams can pose a serious problem. Many polymers can be plasticized or swollen when exposed to hydrocarbons or CO_2 at high pressures. Their separation capabilities can be dramatically reduced or the membranes can be irreparably damaged. Therefore, gas pre-treatment and condensate handling are critical for proper operation of gas separation modules. The development of inorganic membranes (e.g., silica, zeolites etc.) and carbon based molecular sieves is particularly interesting because they can withstand aggressive chemicals as well as high temperatures. However, these materials have drawbacks, including high cost, modest reproducibility, brittleness, low membrane area to module

volume ratio, low permeability in the case of highly selective dense membranes (e.g., metal oxides at temperatures below 400°C) and difficult sealing at high temperatures (greater than 600°C) (Bernardo et al., 2009).

2.4.1 Polymeric membranes

Although a large number of polymeric materials have been developed and investigated for gas separation applications, the actual number of polymers used in commercial systems is still limited. The main rubbery and glassy polymers employed for gas separation membranes are listed in Table 2.1.

The overall amount of free-volume and the distribution of the effective micro-pore sizes (if the free-volume elements are interconnected) have a significant influence on the intrinsic permeability of the polymer. Typically, rubbery polymers have high permeabilities, and their selectivity is mainly influenced by the difference in the condensabilities of the gas species. Polymer in rubbery state presents a relatively large amount of free-volume owing to transient voids between the highly mobile polymer chains. When the temperature is lowered below its glass transition temperature (T_g), the polymer behaves as a rigid glass. When applied to separate an organic vapor from nitrogen, rubbery membranes preferentially permeate the organic molecules. Silicone rubber is extremely

Table 2.1: Glassy and rubbery polymers used in industrial membrane gas separation (Bernardo et al., 2009).

Rubbery Polymers	**Glassy Polymers**
poly (dimethylsiloxane)	cellulose acetate
ethylene oxide/propylene oxide-amide copolymers	polyperfluorodioxoles
	polycarbonates
	polyimides
	poly (phenylene oxide)
	polysulfone

permeable and has adequate vapor/inert gas selectivities for most applications; composite membranes of silicone rubber are used in almost all of the commercial vapor separation systems (Baker, 2004; Bernardo et al., 2009).

Due to high gas selectivity and good mechanical properties, majority of the industrial membrane gas separation processes utilize glassy polymers. For glassy polymers, usually the more permeable species are those with small molecular sizes, and the membrane selectivity is due to differences in molecular dimension. The glassy state is characterized by a relatively small fraction of free volume. Medium to high free-volume glassy polymers (e.g., polyimide, polyphenyleneoxide, etc.) are used to produce membranes since the micro-voids aid the transport of gas or liquid through the material (Bernardo et al., 2009).

Although almost all industrial gas separation processes use polymeric membranes, however, interest in metal membranes continues, mostly for the high-temperature membrane reactor applications. The study of gas permeation through metals began with the observation of hydrogen permeation through palladium. Pure palladium absorbs 600 times its volume of hydrogen at room temperature and is measurably permeable to the gas. Hydrogen permeates through a number of other metals including tantalum, niobium, vanadium, nickel, iron, copper, cobalt and platinum (Alefeld and Voelkl, 1978). In most cases, the metal membrane must be operated at high temperatures (> 300^{o}C) to obtain useful permeation rates and to prevent embrittlement and cracking of the metal by sorbed hydrogen. Although most work on gas permeation through metal membranes has focused on hydrogen, oxygen-permeable metal membranes are also known. However, the oxygen permeabilities are low. The high cost of metal membranes and the need to operate at high temperatures to obtain useful fluxes make the process uncompetitive with other hydrogen recovery technologies (Baker, 2004). Several other membranes/materials (i.e., ceramic, zeolite, mixted-matrix) are also being developed for gas separation applications.

2.5 Types of membrane modules: Hollow fibers

The unit into which the membrane is packed is called a module. Technology development to produce low-cost membrane modules was one of the breakthroughs that led to commercial membrane processes in the 1960's and 1970's (Baker, 2004). Large surface areas can be packed in membrane modules through the compact design of membrane modules. Among the compact designs, hollow fiber membranes are advantageous over flat membranes as a large membrane area density can be packed in hollow fiber modules. These membranes offer the highest membrane area per unit volume, which can be as high as 4000 ft^2/ft^3, while spiral wound and plate and frame modules with flat membranes offer 200-250 and 100-150 ft^2/ft^3, respectively (Koros and Fleming, 1993). Polymeric hollow fibers are formed by extruding a polymer solution (commonly called polymer dope) through the annulus of a spinneret. A liquid or a gas is coextruded in the core of the annulus to form the hollow region. Figure 2.3 represents a cross section of a spinneret initially designed by Dow (Baker, 2004). The thickness of hollow fiber membranes is

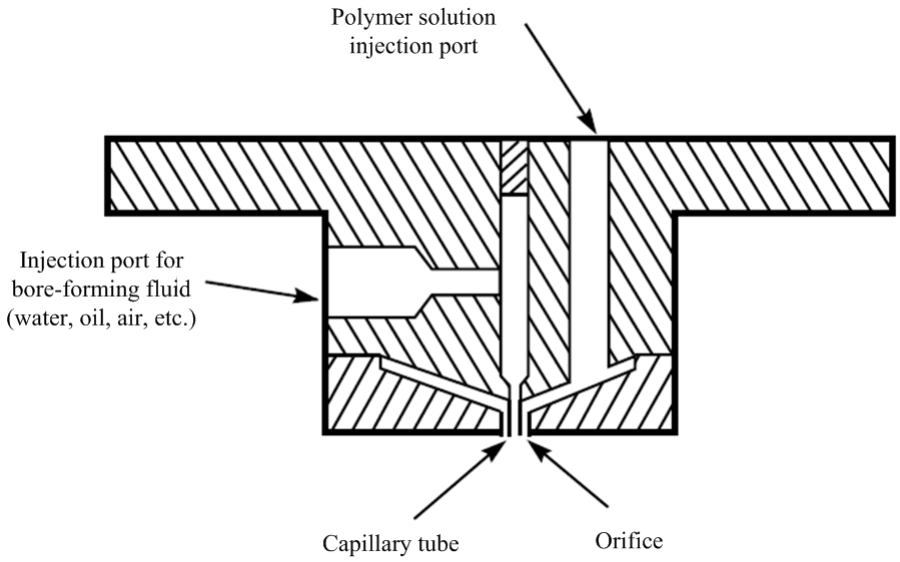

Fig. 2.3: Twin-orifice spinneret design used in solution-spinning of hollow fiber membranes (Baker, 2004).

usually greater than their flat sheet equivalent since the fibers must withstand the applied pressure without collapsing. The diameter of hollow fibers varies over a wide range, from 50 to 3000 μm. Fibers of 50 to 200 μm diameter are usually called hollow fine fibers. Such fibers can withstand very high hydrostatic pressures applied from the outside, so they are used in reverse osmosis or high-pressure gas separation applications. For low pressure gas applications, larger diameter fibers can be used (Baker, 2004).

2.6 Modeling of hollow fiber permeators

For the current study as well as for many theoretical studies in the literature, hollow fiber membrane modules are the focus of the modeling efforts due to their high packing densities and widespread industrial uses for gas separations. Theoretical analysis is essential for the knowledge of variation in process (design and operating) parameters affecting permeator performance. Process design, scale up from pilot plant to large-scale units, existing process improvement, new process development, optimization and economics of the overall separation process can be investigated using mathematical models. The mathematical models for hollow fiber permeator should include:

- governing transport equations across the membrane,
- pressure drop relations, and
- boundary conditions reflecting permeator configurations

Weller and Steiner (1950) pioneered the modeling of gas permeation, and their analysis was based on binary gas mixtures. Two specific cases were investigated, i) complete mixing of both the residue and permeate streams (as shown in Figure 2.4a), and ii) cross-flow permeation where permeate is withdrawn perpendicular to the feed flow (as shown in Figure 2.4b). Naylor and Backer (1955) analyzed the cross flow permeation for binary gas separation. Though the models did not address cocurrent or countercurrent flows and cell geometry, they provided the much needed foundation for subsequent development of sophisticated models. Brubarker and Kammermeyer (1954) accommodated ternary and quaternary gas mixtures to the complete mixing model of Weller and Steiner (1950). Stern et al. (1965) extended the model of Weller and Steiner (1950) for cross flow (case ii)

permeation of multicomponent systems for helium recovery from natural gas. In subsequent years, more complex mathematical models were eventually developed for better understanding with the aid of advanced computing facilities.

Hollow fibers are normally arranged in a shell and tube configuration. In principle, the feed gas may be supplied to either the shell side or the bore side of the hollow fiber permeator. In the shell-side feed configuration, the feed gas enters the permeator on the shell side and the permeate is collected from the fiber bores. In the simplest version, only one active tube sheet is needed to allow for permeate removal from the fiber lumens. This design is simple and the module assembling is straightforward, but provisions must be,

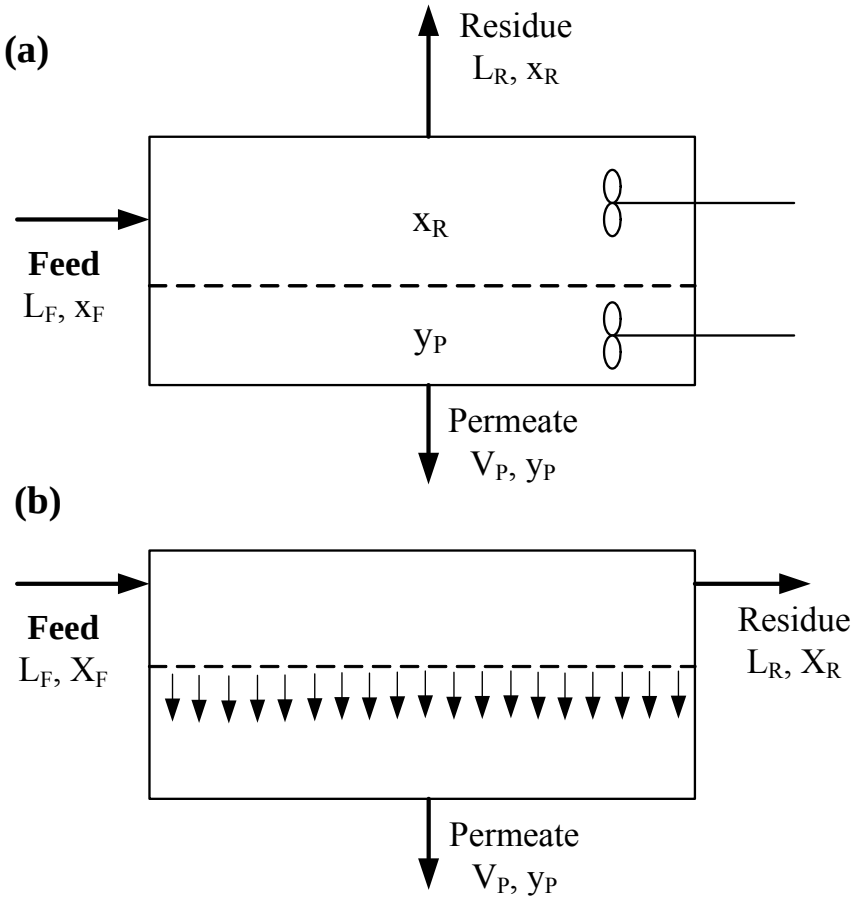

Fig. 2.4: Membrane model with (a) completely mixed flow, and (b) cross flow pattern (Zakaria, 2006).

made to pack the fibers uniformly in order to achieve a uniform flow distribution. In the bore-side feed configuration, on the other hand, the feed gas enters the fiber bores at one end of the hollow fibers, and the residue exits from the fiber lumens at the other end whereas the permeate is removed from the shell side of the device. This requires two active tube sheets, one at each end of the hollow fibers. In the latter configuration, a more even flow distribution of feed on the membrane surface is achieved, which is beneficial to an efficient operation. Also, only the fiber wall and the end caps of the membrane device are pressurized, and the pressure at the shell side is substantially low. Therefore, the mechanical strength requirement to the shell casing of the permeator is minimized. However, when the pressurized gas stream moves to or from the fiber bores, both tube sheets are under significant compressive and sheer stresses. Consequently, the bore-side feed permeator design is more complicated than the shell-side feed design because of the problems associated with supporting the tube sheets (Feng et al., 1999).

Flow patterns inside a hollow fiber permeator can be configured in various ways. The most common practical configurations are shown in Figure 2.5. Different flow patterns expected to result in different patterns of driving force in the module (Zakaria, 2006). Walawender and Stern (1972), and Blaisdell and Kammermeyer (1973) initially proposed incorporation of the effect of cocurrent and countercurrent flow patterns in the

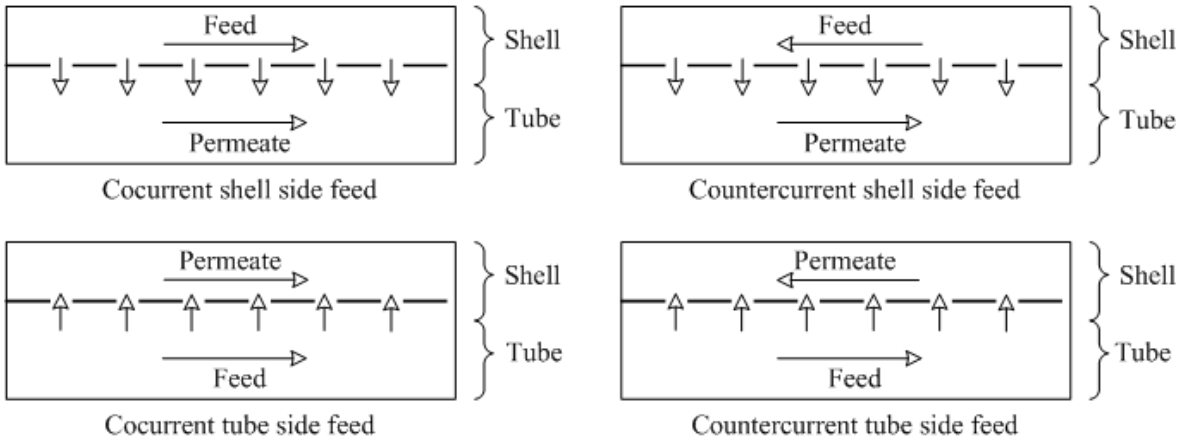

Fig. 2.5: Countercurrent and cocurrent flow patterns in hollow fiber permeator.

mathematical models. Blaisdell and Kammermeyer (1973) investigated the performance of different flow patterns for binary gas separation. Their model prediction agreed well with the experimental results, and it was concluded that countercurrent flow pattern was the best option for commercial gas separation application. Pan and Habgood (1974) extended the model of Walawender and Stern (1972) to the case with a non-permeable component in the system, and investigated the effect of permeability ratio and the sweep gas on the separator performance. Pan and Habgood (1974) also confirmed theoretically that the countercurrent flow pattern is the best possible arrangement.

Li et al. (1990) developed mathematical models for separation of gas mixtures involving three or more permeable components without consideration of pressure drop. Theoretical analysis of CO_2 separation from multi-component gas mixtures was performed using five different flow patterns of the permeated and unpermeated stream. The solution from the different flow models was compared, and a parametric analysis was performed to investigate the effect of flow pattern, pressure ratio, and stage cut on the separation performance. Rautenbach and Dham (1985) also provided derivations of equations for multi-component gas separation for four different flow patterns. Their results were compared with those of a short-cut method based on pseudo-binary gas mixtures, and it was demonstrated that pseudo-binary components can only be used for component with similar permeabilities. Thundyil and Koros (1997) presented a new approach to solve the mass transfer problem posed by the permeation process in a hollow fiber permeator for radial crossflow, countercurrent and cocurrent flows. More recently, Marriott et al. (2001), and Marriott and Sorenson (2003) developed a more rigorous model based on mass, energy and momentum balances to describe a generic membrane separation in contrast to a process specific model. The model was compared with Pan's (1986) experimental data, and an excellent agreement was found. However, the main drawback of their model is that knowledge of molecular diffusivity and solubility is necessary rather than permeability or permeance, which are difficult to determine and not handy. This is especially the case when asymmetric composite membranes are used.

2.6.1 High flux asymmetric membranes

Asymmetric membranes consist of a dense skin on one side with a backing of porous support structures where the porosity changes from top surface to the bottom. Pan and Habgood (1978a) initially suggested that the permeation through a high flux asymmetric membrane follows a cross-flow pattern because the porous support layer prevents mixing of the local permeate. Figure 2.6 represents a schematic of cross-flow permeation in an asymmetric membrane. According to Pan (1983, 1986), the gas composition inside the pores in the backing will be different from that in the bulk permeate (y' as opposed to y, Figure 2.6). The permeate inside the porous backing is considered to be unaffected by the bulk permeate composition and unmixed with that from any adjacent layers. The composition y' is essentially controlled by the relative local permeation rates, which in turn are dictated by the local feed composition and total pressures only. The bulk permeates at any point along the permeator represents the accumulated effect of all permeation prior to that point. However, it does not affect the local permeation rate. This is called the 'crossflow model' and should be distinguished from the 'crossflow pattern' inside the permeator module. Similar models can be used for a truly composite membrane, which

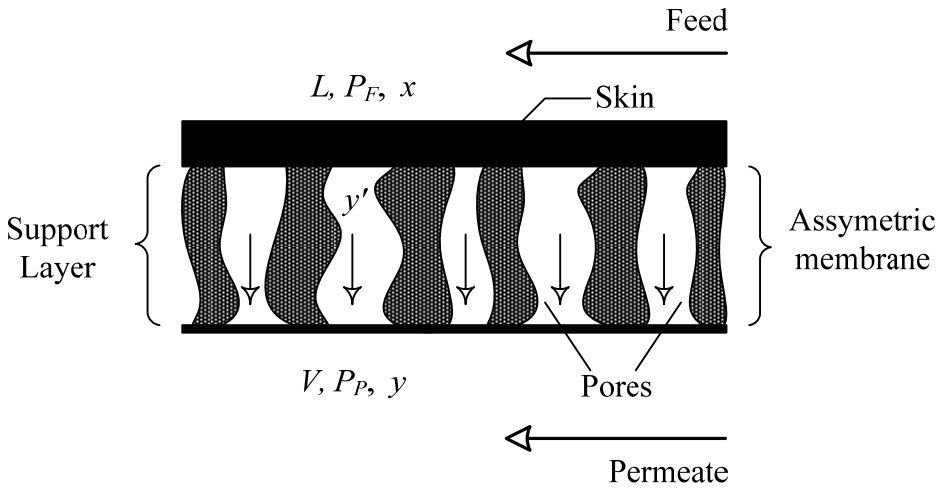

Fig. 2.6: Schematic of cross-flow pattern permeation in asymmetric membrane (Sengupta and Sirkar, 1995).

has a thin, distinct selective layer backed by a porous support. However, it is to be noted that the above model for asymmetric or composite membranes is insufficient for describing the permeation if the flux is very high or the membrane is extremely thin because the permeation resistance of the porous backing starts to become important under these situations (Baker, 2004). However, in a homogenous symmetric model, the bulk permeate concentration, y, is assumed to be the same as y' due to radial mixing of permeate (Zakaria, 2006).

A calculation method for multi-component separation based on the cross flow model was presented by Pan (1978a), and a parametric analysis on cascade operation was provided. The cross flow model for asymmetric membrane was extended to include the effect of pressure build-up for binary and multi-component gas mixtures (Pan, 1983, 1986). It was found that the countercurrent flow pattern is not necessarily the best flow pattern for asymmetric membranes, and the effect of the flow pattern is not significant for most practical operating parameters. A model to describe the transport across asymmetric membranes using a two-layer concept was presented by Sirkar (1977). It was suggested that the gas species are transported through the dense skin layer by Fickian diffusion, while Knudsen diffusion is assumed to control the transport across the microporous backing. The overall flux equation is derived from the combination of both transports in series.

Experiments for the separation of O_2/N_2 and helium/N_2 using proprietary composite hollow fiber membranes were conducted by Giglia et al. (1991), and experimental results were compared with cocurrent and countercurrent homogenous models and a cross flow asymmetric model. It was concluded that the experimental observations closely resemble with the homogenous cocurrent and countercurrent models than that of the cross flow model. Sidhoum et al. (1988) investigated separation of CO_2/N_2 and O_2/N_2 and also confirmed the findings by Giglia et al. (1991). Feng et al. (1999) showed experimentally that the permeation of O_2/N_2 through asymmetric hollow fiber membrane does not give rise to cross-flow permeation and that tube side feed countercurrent flow yields the best separation performance. Narinsky (1991) also advocated that permeation in asymmetric membrane follows the homogenous cocurrent or countercurrent model.

2.6.2 Feed compression, vacuum pumping and sweep gas operation

Separation effect can be achieved in membrane permeation only at the expense of a specific driving force exerted on each component of the feed mixture in terms of chemical potential gradient. Basically, two distinct options can be taken in order to achieve that purpose. The first is to increase the chemical potential on the feed side. This can be best induced by a compression step exerted on the feed mixture. Such an option is classically applied in gas permeation and reverse osmosis. The other is to decrease the chemical potential on the downstream side. Vacuum pumping is interesting since it minimizes the overall permeate flow rate, but it necessitates a compression step which is energy consuming. Conversely, gas sweep is appealing due to the possibility it offers to work under higher total downstream pressure conditions (lower compression cost), but it generates an increased permeate flow rate and requires an additional component (i.e., an inert gas such as nitrogen or air), which can be costly. From an industrial point of view, gas sweep will generally offer the lowest raw energy consumption (pump work), unless a low vacuum level can be practically achievable. Vacuum operation is however systematically preferable when the integral work of separation (i.e., the work needed to recover pure component) is taken into account (Vallieres and Favre, 2004). Vacuum sweep has been reported beneficial for several applications (Skoulidas and Sholl, 2005; Vallieres and Favre, 2004; Xie et al., 2009; Xu et al., 2006). However, vacuum pumping does not save much power but uses lots of membrane (Lin et al., 2007).

2.6.3 Pressure build-up in hollow fiber membranes

Pressure drop generally occurs in the bulk flow directions as gas flows through the membrane module. A significant pressure drop can occur in a hollow fiber permeator in case of small lumen sizes (inside diameter 50-100 μm). The permeate pressure increases from the open end to the close end if the permeate is in the tube side of the hollow fibers. The feed pressure reduces from the feed inlet to outlet if the feed is in the tube side, as shown in Figure 2.7. Both situations will cause a reduction in the local pressure difference

across the membrane, and thus reduces the driving force. Berman (1953) obtained a solution for laminar flow in a channel with porous walls from the Navier-Stokes equations. The solution reduces to the differential form of the Hagen-Poiseuille equation when the Reynolds number is less than 1.

$$\frac{dP_P}{dz} = \frac{-128\mu RTV}{\pi D_i^4 N_T P_P} \tag{2.6}$$

The Hagen-Poiseuille equation quantifies pressure drop in the narrow channel of hollow fibers. The equation assumes that the gas is incompressible (ideal gas) and the permeation flux is low (laminar flow). Thorman and Hwang (1978) investigated several factors affecting tube side pressure drop (i.e., radial and axial deformation, radial flow and gas expansion), and incorporated them into a refined pressure drop model. An effort was made by Coker et al. (1998) and Lim et al. (2000) to improve the Hagen-Poisseuille equation by taking into account the gas permeability and compressibility. However, it was found that the effect of gas compressibility and permeate flow is negligible and the pressure drop can still be described by the Hagen-Poiseuille equation. A new pressure drop equation was developed by Lim et al. (2000) from the continuity and the momentum balance equations with the consideration of gas compressibility and permeability. However, it was reported that the proposed equation reduces to Hagen-Poiseuille equation for low permeation fluxes. It was also reported that the use of Hagen-Poiseuille equation for defining pressure drop relations will result in overestimation or underestimation of the

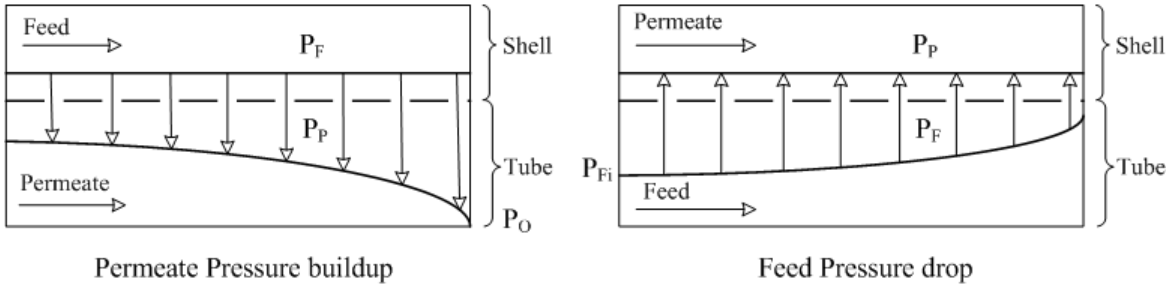

Fig. 2.7: Permeate pressure build-up or feed pressure drop in hollow fiber permeator (Zakaria, 2006).

membrane area required at the stipulated stage cut depending on the feed mode operation.

Several permeator models incorporated the Hagen-Poiseuille equation to account for the effect of pressure build-up in the separation (Chern et al., 1985; Pan and Habgood, 1978b; Pan, 1983, 1986). A comparison of the permeator performance achieved with and without taking into account the pressure build-up was portrayed by Pan (1978b). Chern et al. (1985) developed a model for simulating the performance of an isothermal hollow fiber permeator for binary gas mixtures. The model considered permeate pressure build-up and concentration dependence of the permeabilities by using the dual-mode sorption and transport models. The effects on separator performance caused by changes in fiber dimensions, feed pressure, membrane area and feed composition were investigated. Shao and Huang (2006) made and effort to provide an analytical approach to analyze the extent of pressure build-up. A dimensionless parameter that contains all the dominant factors responsible for generating the pressure build-up was proposed to serve as an indicator on the extent of pressure build-up in hollow fibers. However, a big pressure build-up in hollow fibers should be avoided since it represents a sacrifice of the driving force for gas permeation. Shao and Huang (2006) estimated the optimum length of the fiber as 12 cm, corresponding to the permeance of the fiber of 9.0 GPU, which otherwise will significantly inhibit gas permeation due to pressure build-up in fibers. It suggests that attention should be given to the fiber length while evaluating the fiber's gas permeance. It was also pointed out that influences of permeance and inner diameter are equivalent to that of the fiber length, so fiber length should be handled with caution particularly when the inner diameter of the fiber is small, and/or the intrinsic permeance of the fiber for the permeating gas is high (Shao and Huang, 2006).

2.6.4 Apparent and intrinsic permeances

The permeance of gases through hollow fiber membranes is essentially independent of feed pressure, which is normally the case for permeation of permanent gases in glassy polymers and may be attributed to the constant diffusivity at different pressures. Other studies also reported that the intrinsic permeability of non-condensable gases in glassy

polymers is constant or slightly decreasing with pressure (Haraya et al., 1989; Haraya and Hwang, 1992).

Gas permeance is measured normally with pure gases, and the ratio of pure gas permeance gives the ideal membrane selectivity, which is an intrinsic property of the membrane material. The magnitude of selectivity depends sensitively on the gas pair under consideration. In case of air separation, the selectivity varies from approximately 2 to 15 in polymers, in contrast with 5 to 1000 or more for H_2/CH_4 separation (Robeson, 1991). However, practical gas separation processes are performed with gas mixtures. If the gases in a mixture do not interact strongly with the membrane material, the intrinsic selectivity based on pure gas permeability and the mixed gas selectivity will be equal. This is usually the case for mixtures of oxygen and nitrogen, for example. In many other cases, such as a carbon dioxide and methane mixture, one of the components (carbon dioxide) is sufficiently sorbed by the membrane to affect the permeability of the other component (methane). Neglecting the difference between these two values, however, has led to a serious overestimate of the ability of a membrane to separate a target gas mixture (Baker, 2004; Lee et al., 1988). The hollow fiber membranes used in gas separation are often very fine. However, the pressure build-up on the lumen side of the membrane for these fine fibers can become enough to seriously affect membrane performance. Permeance determined from pure gas permeation experiments (apparent permeance) does not necessarily represent the true permeance of the membrane due to pressure build-up in the fiber lumen. In the production of nitrogen enriched air, the pressure-normalized fluxes are relatively low, from 1 to 2 GPU, and the pressure drops are not a significant problem. However, in the separation of hydrogen from nitrogen or methane, or carbon dioxide from natural gas, the pressure-normalized fluxes are higher, and excessive permeate pressure drops can develop in hollow fine fibers (Baker, 2004). Pressure build-up increases for longer fibers, fine fibers and for high pressure applications. For identical feed pressure and membrane area, permeate flow is less in the long fiber than that of shorter one, which can be attributed to the reduced driving force resulting from the permeate pressure build-up. In an industrial scale, the membrane length is usually more than 1 m and a considerable pressure build-up in the lumen can occur, resulting in discrepancy in the predicted

membrane performance if this effect is neglected. It is also important to ensure that all of the fibers have identical fiber diameters. Even a variation as small as ±10% from the average fiber diameter can lead to large variations in module performance (Crowder and Cussler, 1997; Lemanski and Lipscomb, 2000). Moreover, the length of potted section in the tube sheet contributes some pressure drop, and exclusion of the potted length section in theoretical analysis could possibly exacerbate prediction of module performance.

Wang et al. (2002) employed binary simulation models as an analytical tool to calculate the true permeation characteristics of hollow fiber membranes for a gas mixture of CO_2 and CH_4. Lababidi et al. (1996) employed an approximation method to estimate the permeance of each gas component in the gas mixture. Permeances measured from mixed gas permeation experiments do not represent the true intrinsic property of the membrane. Determination of mixed gas permeance through simulations are not straightforward and require consideration of competitive sorption, plasticization, concentration polarization, non-ideal behaviour of gases, and knowledge of thermodynamic properties (Chenar et al., 2006; Wang et al., 2002). However, pure gas permeances and selectivities are much more commonly reported in the literature than gas mixture data because they are easier to determine.

2.6.5 Numerical techniques and solution scheme

The numerical solution techniques for hollow fiber permeators involve solving a set of nonlinear ordinary differential equations (ODEs), which generally constitute boundary value type problems. Several solution techniques have been reported in the open literature including trial and error shooting techniques (Pan and Habgood, 1978b), finite difference with iteration approach (Coker et al., 1998), finite element (Thundyil and Koros, 1997), finite volume method (Cruz et al., 2005), and orthogonal collocation (Kaldis et al., 1998; Kaldis et al., 2000; Marriott and Sørensen, 2003).

Numerical solution to the set of ODEs can result in substantial computational time and effort. Instead of solving the complex set of ODEs, approximate solutions to the model

equations have been developed by several workers (Boucif et al., 1984; Boucif et al., 1986; Krovvidi et al., 1992; Pettersen and Lien, 1994a) in order to reduce computational difficulties, time and to provide quick solution especially for initial design purposes. A linear approximation model to solve the multicomponent countercurrent gas permeator transport equations considering pressure variation inside the fiber was presented by Kovvali et al. (1994). A linear relationship between the permeate and feed stream compositions was assumed, which reduced the computational efforts and also yielded analytical expressions for flow rates, permeate pressure, and compositions along the length of the permeator. A robust algebraic model for multi-component separation based on analogy with countercurrent heat exchangers was developed by Peterson and Lien (1994a). The algebraic nature of their model would make it easier to optimize membrane system and operating conditions. For a multi-component system, the solution using trial and error techniques is much more complicated than the binary case due to the need to converge an increased number of boundary conditions. A systematic method to find multi-component solution vectors using direct search maximizing routine adopted from box complex method was presented by McCandless (1990). More recently, a new numerical approach to solve the ODEs using Adams-Moulton's or Gear's backward differentiation formulas was developed by Chowdhury et al. (2005). This method allows the model equation to be solved as an initial value problem without initial estimates of the pressure, flow and concentration profiles.

2.7 Membrane process modules and cascade configurations

Since the membrane selectivity and pressure ratio achievable in a commercial membrane system are limited, single stage membrane system may not provide the separation desired. If the desired separation cannot be accomplished in a single stage or if a higher purity or recovery is needed, stream recycles or multi-stage operations could be a solution to improve the overall separation performance (Zakaria, 2006). A number of possible module configurations have been proposed by researchers and industries, including single permeation stage, recycle/reflux, and cascade configurations of multi stages. With the current generation of membranes, single-stage permeation, simple to

operate and control, is often capable of meeting a wide range of separation requirements. For many applications, a simple single-stage configuration is sufficient and offers the lowest capital investment (Bhide and Stern, 1991a). Multistage/multistep combinations can be designed but are seldom used in commercial systems in the first instance due to their complexity and being uncompetitive with alternative separation technologies (Baker, 2004). However, more complex designs are economically justified as the size of the processes expands and the costs of the separated components increase. More commonly, some form of recycle designs are used commercially and preferred over Multistage/multistep combinations. The enrichment of the more permeable component can be improved by recycling a part of the permeate stream to the feed stream. Pettersen and Lien (1994b), from their mathematical analysis of two cell configurations with a recycle of reject or permeate streams, reported that the reject recycle improves species recovery and product purity. On the other hand, the permeate recycle reduces the compressor duty which in turn improves the process economics.

2.7.1 Recycle and multiple stage permeators

A well known method for increasing the product purity is by cascade operation in which the permeate from a first permeator is recompressed and fed to a second permeator while the unpermeated stream from the second permeator is returned to the first permeator (Stern et al., 1984). A potentially more efficient way is to recycle a fraction of the concentrated permeate back to the feed stream. A parametric analysis of the permeate recycle to feed stream was conducted by Stern et al. (1984) for oxygen enrichment of air, while Majumdar et al. (1987) performed both experimental and theoretical analysis of the same system. An increase in the recycle ratio was found to increase the product purity but the membrane area requirement and compression power also increased rapidly with increased recycle ratio.

Multiple stage process designs usually involved tradeoffs between higher product recovery and increased equipment and operating costs. Several studies have been carried out to compare the performance of various multistage permeator designs (McCandless,

1985; Schulz, 1985; Spillman, 1989). An economic study by Spillman (1989) shows multiple stage designs have the same or lower process cost than a single stage process for some particular applications. An economic study of H_2 and N_2 separation from coal gasification was conducted by Gottschlich et al. (1989), and the performance of a single stage design was compared with several multistage designs. It was concluded that the single stage operation is the most economical for easy separations (when the feed and product compositions are not greatly different), while multiple stages are more economical for medium to difficult separations. An alternative method to choose optimal configurations for gas separation was proposed by Laguntsov et al. (1992), and it was shown that the use of high selectivity membranes in a conventional permeator does not always give better economics, however, the use of low selectivity membranes in a recycle system sometimes would.

Instead of an independent second permeator at the downstream of a first permeator, an internal second stage can be provided in the same permeator, which is referred to as an internally staged permeator (ISP) (Sidhoum et al., 1989). In an ISP, as the feed gas in the first tube set (first permeator) permeates to the shell side, a fraction of the permeate passes to the second tube set (internal second stage) which is maintained at a lower pressure than the shell side. Therefore, at every axial location of the permeator, permeate from the first membrane is fed to the second membrane. For air separation producing high purity nitrogen, it was shown by Sidhoum (1989) that ISP gives a slightly better separation than a two-stage cascade. However, the physical manufacturing of an ISP is more difficult than the conventional hollow fiber modules. A great deal of recycle and multiple stage permeators used commercially can be found elsewhere (Baker, 2002; Baker, 2004; Baker and Lokhandwala, 2008; Basu et al., 2004; Bernardo et al., 2009; Lokhandwala et al., 2010).

2.7.2 Unsteady state and cyclic operations

The advantages with steady-state operation include easy start-up and shout-down, simplicity of pressure and flow controls, large throughput of permeation, and low

maintenance requirements. However, several gas pairs of industrial interest cannot be separated effectively by current polymeric membranes due to limited permselectivity. These characteristics prompt researchers to consider the potential advantages of improved permselectivity in transient state conditions (Wang et al., 2011). Membrane gas separations under transient state conditions are rather unexplored compared to steady-state operations. However, unsteady state permeation is shown to be sometimes more beneficial to enhance the separation efficiency (Beckman et al., 1991; Higuchi and Nakagawa, 1989; Paul, 1971). The solution-diffusion mechanism states that the permeability coefficient can be considered equal to the product of solubility coefficient and diffusion coefficient (Nunes and Peinemann, 2006). Unfortunately, for most membrane materials, a trade-off relationship between permeability and selectivity often exists, and there appears to be an upper bound in permeability vs. selectivity plot above which virtually no data exist (Robeson, 1991). Once the membrane material is fixed, the intrinsic selectivity is essentially fixed as long as steady-state operation is used. However, transient and, in particular, steady cyclic operation of the membrane can be used to alter the selectivity characteristics.

To the best of our knowledge, the first theoretical study dedicated to a membrane separation process operating in a cyclic transient fashion was performed by Paul (1971) in 1971. Paul's design theoretically improved the separation when the membrane's mobility selectivity is significantly greater than permselectivity. If the feed is admitted intermittently at appropriate time intervals, the difference in the desorption fallout rates (due to the difference in the permeant diffusivity) can be exploited to effect the separation. Two cuts of permeate can be taken periodically in a time sequence in phase with the upstream pressure variations, and they are enriched in the component with the higher and lower diffusion coefficients, respectively. Corriou et al. (2008) optimized Paul's (1971) mode of operation and reported that synchronous operation offers the best performances. Corriou et al. (2008) also reported that based on current membrane material, the cyclic operation could potentially compete with the most selective polymers available to date, both in terms of selectivity and productivity.

Kao et al. (1991) reported a pressure swing scheme similar to pressure swing adsorption to carry out the transient permeation where the opposite solubility and diffusivity selectivity can operate synergistically. By periodically pressurizing the feed gas on one side of the membrane, a product enriched in the less soluble species can be collected during the high pressure cycle. A variant of the process is also described by LaPack and Dupuis (1994) to exploit the differences in the rates of either attainment of steady-state permeation or fall-off from steady-state permeation. Ueda et al. (1990) described air separation by a cyclic process comprising of the steps of feed pressurization and permeates evacuation using a compressor and a vacuum pump separately or using a single pump suitable for both pressurization and suction. Bowser (2004) and Nemser (2005) extended the application of cyclic process for controlling environmental emissions of volatile organic compounds (VOC) for vapour recovery in storage and reported reduction in overall VOC emissions. Feng et al. (2000) reported an unsteady state permeation process called pressure swing permeation for gas separation. The relatively low permeate pressure was elevated by periodically "pushing" the permeate by the high pressure feed gas, producing a permeate stream at a pressure as high as the feed pressure, which is impossible to achieve with conventional steady-state permeation. Transient and, in particular, steady cyclic operations can achieve a selectivity beyond the conventional processes; however, it has been overlooked despite its potentials.

2.7.3 Membrane hybrid systems

Hybrid processes are integrated processes in which a membrane system operates in combination with another unit operation, or processes in which the basic functioning of the membrane is joined with another physical or chemical process in a single unit operation. A properly designed hybrid process will balance the drawbacks of the specific process and favorably combine their advantages. The result will be a better separation that neither process could achieve individually, contributing to a sustainable process improvement by allowing the reduction of investment and operational costs (Bernardo et al., 2009).

Typically, membranes offer bulk removal properties with a relatively small area i.e., moderately pure product at low cost, that may be economically upgraded by a subsequent process. Davis et al. (1993) reported a pilot BP distillation/membrane hybrid process for propane/propylene separation, where a part of the vapor mixture from the cryogenic distillation column is sent to the membrane system which extracts the propylene using an aqueous solution of silver nitrate. The integration of membranes with such other separation processes as PSA (Bernardo et al., 2009; Doshi et al., 1989; Feng et al., 1998a) is well-established in the chemical and petrochemical industries. Membrane permeation can be effective to aid the pressurization and high-pressure adsorption steps of a typical PSA process. The pressure difference available from the PSA can be used for operating the membrane incorporated into the blow down step of the PSA cycle (Esteves and Mota, 2007; Bernardo et al., 2009). Usually, a combination of membranes with PSA is considered in H_2 separation, while hybrid membranes with amine absorption are applied to the CO_2 separation. Belaissaoui et al. (2012) studied a hybrid membrane cryogenic process for post-combustion CO_2 capture and reported that the energy requirement of the hybrid process is lower than that of the energy required for an independent cryogenic process, and the overall energy requirement of the hybrid process could possibly be significantly decreased. A case study of hybrid process combining oxygen enriched air combustion and membrane separation for post-combustion CO_2 capture was investigated from an energy requirement perspective (Favre et al., 2009a) and the hybrid process could lead to a 35% decrease in the energy requirement compared to oxycombustion. A comparison of the separation cost for the membrane process with diethanolamine (DEA) absorption showed that the membrane process is more economical for CO_2 concentrations in the feed in the range 5-40 mol % (Bhide et al., 1998). If the feed contains H_2S, the cost for reducing CO_2 and H_2S concentrations to pipeline specifications increases with increasing H_2S concentration (1000-10000 ppm). If membrane processes are not economically competitive because of the high H_2S concentration in the feed, the separation cost could be significantly lowered by using hybrid membrane processes. In such processes, the bulk of CO_2 and H_2S are separated from sour natural gas with membranes and the final purification is performed by means of suitable gas-absorption processes (Bhide et al., 1998). A hybrid system (Cynara membranes with amine absorption) has been operating since 1994 in Mallet (Texas,

U.S.A.) to perform the bulk removal of CO_2 from associated gas (90% CO_2 and heavy hydrocarbons), before downstream treating. The membrane system offered a 30% reduction in operating cost when compared with a methyl diethanolamine (MDEA) system and significantly reduced the size of the subsequent operations (Blizzard et al., 2005). Several EOR projects in Texas integrate membranes and amine technologies to produce pipeline quality natural gas and at the same time to recover CO_2 (Chowdhury, 2012; Echt, 2002). The economic viability of membrane-amine hybrid processes for the removal of acid gases (i.e., CO_2 & H_2S) from crude natural gas could be found elsewhere (Bhide et al., 1998; Echt, 2002; McKee et al., 1991).

2.8 Industrial applications of membrane gas separation

The membrane gas separation industry is still growing and changing. Most of the large industrial gas companies now have membrane affiliates: Air Products (Permea), MG (Generon), Air Liquide (Medal) and Praxair (IMS). The affiliates focus mainly on producing membrane systems to separate nitrogen from air, but also produce some hydrogen separation systems. Another group of companies including UOP (Separex), Natco (Cynara), Kvaerner (GMS) and ABB Lummus Global produce membrane systems for natural gas separations. A third group of smaller independents are focusing on the new applications including vapor separation, air dehydration and oxygen enrichment. The main industrial applications of membrane gas separation are summarized in Table 2.2. Overviews on the main gas separation applications can be found in Koros and Fleming (1993); Baker (2002); and Bernardo et al. (2009).

2.8.1 CO_2 removal and capture

The recovery of carbon dioxide from large emission sources is a formidable technological and scientific challenge which has received considerable attention for several years (Favre, 2007). Polymeric membranes are well developed today and commercially available for CO_2 capture. Recovery of carbon dioxide from flue gas streams is particularly

Table 2.2: Main industrial applications of membrane gas separation (Bernardo et al., 2009).

Separation	Process
H_2/N_2	Ammonia purge gas
H_2/CO	Syngas ratio adjustment
H_2/hydrocarbons	Hydrogen recovery in refineries
O_2/N_2	Nitrogen generation, oxygen-enriched air production
CO_2/hydrocarbons (CH_4)	Natural gas sweetening, landfill gas upgrading
$CO_2/N_2/O_2$	Carbon dioxide removal from flue gas or Enhanced coal bed methane application
H_2O/hydrocarbons (CH_4)	Natural gas dehydration
H_2S/hydrocarbons	Sour gas treating
He/hydrocarbons	Helium separation
He/N_2	Helium recovery
hydrocarbons/air	Hydrocarbons recovery, pollution control
H_2O/air	Air dehumidification
Volatile organic species (e.g., ethylene or propylene)/light gases (e.g., nitrogen)	Polyolefin purge gas purification

interesting both for the product value of CO_2 (e.g., enhanced oil recovery) and for environmental reasons (reducing the greenhouse effect). The key issue for CO_2 capture is minimizing the energy required in the overall process (capture and sequestration).

Post-combustion capture involves the separation of CO_2 from the flue gas produced from the combustion of fossil fuels (e.g., from a standard gas turbine combined cycle, a coal-fired steam power plant). This technology involves CO_2 separation at a relatively low temperature, from a gaseous stream at atmospheric pressure and with a low CO_2 concentration (5-15 vol % if air is used during combustion). Suitable methods for CO_2 capture may include absorption, adsorption, and membrane processes. Amine absorption is today's best technology for post-combustion capture, with an energy cost in the range of 4-

6 GJ/ton CO_2 recovered (mainly due to significant energy consumption in the solvent regeneration step). However, the amine process requires large-scale equipment for the CO_2 removal and chemicals handling. In post-combustion capture, CO_2 must be separated from the flue gases (where N_2 is the main component). Due to the low CO_2 concentration and pressure in this gas, the commercial membranes used to separate CO_2 from natural gas at high pressures are not particularly suited. Their use will result in a large membrane area and in high compression costs (Bernardo et al., 2009). Bounaceur et al. (2006) presented a simulation study on the separation performance and energy cost of a single-stage membrane module for post-combustion applications considering binary dry CO_2/N_2 feed mixtures with a wide range of compositions and membrane CO_2/N_2 selectivities. It was shown that most membranes currently available (CO_2/N_2 selectivity less than 50) are not adequately capable of producing the recovery and permeate compositions (specified by the government regulations), but membranes with selectivity above 100 are required. However, for flue streams containing 20% or more CO_2, reasonable recoveries and permeate compositions (that do not exceed 80%) can be attained with currently available membranes and the related cost will be only about 0.5-1 GJ/ton CO_2 recovered, which is lower than the amine absorption.

Carbon dioxide removal from natural gas (i.e., natural gas sweetening) is needed to meet the pipeline specifications (e.g., down to 2% vol. in U.S.A.), since CO_2 reduces the heating value of natural gas, renders corrosion, and freezes at a relatively high temperature, forming blocks of dry ice that can clog pipelines and damage pumps. Membrane technology is attractive for CO_2 removal from natural gas since it offers a high recovery of the acid gases without significant loss of pressure in the pipeline product gases, and the treatment can be accomplished using the high wellhead gas pressure as the driving force for the separation. A high natural gas recovery (> 95%) can be achieved in multistage systems. Membrane systems are typically installed for small size applications (less than 6000 Nm^3/h) and in remote locations since amine processes are too complicated for small productions. Membrane and amine systems become competitive for a size of 6000-50000 Nm^3/h, while bigger plants are installed for offshore platforms or for enhanced oil recovery. Membrane gas separation presents significant advantages for the offshore

industry; moreover, it is an environmentally friendly alternative to traditional amine absorption (Bernardo et al., 2009).

Methane is the second largest contributor to global warming, after carbon dioxide. Landfills and sewage treatment digesters produce methane-rich biogas that contains approximately 50% carbon dioxide. Although biogas is expensive to upgrade, the gas is essentially free and its collection will satisfy certain environmental interests. Also, such gas is usually located near industrialized areas where energy values are high. Several landfills currently use membranes to upgrade to a high-quality gas. In this application, membranes compete directly with water-scrubbing, amine treatment and PSA. It also competes with the use of the untreated gas as a low BTU fuel. The competitiveness of membranes for biogas applications is strongly dependent on the pressure requirements of the product gas. Low pressures penalize membrane economics. If a high-pressure gas is required, then membranes offer clear advantages (Noble and Stern, 1995). Membrane Technology and Research (MTR) along with United States Environmental Protection Agency (USEPA) has been developing simple and low cost membrane process to convert landfill gas and other dilute methane waste gas streams into useful fuel. Such streams, containing 10-40% methane, are often vented without capturing the fuel value (estimated at $US200-300 million per year), and contribute up to 1 Tg (= 1 million tons) of methane to U.S. greenhouse gas emissions (Membrane Technology and Research, 2012). Several other gas companies (Pall Corporation, Monarflex, Evonik Industries, Air Products, Sioen Industries) have been developing membranes to capture the fuel value of biogases worldwide.

2.8.2 Nitrogen- and oxygen-enriched air production

Air separation to produce nitrogen and oxygen (or oxygen-enriched air) by selective permeation through membranes is widely investigated. Membrane air separation is now accepted as an economic process to produce moderate purity streams containing up to 99.5% nitrogen or 30~50% oxygen (Feng et al., 1999). It is estimated that air separation by membranes represents about 60% of the overall membrane gas separation business. According to the forecast made in 2002 (Baker, 2002), the total market of membrane gas

separation in 2010 would be 350 million USD. However, its actual growth rate was faster than expected, and it amounted to about 500 million USD in 2010, mainly because of the expansion of the processes of air membrane separation (Yampolskii, 2012). For the present generation of membranes, the permeation selectivity to oxygen and nitrogen is relatively low (the permeability ratio or permselectivity is generally between 2 and 7). Consequently, the production of relatively pure oxygen would require multistage operations, each stage requiring recompression of the oxygen-enriched permeate stream from the previous stage. Currently, there are no membrane systems that produce high purity oxygen by membrane alone, while the membrane processes for the production of moderate purity nitrogen is practically viable. When high purity nitrogen is desired, hybrid separation processes that incorporate membranes with other ‘‘finishing’’ technologies such as PSA, liquefaction, and deoxo process have been developed to eliminate the purity limitations of the membrane process while taking advantage of its efficient bulk separation characteristics.

2.9 MEA-based CO_2 capture technology

Monoethanolamine (MEA) used in MEA-based chemical absorption process was developed over 70 years ago as a general solvent to remove acid gases (i.e., CO_2 and H_2S) from natural gas streams. The idea of separating CO_2 from flue gas streams started in the 1970’s, not with concern about the greenhouse gas effect, but as a potential economic source of CO_2 for different applications such as enhanced oil recovery (EOR). Fluor Daniel Inc., Dow Chemical Co., ABB Lummus Crest Inc., and Kerr-McGee Chemical Corp. were few of the initial developers of MEA-based technologies for CO_2 capture (Chowdhury, 2012; Hassan, 2005; Rao and Rubin, 2002). MEA-based technology can capture more than 95% of the CO_2 from flue gases to yield a fairly pure (> 99%) CO_2 product stream. Most commercial CO_2 capture plants use processes based on chemical absorption with MEA solvent until to date.

Flue gas from power plant is first treated to reduce the levels of particulates and other impurities present, pressurized to overcome the pressure losses in the downstream processing section, and cooled before sending to an absorption tower (absorber). The amine

process has two major units, one for absorption and the other for stripping, as illustrated in Figure 2.8. The cooled flue gases entering the absorption column flow upwards through the vessel, countercurrent to the absorbent (MEA solution, with some additives). Amines in water solution react with CO_2 in the absorption column to form carbamate, while the scrubbed gas is vented to the atmosphere. The CO_2-rich solution leaves the absorber from the bottom and is preheated in a heat exchanger by the hot lean solution returning from the stripper on its way back to the absorber. The rich solution is further heated in a reboiler using steam. The carbamate formed during CO_2 absorption is broken down by heat, thereby regenerating the sorbent and producing a concentrated CO_2 stream. The hot CO_2-lean solvent is then pumped from the bottom of the stripper to the exchanger, where the lean solution transfers heat to the rich solution. The lean solution is further cooled before being recycled back to absorber to match design specifications. Some fresh MEA is added to make up for losses incurred in the process.

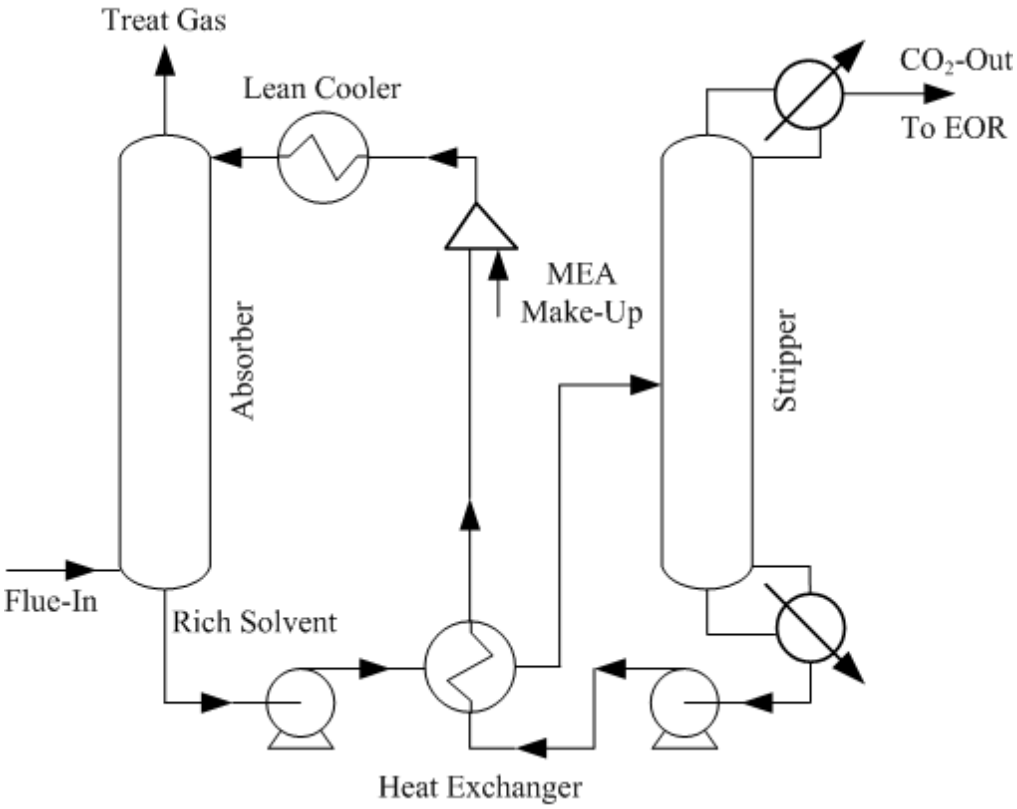

Fig. 2.8: Schematic of MEA process.

The CO_2 product is separated from the sorbent in a flash separator, and then taken to the drying and compression unit. In order to be an effective climate change mitigating solution, the captured CO_2 must be stored safely and securely or it should be utilized. The captured CO_2 may be compressed to high pressures so that it is liquefied and can be transported to long distances to the designated storage or disposal facility or it may utilized for different applications (Chowdhury, 2012).

Since the carbamate formed during absorption is quite stable, it takes substantial heat energy to break the bonds and to regenerate the sorbent. Although MEA-based absorption process is a very most suitable technology available for capturing CO_2 commercially from power plant flue gases and is considered a state-of-the-art technology for acid gas removal, it has its own limitations. As mentioned above, one of the major drawbacks is excessive energy penalty due to regeneration of the solvent for reuse. Moreover, amine units use more energy when the CO_2 concentration increases. The other two factors are corrosion and loss of solvent. Corrosion control is very important in amine systems for processing of oxygen-containing flue gases. Excessive corrosion has a great impact on the plant's economy as it can result in unplanned downtime, production losses, reduction in life of machineries and limiting operational ranges of process parameters. In order to reduce the corrosion rates, corrosion inhibitors, lower concentrations of MEA, appropriate materials of construction and mild operating conditions are required (Barchas and Davis, 1992). Some of the sorbent is lost during the process because of a variety of reasons including mechanical, entrainment, vaporization and degradation. Not all the sorbent entering the stripper are regenerated. Flue gas impurities, especially oxygen, sulfur oxides and nitrogen dioxide react with MEA to form heat-stable salts, thus reducing the CO_2-absorption capacity of the sorbent (Rao and Rubin, 2002).

2.10 Conclusions

Though membrane gas separation is comparatively a new process, a great deal of research has been carried out to date. It is beyond our scope to discuss everything in details. Salient features of polymeric membranes, hollow fiber permeators, unsteady state

permeation, and membrane hybrid systems have been discussed. Membrane based gas separations are well established today and can outperform conventional techniques in many aspects. The current trend in membrane gas separation industry is to develop robust membranes with superior separation performance, in order to meet the key criteria of reliability and durability for industrial applications. In accordance with that, process analysis such as modeling, simulation, optimization and sorting optimal operating conditions/modular configuration/economics are deemed necessary for better understanding of the membrane separation technology. With the development of new process concepts, new membrane applications will emerge. An optimal operating condition and/or module configuration could possibly yield a better separation performance as well as cost savings. Moreover, the potential of hybrid separation processes in industrial scale is not fully exploited because of the lack of general design methodologies and detailed process know-how. It is our understanding that although significant positive outcomes have been found through research in membrane gas separation, the possibilities are endless.

Chapter 3

Simulation of binary gas separation with asymmetric hollow fiber membranes and case studies of air separation[†]

3.1 Introduction

Membrane process is an attractive alternative to conventional technologies for gas separations due to its simplicity in operation, moderately low capital cost, small size, low energy consumption, low maintenance and reliable performance. Polymer membranes have found applications in variety of industrial processes such as air dehumidification, nitrogen production, oxygen enrichment of air, hydrogen recovery from refinery and ammonia synthesis purge gases, landfill gas upgrading, sweetening of natural gas, recovery of carbon dioxide for enhanced oil recovery, helium recovery, syngas ratio adjustment, and volatile organic compound recovery. Remarkable efforts have been put forward on developing membrane materials to offer high permselectivities. However, the overall process design and operating conditions also play an important role in successful and economic application of membranes for gas separations. The prediction of the separation performance and the evaluation of the membrane process are essential to process engineers. Identifying optimal operation and design conditions is difficult without a valid model of the system and justified solution technique. Modeling and simulation of the membrane process is a viable means to provide valuable information to the design, operating and economics of the separation process with minimum cost.

Various aspects in membrane gas separation (e.g., permeation analysis, permeator simulation, module design and economic evaluation) have been addressed using a variety of structures and forms. Since the earlier work of Weller and Steiner (1950), who were among the first to address mathematical modeling of membrane gas separators, a number of mathematical models and calculation techniques with different flow patterns and module configurations for symmetric and high flux asymmetric membranes have been investigated. A great deal of modeling studies has been accomplished on symmetric membranes, but not

[†] Part of Chapter 3 has been published in Can. J. Chem. Eng. 90, 1253-1268; cited as Kundu et al. (2012a).

much work was done on modeling of asymmetric membranes where the porous substrate layer prevents back mixing of local permeate. Most of the models refer to binary systems (Boucif et al., 1986; Feng et al., 1999; Kaldis et al., 1998; Pan and Habgood, 1978a, b; Pan, 1983; Sidhoum et al., 1988; Weller and Steiner, 1950) and only a few of them deal with ternary or multicomponent systems (Coker et al., 1998; Kaldis et al., 2000; Chowdhury et al., 2005; Sada et al., 1992; Sengupta and Sirkar, 1987; Weller and Steiner, 1950). For hollow fiber membranes, the permeate pressure build-up in the fiber lumen has been considered in a limited number of studies. The mathematical model developed by Pan (1983) is widely accepted for calculating the performance of hollow fiber permeators with high-flux asymmetric membranes. It takes into account the pressure build up inside the fiber lumen and is applicable to the basic operating modes (i.e., countercurrent, cocurrent and crossflow). However, the solution technique for the boundary value problem was very complicated and demanded significant computational efforts. Moreover, prior initial estimates of the pressure and concentration profiles along the fiber length were required. Since commercial membrane modules have a predetermined length of fibers, this solution technique leads to considerable numerical difficulties in such cases because of the trial-and-errors involved. To overcome the computational complexities in solving the boundary value problems, several modifications and alternative approaches to solving the model equations have been proposed (Coker et al., 1998; Kaldis et al., 2000; Kovvali et al., 1994; Marriott et al., 2001; Marriott and Sørensen, 2003). These models aim at simplifying the governing equations and introducing additional assumptions that lead to approximate solutions with less computational effort and time. Basaran and Auvil (1988) solved the governing equations for the case of binary gas mixtures in a crossflow mode by asymptotic solutions based on Navier-Stokes equations. However, these solutions do not really alleviate the computational problems but rather the solutions appear to be inadequate at low permselectivities. Singh et al. (1995) investigated the gas diffusion resistance inside the porous supporting layer, which Pan (1983) considered negligible as compared to the mass transfer resistance of the membrane skin layer. It was shown that gas diffusion within the substrate pores is very fast compared to bulk transport in the fiber bore under certain operating conditions, which leads to a simplifying assumption that the gas phase composition at the porous layer interface is identical to that in the bore. This simplifies the

governing equations, and the requirements for non-linear equations to describe local permeate concentrations are bypassed. However, cases where gas diffusion is relatively slow have not been discussed. Following the assumption of Singh et al. (1995), Giglia et al. (1991) analyzed the concentration profiles along the fiber. The boundary conditions at fiber entrance and exit were considered fixed to initial and final values, which is actually not true, especially at the closed end of the fiber or at the residue exit. The solution technique requires guessing of certain operating variables (e.g., the residue concentration at exit). Sidhoum et al. (1988) studied binary gas separation with asymmetric hollow fiber membranes by considering cocurrent or crossflow configuration, but the pressure build up inside the fiber lumen was not taken into consideration. The problem was reduced to an initial value problem and the obtained dependent variable profiles (with initial estimates being supplied for the actual boundary value problem) were solved using the Runge-Kutta method. Kaldis et al. (1998) developed a model based on Pan's (1986) initial theoretical formulation, and the orthogonal collocation technique was adopted to solve the basic differential equations. This strategy conduces to a system of non-linear equations in which the convergence is dependent on the estimated composition profile. Solution techniques for the model equations differ depending on simplifications and specific applications.

Significant contributions have been provided by Agrawal and Xu (1996), Agrawal (1997), Bhide and Stern (1991a, b), Ettouney et al. (1998), Feng et al. (1998a, b; 2000), Pan (1986), and Sengupta and Sirkar (1983; 1987; 1988) to address some of the important aspects in producing acceptable product purity with membranes. A number of possible module configurations have been proposed, including single permeation stage, recycle, and multi-stage cascades. With current generation of membranes, single-stage permeation, which is simple to operate and control, is often capable of meeting a wide range of separation requirements. For many applications, a simple single-stage configuration is sufficient and requires the lowest capital investment (Bhide and Stern, 1991a). However, more complex designs are economically justified as the size of the processes expands and the costs of the separated components increase. The enrichment of the more permeable component can be improved by recycling a part of the permeate stream to the feed stream. Pettersen and Lien (1994b), from their mathematical analysis of two-cell configurations

with recycle of reject or permeate streams, reported that reject recycle improves species recovery and product purity. On the other hand, permeate recycle reduces the compressor duty which in turn improves the process economics.

In this study, a mathematical model for high-flux asymmetric hollow fiber membrane was developed on the basis of Pan's (1986) original model. The basic model was simplified in a way different from Pan's (1986) original simplification. In simplifying the governing equations, the approach taken by Sengupta and Sirkar (1995) was followed. The model takes into account Pan's (1983) approach of crossflow pattern with respect to the membrane skin, irrespective of the flow direction of the bulk permeate stream outside of the porous substrate layer. The permeate pressure build-up inside the fiber bore was taken into account in the model. Finally, a set of coupled first order ordinary differential equations for flow rate, composition and pressure profile were derived. A new solution technique was developed to solve the model equations, which constitute a boundary value problem. A set of ordinary differential equations (ODE's) was solved as an initial value problem (IVP) in two successive steps using Gear's backward differentiation formulae (BDF) method (DIVPAG subroutine in the IMSL library). An iterative approach was employed since all quantities at any specific end are not known. The solution technique was applied to different flow and module configurations (i.e., cocurrent and countercurrent, shell-side feed, and bore-side feed). The model predictions were validated with experimental results, and its robustness was demonstrated. The model as well as the solution technique can be implemented for a variety of membrane gas separations.

Using the model, the separation characteristics of air by representative hollow fiber membranes were investigated. In membrane air separation, air is fed to one side of the membrane, and nitrogen is obtained in the residue side at a pressure equal to the feed, while the permeate stream is enriched with oxygen at a substantially lower pressure. The primary target is usually to have either nitrogen or oxygen enriched air as the product due to purity and recovery considerations. In addition to membrane permselectivity and operating pressures, the flow patterns (i.e., countercurrent, cocurrent, or crossflow) also influence the separation performance of a membrane permeator. The feed gas can be supplied to either

the shell-side or the bore-side of the hollow fibers. Both modes of feeding are being used commercially for nitrogen production, and the choice is often determined by the cost of module manufacturing and the separation performance. The configurations studied here included single-cell, single-cell with permeate recycle, single-cell with retentate recycle, air bleeding, and two cells in series. The results were presented in terms of species recovery, productivity, stream enrichment and energy requirement. There is a complex interplay between the process parameters. An optimization study or rigorous parametric study is required for better understanding of the different module configurations and associated economics.

3.2 Mathematical modeling

According to Pan (1983; 1986), the composition of the permeate leaving the membrane skin surface differs from that of the bulk permeate outside the porous supporting layer (y' as opposed to y, see Figure 3.1). It was considered that the permeate inside the porous support is not affected by the bulk permeate composition, and the bulk permeate composition at any point along the permeator length represents the accrued effect of all permeation prior to that point. The composition y' is restrained by the relative local permeation rates, which in turn are dictated by the local feed composition and local pressures. The permeation rate of component A can be described as:

$$dJ_A = Q_A dA\left(P_F x - P_P y'\right) \tag{3.1}$$

where

$$y' = dJ_A / (dJ_A + dJ_B) \tag{3.2}$$

The assumptions employed in the analysis are:

1) The porous support layer has negligible resistance to the gas flow, and back diffusion along the pore path is insignificant due to high permeate flux.
2) No mixing of different permeate compositions occurs inside the porous support layer.
3) The deformation of the hollow fiber under pressure is negligible.
4) The permeance of each species is constant at a given temperature.

5) The gas viscosities are independent of pressure.
6) The pressure drop on the shell-side of the module is negligible.
7) The pressure drop inside the fiber lumen can be described by the Hagen-Poiseuille equation.
8) The gas flows are evenly distributed, and the end effects resulting from flow direction change are negligible.

The flow pattern inside the module can be either cocurrent or countercurrent, as shown in Figure 3.1. The basis for the model is mass balance over a differential element of the hollow fiber module, and the model equations for all the modules and flow configurations can be deduced in a similar way. However, only the equations for shell-side

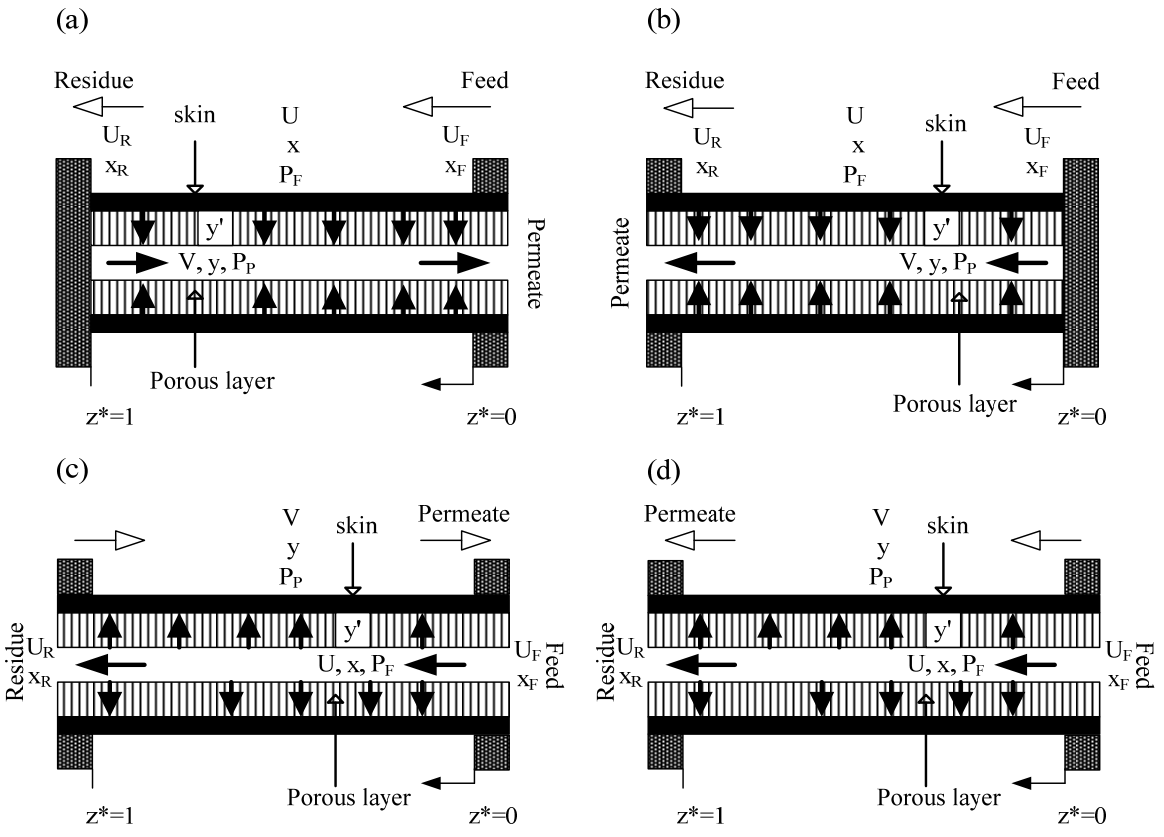

Fig. 3.1: Schematic of (a) countercurrent flow shell-side feed; (b) cocurrent flow shell-side feed; (c) countercurrent flow bore-side feed and (d) cocurrent flow bore-side feed pattern in a hollow fibre permeator.

feed countercurrent flow conditions are described here in details for brevity. Consider the separation of binary gases with a hollow fiber membrane. Referring to Figure 3.1a, the mass balance for the faster and slower permeating components over the differential permeator length *dz* can be written as Eqs. (3.3) and (3.4), respectively:

$$-\frac{d[Ux]}{dz} = Q_A(\pi D_o N_T)(P_F x - P_P y') = -\frac{d[Vy]}{dz} \tag{3.3}$$

$$-\frac{d[U(1-x)]}{dz} = Q_B(\pi D_o N_T)\{P_F(1-x) - P_P(1-y')\} = -\frac{d[V(1-y)]}{dz} \tag{3.4}$$

Combining Eqs. (3.3) and (3.4) yields an expression for the total molar flow rate over the differential permeator length *dz*:

$$-\frac{dU}{dz} = (\pi D_o N_T)[Q_A(P_F x - P_P y') + Q_B\{P_F(1-x) - P_P(1-y')\}] = -\frac{dV}{dz} \tag{3.5}$$

The local relative rate of permeation can be described by

$$\frac{d[Ux]}{dU} = y' \tag{3.6}$$

The pressure variation in the fiber lumen can be represented by the Hagen-Poiseuille equation,

$$\frac{dP_P}{dz} = \frac{-128\mu RTV}{\pi D_i^4 N_T P_P} \tag{3.7}$$

The overall material balance and component balance yield

$$U = U_R + V \tag{3.8}$$

$$Ux = U_R x_R + Vy \tag{3.9}$$

The local mole fraction of the permeate in the porous substrate y' upon permeate leaving the membrane skin layer is obtained from Eq. (3.6) with the help of Eqs. (3.3) and (3.5):

$$y' = \left\{1+(\alpha-1)(x+\gamma) - \left[\{1+(\alpha-1)(x+\gamma)\}^2 - 4\alpha(\alpha-1)\gamma x\right]^{0.5}\right\} / [2(\alpha-1)\gamma] \tag{3.10}$$

For convenience, the following dimensionless quantities are defined:

$$\alpha = \frac{Q_A}{Q_B}, \qquad \gamma = \frac{P_P}{P_F}, \qquad z^* = \frac{z}{l_E}, \qquad U^* = \frac{U}{U_F}, \qquad V^* = \frac{V}{U_F}, \qquad K_1 = \frac{\pi D_o l_E N_T Q_B P_F}{U_F},$$

$$K_2 = -\frac{128\mu RTl_E U_F}{\pi D_i^4 N_T P_F^2}$$

The differential equations for the molar flow rates at the residue and permeate sides are obtained from Eq. (3.5) with the aid of the dimensionless quantities,

$$dU^*/dz^* = -K_1[\alpha(x-\gamma y')+(1-x)-\gamma(1-y')] \tag{3.11}$$

$$dV^*/dz^* = -K_1[\alpha(x-\gamma y')+(1-x)-\gamma(1-y')] \tag{3.12}$$

The differential equation for the variation of residue side mole fraction along the permeator length is obtained from Eqs. (3.3) and (3.5):

$$dx/dz^* = -K_1[\alpha(1-x)(x-\gamma y')-x\{(1-x)-\gamma(1-y')\}]/U^* \tag{3.13}$$

The differential equation for the permeate side pressure build up along the fiber length is obtained from Eq. (3.7),

$$d\gamma/dz^* = K_2 V^*/\gamma \tag{3.14}$$

The four simultaneous differential Eqs. (3.11-3.14), together with Eq. (3.10), describe the molar flow rates of residue and permeate sides, the residue mole fraction, the permeate pressure build up and the local permeate mole fraction along the dimensionless fiber length. The solution is expected to give the molar flow rate and composition of the residue stream from which the bulk composition of the permeate stream exiting the permeator can be evaluated from the overall material balance (Eqs. 3.8-3.9).

The boundary conditions depend on the mode of operation. For countercurrent operation, the boundary conditions are as follows:

$$\text{At fiber exit } (z^*=0): \quad x = x_F \;;\; U^* = 1 \;; \text{and } \gamma = \gamma_o = P_{Po}/P_{Fi} \tag{3.15a}$$

$$\text{At fiber closed end } (z^*=1): \quad V^* = 0 \tag{3.15b}$$

Alternatively, the bulk permeate concentration profile along the fiber length can be obtained from Eq. (3.16),

$$dy/dz^* = -K_1[\alpha(1-y)(x-\gamma y')-y\{(1-x)-\gamma(1-y')\}]/V^* \tag{3.16}$$

A similar procedure can be applied for deriving the governing equations for shell-side feed cocurrent flow configuration (Figure 3.1b), with slight modifications as follows:

1) The overall material balance for cocurrent flow

$$U_F = U + V \tag{3.17}$$

2) Eqs. (3.11-3.14) and (3.16), together with Eq. (3.10), can describe the molar flow rates of residue and permeate, residue composition, permeate pressure build up in the fiber lumen and bulk permeate composition, respectively, with the signs for V^*, y and γ being reversed:

At closed end of the fiber, $z^* = 0$: $U^* = 1$; $V^* = 0$; $x = x_F$; and $y = y'$ (3.18a)

At fiber exit, $z^* = 1$: $\gamma = \gamma_o = P_{Po}/P_{Fi}$ (3.18b)

For bore-side feed flow (Figure 3.1c and d), the feed pressure P_F decrease along its direction of flow inside the hollow fibers, while the permeate pressure P_P can be taken as constant. Therefore, the dimensionless quantities and other variables can be defined using the feed inlet pressure P_{Fi}, instead of P_F:

$$\gamma_o = P_P/P_{Fi}\ ,\ K_1 = \pi D_o l_E N_T Q_B P_{Fi}/U_F\ ,\ K_2 = -128\mu RTl_E U_F/\left(\pi D_i^4 N_T P_{Fi}^2\right) \quad (3.19)$$

The variation in the feed pressure inside the fiber lumen can be described using a new dimensionless variable β defined as

$$\beta = P_F/P_{Fi} \quad (3.20)$$

The governing equations will now incorporate the change of β with fiber length and will replace γ in the pressure drop equation used in the shell-side feed configuration. The final governing equations for the bore-side feed configuration can be formulated similarly as for the shell-side feed configuration.

3.3 Solution technique of model equations

For the permeator performance study, the known variables are: input feed conditions (i.e., feed flow rate, composition, temperature and feed pressure), permeate pressure at fiber exit, membrane permselectivity (i.e., permeance and permeance ratio) and the membrane module information (i.e., fiber inside and outside diameters, length and number of fibers). The variables to be observed are: stage cut (i.e., permeate to feed flow rate ratio), and the concentrations of the permeate and residue streams. Though the model equations appear to be of boundary value problem (BVP) nature, they can be solved numerically as an initial value problem (IVP) for both shell-side feed and bore-side feed

with countercurrent or cocurrent flow pattern. Unlike Pan's approach, the present technique does not require initial estimates of the pressure, flow or concentration profiles inside the hollow fiber. The system of ordinary differential equations was solved using the Gear's BDF method based on the DIVPAG subroutine in the IMSL library. The BDF method is particularly useful for stiff differential equations and differential algebraic equations. It is to be noted that for binary gas separation, the local permeate concentration equation is an explicit algebraic equation. However, for the separation of multicomponent gas mixtures, the corresponding equations will be implicit non-linear equations. Details of multicomponent gas separation have been addressed in a separate study (Kundu et al., 2012b).

The steps followed for shell-side feed countercurrent flow configuration are as follows:

1) Algebraic Eq. (3.10), differential Eqs. (3.11-3.14) together with boundary conditions (Eq. (3.15a and 3.15b)) define the operation of shell-side feed countercurrent flow configuration.
2) Since the initial condition (at $z^* = 0$) for V^* is not explicitly known, an iterative approach was adopted in order to solve the equations. The initial value of V^* at $z^* = 0$ was guessed at first instance. The local permeate mole fraction (y') at $z^* = 0$ was estimated using Eq. (3.10) and the initial conditions.
3) Using the initial conditions of U^*, V^*, x and γ at $z^* = 0$ as well as y' from step (2), Eqs. (3.11-3.14) were integrated from $z^* = 0$ by calling DIVPAG subroutine from the IMSL library to calculate U^*, V^*, x and γ for the next plate. After the integration step, the value of y' was updated.
4) Based on the values of U^*, V^*, x, γ and y' from the first plate, new values of U^*, V^*, x, γ and y' were calculated for the next plate according to step (3). The procedure was repeated till the N^{th} discrete point/plate or $z^* = 1$.
5) If the calculated value of V^* at the other boundary $(\text{i.e., } z^* = 1)$ did not match the specified value (i.e., $V^* = 0$) with a preset tolerance limit, steps (2-4) were repeated with different guesses until the value was matched.

6) After satisfying step (5), bulk permeate mole fraction at the fiber exit and bulk permeate concentration profile along the fiber length were calculated from mass balance. Alternatively, the values of V^*, x, γ, y and y' at $z^* = 0$ were used as initial values to initiate integration of Eq. (3.16) only, by calling DIVPAG subroutine from the IMSL library to calculate bulk permeate concentration profile.

For the shell-side feed cocurrent flow configuration, five differential Eqs. (3.11-3.14, and 3.16) together with algebraic Eq. (3.10) were simultaneously solved by assuming a γ at $z^* = 0$ (instead of V^*). The solution procedure for bore-side feed countercurrent flow configuration is essentially the same as the procedure for the shell-side feed countercurrent flow. It may be mentioned that the bore-side feed cocurrent flow configuration is the easiest to execute and does not require any trial and error since all the boundary conditions are explicitly specified at $z^* = 0$.

It may be mentioned that in Chowdhury et al. (2005), who used a set of implicit non-linear algebraic equations for local permeate concentrations, the bulk permeate concentration at the fibre exit was obtained by applying the L'Hospital's rule. The present study uses explicit linear algebraic equations, and the bulk permeate concentration profile was evaluated with a differential equation. The numerical technique of Chowdhury et al. (2005) was a combination of modified Powell hybrid algorithm, the Gear's BDF method, the L'Hospital's rule and secant method. With the present technique, the equations have been simplified such that the Gear's BDF method alone is adequate for solving the equations.

3.4 Validation of the model and solution technique

In order to validate the mathematical models and the solution technique, the model predictions have been applied to simulate and compare the experimental data of air separation using cellulose acetate-based asymmetric hollow fiber membranes (Feng et al., 1999). Figure 3.2 represents the experimental and calculated oxygen and nitrogen

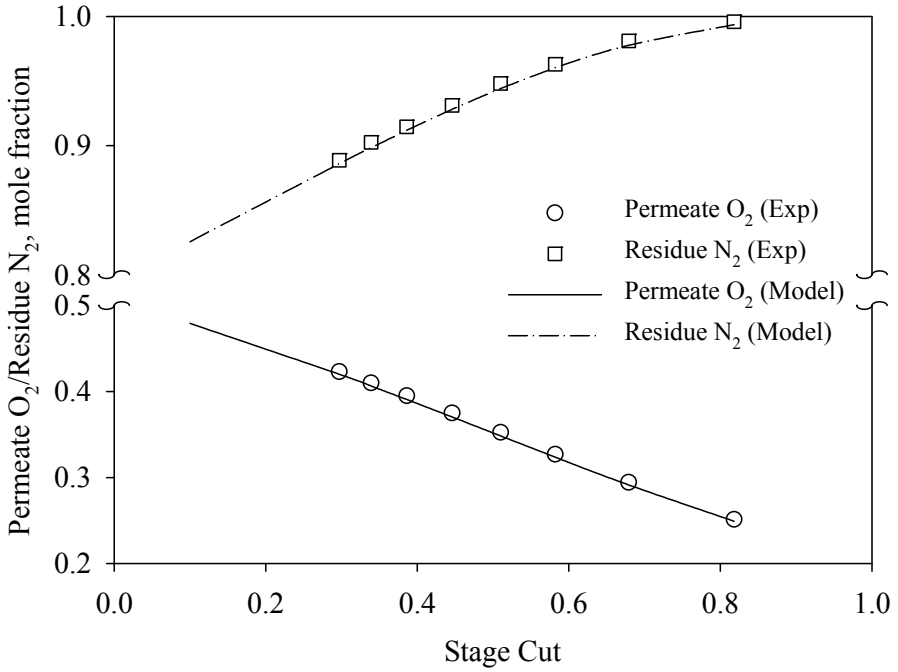

Fig. 3.2: Comparison of model predictions with experimental data (Feng et al., 1999) for air separation with shell-side feed/countercurrent flow.

concentrations in permeate and residue stream, respectively, as a function of stage cut (θ) for shell-side feed countercurrent flow conditions. The agreement between the experimental data and the calculated predictions is good over a wide range of stage cuts. Figures 3.3a and b represent the calculated local permeate (y') and bulk permeate (y) concentrations for air separation (Feng et al., 1999) with an active fiber length of 1.25 m, and H_2/N_2 separation (Zakaria, 2006), respectively, along the fiber length for different stage cut operations. The pores in the substrate of the asymmetric hollow fiber membrane allows the gas permeated through the membrane skin layer to reach the bulk of the permeate stream, but the gas composition leaving the membrane skin is not affected by the one in the permeate side (y) because there is little radial mixing along gas flow in the pores. This is especially the case for membranes with high fluxes, as shown in Figure 3.3 where the difference between y' and y for H_2/N_2 separation is shown to be greater than that for O_2/N_2 separation. Thus, the concentration of the reference component in the void volume is always higher than that in the permeate side. For a given feed concentration, the local

driving force for permeation (i.e., partial pressure differential across the membrane) is directly affected by y'. However, in case of homogeneous symmetric model, the bulk permeate concentration, y, is assumed to be the same as y' due to radial mixing of local permeate. The fiber length is usually around 1-1.5 m for industrial applications, and considerable pressure build-up in the lumen can occur, resulting in reduced driving force

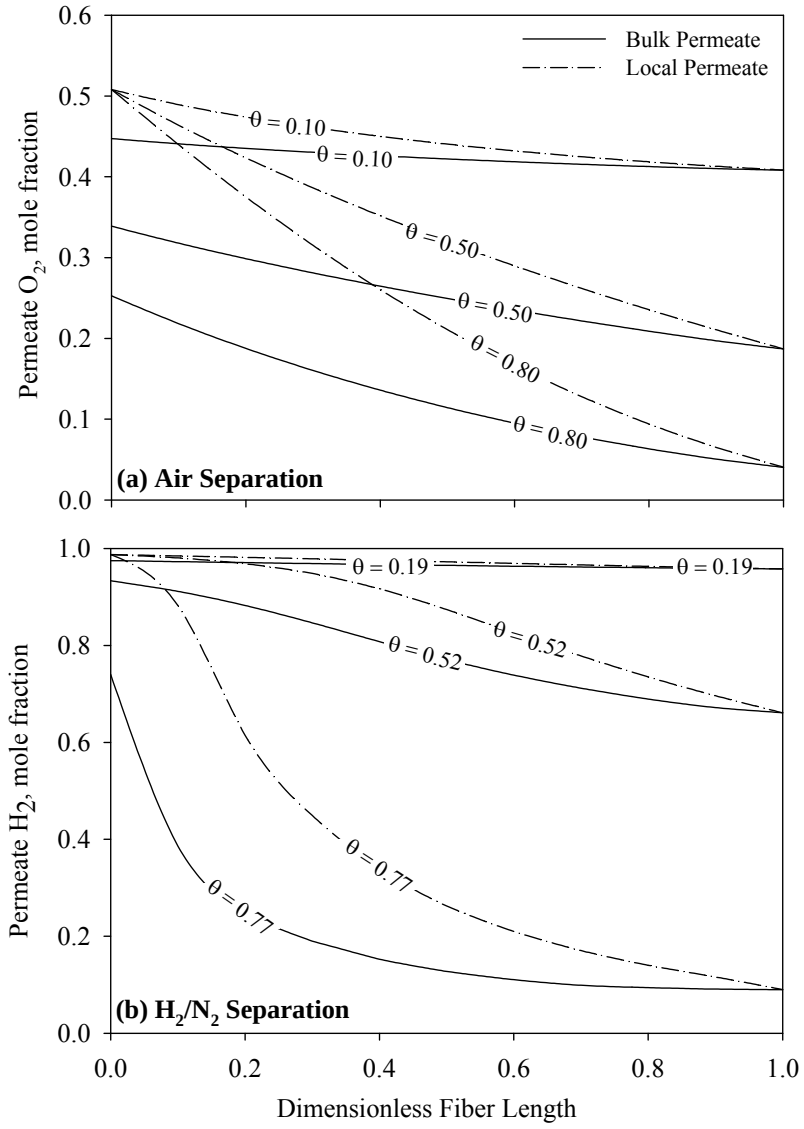

Fig. 3.3: Variations of bulk permeate (y) and local permeate (y') mole fraction along fibre length at different stage cuts (θ) under shell-side feed/countercurrent flow conditions for (a) air separation (Feng et al., 1999) with an active fibre length of 1.25 m, and (b) H_2 separation (Zakaria, 2006).

and thus a discrepancy in the predicted membrane performance if this effect is neglected. Figure 3.4a shows the productivity versus purity of oxygen in the permeate stream with and without considering permeate pressure build-up in the fiber lumen for a permeator length of 1.25 m. The effect of permeate pressure build-up is more significant for oxygen

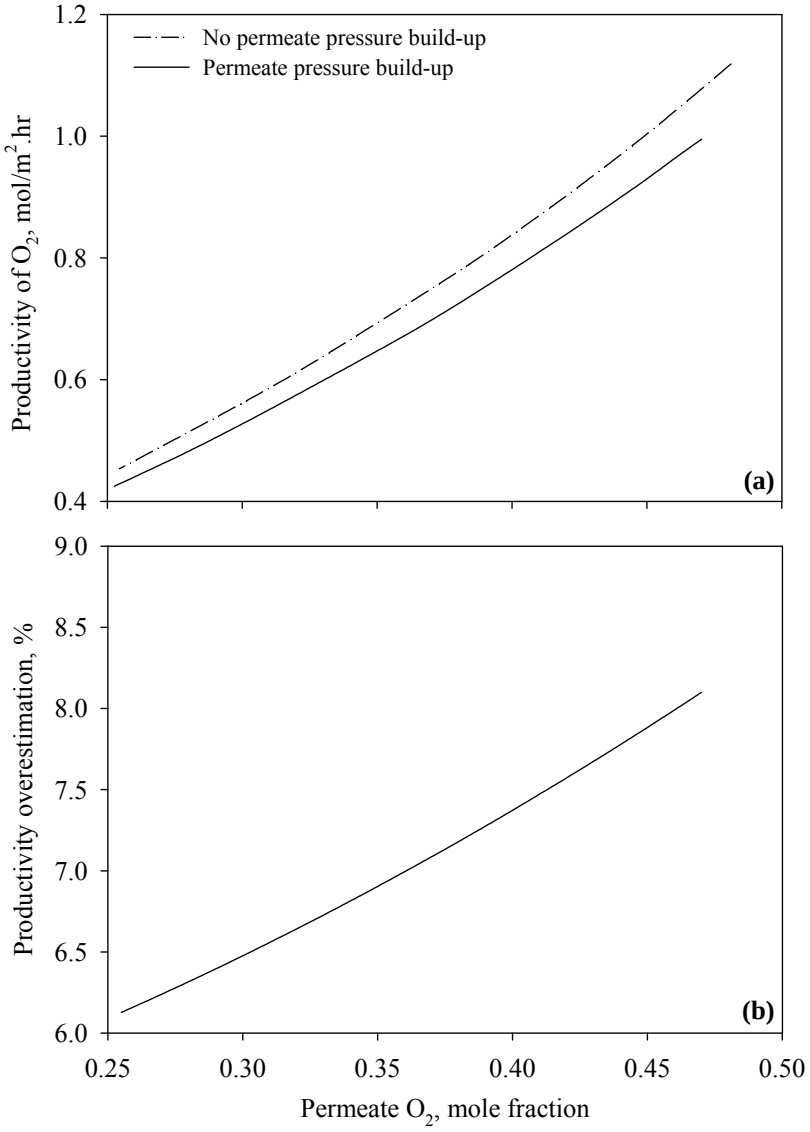

Fig. 3.4: (a) Oxygen productivity versus oxygen purity in permeate for air separation with shell-side feed/countercurrent flow configuration with/without considering permeate pressure build-up. The membrane performance is overestimated if the permeate pressure build up is not considered. (b) Percentage of productivity overestimation with oxygen purity in permeate while pressure build-up was neglected.

permeation since oxygen is more permeable than nitrogen. Obviously, should the permeate pressure build-up not been taken into account, the model predictions will overestimate the permeate purity and productivity. Figure 3.4b shows the percentage of productivity overestimation. The effects of the pressure build-up will be more significant for smaller fiber diameters, longer fiber lengths and higher permeances.

The validity of the model was further tested by comparing the model predictions with experimental data of hydrogen separation from a mixture of gases (i.e., mixtures of hydrogen and nitrogen) using cellulose acetate-based asymmetric hollow fiber membranes (Zakaria, 2006). As shown in Figure 3.5, the model prediction was quite satisfactory under

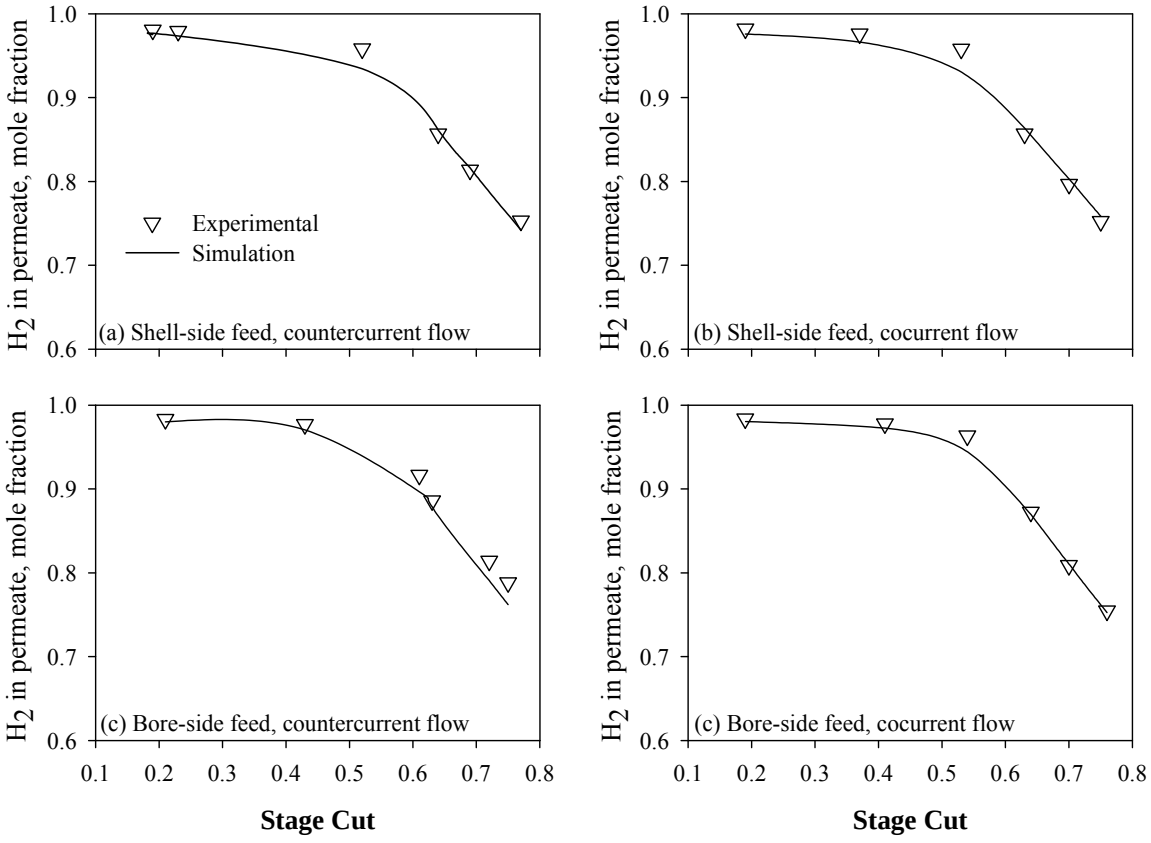

Fig. 3.5: Comparison of model predictions with experimental data (Zakaria, 2006) for hydrogen recovery to illustrate the validity of the model for various configurations: (a) shell-side feed/countercurrent flow, (b) shell-side feed/cocurrent flow, (c) bore-side feed/countercurrent flow and (d) bore-side feed/cocurrent flow.

different operating conditions and module configurations, which supports its robustness and reliability. For the binary system, the asymmetric model predicted the membrane performance well for all flow configurations studied here (Figure 3.5). Particularly for the cocurrent flow, the asymmetric model appeared to work better than countercurrent flow configuration. Furthermore, as shown in Figure 3.5, the flow configuration, whether cocurrent or countercurrent, does not seem to influence the separation performance significantly although the bore-side feed does give a slightly better result than the shell-side feed arrangement. This supports the hypothesis made earlier that the flux through the membrane porous substrates was not radially mixed with the bulk permeate stream,

Table 3.1: Module design and operating conditions of membrane systems used for model validation.

	Membrane Module	
	(Zakaria, 2006)	(Feng et al., 1999)
Membrane material and type	asymmetric cellulose acetate hollow fiber	asymmetric cellulose acetate hollow fiber
Flow configuration	cocurrent and countercurrent, shell-side and bore-side feed	cocurrent and countercurrent, shell-side and bore-side feed
No. of fibers	9	368
Inner diameter (μm)	80	80
Outer diameter (μm)	200	160
Active length (cm)	87	25
Feed composition	57.39 % H_2 42.61 % N_2	20.5 % O_2 79.5 % N_2
Temperature (K)	298.15	296.15
Feed pressure (kPag)	600.0	690.0
Permeate Pressure (kPa)	101.3	101.3
Permeance (10^{-10} mol/s m^2 Pa)	H_2 : 201 N_2 : 2.453	O_2 : 30.78 N_2: 5.7

resulting in a crossflow type of permeation behaviour. The module design and operating parameters studied for the validation and comparison of the membrane systems are summarized in Table 3.1.

3.5 Membranes air separation: Case studies

Table 3.2 lists the permeabilities and selectivities of some membrane materials as well as the permeance of representative membranes used for air separation. High oxygen/nitrogen selectivity is required for an economical nitrogen production process. The effect of improved membrane selectivities on the efficiency of nitrogen production from air has been assessed (Baker, 2004), and it was shown that even membranes with an oxygen/nitrogen selectivity as low as 2 can still produce better than 99% nitrogen though at very low recoveries. Currently, membrane nitrogen production is competitive with alternative technologies, but it is much more difficult to produce high purity oxygen. Even at the extremes of zero stage-cut and infinite pressure ratio, the best available membrane (with an oxygen/nitrogen selectivity of 8) can only produce 68% oxygen. These constraints limit membrane systems to the production of oxygen-enriched air in the 30 -50% oxygen range.

As a case study, four representative hollow fiber membranes i.e., polydimethylsiloxane (PDMS, silicone rubber), cellulose acetate, polysulfone and poly(ether block amide) (PEBA) were investigated here. The membranes were assumed to have an asymmetric structure with an outer dense skin layer supported on a porous substrate. The active fiber length for all types of membranes is 25 cm. The effective membrane area for permeation is 1300 cm^2 based on a nominal outside diameter of 450 μm for all the membranes except cellulose acetate, which has membrane area of 462 cm^2 based on a 160 μm nominal outside diameter. Air is considered to contain 20.5 mol% O_2 (balance nitrogen). Other trace components (e.g., argon, neon, helium) in air were ignored for simplification. The separation performance was investigated for three different feed pressures: 345, 690 and 1035 kPa. Unless specified otherwise, the permeate stream exited

Table 3.2: Permeabilities and selectivities of polymers of interest in air separation.

Polymer	N_2 Permeability or Permeance		α (O_2/N_2)	References
	Barrer	GPU		
Poly (1-trimethylsilyl-1-propyne) (PTMSP)	5400	-	1.4	(Baker, 2004)
Teflon AF2400	760	-	1.7	(Baker, 2004)
Poly(dimethyl siloxane) (PDMS)	-	0.61	2.2	(Baker, 2004)
Ethyl Cellulose	3.3	-	3.4	(Baker, 2004)
Poly (4-methyl-1-pentene) (TPX)	7.1	-	4.2	(Baker, 2004)
Poly (Phenylene oxide) (PPO)	3.8	-	4.4	(Baker, 2004)
Poly(ether block amide)	-	1.5	5.0	(Liu et al., 2005)
Cellulose acetate	-	1.7	5.4	(Feng et al., 1999)
6FDA-DAF (polyimide)	1.3	-	6.2	(Baker, 2004)
Polysulfone	-	2.0	6.75	(Feng et al., 2002)
Polyaramide	0.46	-	6.8	(Baker, 2004)
Tetrabromo *bis* polycarbonate	0.18	-	7.6	(Baker, 2004)

the membrane at atmospheric pressure. Most of the simulations were carried out assuming isothermal conditions at the ambient temperature (23^{o}C). The study is limited to single-stage and two-stage processes, as shown in Figure 3.6.

The feed gas was compressed before feeding to the membrane to provide the driving force for separation. For this simulation study, the compressor was assumed to be polytropic with inter-stage cooling. The polytropic index of air ranges between 1.25 and 1.35 (Helmut, 2005). Assuming a polytropic efficiency of 85% for the compressor, the energy required for compression was calculated to be 0.25–0.30 MJ/kg at the feed pressures considered here. Though the simulation study is performed for small scale operation, it provides a platform to compare power requirement with different configurations/modules since the membrane process can be scaled up linearly.

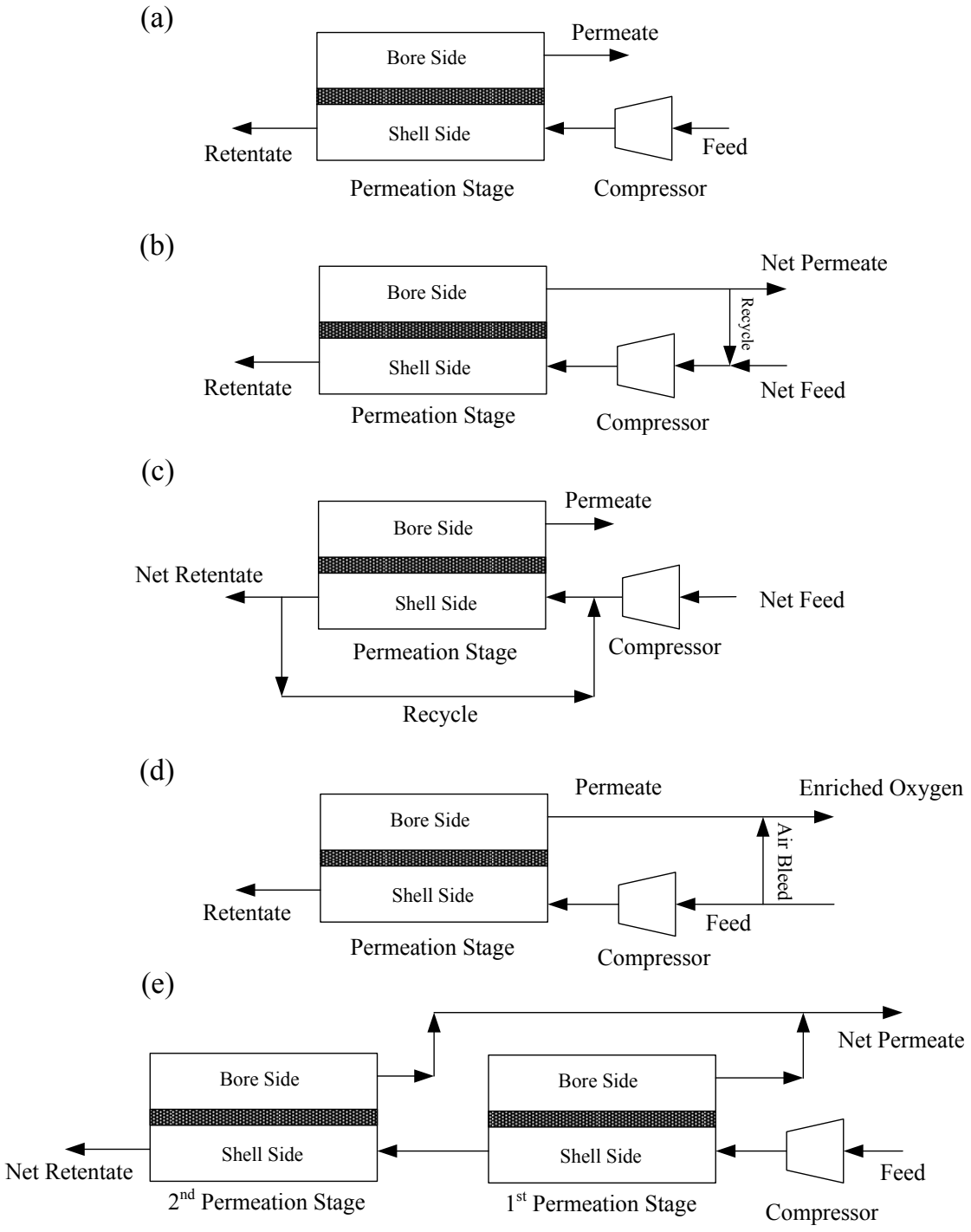

Fig. 3.6: Different configurations analysed in this study: (a) single-stage, (b) single-stage with permeate recycle, (c) single-stage with retentate recycle, (d) single-stage permeate blending with air bleed, (e) two stages in series.

3.5.1 Performance in single-stage without recycle

The pressure range used in the simulation study is 345-1035 kPa. Feng et al. (1999) showed that the permeability of pure nitrogen remains constant over a pressure range of 100-1,000 kPa irrespective of shell-side feed or bore-side feed, while the oxygen permeability in the bore-side feed mode has been found only slightly higher (< 3%) than in the shell-side feed. Hence, the pure gas permeability and the permeability of the gas component in a mixture are assumed to be the same.

In assessing the performance of a permeator, three issues are particularly important: product purity, recovery and productivity. Here the product recovery is defined as the fraction of nitrogen or oxygen in air recovered as product, and the productivity is defined as the quantity of product in terms of equivalent pure nitrogen or oxygen generated per unit membrane area per unit time. Figures 3.7a, b and c represent oxygen concentration in the permeate stream as a function of stage cut for different feed pressures. Figures 3.7d, e and f represent nitrogen concentration in the residue stream as a function of stage cut for different feed pressures. Among the four membranes studied here, silicone rubber has the least and polysulfone has the most oxygen to nitrogen selectivity. It is possible to produce a permeate stream containing 50.2% oxygen at a stage cut of 0.2 from polysulfone permeator at a feed pressure of 1035 kPa. Also, at the same stage cut, it is possible to produce a permeate containing 47.5% oxygen at 690 kPa. An increase in feed pressure increases the driving force for permeation and causes passage of a larger amount of gas through the membrane. For a fixed feed pressure, a higher feed flow rate results in a reduction in stage cut. It is apparent that the silicone rubber membrane shows the least improvement in oxygen purity when the pressure is increased. At a stage cut of 0.2, increasing the feed pressure from 690 to 1035 kPa will increase the oxygen concentration in the permeate from 31.2% to 32.1%. This is because silicone rubber has a considerably higher permeability than others but is less selective. At higher stage cuts, a larger amount of gas is removed as permeate, with a major portion being O_2. As a result, the reject becomes highly enriched in N_2. In spite of this favourable behaviour for N_2 enrichment, the N_2 recovery in the reject stream is generally low. At high stage cuts, it is possible to produce better than 99%

nitrogen at considerably low feed pressures using cellulose acetate, polysulfone and poly (ether block amide) membranes. At a stage cut of 0.9, the polysulfone membrane can produce 99.2% and 99.9% nitrogen at 345 kPa and 690 kPa feed pressure, respectively,

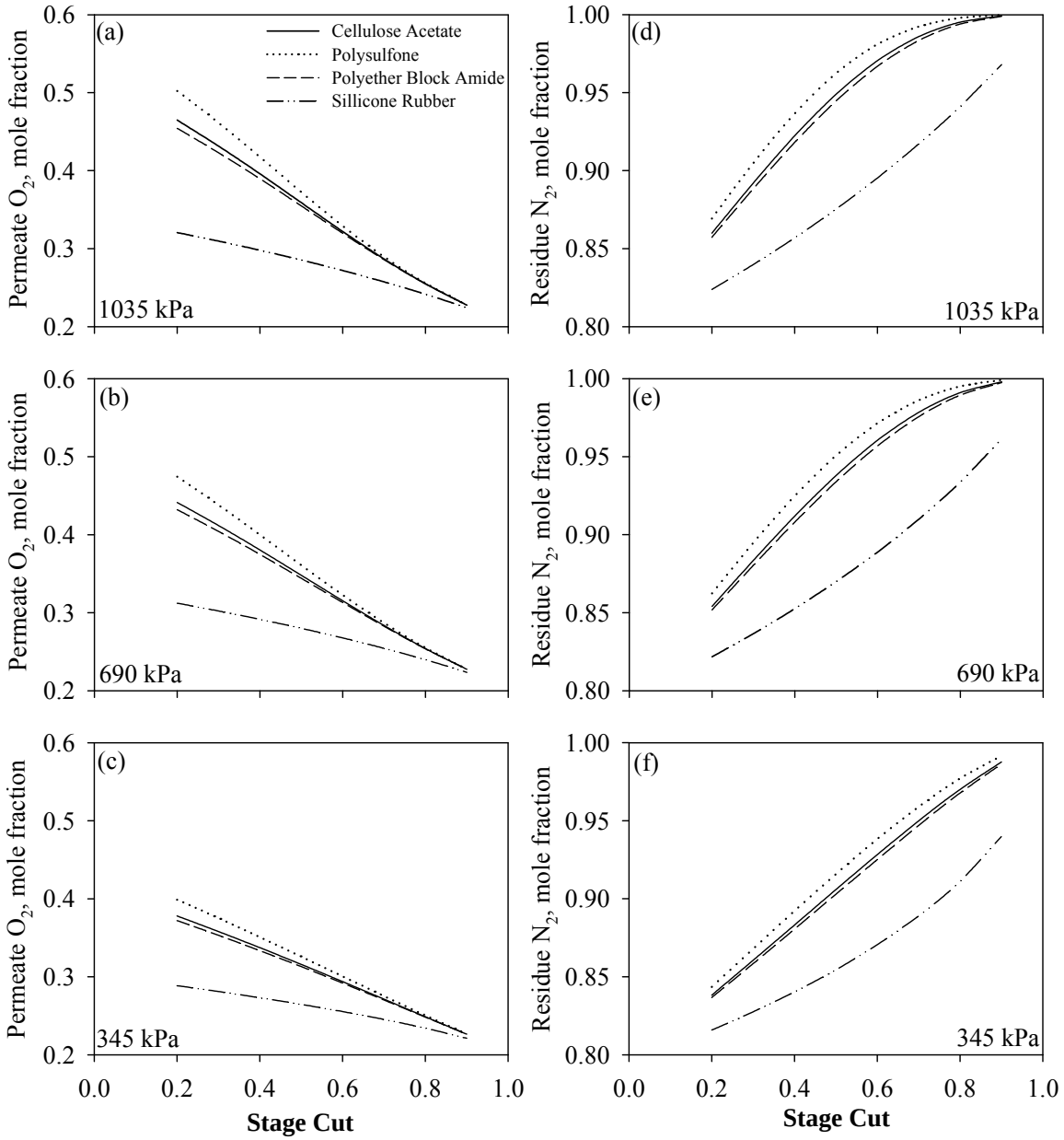

Fig 3.7: Concentrations of oxygen (a–c) and nitrogen (d–f) in permeate and residue, respectively, as a function of stage cut at different feed pressures (single-stage). Membrane configuration: shell side feed and counter-current flow.

but, the rate of recovery for nitrogen is fairly low in these cases. At a moderately high pressure, it is possible to produce 99.9% nitrogen with reasonably good recoveries (i.e., at moderate stage cut), but the enhanced purity comes with additional cost for compression.

The trade-off relationship between recovery and concentration for oxygen enrichment of air at different feed pressures is illustrated in Figures 3.8a, b and c. Similar results are shown in Figures 3.8d, e and f for the trade-off relationship for nitrogen production. For both oxygen enrichment and nitrogen production, increasing the product purity always reduces the product recovery, and the reduction in the recovery becomes more profound at higher product purities. Figure 3.9 represents the productivity of oxygen in permeate and the productivity of nitrogen in residue, respectively, as a function of the product concentration. It is obvious that while the productivity of nitrogen decreases with an increase in its purity, the opposite appears to be true for oxygen enrichment, which asserts again the trade-off relationship between product recovery and purity. A high recovery or a high purity can be obtained in the membrane processes, but not at the same time. For a required purity, a higher recovery rate accounts for lower specific energy consumption, which is often the major operating cost. Therefore, it is essential to optimize the operating conditions of a given membrane system in order for the separation potential of the membrane to be maximized. It is apparent from Figures 3.8 and 3.9 that for a given product purity, increasing the feed pressure increases the product recovery and productivity.

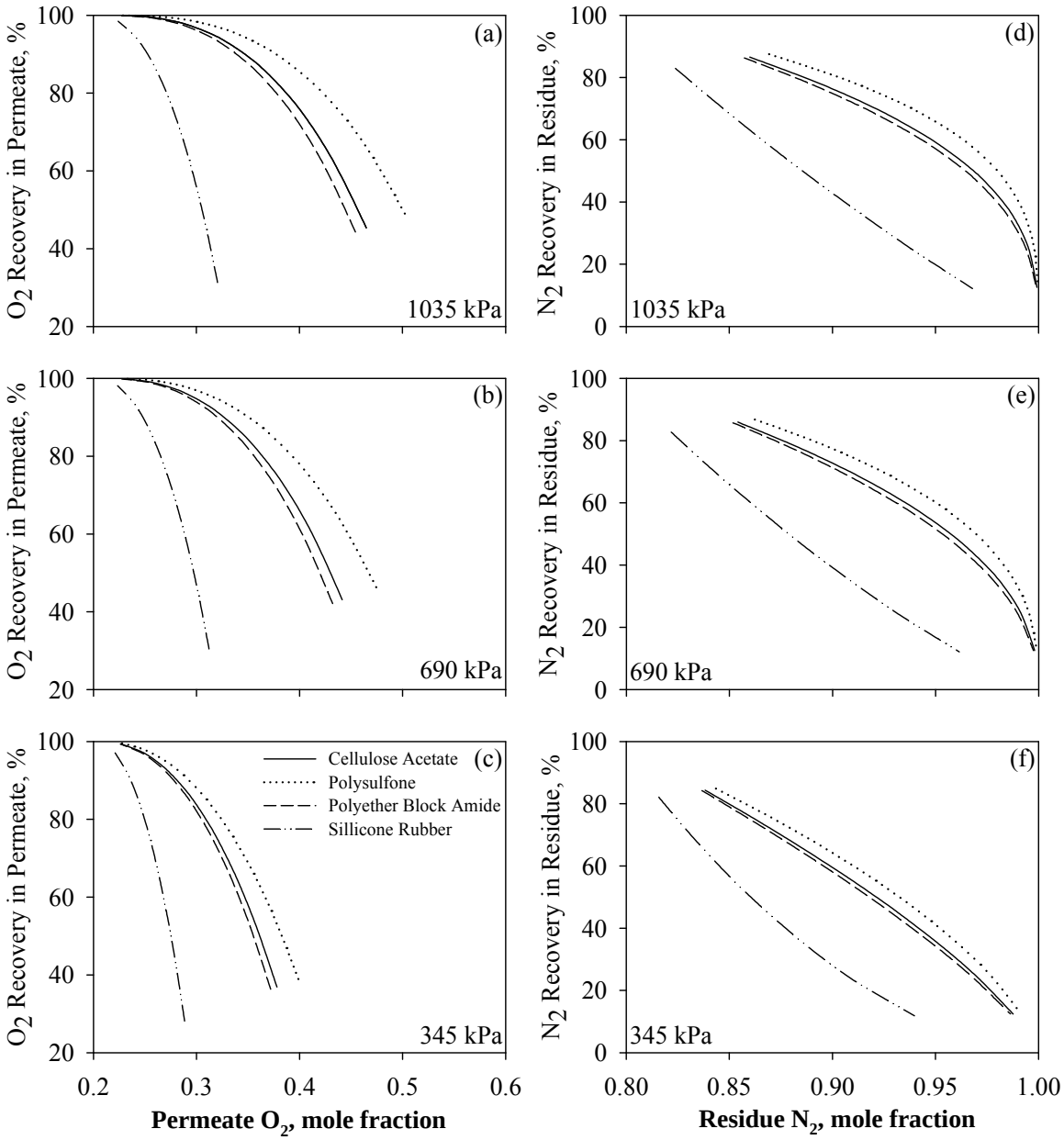

Fig. 3.8: The trade-off relationship between recovery and concentration for air separation at different feed pressures (single-stage) to produce oxygen-enriched air (a–c) and nitrogen-enriched air (d–f). Membrane configuration: shell side feed and counter-current flow.

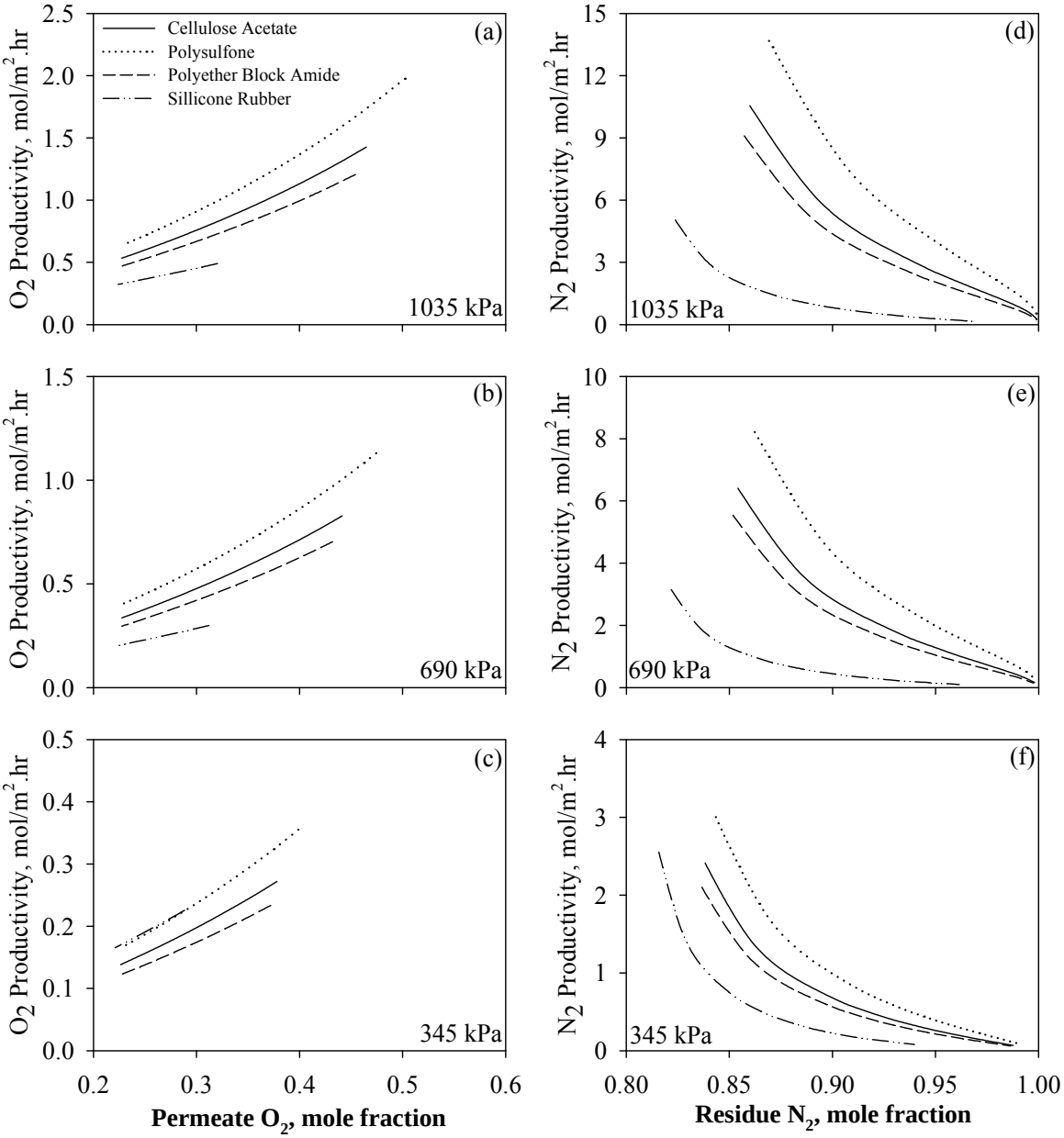

Fig. 3.9: Productivity versus product concentration for air separation (single-stage) to produce oxygen-enriched air (a–c) and nitrogen-enriched air (d–f). Membrane configuration: shell side feed and counter-current flow.

3.5.2 Single-stage with permeate recycle to feed stream

Membrane processes are currently considered to be economical and convenient

when the target oxygen concentration is in the range 25-50%. It is understandable that membranes are not currently capable of producing high purity oxygen and cannot compete with other conventional technologies that produce high purity oxygen. One way to improve the product purity in membrane air separation is to recycle a portion of the permeate stream to the feed stream (Figure 3.6b). The permeate stream is at atmospheric pressure and the portion of the stream to be recycled needs recompression before mixing with the fresh feed. In this way, the product purity (oxygen) can be greatly enhanced. This, however, is at the expenses of reduced recovery of product oxygen and the added recompression of the recycle stream. Similarly, the productivity also suffers as a part of the permeate stream is recycled. It should be assessed based on economic consideration if the reduced recovery and productivity can be paid off by the enhanced product purity. It looks this process would be particularly useful for specific applications where a higher purity product is desired. Figures 3.10a and b represent the dependencies of product purity with product recovery for permeate recycle operation using polysulfone membranes at different feed pressures. Figures 3.10c and d represent the relation of productivity of oxygen with product recovery at different pressures. It was found that at a feed pressure of 1035 kPa, when 70% of the permeate was recycled to feed stream, oxygen concentration could reach 59.3% in the enriched air stream. Since air is the feed, which is abundant in nature, the rate of recovery is considered less important here. As expected, an increase in the recycle ratio increases the concentration of the permeate stream. The increase in oxygen concentration and the power enriched air stream. Since air is the feed, which is abundant in nature, the rate of recovery requirements with increasing recycle fraction are greater at lower stage cuts, which correspond to a higher N_2 recovery (or lower O_2 recovery). It is calculated that total power requirement for gas compression in recycle operation is 8-25% more than the power requirement for single-stage operation without permeate recycle. The power consumption decreases with an increase in the stage cut and increases with a reduction in the recycle fraction.

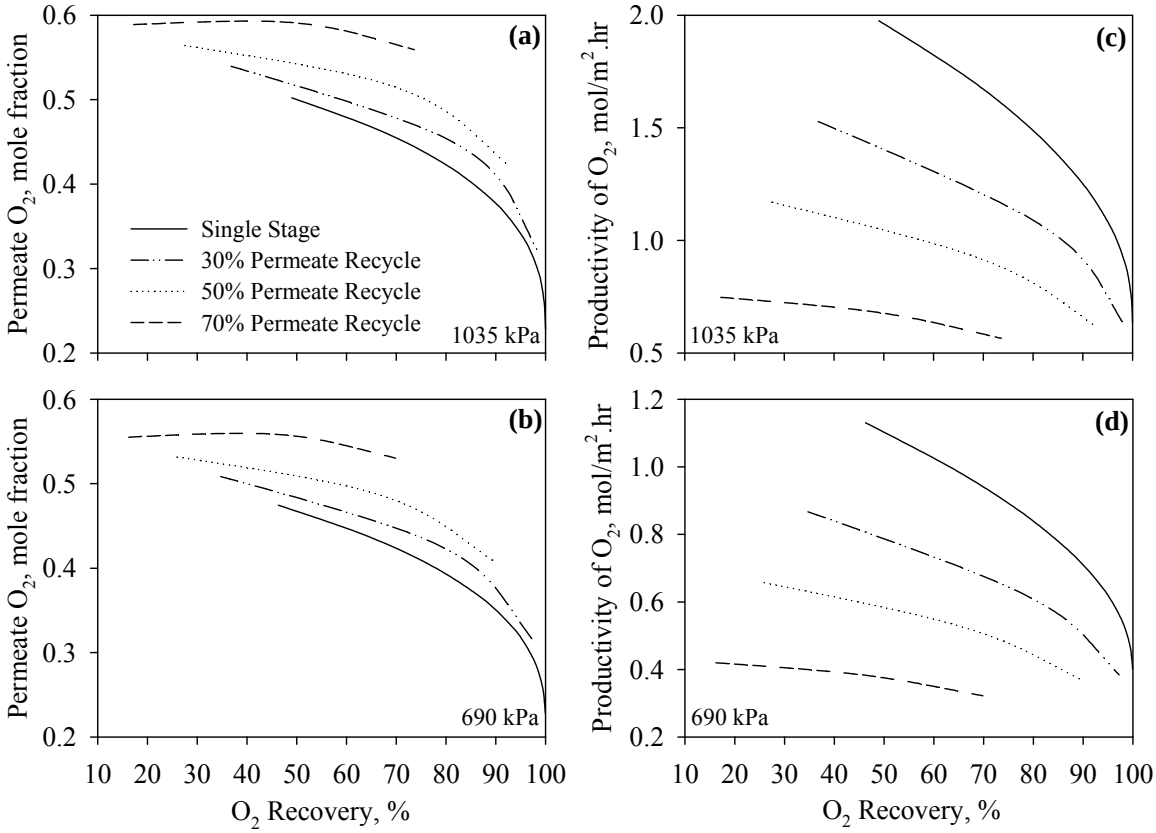

Fig. 3.10: Oxygen concentration (a and b) and productivity (c and d) versus recovery for single-stage operation with permeate recycle using polysulfone membrane at different pressures (690 and 1035 kPa). For comparison, single stage without permeate recycle is also shown (solid line). Membrane configuration: shell side feed and counter-current flow.

3.5.3 Single-stage with retentate recycle to feed stream

Retentate recycle (Figure 3.6c) is sometimes useful if the residue stream is the desired product. The retentate recycle will be especially effective for the system in which the feed gas is relatively cheap and the product (the retentate) is relatively valuable. It should be noted that the retentate recycle stream does not require significant recompression as the retentate pressure is essentially the same as feed pressure, which is advantageous over the aforementioned permeate recycle that involves additional capital and energy costs due to recompression. It may be conceived that when the feed is blended with a portion of the retentate stream which is enriched with the low permeable component, both the purity

and recovery of the low permeable component in the retentate stream will be enhanced. As in the case of He/N_2 or H_2/N_2 separation systems where the membrane selectivity is relatively large, the retentate recycle may be effective for enrichment of the less permeable component in the retentate stream. However, in case of air separation where the membrane selectivity is rather low, the retentate recycle does not lead to a considerable improvement in the separation performance, as shown in Figure 3.11. It is apparent from Figure 3.11a and b that only a slight improvement in the recovery is obtained at a low stage cut with a low fraction of retentate recycle. At a feed pressure of 1035 kPa, the recovery of N_2 increases from 87.4% to 88.4% when 2% of the retentate stream is recycled to the feed stream, but there is little improvement in the nitrogen purity in the retentate. A marginal

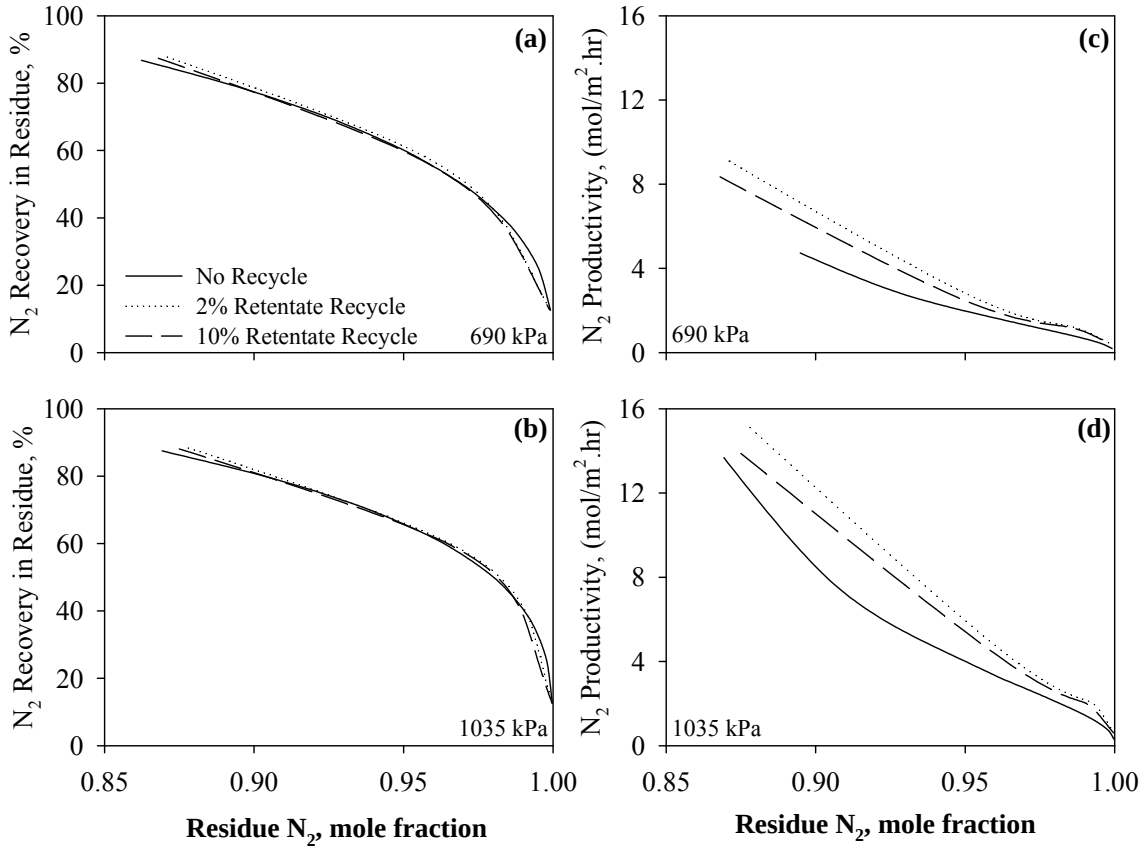

Fig. 3.11: Nitrogen recovery and productivity versus purity for single-stage operation with retentate recycle using polysulfone membrane at different pressures (a and c) 690 kPa (b and d) 1035 kPa. Membrane configuration: shell side feed and counter-current flow.

improvement in nitrogen recovery can be obtained by recycling 10% of the retentate to the feed, but no improvement is noticeable above 10% of the retentate recycling. This is due to the fact that a higher recycle ratio will eventually lower the concentration of the more permeable component on the feed side of the membrane, making it slower to permeate through the membrane. The concentration of nitrogen in the retentate decreases with the retentate recycle because the processing capacity of the module is increased. As a result, the separation does not improve especially when a high purity retentate is the target product. It was also observed that the retentate recycle requires a higher feed flow rate than the feed flow rate without recycle in order to produce the same amount of product, which eventually increases the total compressor load. As shown in Figure 3.11c and d, the turn results in low stage cuts. The productivity of N_2 decreases as the recycle ratio increases. Hence, there is in principle an optimum recycle ratio with respect to the productivity of N_2 increases at low recycle ratios due to higher feed flow rates which in turn results in low stage cuts. The productivity of N_2 decreases as the recycle ratio increases. Hence, there is in principle an optimum recycle ratio with respect to the concentration of nitrogen in the retentate, but since this configuration offers no significant practical benefits for air separation to produce nitrogen, the retentate recycle to feed stream has rarely been discussed in the literature.

3.5.4 Single-stage with permeate blending with a portion of feed

In some applications where the permeate stream is the desired product and a moderate product purity is required, the membrane area requirement may be reduced through the use of feed gas bypass (Kimura and Browall, 1986). It is equivalent to mixing a portion of the feed with the permeate whose concentration is higher than the target product concentration. Figure 3.6d illustrates such a design. Consider production of a 30% oxygen enriched air by mixing air with the permeate containing ~40% oxygen. Figure 3.12 represents the productivity of oxygen as a function of permeate oxygen concentration at different feed pressures using the polysulfone membrane with and without air bleed. It is clear that the productivity rises if a 40% oxygen permeate is blended with air (20.5%

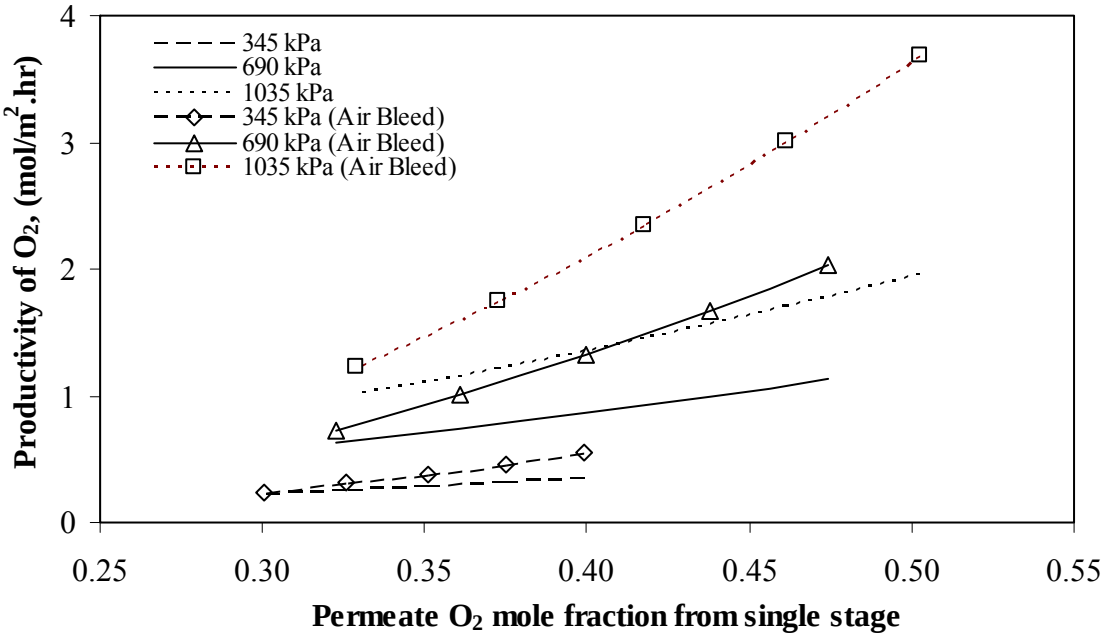

Fig. 3.12: Productivity of oxygen as a function of permeate oxygen concentration at different pressures using polysulfone membrane with and without air blending. Membrane configuration: shell side feed and counter-current flow.

oxygen) to get 30% oxygen enriched air. This means less membrane area is required for a target purity, which represents savings in the capital costs. Furthermore, the energy requirement is less since a portion of the final product comes directly from the feed air. It, however, should be mentioned that although permeate blending is simple in operation, but it may not be advantageous unless a considerably low purity of the product is required. Rice (2007) disclosed a similar process design based on blending the permeate with a portion of the feed to reduce membrane area requirement.

The use of membranes to produce moderate oxygen enriched air is a potential approach for industries using oxygen enriched air (e.g., combustion, personal oxygen generation bars). As the cost of fuel, particularly natural gas, increases, the use of oxygen-enriched air for combustion as a means of reducing fuel consumption in certain industrial combustion applications becomes increasingly attractive. It has been reported that the fuel consumption for furnaces can be reduced by 13% if oxygen enriched air containing 30%

oxygen is used (Kimura and Browall, 1986). The use of oxygen enriched air results in higher flame temperatures and reduces the volume of parasite nitrogen that will be heated with the latent heat being lost in the vent.

3.5.5 Two permeators in series

When a single-stage operation is unsatisfactory in terms of product purity or recovery, multistaging (as illustrated in Figure 3.6e) is an attractive approach. In fact, many industrial processes use multi-stage operations. Since the residue from the first stage is already at a high pressure, recompression of this stream prior to feeding to the second stage is not required. Moreover, splitting a long module into two stages can reduce the pressure build-up in the fibre bores as the permeate is removed from both stages. In the two modules-in series design, the stage cuts for both stages can be varied to obtain the intended purity of the product stream. Figure 3.13 illustrates the productivity and recovery of nitrogen from the two modules in series design as a function of product nitrogen concentration using a polysulfone membrane; for the purpose of comparison, the single stage performance with the same total membrane area is also presented in Figure 3.13. It is apparent from the data in Figure 3.13 that the overall performance of the two modules-in-series operation is much better than the single stage operation in terms of productivity and recovery of the nitrogen product at a given nitrogen purity. At a feed pressure of 1035 kPa, the productivity of the two modules-in-series operation is 18% more than the productivity of the single stage operation for the production of 95% nitrogen purity. The improvements in both the productivity and recovery become more significant when a higher purity of nitrogen in the residue stream is needed, as shown more clearly in Figure 3.14 which shows the percentage increases in productivity and recovery at a given nitrogen purity as compared to a single-stage operation. It becomes clear that the two modules-in-series operation is especially advantageous when a high purity of nitrogen is required. In addition, by using the two-stage operation, one may also take advantage of the differences in the permeate oxygen compositions coming from each stage because the permeate stream from the first stage will be more enriched in oxygen as compared to the oxygen concentration that would be produced in a single stage operation. A comparison of feed compression and

permeate vacuum operation has been provided in Appendix A for reference.

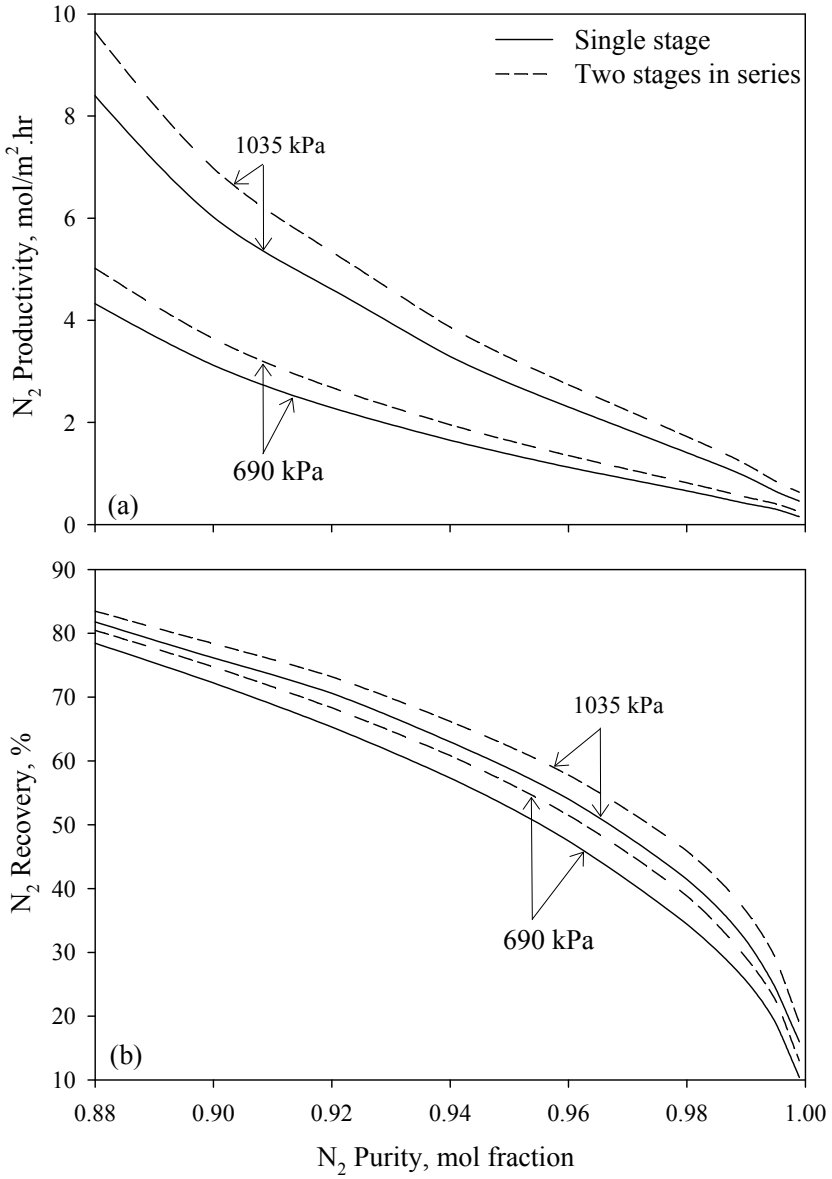

Fig. 3.13: A comparison of two modules in series with a single stage operation in terms of productivity (a) and recovery (b) for nitrogen production as a function of nitrogen purity. Membrane configuration: shell side feed and counter-current flow.

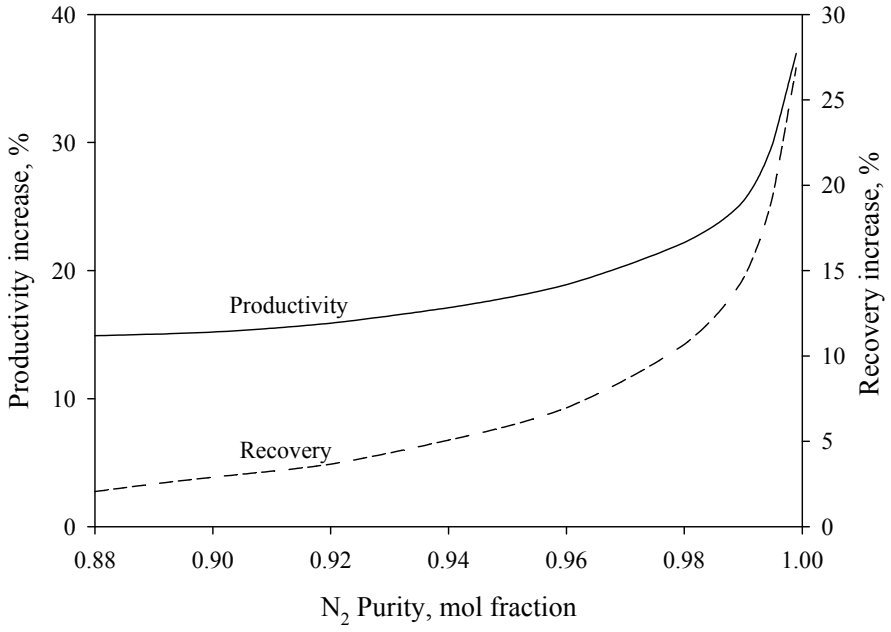

Fig. 3.14: Percentage increases in productivity and recovery for nitrogen production using the two modules in series operation as compared to the single stage operation. Feed pressure 1035 kPa.

3.6 Conclusions

The developed mathematical model can generate profiles for the residue and permeate flow rates, the residue and permeate compositions, and the pressure build up in the fibre bore along the fibre length. The solution technique has merits over other techniques commonly used since it offers minimum computational time and effort with improved solution stability. Moreover, the computational complexity does not multiply as the number of components increases. The model predicted the binary gas separation behaviour with different flow and module configurations quite satisfactorily. In a comparison of the four representative membranes for air separation, it was found that all the membranes (except silicone rubber) can produce 99.9% nitrogen in the residue stream. It was also shown that these membranes can be used to produce up to 50% oxygen-enriched air as a permeate stream from the single-stage operation. Further enrichment in oxygen up to 60% was possible with permeate recycle, but the retentate recycle did not considerably improve the productivity and recovery of nitrogen. Single-stage operation

with permeate blending with air can be used to increase productivity of oxygen-enriched air for applications requiring only moderate enrichment (e.g. 30% concentration). Two modules in series can be used to enhance the overall performance for nitrogen production, especially when a high concentration of the nitrogen is needed.

Chapter 4

Modeling of multicomponent gas separation with asymmetric hollow fiber membranes - methane enrichment from biogas[†]

4.1 Introduction

Membrane separation is favourable over other separation technologies due to its simplicity in operation, small size, ease in maintenance, energy efficiency, and reliable performance. These endearing characteristics make membrane technology very competent to penetrate a wide variety of applications. Although most membrane separation studies deal with binary gas mixtures, many applications of industrial importance involve multicomponent gas mixtures (i.e., recovery of helium from natural gas or deep sea diving gas, separation of H_2 from a reformed natural gas or other producer gases containing substantial amounts of CO_2 and N_2, recovery of H_2 from ammonia synthesis purge stream, and CO_2 removal from flue gas). Membranes are a key component in membrane gas separation; and the overall membrane module design and finding optimal operating conditions also play a significant role in successful application of the membrane processes. The prediction of the separation performance and the evaluation of the membrane processes are deemed important for new process designs and modification of existing designs.

Gas permeation model developed by Pan (1986) is the most practical representation of multicomponent gas separation in high-flux asymmetric hollow fiber membranes. Using the residue concentration as an independent variable, the permeate concentration, pressure and the fiber length required can be calculated. However, most commercial membrane modules have a pre-determined length of fibers, and in such cases the solution technique has considerable numerical difficulties since the fiber length is a computed variable. Moreover, the calculation procedure of iterative shooting method involves significant computational time and effort. To overcome mathematical complexities involved, different modifications and approaches of solving the model equations have been proposed (Coker et

[†] Part of Chapter 4 has been published in Can. J. Chem. Eng.; cited as Kundu et al. (2012b)

al., 1998; Jiang and Kumar, 2008; Kaldis et al., 2000; Kovvali et al., 1994; Makaruk and Harasek, 2009; Marriott et al., 2001; Marriott and Sørensen, 2003; Peer et al., 2008).

Kovvali et al. (1994) used a linear approximation to represent the feed and permeate compositions at certain intervals along the fiber length, and the solution accuracy thus entirely depends on the number of intervals along the fiber. Coker et al. (1998) proposed a stage-wise approach (100-1000 stages) to convert the differential equations to a set of coupled, non-linear ordinary differential equations. This method requires initial guess of the component flow rates on each stage, and the solution is approximated using the first order finite difference method with an iteration of derived tri-diagonal matrices. Sidhoum et al. (1988) developed a model where initial estimates of dependent variables were generated based on cocurrent or crossflow while neglecting pressure build up in the fiber bore. It turns out that the model fit symmetric membranes better than high-flux asymmetric membranes. Kaldis et al. (2000) developed a model based on Pan's (1986) original formulation. To minimize solution complexity, the concentration of the permeate leaving the membrane surface was assumed to be identical to that of the bulk permeate stream. Such a treatment does not appear to be suitable to high-flux asymmetric membranes where the microporous substrate prevents local permeate mixing. The model developed by Sengupta and Sirkar (1987) was limited to only three-component mixtures and its extension to a higher number of components would require considerable calculation effort and time. Marriott et al. (2001), and Marriott and Sørensen (2003) developed a mathematical model for multicomponent gas separation, which requires prior knowledge of diffusion and dispersion coefficients in the fluid phase, and mass transfer coefficient in the porous substrate. These parameters are unfortunately not readily available and the structure of asymmetric membranes can hardly be described accurately. Chowdhury et al. (2005) developed a mathematical model based on Pan's (1986) formulation and the numerical solution was formulated as an initial value problem. However, the overall material balance for cocurrent flow was used as an approximation for that of countercurrent flow for easy incorporation into AspenPlus. Cruz et al. (2005) developed a numerical algorithm for the solution of permeation problems using different discretization techniques, in the context of finite volume formulation. Makaruk and Harasek (2009) developed a model for

multicomponent permeation based on the finite difference Gauß-Seidel method, and the solution was stabilised by adapting a relaxation factor in case of difficulties with convergence. Katoh et al. (2011) utilized a tanks-in-series model to take into account non-ideal mixing flows, and applied relaxation method as a stable computational technique to solve the governing differential equations.

In this study, a mathematical model for high-flux, asymmetric hollow fiber membrane was developed, which is based on Pan's (1986) original formulation but the governing equations were simplified following the approach of Sengupta and Sirkar (1995). The model takes into account of "cross flow" of local permeate with respect to the membrane skin, irrespective of the flow direction of the bulk permeate stream outside the porous substrate. The permeate pressure build up inside the fiber bore was taken into account in the model as well. The solution technique was applied to different flow and module configurations (i.e., cocurrent and countercurrent, shell-side feed and bore-side feed), and found very efficient for the solution of multicomponent systems. The model predictions were validated with experimental results, and its robustness was demonstrated. The model and solution technique were applied to investigate dynamic performance of several membrane module configurations for methane recovery and enrichment from biogas, considering biogas as a mixture of CO_2, N_2 and CH_4. Several recycle operations including continuous membrane column and optimum recycle ratio vital for these operations were studied. Methane recovery from biogas represents not only an opportunity for greenhouse gas emission reduction; the methane recovered is also an energy source. Meanwhile, when methane is recovered, CO_2 is concentrated in the remaining gas stream, which also helps facilitate subsequent carbon capture for greenhouse gas reduction. A great deal of work can be found in open literature about methane separation from biogas using different technologies (Cavenati et al., 2005; Favre et al., 2009b; Knaebel and Reinhold, 2003; Rautenbach and Welsch, 1993; Tsuru and Hwang, 1994). Most of the studies considered biogas as a binary mixture of CO_2 and CH_4, which would appear to be an easy separation. However, the difficulties to separate methane from nitrogen by either membranes or pressure swing adsorption are an important technical issue for practical

applications. Therefore, the limitations that N_2 poses on the separation of CH_4 from biogas using membrane technology were also investigated in this study.

4.2 Mathematical modeling for simulation of asymmetric hollow fiber membranes

Consider the separation of multicomponent mixture containing n species using an asymmetric membrane, where mass balances for individual components have to be addressed. Unlike a binary system where a single selectivity term is needed (Kundu et al., 2012a), a reference component needs to be specified with respect to which the selectivities of the other components in the multicomponent system can be defined. The choice of the reference component depends on the system, and it may be the slowest permeating component in the mixture so that the selectivity values for other components will be greater than 1. For the mathematical formulation, the following main assumptions are made:

- The porous sub layer has negligible resistance to gas flow, and diffusion along the pore path is insignificant due to high permeation flux.
- There is no local mixing of permeate inside the porous sub layer of the membrane.
- The local concentration of the permeate leaving the membrane surface is determined by the relative permeation rates of the component at that point.
- The deformation of the hollow fiber under pressure is negligible.
- Permeance of each species is independent of gas pressure and concentration.
- Pressure drop on the shell-side of the module is negligible. Pressure drop inside the fiber lumen can be described by the Hagen-Poiseuille equation, i.e., the flow is laminar.

The simplification of the model equations for all the module configurations was made in a similar way, but only the shell-side feed countercurrent flow configuration (Figure 4.1a) is described here for brevity. The basis for the model is mass balance over a differential element of the hollow fiber length. For permeation of a mixture comprising n components (one of which is designated as the reference component), the material balance for the i^{th} component gives

$$-d\left[U^* x_i\right]/dz^* = K_1\alpha_i\left(x_i - \gamma y_i'\right) = -d\left[V^* y_i\right]/dz^* \quad \text{, for } i = 1, 2, 3, \ldots\ldots n \tag{4.1}$$

By adding all the equations for component balance (i = 1, 2, 3,…n), the total molar flow rate U^* and V^* can be deduced:

$$dU^*/dz^* = -K_1\left[\sum \alpha_i x_i - \gamma \sum \alpha_i y_i'\right] \tag{4.2}$$

$$dV^*/dz^* = dU^*/dz^* \tag{4.3}$$

The local permeate composition is determined by the relative permeation rates of the components at that point:

$$d[Ux_i]/dU = y_i' \tag{4.4}$$

With the help of Eqs. (4.1) and (4.2), Eq. (4.4) can be re-written as

$$y_i' = \alpha_i(x_i - \gamma y_i')/\left[\sum \alpha_i x_i - \gamma \sum \alpha_i y_i'\right] \quad \text{, for } i = 1, 2, ... n \tag{4.5}$$

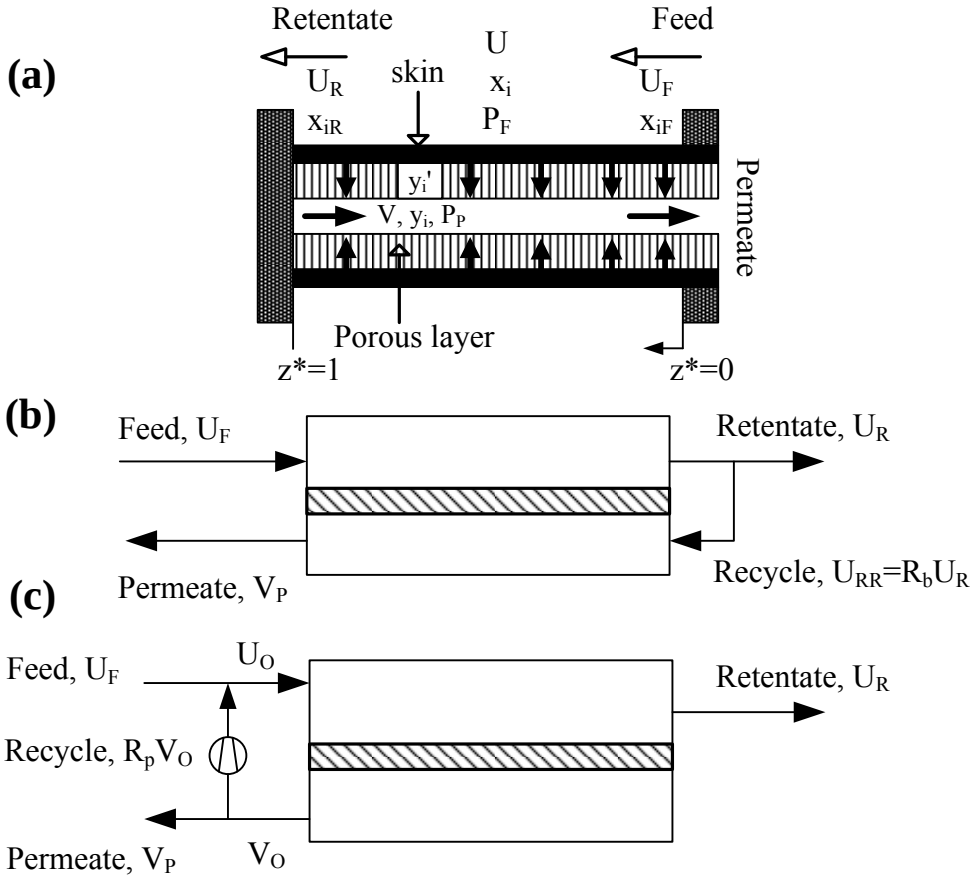

Fig. 4.1: Schematic of (a) single-stage shell-side feed permeator with countercurrent flow configuration, (b) single-stage membrane permeator with retentate recycle to permeate side, and (c) single-stage permeator with permeate recycle to the feed side.

Eq. (4.5) must satisfy the following condition

$$\sum_{i=1}^{n} y_i' = 1 \tag{4.6}$$

The differential equation for the variation of residue side composition along the hollow fiber length is obtained from Eqs. (4.1) and (4.2):

$$dx_i/dz^* = -K_1\left[\alpha_i\left(x_i - \gamma y_i'\right) - x_i\left\{\sum \alpha_i x_i - \gamma \sum \alpha_i y_i'\right\}\right]/U^* \quad \text{, for } i = 1, 2, ...n \tag{4.7}$$

The permeate side pressure build-up along the fiber lumen can be described by

$$d\gamma/dz^* = K_2 V^*/\gamma \tag{4.8}$$

The overall material balance and component balance give

$$U = U_R + V \tag{4.9}$$

$$Ux_i = U_R x_{iR} + Vy_i, \quad \text{for } i = 1, 2, 3, \ldots..n \tag{4.10}$$

Boundary conditions:

$$\text{At fiber exit } (z^* = 0): U^* = 1, \ \gamma = \gamma_o = P_{Po}/P_{Fi}, \text{ and } x = x_{iF} \text{ for } i = 1, 2.....n \tag{4.11a}$$

$$\text{At fiber closed end } (z^* = 1): \ V^* = 0 \tag{4.11b}$$

The differential Eqs. (4.2), (4.3), (4.7) and (4.8), together with Eqs. (4.5) and (4.6), describe the gas flow rates on the permeate and residue sides, gas composition on the residue side, permeate pressure build up in the fiber bore, and the local permeate mole fraction along the dimensionless length. The bulk permeate composition at the fiber exit can be evaluated using Eq. (4.10).

All the differential equations and non-linear implicit algebraic equations have been converted into dimensionless forms using following definitions:

$\alpha_i = J_i/J_{\text{Ref}}$, $\gamma = P_P/P_F$, $z^* = z/L$, $U^* = U/U_F$, $V^* = V/U_F$, $K_1 = \pi D_o LNJ_{\text{Ref}} P_F/U_F$, and $K_2 = -128\mu RTLU_F/\pi D_i^4 NP_F^2$

Note that equations for the reference component are actually not necessary in the computations since the sum of the mole fractions is always unity in both the feed and permeate streams.

4.3 Numerical technique of the proposed model

The numerical technique presented here does not require initial estimates of the pressure, flow or concentration profiles inside the hollow fiber as does in the original Pan's approach. The system of ODE (Eqs. 4.2, 4.3, 4.7-4.8) was solved using Gear's method (DIVPAG subroutine in the IMSL library). The set of non-linear algebraic equations (Eq. 4.5) was solved simultaneously until Eq. (4.6) is satisfied. The system of non-linear implicit algebraic equations for local permeate concentrations were solved using the modified Powell hybrid algorithm and a finite difference approximation of the jacobian (DNEQNF subroutine in the IMSL library), which is a variation of Newton's method. Newton's method is more sophisticated and elegant numerical techniques and can establish an inherently more stable solution methodology (Coker et al., 1999). Through this procedure, the computation was formulated as an IVP inspite of the boundary value nature of the problem. The system of ODE could also be solved by MATLAB *bvp4c* solver as a BVP, which was found to be especially effective for retentate recycle in continuous membrane columns. The advantage of the present technique is that *bvp4c* is not a shooting method, rather it is based on collocation technique. It is well known that a significant difficulty with the shooting method is that the solution of a BVP can be insensitive to changes in the boundary values, even for a perfectly nice BVP, while the solutions to IVPs of shooting are sensitive to changes in the initial values (Shampine et al., 2003). The numerical technique presented here permits easy evaluation of membrane performance with minimum computational time and effort.

4.4 Validation of the proposed model and simulation scheme

Experimental data reported in the literature was used to validate the model and solution technique. Sada et al. (1992) reported a multicomponent gas separation (separation of CO_2 from mixtures of CO_2, N_2 and O_2) by an asymmetric cellulose-triacetate based hollow fiber membrane. The experimental data was compared with the model calculations, and it was found that the model prediction is quite satisfactory, as shown in Figure 4.2. The calculated results for permeate composition as a function of stage cut agree well with the experimental data over a wide range of stage cuts and feed pressures. As mentioned earlier,

the model and solution technique developed is not limited to only ternary mixtures, and it can accommodate a larger number of components. Hence, the model was further validated with experimental data of hydrogen separation from refinery gases by polyimide hollow fiber membranes (Kaldis et al., 2000), where the feed gas consisting of H_2, CH_4, CO_2 and C_2H_6 was fed to the shell side of the membrane and the permeate was collected from the bore side in a countercurrent mode. Figure 4.3 shows a comparison between the experimental data and the model calculations performed here, and a good agreement between them was obtained. Moreover, the model was further validated with separation of gas mixture comprising of CH_4, CO_2 and O_2 by a polyimide hollow fiber permeator with bore-side feed countercurrent flow configuration (Makaruk and Harasek, 2009), where the membrane selectivities for CO_2/CH_4 and O_2/CH_4 were 37.2 and 8.6, respectively. A good agreement between the model calculations and the experimental results was found (not shown here for brevity). As the validity of the model and solution technique was

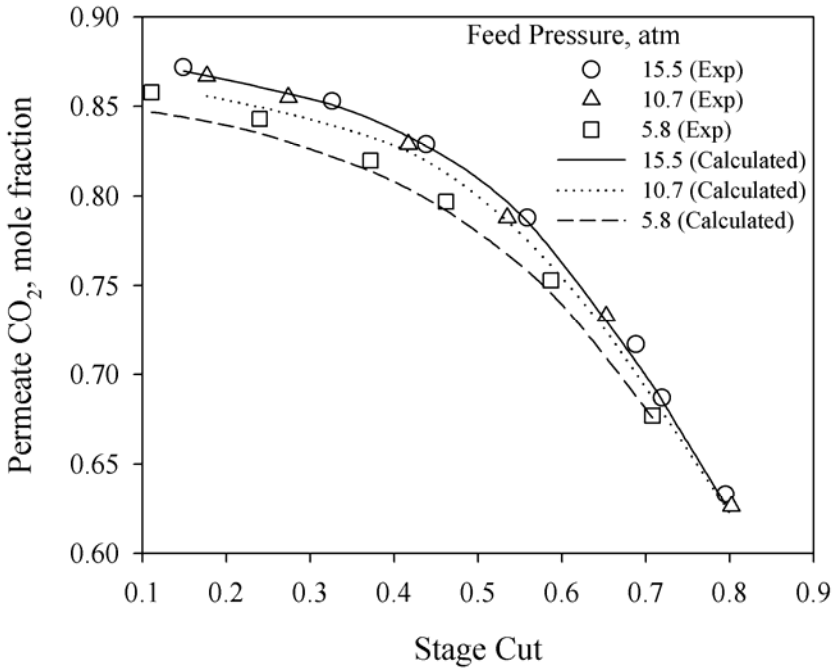

Fig. 4.2: Comparison of model calculations with experimental data (Sada et al., 1992) for CO_2 separation by asymmetric cellulose triacetate hollow fibers with shell-side feed countercurrent flow (feed composition: CO_2 50%, O_2 10.5%, and N_2 39.5%).

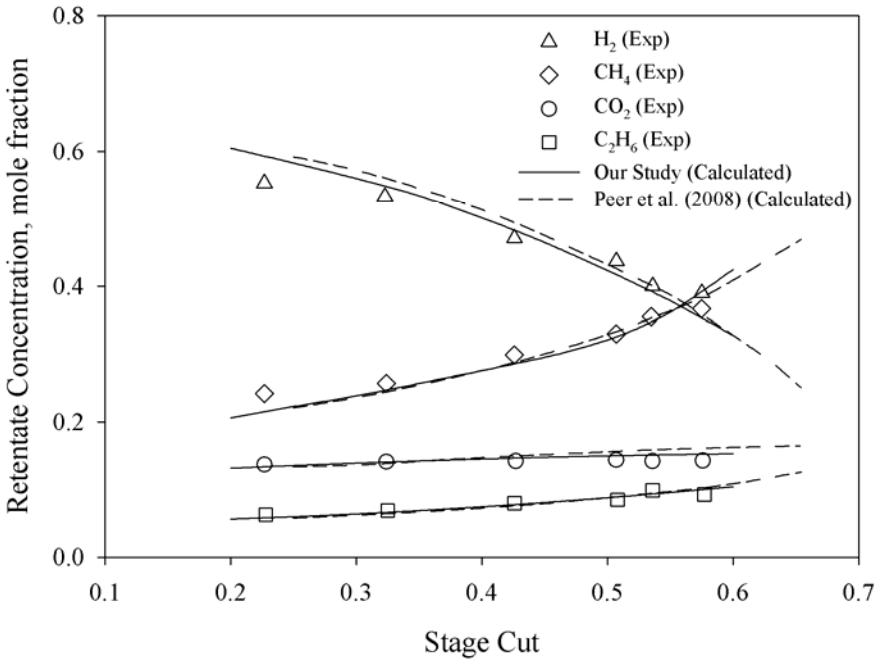

Fig. 4.3: Comparison of model calculation with experimental data (Kaldis et al., 2000) for hydrogen recovery from refinery gas by polyimide hollow fibers with shell-side feed countercurrent flow (feed composition: H_2 67.5%, CH_4 16.7%, CO_2 11.5%, and C_2H_6 4.3%).

confirmed, a case study of methane recovery from biogas by membranes was subsequently carried out to evaluate the membrane performance at different module configurations.

4.5 Characteristics of biogas and challenges in separation of methane from biogas

Biogas contains about 45~70 mol% methane. It is a potential source of energy but has not been well exploited. Despite the increasing importance of thermal and biological disposal techniques, more than 60% of the municipal waste is deposited on landfill dumps (Rautenbach and Welsch, 1993). Presently, only a few dump sites make good use of the biogas (e.g., to run generators or water heating plants) and most biogases are simply disposed of or flared. Among the dozens of components in biogases, methane is obviously the most valuable. On the other hand, methane is 21 times more potent than carbon dioxide in terms of its "greenhouse gas" effect (Knaebel and Reinhold, 2003). When completely

combusted, methane is converted to an equal stoichiometric amount of CO_2. Thus, flaring biogas will reduce the potential greenhouse gas effect of CH_4 in the biogas, but the energy recovery is not effective because of the low BTU values. On the other hand, biogas can be upgraded to produce a high quality fuel if most of the CO_2, moisture and N_2 can be removed. The captured methane can be used in internal combustion engine (most commonly used), gas turbine for power generation, fuel cells, boilers, industrial heaters, manufacturing of chemicals, or can be delivered to an existing gas distribution network (Demirbas et al., 2011; Khan and Islam, 2012).

In principle, adsorption, absorption, membranes and cryogenic distillation can be used for biogas upgrading to improve its heating value. Cryogenic distillation would only be feasible in very large applications, probably beyond the capacity of most landfills at present (Knaebel and Reinhold, 2003), and pressure swing adsorption and liquid scrubbing are still at the early stage of development. Membranes have shown to be efficient for bulk separations. They could be used to remove moisture and the bulk of the CO_2, depending on the type of the membrane used. However, till to date, there are no known membranes that exhibit a good selectivity between N_2 and CH_4. Therefore, membranes are not expected to produce high purities of CH_4 from biogases. As a landfill emits gases at different compositions during different phases of its life, for the purpose of simplicity to demonstrate multicomponent separation performance of membranes, CH_4, CO_2 and N_2 were taken as the key components of biogas in this study. During the methane fermentation phase and the maturation phase, which are the longest period of a landfill's life expectancy, CH_4, CO_2 and N_2 are the major compounds (Gowing, 2001; Tchobanoglous and Kreith, 2002). The above mentioned gases are the major compounds in digester gas too. Table 4.1 shows the typical composition of a landfill gas (from landfills) and digester gas (from anaerobic digestion). Among the many kinds of polymer membranes, cellulose acetate-based membranes are well known for CO_2/CH_4 separation in natural gas processing. They typically have a gas permeance of 40-50 GPU for CO_2 and 1-3 GPU for N_2 and CH_4, with a CO_2/CH_4 and CO_2/N_2 selectivity in the range of 15-35 under normal operating conditions (Baker, 2002; Baker, 2004; Pan, 1986). It has been reported that the permeances of a

Table 4.1: Compositions of biogas through landfills and anaerobic digestion (Tchobanoglous and Kreith, 2002; Rasi et al., 2011; Demirbas et al., 2011).

Component	Gas composition, %		Property
	Landfills	Anaerobic Digestion	
Methane	45-60	55-70	Energetic potential
Carbon dioxide	40-60	30-45	Greenhouse effect
Nitrogen	2-5	0-2	Reduction of heating value
Oxygen	0.1-1	0-2	Danger of explosion
Ammonia	5 ppm	< 100 ppm	Smell, toxic
Hydrogen	0-0.2	0-1	Potential of detonations and fires
Sulfides	0-1	50-5000 ppm	Smell, corrosion

cellulose triacetate membrane are 60, 3.6 and 2.9 GPU for CO_2, N_2 and CH_4, respectively (Coker et al., 1998). These values were used in this study (including all the case studies) to evaluate the possibility of CH_4 enrichment for biogas upgrading with membranes.

4.6 Dynamic membrane module configurations for methane enrichment

In biogas separation, in view of the purity-recovery trade off, a moderate purity of CH_4 with a high recovery is desired otherwise it will be difficult for the process to be economically attractive. For the purpose of evaluating the potential use of membranes for biogas upgrading, the permselectivity of the aforementioned cellulose triacetate membrane was used in the parametric studies. The permeability of the membrane was assumed to be constant over a pressure range of 400-600 kPa, irrespective of shell side feed or bore side feed. Unless otherwise noted, every single unit has an active fiber length of 1 m. A nominal fiber outside diameter of 300 μm, and inside diameter of 150 μm were used in the calculation. For all the simulations performed, countercurrent shell-side feed was employed, unless explicitly noted otherwise. The feed gas was assumed to be at landfill outlet temperature (43.3^{o}C). In the studies, the feed flow rate was normalized by membrane

area, which represents the processing capacity of the membrane unit, and similarly product flow rate was normalized by the membrane area to represent the productivity of the membrane unit. The permeate stream was taken at the atmospheric pressure while the feed pressure was varied between 400 and 600 kPa. To assess the performance of a membrane, the product (methane is collected as retentate) purity and methane recovery are the key parameters.

4.6.1 Single-stage without recycle

The single pass configuration (Figure 4.1a) is simple to operate and control, and is generally capable of meeting a wide range of separation requirements. Figure 4.4 represents the performance of single-stage permeation for separating the landfill gas at feed pressures of 400 and 600 kPa. It is found that at 0.8 stage cut, a moderately pure residue stream containing 93.85% methane is possible (Figure 4.4a), though the methane recovery is only 40% (Figure 4.4b). The retentate stream is almost free from carbon dioxide. However, it contains a small amount of nitrogen since methane and nitrogen are difficult to separate by membranes. A higher purity of methane at the retentate can be obtained but there will be a severe methane loss in the permeate stream. As a result, the productivity of methane in the retentate will go down (Figure 4.4c). Similar trends were observed for a

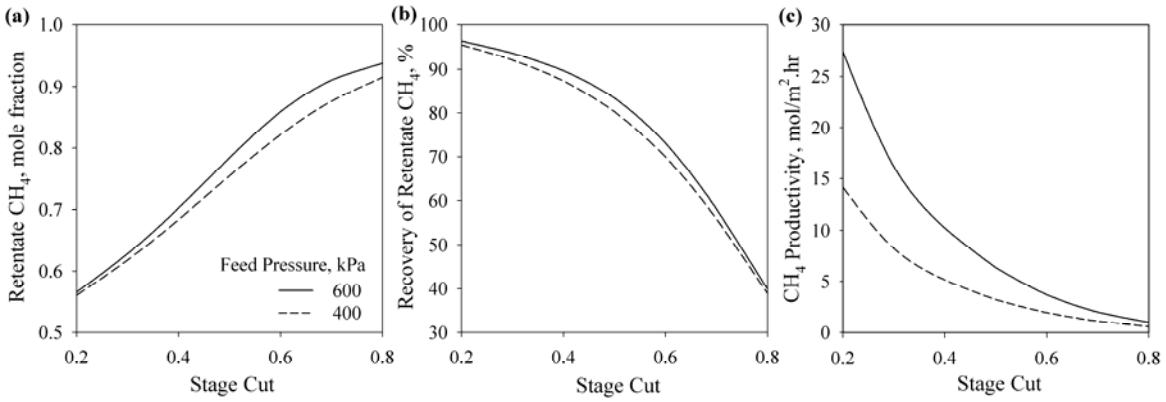

Fig. 4.4: Performance of single-stage permeation at different feed pressures, (a) retentate CH_4 concentration. (b) CH_4 recovery, and (c) CH_4 productivity.

feed pressure of 400 kPa; however compared to an operating pressure of 600 kPa, to achieve the same methane concentration in the retentate, a much higher stage cut will be needed, resulting in a much lower methane recovery and productivity. Single pass configuration is considered the base case here and optimal module configurations are compared with the base case.

4.6.2 Single-stage with retentate recycle to the permeate side

Since the single-stage permeation is not always capable of achieving a desired degree of separation, a number of modular configurations have been proposed to improve the degree of separation. Enrichment of the more permeable component can be improved by recycling a portion of the permeate stream to the feed stream. On the other hand, if a part of the retentate is used to purge the permeate, a higher concentration of the less permeable component in the retentate product is also expected. This is because by passing a small portion of the retentate stream to the permeate, the more permeable component in the permeate side is diluted, thereby lowering the partial pressure of the more permeable component in the permeate side and resulting in an increase in its transmembrane driving force. As a result, a higher purity of the less permeable component in the retentate stream is obtained. Figure 4.1b is a schematic of a permeator with retentate purging to the permeate side, and Figure 4.5 shows the performance of the retentate purging permeator at different feed pressures. The mole fraction of CH_4 in the retentate stream increases with an increase in the recycle ratio (R_b), defined as the molar flow rate ratio of the recycle stream to the retentate stream, as shown in Figure 4.5a. It was possible to produce a retentate stream of 94.40% CH_4 at a feed pressure of 600 kPa. As expected, the mole fraction of CO_2 in the permeate decreases gradually with an increase in the recycle ratio since the permeate stream is diluted by the retentate recycle. A high recovery or a high purity can be obtained in the membrane processes, but seldom both at the same time. The trade-off relationship between methane recovery and purity when the recycle ratio varies at given feed pressures is shown in Figures 4.5a and b. Similarly, the productivity of methane collected in the retentate decreases with an increase in its purity, as shown in Figure 4.5c.

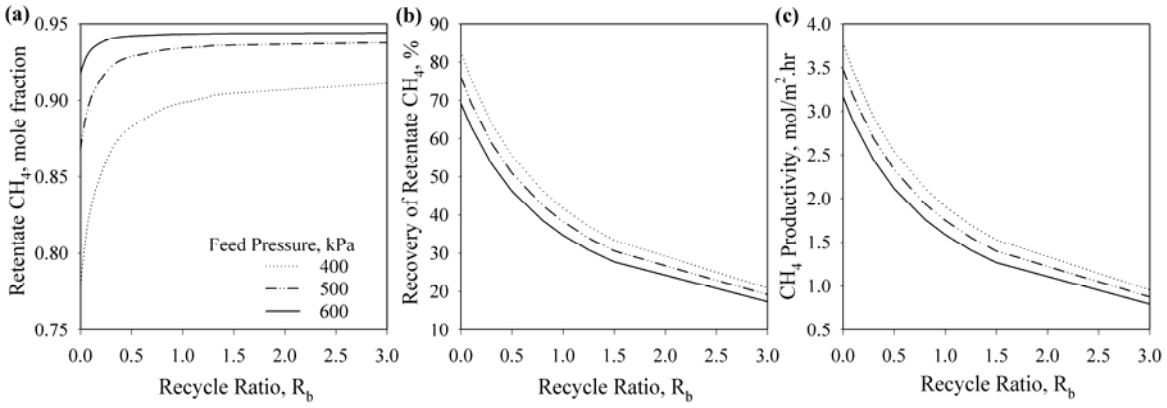

Fig. 4.5: Effects of retentate recycle on the performance of single-stage permeation at different feed pressures. (a) Retentate CH_4 concentration, (b) CH_4 recovery, and (c) CH_4 productivity.

While the retentate recycle operation helps increase the concentration of slow permeating component (i.e., CH_4 in this case) in the retentate, it is not suitable for achieving a high purity of the more permeable component in the permeate. With retentate recycle, a portion of the retentate goes to the permeate stream, and thus the apparent stage cut (that is, the ratio of permeate exiting the permeator to the feed admitted) increases with the recycle ratio. This is shown in Figure 4.6. As expected, at a given retentate recycle ratio, an increase in the stage cut increases the methane concentration in the retentate because more gases on the feed side permeates to the permeate side. The effect of stage cut on the retentate CH_4 concentration becomes more significant at a higher recycle ratio. As the recycle ratio increases, inevitably more CH_4 is lost to the permeate stream, resulting in a reduction in the methane recovery. For the biogas separation studied here, the retentate is the desired product, and a higher throughput and a higher CH_4 concentration are desired. Hence, finding an optimum recycle ratio is vital for the retentate recycle operation. It was also observed from Figure 4.6 that the recycle ratio has a more pronounced effect at lower feed pressures, and the retentate recycle to the permeate side is more effective at lower feed pressures.

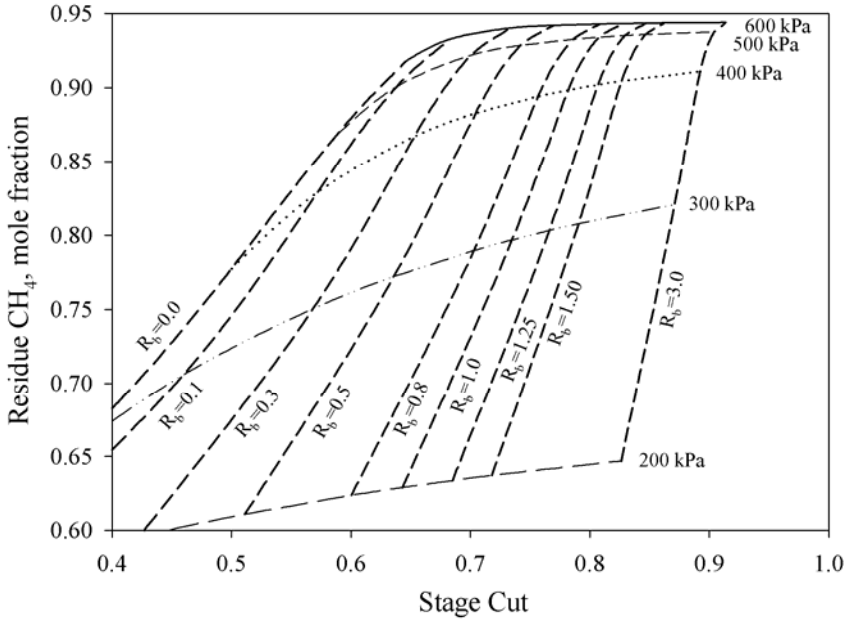

Fig. 4.6: Extent of separation achievable from single-stage permeation with retentate recycle at different feed pressures.

4.6.3 Single-stage with permeate recycle to the feed side

While methane recovery from biogas is of primary interest, CO_2 capture is also important to reduce greenhouse gas emission. The permeate recycle operation was also simulated where a portion of the permeate stream was recycled to the feed stream, as shown in Figure 4.1c. However, because the permeate from the permeator is at a pressure lower than the feed pressure, the portion of the stream to be recycled needs recompression before mixing with the fresh feed. As anticipated, the permeate CO_2 purity is improved by using the permeate recycle since CO_2 on the feed side is concentrated, thus enhancing its transmembrane driving force. This, however, is at the expense of reduced recovery of CO_2 in the permeate. The productivity of permeate CO_2 also suffers when a portion of the permeate stream is recycled to the permeator. This is shown in Figure 4.7, where CO_2 recovery and productivity are plotted versus permeate CO_2 concentration at different recycle ratios (R_P). Here the permeate recycle ratio is defined as the fraction of permeate

from the permeator sent back to the feed stream. At a given recycle ratio, there exists a limit in the maximum CO_2 concentration that can be achieved. The permeate CO_2 concentration approaches maximum when there is no depletion in CO_2 concentration on the feed side, and this corresponds to a limit of zero stage cut (and thus a zero recovery).

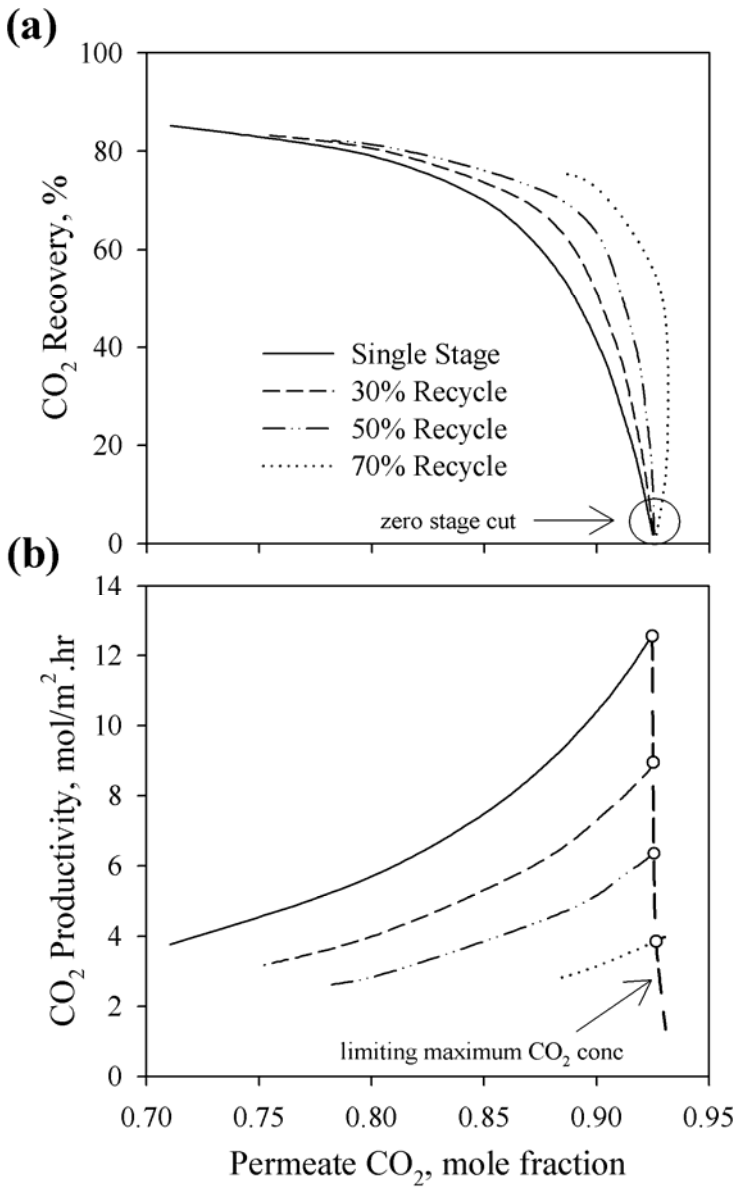

Fig. 4.7: Performance of single-stage permeation with permeate recycle to the feed. (a) Permeate CO_2 concentration, and (b) CO_2 productivity. Feed pressure600 kPa.

Figure 4.8 shows the retentate CH_4 recovery and productivity as a function of retentate CH_4 concentration at different permeate recycle ratios. The purity of retentate CH_4 is restrained in permeate recycle operation since the less permeable component (i.e., CH_4) in the feed side is diluted with the methane-depleted permeate recycle stream. However, the recovery

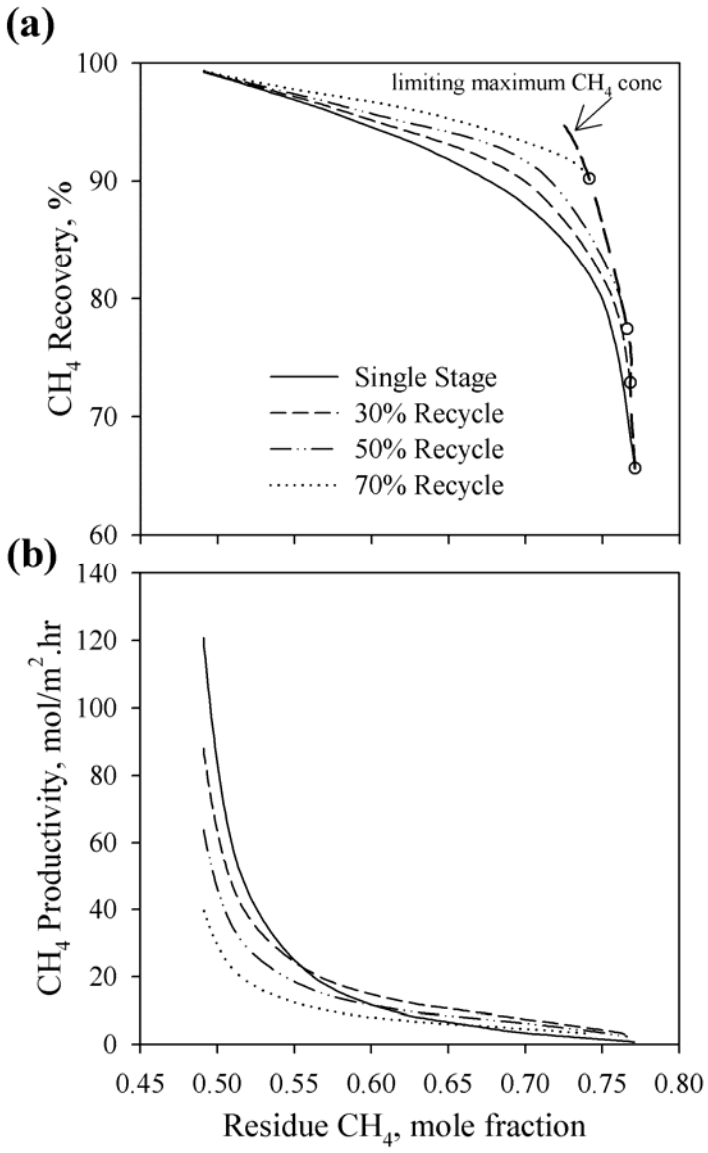

Fig. 4.8: Performance of single-stage permeation with permeate recycle to feed. (a) Retentate CH_4 concentration, and (b) CH_4 productivity. Feed pressure 600 kPa.

of retentate CH_4 increases in the permeate recycle operation. The permeate recycle operation needs to be assessed based on economic considerations if a moderate CH_4 purity can be paid off by the enhanced CH_4 recovery. This process would appear to be particularly useful for specific applications where a higher permeate CO_2 purity and/or higher retentate CH_4 recovery is targeted.

4.6.4 Continuous membrane column

In view of the characteristics of retentate recycle and permeate recycle, the concept of continuous membrane column, which may be viewed as a combination of the retentate and permeate recycles described above, for biogas processing was further investigated. In this case, the permeation cell is no longer regarded as a single stage, rather as a continuous cascade, as shown in Figure 4.9. For simplicity of simulating the membrane column, the membrane column was assumed to consist of two permeation cells with identical membrane areas and the effect of permeate pressure build-up in the membrane column was neglected. The retentate recycle ratio R_b was varied from 0 to 0.7, and the permeate recycle ratio R_p was adjusted to match a stage cut of 0.5. As the more permeable component preferentially permeates through the membrane, the less permeable component is concentrated on the high pressure side. Figure 4.10 shows the effects of R_b on the concentrations, recoveries and productivities of the retentate CH_4 and permeate CO_2 for the membrane column at a feed pressure of 600 kPa. It was shown in Figure 4.10a that not only was the CH_4 in the retentate but also CO_2 in the permeate more concentrated than those obtained without the retentate and permeate recycles. The retentate CH_4 and permeate CO_2

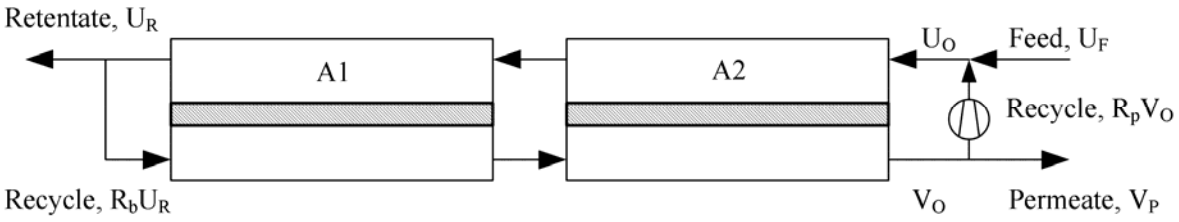

Fig. 4.9: Schematic of retentate recycle and permeate recycle in a continuous membrane column.

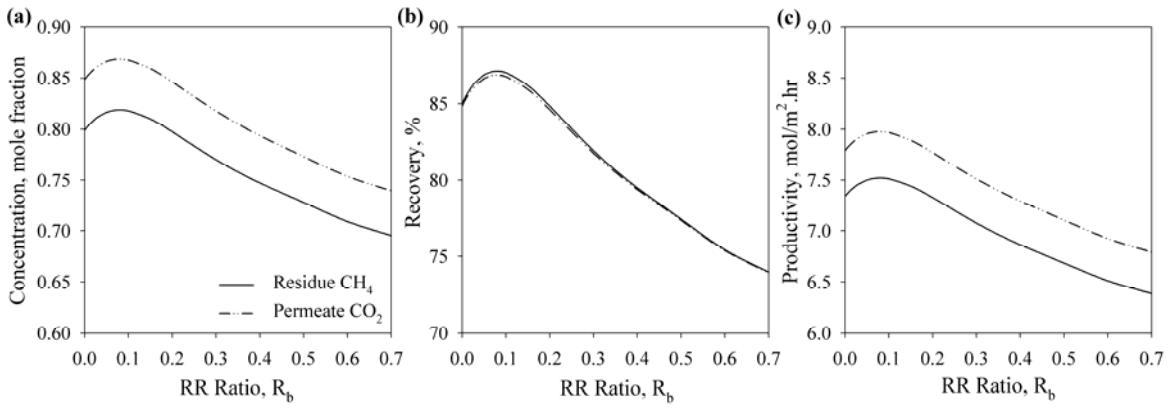

Fig. 4.10: Performance of continuous membrane column. (a) Retentate CH_4 and permeate CO_2 concentrations, (b) CH_4 and CO_2 recoveries, and (c) CH_4 and CO_2 productivities.

reached maximum values of 82.2% and 87.1%, respectively, in the range of R_b = 0.08 - 0.1 (Figure 4.10a). This suggests that a small amount of retentate recycle can enhance the degree of separation to obtain higher concentrations of both retentate CH_4 and permeate CO_2. However, beyond a certain R_b value, a further increase in R_b would decrease these concentrations gradually since the favouring effects (i.e., lowered partial pressure of CO_2 on the permeate side due to retentate recycle, and increased partial pressure of CO_2 on the feed side due to permeate recycle) that enhance transmembrane driving force begin to nullify.

It was also observed that the recovery and productivity of both the retentate CH_4 and the permeate CO_2 with respect to R_b follow a similar trend, as shown in Figures 4.10b and 10c, respectively. Interestingly, the CH_4 recovery in the retentate and CO_2 recovery in the permeate are very close over a broad range of R_b values. Figure 4.11 shows the permeate recycle ratio R_p corresponding to different R_b values; the permeate recycle ratio is greater than the retentate recycle ratio in the membrane column, unless the retentate recycle ratio is high enough. In the latter case, the membrane column is no longer efficient. In spite of their potential advantages, membrane columns have not been exploited industrially, presumably due to the complexities involved in their design and operation.

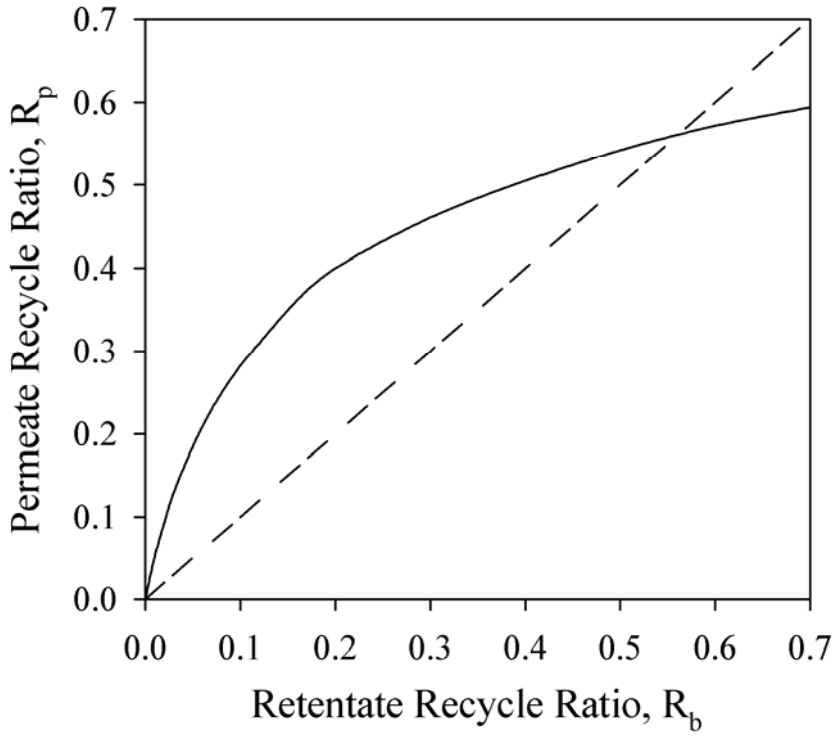

Fig. 4.11: Relationship between retentate recycle ratio R_b and permeate recycle ratio R_p in the membrane column.

4.6.5 Two-stage cascade with reflux and two stages in parallel/series

When a single-stage design is unsatisfactory in terms of product purity or recovery, multistaging or cascading is sometimes an attractive approach. One of the configurations is a two-stage cascade with reflux, where retentate from the first stage serves as the feed to the second stage and the permeate from the second stage is fed to the first stage, as shown in Figure 4.12. This configuration was simulated by varying the stage cut of the second stage until the permeate composition from the second stage matched the feed composition, assuming the same membrane area for both stages. It was possible to produce a retentate stream with 90.0% CH_4 at a CH_4 recovery rate of 84.2%. As a comparison, to produce a comparable methane purity in the retentate, the simple two stages in parallel (Figure 4.13) and two stages in series (Figure 4.14) would yield a recovery of 73.4% and 71.7%,

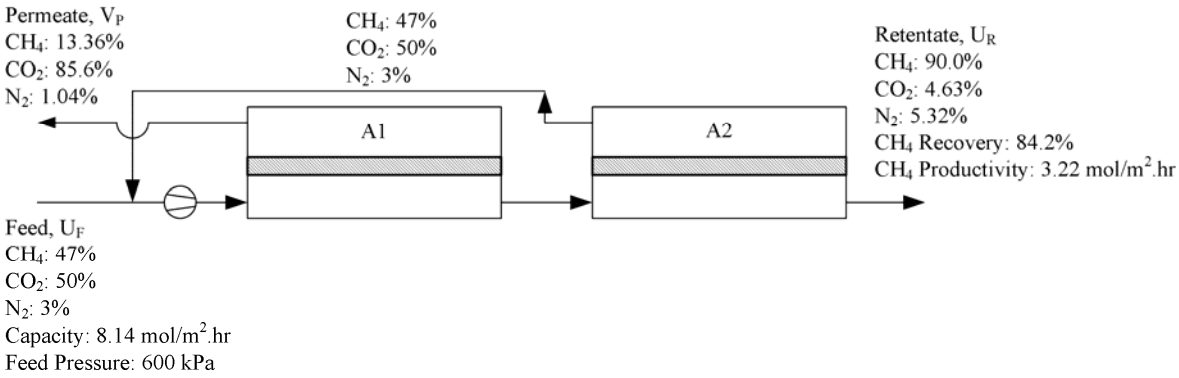

Fig. 4.12: Two-stage cascade with reflux.

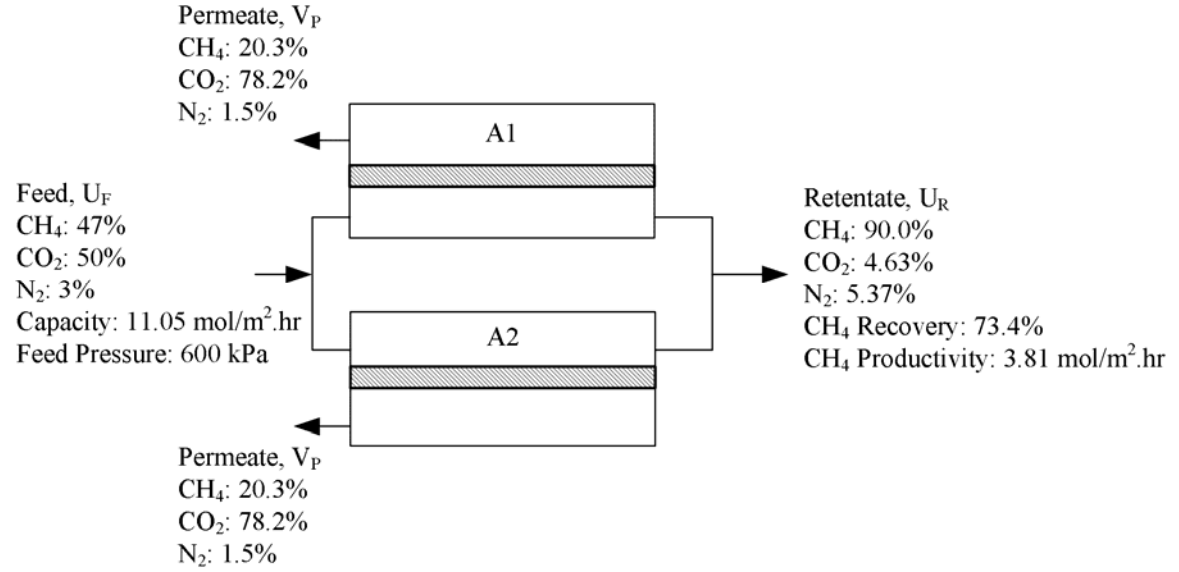

Fig. 4.13: Two modules in parallel.

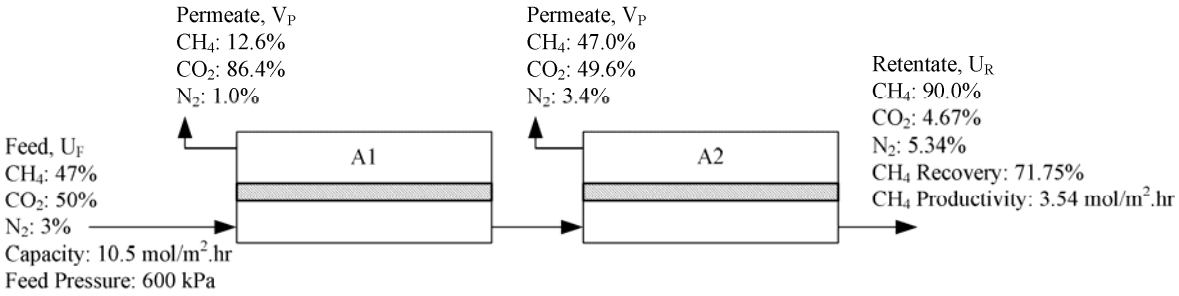

Fig. 4.14: Two modules in series.

respectively. Clearly, the configuration shown in Figure 4.12 performs better in terms of product purity and recovery, though its CH_4 productivity is about 10-18% lower.

4.6.6 Nitrogen removal with methane-selective membranes

The extent of separation is limited by membrane selectivity, process configuration and operating conditions. The above results show that it was possible to obtain as high as 94.4% of CH_4 in the retentate with recycle operations, but it is difficult to meet the pipeline specifications due to presence of nitrogen. The purified gas has a heating value (979 BTU/cf or 36.5 MJ/m^3) (Lyons, 1996) close to pipeline standard natural gas (1032 BTU/cf or 38.4 MJ/m^3) (Perry and Green, 1997), which is much higher than that of the heating value of biogas (403-564 BTU/cf or 15-21 MJ/m^3, depending on the composition of methane) (Williams, 2005). The purified gas has fuel values and can be used in many applications. However, in order to deliver the purified gas to pipeline grids, the N_2 content needs to be lowered below 4%. Unfortunately, there are no efficient technologies available at the present time to separate nitrogen from methane, and membranes with an adequate N_2/CH_4 selectivity are still lacking. Typical rubbery membranes (e.g., polydimethylsiloxane) for N_2/CH_4 separation have a selectivity of only 2-3 at ambient temperatures. It was thus decided to carry out a parametric study for N_2/CH_4 separation using methane-selective membranes that could bring the aforementioned methane-enriched retentate to a methane concentration of 96%. For calculation purposes, the permeator was assumed to have the same membrane area as described above, and the permeance of nitrogen was assumed to be 3.6 GPU. Simulation was performed to determine the membrane selectivity required for a targeted separation to produce a pipeline quality permeate stream (≤ 4% N_2 content) and a retentate stream with 50% N_2 in a single-stage operation. It was found that for a feed gas containing 90% CH_4, a methane-permeable membrane with a methane/nitrogen selectivity of 8 can achieve the target separation (Figure 4.15a) at a methane recovery and productivity of 92.7% and 12.4 mol/(m^2.h), respectively. If the feed gas contains 94% CH_4, a membrane selectivity of 4.5 would be

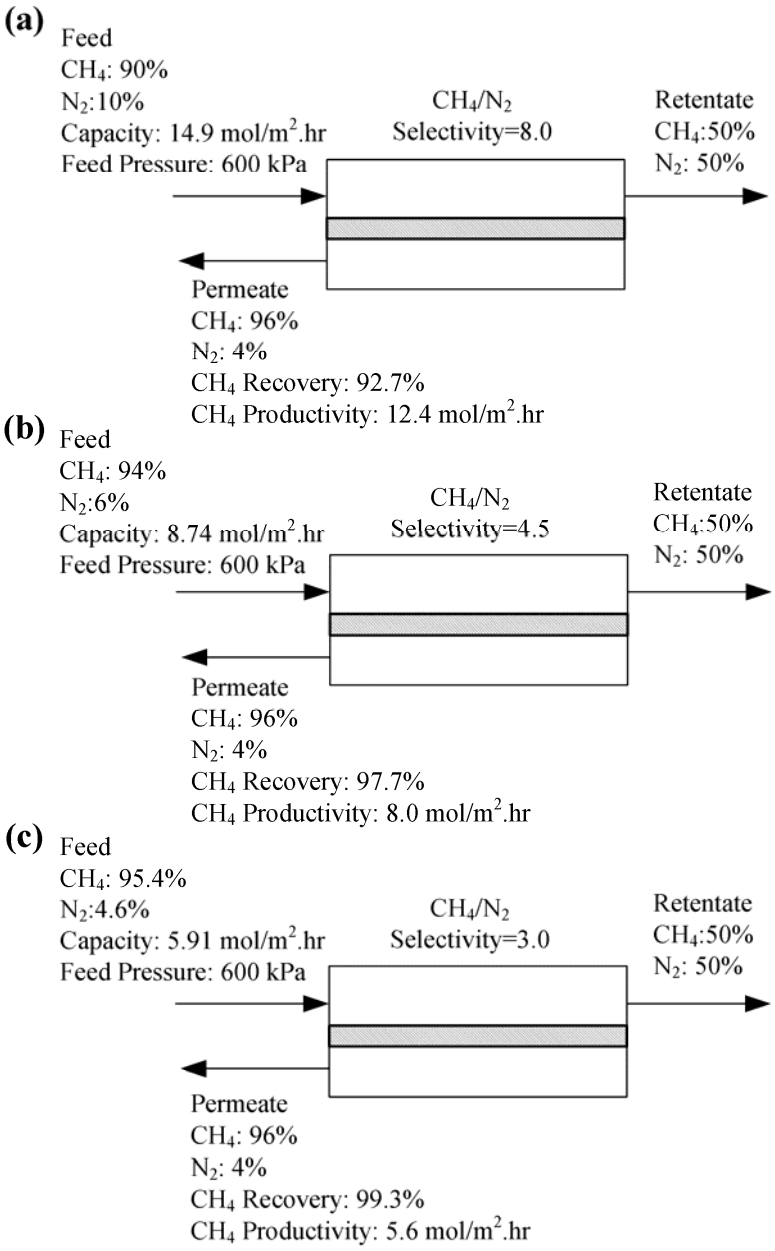

Figure 4.15. Case studies of nitrogen removal from CH_4/CO_2 mixtures with methane-selective membranes to produce a 50% CH_4/50% N_2 retentate stream and a 96% CH_4/4% N_2 product gas stream. (a) Feed composition 90% CH_4/10% N_2, membrane selectivity 8.0, (b) Feed composition 94% CH_4/6% N_2, membrane selectivity 4.5, and (c) Membrane selectivity 3, feed CH_4 concentration required 95.4%.

required (Figure 4.15b), and the methane recovery and productivity were 97.7% and 8.0 mol/(m^2.h), respectively. Current rubbery polymeric membranes exhibit a

methane/nitrogen selectivity of 3-4 at low temperatures (Baker and Lokhandwala, 2008; Lokhandwala et al., 2010). As Figure 4.15c shows, with a methane/nitrogen selectivity of 3, a feed methane concentration of 95.4% was required in order to produce a permeate methane concentration of 96%. This means the intended separation is difficult to achieve using current membranes but it does not look like an elusive target to reach in near future as more permselective membranes are developed. It can be estimated that if a nitrogen-selective membrane is to be used, the membrane must have a much higher nitrogen/methane selectivity than the best nitrogen-selective membrane currently available (nitrogen/methane selectivity of 2.5) to achieve the same separation (Baker and Lokhandwala, 2008). In this case, the purified methane is obtained in the residue stream at a pressure close to the feed pressure, which favours subsequent delivery in terms of recompression costs. It is to be noted that single-stage membrane units would rarely be used in practice for the separations; however, they do provide a basis for comparison.

The renewable methane from Canadian municipal solid wastes has not been properly exploited yet, and there exists enormous opportunities for methane recovery from biogas in order to harness energy production and to mitigate its greenhouse gas effect. The current scenario of Canadian landfills and potential renewable methane generation from municipal solid wastes has been discussed in Appendix B. Based on the current scenario of Canadian landfills and potential renewable methane generation from municipal solid wastes, there appears to be an enormous potential to capture methane for biogas from both an energy recovery and environmental perspectives.

4.7 Conclusions

A simple approach was taken to formulate and solve the multicomponent gas permeation problems with asymmetric hollow fiber membranes. The solution technique offers minimum computational time and effort, with improved solution stability. Moreover, the computational complexity does not multiply as the number of components increases. The model and solution technique were applied to investigate dynamic performance of several membrane module configurations for methane recovery and enrichment from

biogas. It was found that a moderately pure residue stream with 93.85% CH_4 could be produced from single-stage permeation at a methane recovery of 40%. The retentate-to-permeate recycle and permeate-to-feed recycle operation for enhanced separation were explored, and the optimum recycle ratio vital for these operations were found. A higher purity of retentate stream up to 94.4% CH_4 was possible with the retentate-to-permeate recycle mode of operation. The recovery of retentate CH_4 also increased with the permeate-to-feed recycle mode. Complexities involved in the design and operation of continuous membrane column, which involve essentially both modes of recycles, was further investigated; and both concentrations of CH_4 in retentate and CO_2 in permeate were enhanced. It was also observed that methane loss in permeate stream could be lowered using a membrane column. In addition, two-stage cascade with reflux was shown to improve both the product purity and recovery. However, with current CO_2-selective membranes, it is difficult for the methane-enriched retentate stream to reach a pipeline quality natural gas primarily due to the presence of a small amount of nitrogen, and an additional separation step to remove nitrogen is needed. Rubbery polymer membranes may be used for the denitrogenation step, but the methane/nitrogen selectivity currently available is relatively low and more permselective membranes need to be developed.

Chapter 5

Effect of permeate pressure build-up on intrinsic separation performance of asymmetric hollow fiber membranes[†]

5.1 Introduction

An important advantage of hollow fiber membrane modules is their ability to pack a very large membrane area into a single module. Hollow fibers enable substantially higher membrane packing than are possible with either of the flat-sheet or spiral-wound designs. For high-pressure gas separation applications, hollow fine fibers have a major segment of the market, and can withstand high-pressures of 1000 psig or more in shell-side feed modules (Baker, 2004). Operating at a higher pressure consumes more gas, and therefore sometimes membrane module is tested or characterized at lower pressure to save gas consumption. The pressure build-up in the lumen side increases for high pressure applications and can become enough to seriously affect the membrane performance. It is also considered that there is little or negligible pressure build-up for shorter fibers, though the pressure build-up increases for longer fibers. It is thus perceived that the effect of the pressure build-up is significant only for long fibers, especially at high feed pressures. This, however requires rectification and interpretation, and these perceptions are sometimes misleading.

The permeance of gases through a membrane is normally independent of feed pressure, which is normally the case for permeation of permanent gases in glassy polymers and may be attributed to the constant diffusivity and solubility at different pressures. The hollow fiber membranes used in gas separation are often very fine. Pressure build-up on the lumen side of these fine fibers reduces the driving force across the fiber wall available for permeation, and this loss can become enough to seriously affect membrane performance. Because of the pressure build-up in the fiber lumen, the permeances calculated from pure gas permeation experiments (apparent permeances) do not necessarily represent the true permeances (intrinsic property) of the hollow fiber membrane unless the pressure build-up

[†] Part of Chapter 5 will be submitted shortly for publication

in the fiber lumen is taken into account. A number of examples can be cited from open literature where permeance was found independent of pressure difference for flat homogeneous membrane but a dependent function for hollow fibers, though the pressure dependence is not caused by membrane material. The permeate pressure build-up is significant for long fibers, fine fibers and for high pressure applications. To minimize gas consumption, lab tests are often performed at low pressures on miniature fiber modules of short fibers (Pan, 1986). However, the percentage loss in the driving force at low pressures can still be enough to deteriorate the actual permeation performance than that at high pressures. On the contrary, the reduction in the driving force at high pressures is in fact less critical as the membrane permeance will be close to its actual permeance. On the other hand, the pressure build-up is not always negligible for short fibers. In an industrial scale, the hollow fiber length is usually more than 1 m and a considerable pressure build-up in the lumen can occur, resulting in discrepancy in the measured membrane performance if this effect is neglected. For the separation of hydrogen from nitrogen or methane, or carbon dioxide from natural gas, pressure-normalized fluxes are considerably high, and hollow fiber modules can develop excessive permeate-side pressure drops. On the other hand, for the production of nitrogen from air, the membrane pressure-normalized fluxes are relatively low, from 1 to 2 GPU, and parasitic pressure drops are not likely a problem (Baker, 2004). However, depending on the module geometry, the effect of permeate pressure build-up could be significant for slow permeating gases as well. Moreover, the potted section of the hollow fibers does not take part in permeation but contributes additional pressure drop, and this section adds up driving force loss which can influence the apparent permeance calculated from the permeate flow.

In our study, the apparent permeances of H_2 and N_2 were evaluated from pure gas permeation experiments with short and long module. The true separation performance of the hollow fiber membranes was calculated by taking into account the effect of permeate pressure build-up in the fiber lumen (including the potted section). A correlation between the apparent membrane permeance and pressure difference was observed. The observations were explained theoretically and compared with some of the pure gas permeation experiments reported in literature. The pressure build-up effect was further investigated by

calculating the average loss and percentage loss in the driving force due to pressure build-up inside the fiber lumen for pure gas permeation of H_2 at different pressures. The nominal internal diameter of the fibers was accurately estimated through theoretical analysis, which was otherwise difficult to image due to inconsistent shape of the fiber. The mixed gas permeances were also measured from mixed gas experiments, and were compared with permeances measured from pure gas experiments and approximation method. The study will rectify some general perceptions, which are usually believed in case of pressure build-up with high flux asymmetric hollow fiber membranes. The analysis may also provide an insight into the characteristics of gas permeation through hollow fiber membranes.

5.2 Materials and methods

5.2.1 Gas permeation experiment

Details of the gas permeation experiments can be found in Zakaria (2006). A short membrane module was prepared by inserting a bundle of 23 asymmetric cellulose acetate-based hollow fibers in a ¼-in copper tubing of about 4 cm in length, and potted with epoxy resin to form a gas-tight tube sheet as shown in Figure 5.1. The tube sheet was carefully cut to make the fibers fully open for gas flow. The effective length of the fiber was 23.5 cm, and the inner and outer diameter of the fiber was 80 and 200 μm, respectively. Pure gas permeation of H_2 and N_2 was conducted (Figure 5.2). The feed gas at a specific pressure was admitted to the membrane module to contact with the selective layer of the membrane, and the permeate stream exited the module from the lumen side at atmospheric pressure. The residue end was completely closed. The permeation rate was determined volumetrically using a bubble flow meter. The gas permeance through the membrane can be calculated by:

$$J = Q/A\,\Delta p \tag{5.1}$$

where J is the apparent membrane permeance, which is customarily expressed in units of GPU (1 GPU = 10^{-6} cm^3 (STP)/cm^2. s. cm Hg = 3.35×10^{-10} mol/m^2. s. Pa), A the effective

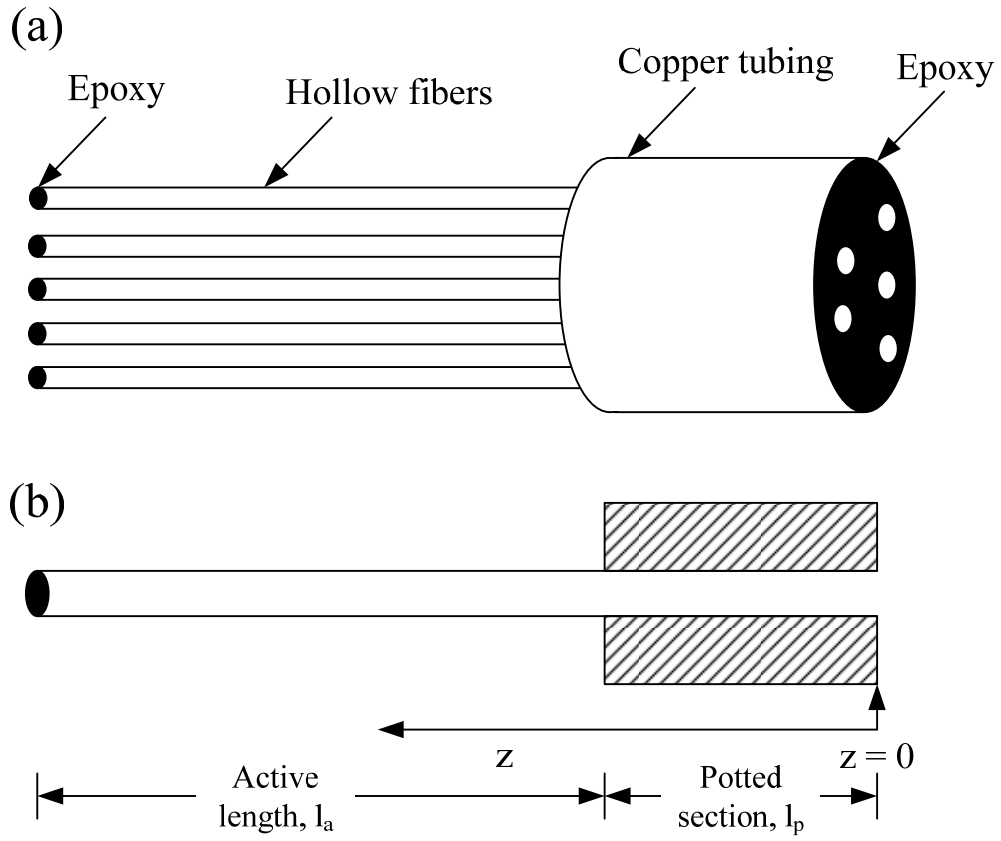

Fig. 5.1: (a) Schematic of assembled hollow fiber membranes, and (b) active and potted section.

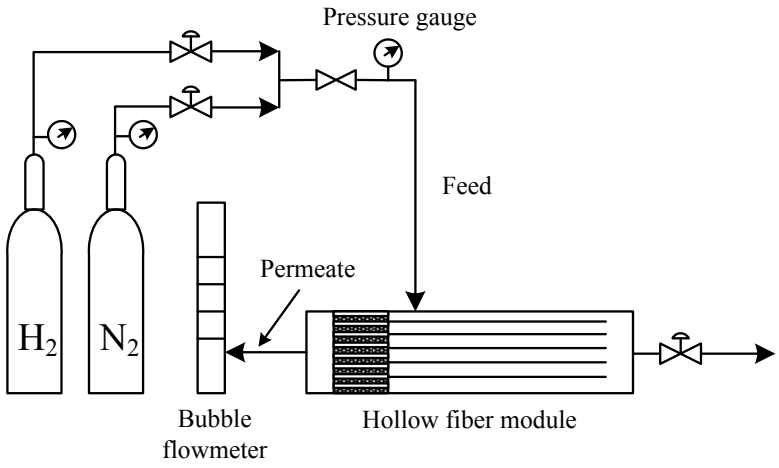

Fig. 5.2: Apparatus of gas permeation experiment.

membrane area for permeation (excluding potted section) in cm^2, Q gas permeation rate in cm^3 (STP)/s, and Δp the pressure difference across the membrane in cmHg. The permeation selectivity is characterized by the permeance ratio of a pair of gases. A longer membrane module, consisting of 9 fibers with 105 cm in length, was also prepared to determine the effect of pressure build-up on the apparent permeance and the selectivity of the membrane module. Another module, consisting 9 fibers and 87 cm in length, was prepared for mixed gas permeation experiment. For the mixed gas permeation experiments, the gas mixture was prepared in-house by blending hydrogen and nitrogen until the required composition was achieved. The feed gas was analyzed using a gas chromatograph and the composition was 57.39% hydrogen and the balance was nitrogen. The composition of the feed, permeate, and residue streams were measured using a gas chromatograph equipped with a thermal conductivity detector. The experiments were carried out at various stage cuts by controlling the residue flow rate. Both the pure gas and mixed gas permeation experiments were carried at 25°C.

5.2.2 Numerical analysis

The trend of permeate pressure build-up was investigated analytically. The permeate pressure build-up can be calculated by the permeation equation and Hagen-Poiseuille equation. The length of hollow fiber consists of two sections i.e., active fibers and potted sections (Figure 5.1b). However, no permeation occurs at potted sections, and the pressure build-up in the potted sections can be described by Eqn. 5.2.

$$\frac{dP_P}{dz} = -256\,R\,T\,Q\mu \big/ 2\,\pi\,D_i^{\,4}\,P_P\,N \tag{5.2}$$

The initial condition for potted section:

At fiber exit : $z = 0,\ P_P = 1\,\text{atm}$;

solving Eqn. 5.2 will provide the permeate pressure at $z = l_p$, which will be used as initial condition for the simulation of active length. In the active fibers section, both permeation and pressure build-up occurs. The pressure build-up can still be described by Eqn. 5.2, while the permeation can be described by Eqn. 5.3.

$$\frac{dQ}{dz} = \pi D_o J (P_F - P_P) N \quad (5.3)$$

For active fibers sections, Eqns. 5.2 and 5.3 form a two point boundary value problem. At the end of potted section (z = l_p or beginning of active action), P_P and Q are known from simulation of the potted section and from the gas permeation experiment, respectively. At the fiber's closed end (z = l_a), Q = 0. The intrinsic permeance J was kept as an unknown parameter in the problem. The two point boundary value problem with unknown parameters can be solved by the collocation technique. The solutions will provide the value of intrinsic permeance for the pure gas and the permeate pressure profile along the fiber length. Again, mixed gas permeances of hollow fiber membranes in a binary mixed-gas membrane permeator were also calculated as unknown parameters from the mathematical model of binary gas separation with the aid of mixed gas separation experimental results. Several mathematical models of binary gas separation in hollow fiber membranes available in open literature (Kaldis et al., 2000; Kundu et al., 2012a; Murad Chowdhury et al., 2005; Wang et al., 2002) can be used for mixed gas permeance calculation. The model can also be used to predict the performance of a permeator if the permeances of the gas pair are known.

5.3 Results and discussion

In the membrane module, the epoxy-filled tube sheet is not included in the effective length since there is no permeation in this section (Figure 5.1). However, this section still incurs some pressure drop. Figures 5.3 and 5.4 represent the pressure profile along the fiber bore for the short and long module, respectively. It suggests that the pressure build-up in the potted section is not negligible and excessive pressure build-up can affect the actual performance if that effect is neglected. The tube sheet comprises about 17% and 4% of the effective fiber length for the short (potted length 4 cm and active length 23.5 cm) and long module (potted length 4 cm and active length 105 cm), respectively. The uncertainties in the measured fiber length due to the epoxy potting will result in greater inaccuracy for a short hollow fiber compared to a long hollow fiber.

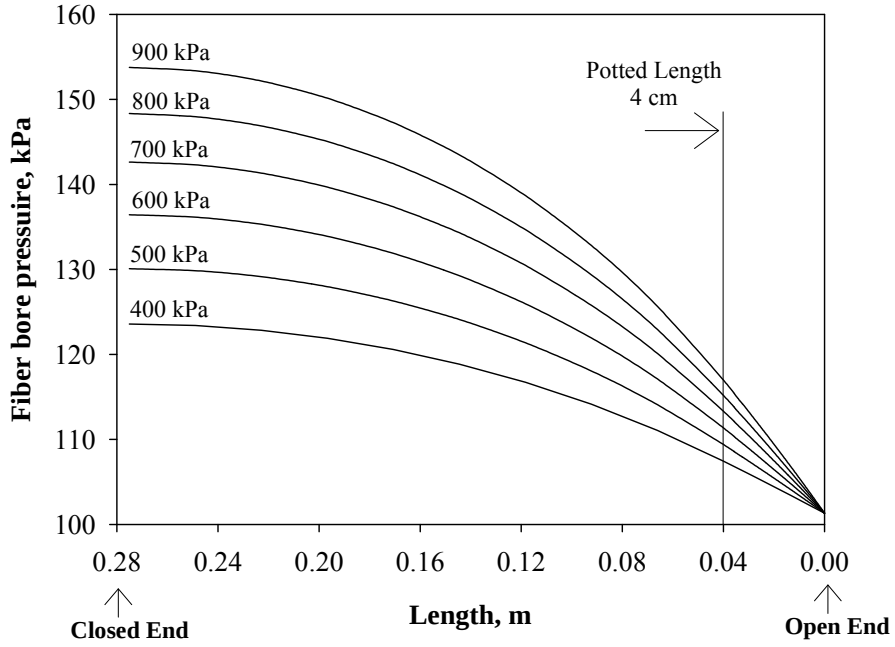

Fig. 5.3: Permeate pressure profile along the fiber bore for short module including potted section.

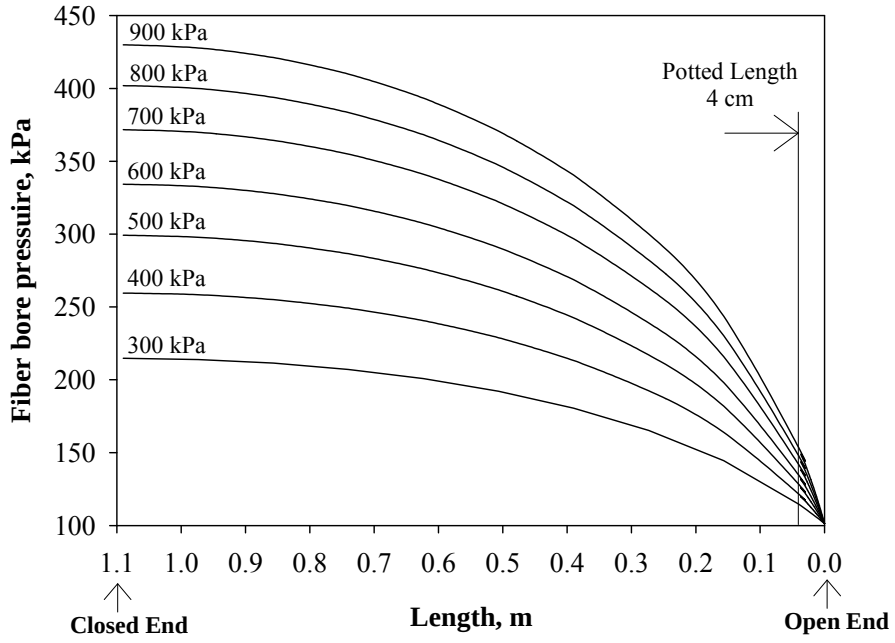

Fig. 5.4: Permeate pressure profile along the fiber bore for long module including potted section.

The apparent permeances of pure H_2 and N_2 in both the short and long modules were calculated using Eqn. 5.1, and they are presented in Figure 5.5. The calculated apparent permeances do not take into account the permeate pressure build-up. It was observed that the apparent permeances of H_2 and N_2 obtained with the long module were always less than the apparent permeances obtained with the short module (Figure 5.5). This

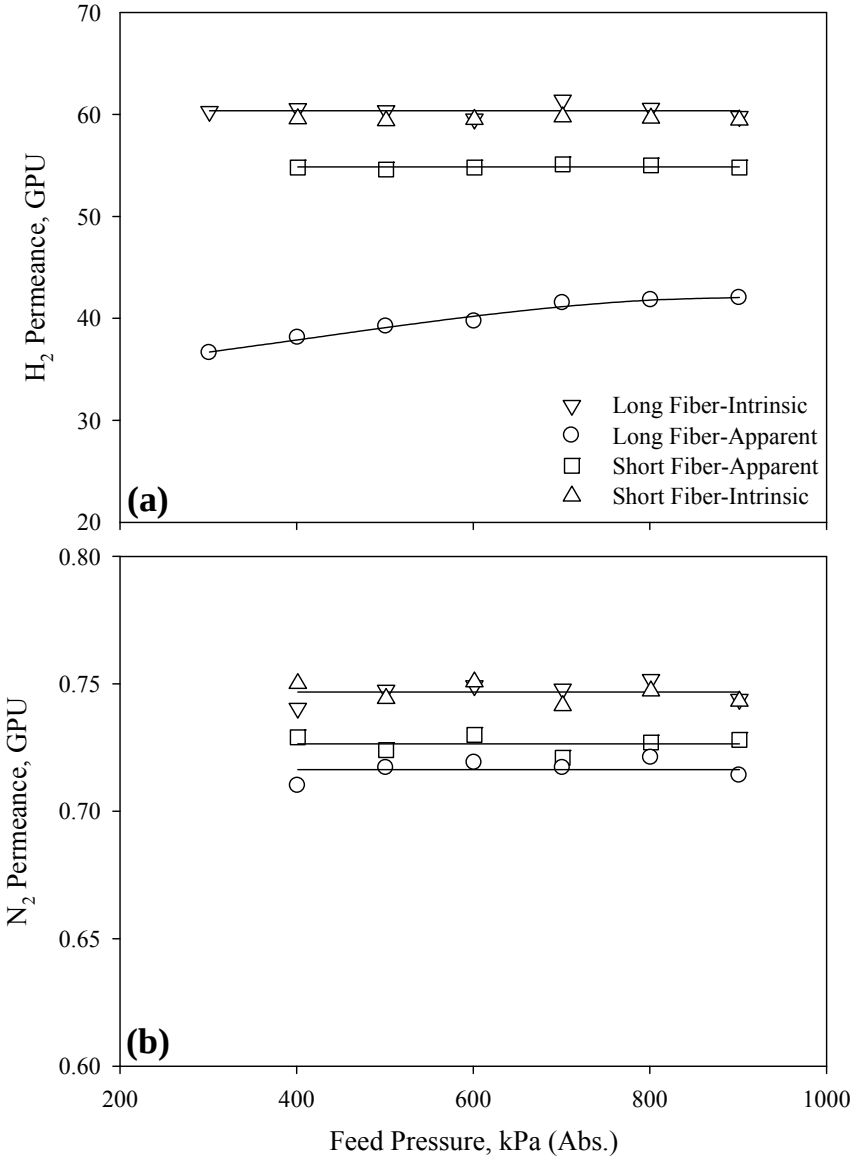

Fig. 5.5: Comparison of apparent and intrinsic permeances of short and long modules at different feed pressures for, (a) pure H_2, and (b) pure N_2.

clearly shows that at a given feed pressure, less permeate flow is generated from the long fiber than from the short fiber for a given membrane area, which can be attributed to the reduced driving force resulting from the permeate pressure build-up. The effect of permeate pressure build-up is more significant for H_2 since H_2 is much more permeable (~60X) than N_2.

The intrinsic or true permeances were calculated at different feed pressures from the permeation rate data by solving Eqns. 5.2 and 5.3, which incorporates the effect of permeate pressure build-up. The pressure build-up in the potted section of the tube sheet was calculated first from permeate flow rate data, and was used as boundary condition along with the permeate flow rate data to calculate the intrinsic permeance. As expected, the intrinsic permeance obtained for the long module is essentially the same as that obtained using the short module and that the permeance is independent of feed pressure (Figure 5.5). For instance, the intrinsic permeance of H_2 was calculated to be 60.4 GPU (Figure 5.5a), while the intrinsic permeance of N_2 was found to be 0.75 GPU (Figures 5.5b). It is apparent from Figure 5.5 that pressure build-up occurs in short fiber too.

Since the permeation rate of H_2 is high, the permeate pressure build-up reduces the permeation of H_2 more than N_2, resulting in a substantial underestimation of H_2 permeance. For the long module, the deviation between the intrinsic and apparent permeance of H_2 was found larger at lower feed pressures than at higher feed pressures. It infers that though the permeate pressure build-up in the lumen increases with feed pressures, the effect of pressure build-up on membrane performance is in fact more significant at low feed pressures than at high feed pressures. It was observed that the apparent permeance of H_2 for long module tends to approach that of the intrinsic permeance at high feed pressures (Figure 5.5a). This suggests that the membrane performs close to its full potential as dictated by the intrinsic property of the membrane if it is operated at a high feed pressure, and in spite of greater pressure build-ups, the effect of pressure build-up on the membrane performance is actually minimized. The apparent selectivity of H_2/N_2 for longer fiber was found less than the selectivity of the membrane measured from that of the short fiber

(Figure 5.6). The intrinsic selectivity of the aforementioned membrane was calculated to be 80.5.

Table 5.1 lists the measured pure gas permeances of some permanent gases and dimensions of some hollow fiber membranes reviewed here. Kumazawa et al. (1994) studied the gas permeance of pure helium in cellulose triacetate hollow fiber membranes. The permeance of helium for a short module (active length of 26 cm and internal diameter of 88 μm) was found to be dependent on the pressure difference up to 5 atm. An increasing trend with the pressure difference was noticed. However, the permeance was found to become independent of the feed pressure at pressures over 5 atm, and the permeance value was reported to be 200 GPU. On the contrary, for a long module (active length of 87 cm), the permeance was reported to increase with an increase in the feed pressure. The permeance increased from 70 to 130 GPU when the pressure was increased from 2 atm to 20 atm (Kumazawa et al., 1994). It is interesting that the permeance of flat membranes of

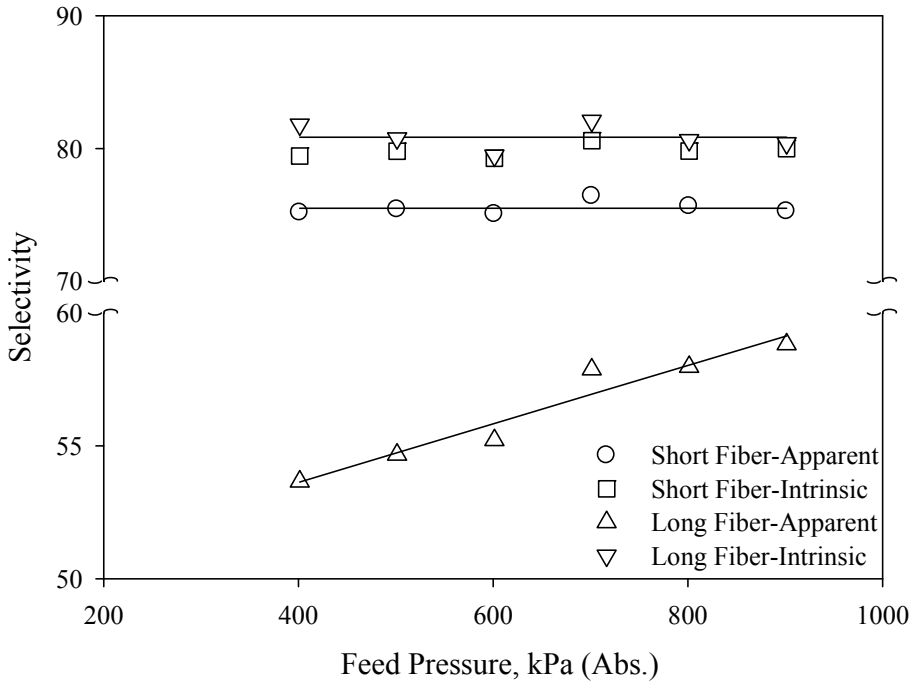

Fig. 5.6: Comparison of apparent and intrinsic selectivity of H_2/N_2 at different feed pressures.

Table 5.1: Measured pure gas permeances in different membrane modules.

Pure Gas	Membrane	Length, cm	D_o, μm	D_i,μm	Permeance, GPU	Reference
He	Cellulose Triacetate	87 21	191 191	88 88	70-130 200	(Kumazawa et al., 1994)
He	Sillica	-	45	35	19.7-98.5	(Hassan et al., 1995)
He	Cellulose Acetate	50	230	84	23	(Sengupta and Sirkar, 1987)
H_2	Polyimide	100	400	-	100-105	(Peer et al., 2009)
CO_2	Polyimide	20	500	370	90-110	(Chenar et al., 2006)
CO_2	PPO	30	520	370	180-210	(Chenar et al., 2006)
CO_2	Cellulose Triacetate	26 22 20	156 148 184	63 56 91	61-120 45-88 40-77	(Sada et al., 1992)
CO_2	Sillica	-	45	35	0.59-1.97	(Hassan et al., 1995)
O_2 CH_4	Polysulfone Polysulfone	60 60	450 450	150 150	13.33-26.66 3.67-4.67	(Ettouney and Majeed, 1997)
N_2	Polysulfone	60	450	150	2.0-4.67	(Ettouney et al., 1998)

cellulose triacetate was found to be independent of the pressure, which suggests the pressure dependence of permeance for helium is not caused by the membrane material. It is certain that the reduction in the driving force is more at lower pressures, and the membrane performs close to its intrinsic performance if operated at higher pressures. The pressure dependence of permeance for faster permeating gases such as helium and hydrogen in hollow fiber membrane modules were also reported by Wang et al. (1995), Hassan et al. (1995) and Peer et al. (2009). A 400% increase in Helium permeance was reported by Hassan et al. (1995) for fine hollow fibers at high pressures.

It has been reported that pure gas permeance of CO_2 increases with the feed pressure and the increasing trend of CO_2 permeance with pressure is due to plasticization effect (Chenar et al., 2006; Omole et al., 2010; Visser et al., 2005). Sada et al. (1992) observed permeance of CO_2 increases with increasing pressure difference for cellulose triacetate based asymmetric hollow fiber membranes. The dimension of the membrane modules has been provided in Table 5.1. In order to find out whether the above-mentioned pressure dependence is caused by the membrane material (cellulose triacetate) or just by module geometry, permeability coefficient for CO_2 through a flat homogeneous membrane of cellulose triacetate (thickness 50 μm) was measured, and the permeability coefficient of CO_2 was found to increase with an increase in the pressure difference. This result conforms to the permeation results of the hollow fiber membrane module. However, we calculated the percentage increases in CO_2 permeance for both module geometries and they are plotted in Figure 5.7. It is found that percentage increase in CO_2 permeance for flat homogeneous membrane is comparable with that of the hollow fiber geometry at low pressures. It was expected that percentage increase in CO_2 permeance with pressure for both module geometry would be comparable. However, the percentage increase in CO_2 permeance in hollow fibers was higher than the flat homogeneous membrane at high pressures. The discrepancy may be due to reduced effect of pressure build-up on the apparent permeance for hollow fibers at high pressures.

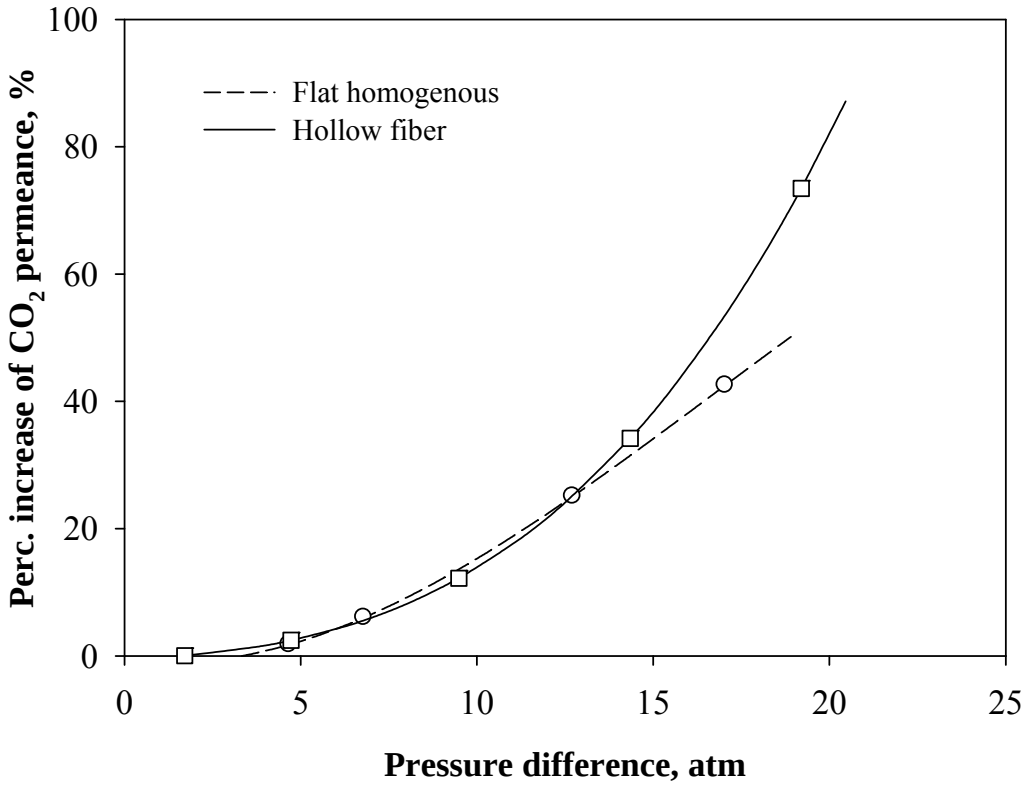

Fig. 5.7: Percentage increase of CO_2 permeance with pressure differences for cellulose triacetate based flat homogeneous and hollow fiber membrane (Sada et al., 1992).

It has been reported that pure gas permeances for moderate to slow permeating gases (O_2, CH_4 and N_2) remain constant over a certain feed pressure range for both hollow fibers and flat homogeneous membranes of some glassy polymers (Du et al., 2007; Haraya et al., 1989; Hughes and Jiang, 1995; Lee et al., 2000; Peer et al., 2009). However, Ettouney and Majeed (1997) observed that pure gas permeance of O_2 and CH_4 slightly increases with feed pressure for polysulfone hollow fibers. Ettouney et al. (1998) also observed that the permeance of pure N_2 slightly increases as feed pressure increases for polysulfone hollow fibers. However, the permeances of these gases were found essentially constant in case of flat homogeneous membrane (Haraya and Hwang, 1992; Ilconich et al., 2003; Lee et al., 2000; Pfromm et al., 1993). This suggests that effect of permeate pressure build-up could be significant for slower permeating gases too and the membrane will

perform close to its intrinsic properties at high pressures due to minimization of pressure build-up effect.

To further investigate the pressure build-up effect, we analytically calculated the average loss in driving force due to pressure build-up inside the fiber lumen for pure gas permeation of H_2 at different pressures. The percentage loss in the driving force at different pressures was also calculated using Eqn. 5.4.

$$\text{Perc. loss in the driving force} = \frac{\text{total pressure drop (integrated)}}{\text{feed inlet pressure - permeate exit pressure}} \times 100\% \qquad (5.4)$$

The active length of the fiber, inside diameter and permeance were varied independently for this parametric analysis. It was observed that average loss in the driving force due to pressure build-up is higher with a longer fiber (Figure 5.8a), with a smaller fiber diameter (Figure 5.9a) and higher permeability (Figure 5.10a). However, it was also observed that the percentage loss in driving force is higher at low pressures and the percentage loss of driving force reduces at higher pressures (Figures 5.8b, 5.9b and 5.10b). It infers that though pressure build-up increases at higher pressures, the effect of pressure build-up on membrane performance reduces at higher pressures. Since the percentage loss in driving force is high at lower pressures, the deviation of apparent permeance of H_2 from intrinsic permeance was found larger at low feed pressures.

It is difficult to measure the internal diameter precisely since the fibers are not perfectly circular at the open end, and the diameter varies to some extent from one fiber to another. Since the internal diameter appears as power of four in Hagen-Poiseuille equation, even a small variation in the internal diameter will affect the calculated permeances greatly. The calculation was carried out using various internal diameters for all feed pressures and the value of internal diameter that gives constant permeance with respect to the feed pressure can be considered the accurate fiber diameter. It was found that when an internal diameter of 80 μm was used, the permeance was constant with respect to feed pressure (Figure 5.11). The permeance thus measured was considered the intrinsic permeance, since the permeance is an intrinsic property of membrane and is not a function of feed pressures.

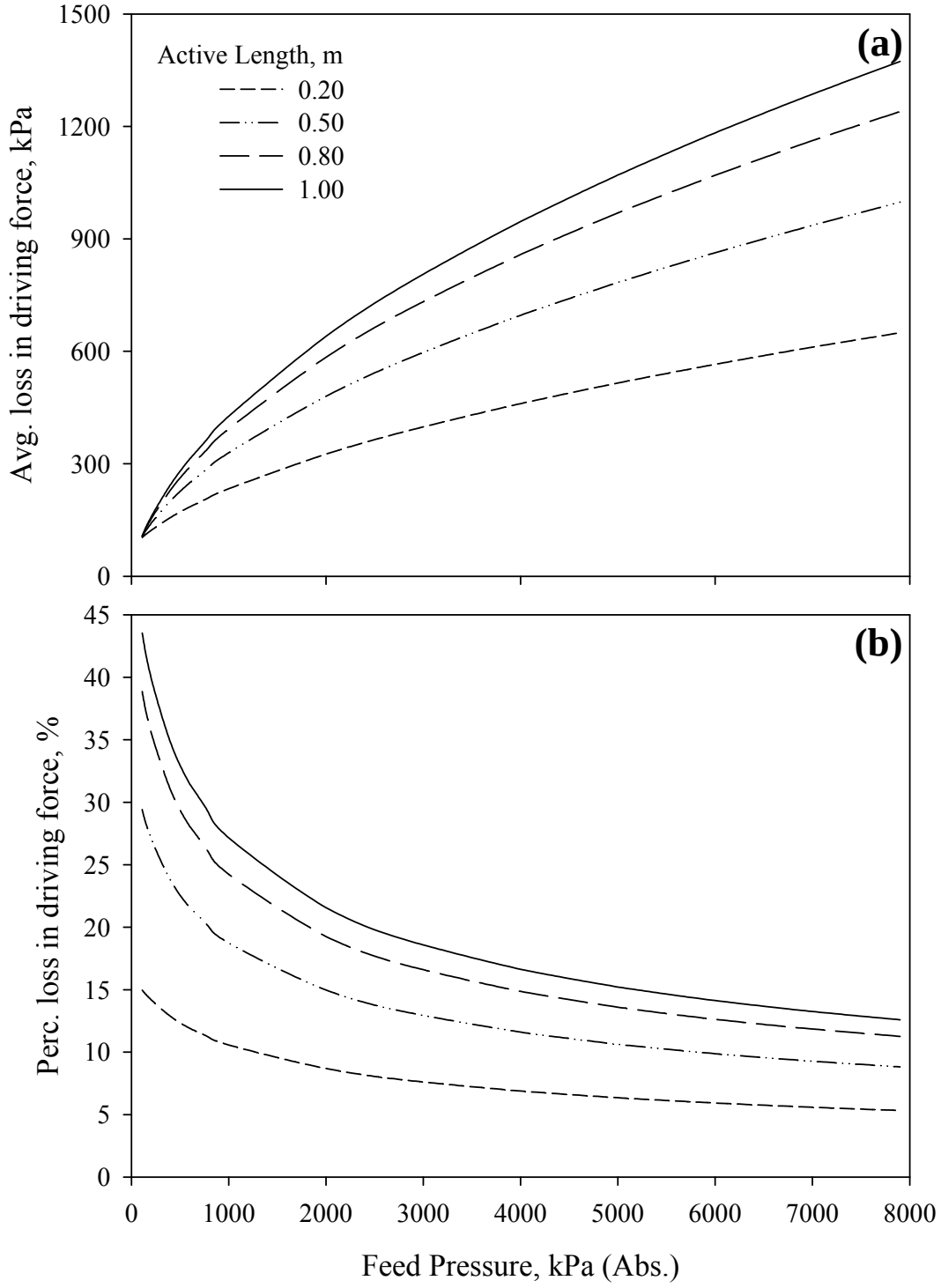

Fig. 5.8: (a) The average loss in driving force, and (b) percentage loss in driving force with the feed pressures at different active length.

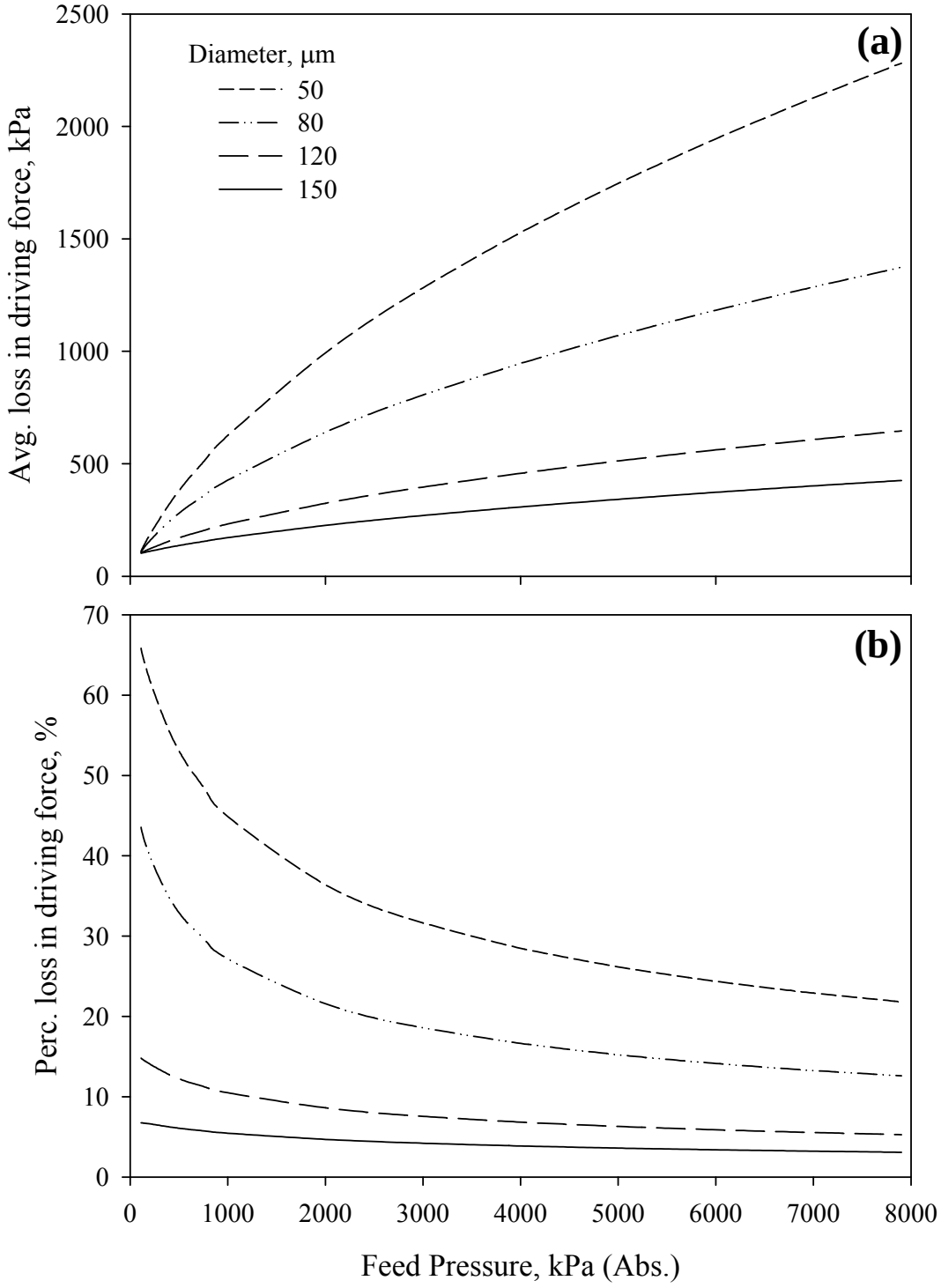

Fig. 5.9: (a) The average loss in driving force, and (b) percentage loss in driving force with the feed pressures at different fiber inside diameter.

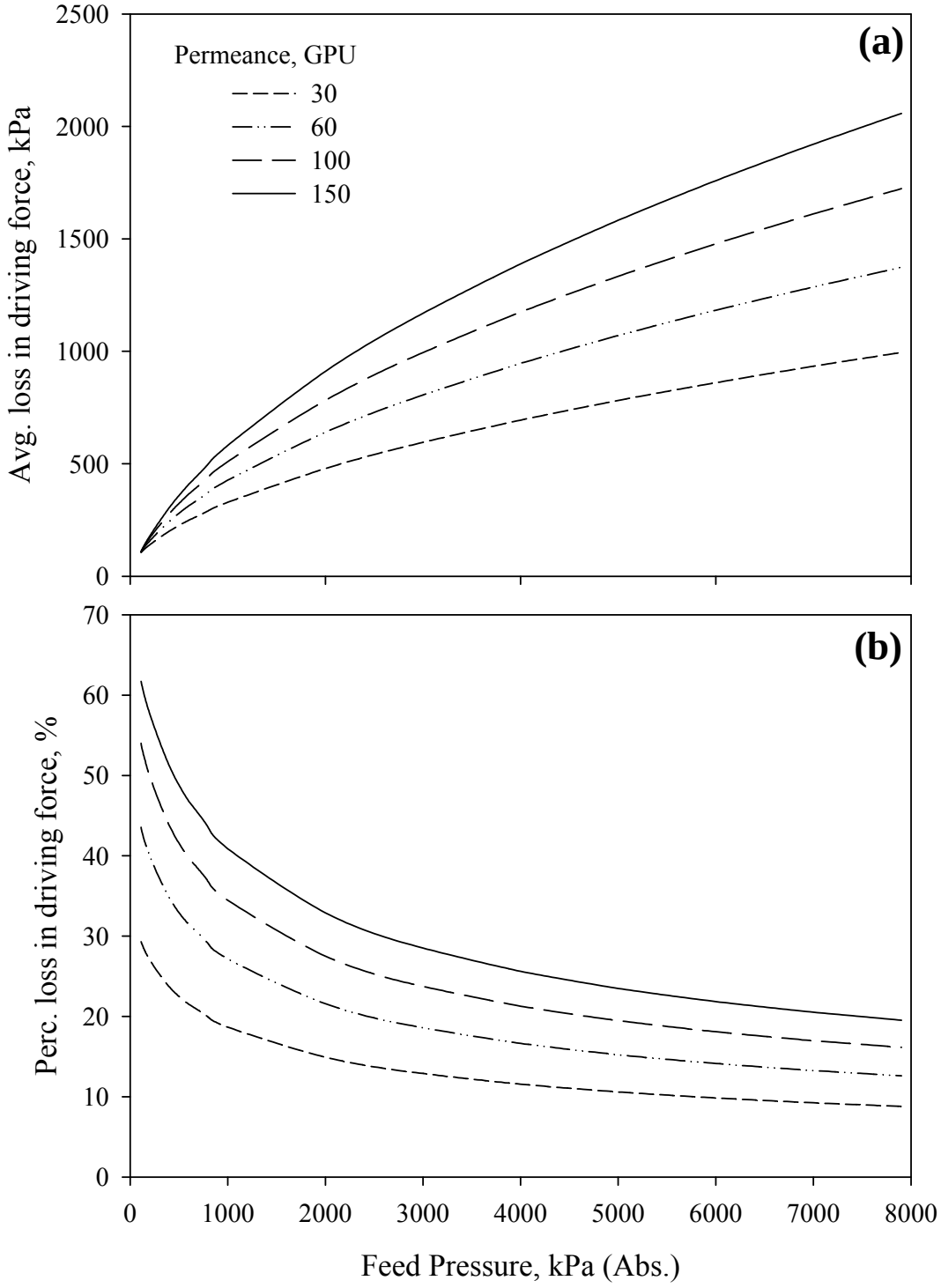

Fig. 5.10: (a) The average loss in driving force, and (b) percentage loss in driving force with the feed pressures at different permeances.

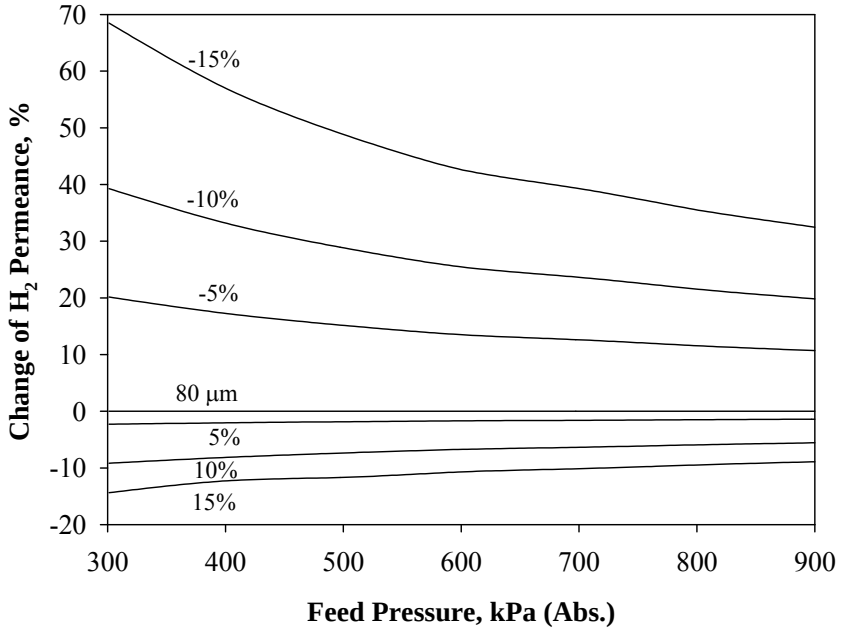

Fig. 5.11: Percentage change of H_2 permeance with percentage change in inside diameter at different feed pressures.

An internal diameter of 80 μm was considered the nominal inside diameter of the hollow fibers, which was otherwise difficult to measure due to inconsistent shape of the fiber. Figure 5.11 represents the percentage change of H_2 permeance with percentage change in inside diameter at different feed pressures, considering internal diameter of 80 μm as the basis for comparison. It is also apparent from Figure 5.11 that effect of pressure build-up maximizes at low feed pressures.

Figure 5.12 shows a comparison of H_2 permeance as a function of stage cut calculated as an unknown parameter from the mathematical model of binary mixed-gas membrane permeator, pure gas intrinsic permeance, and permeance calculated by the approximation methods previously developed (Lababidi et al., 1996). The approximation methods underestimated permeance values as they do not consider the effect of pressure build-up in the fiber lumen. The mixed gas permeances and pure gas intrinsic permeances were found comparable at low stage cuts as shown in Table 5.2. However, the mixed gas

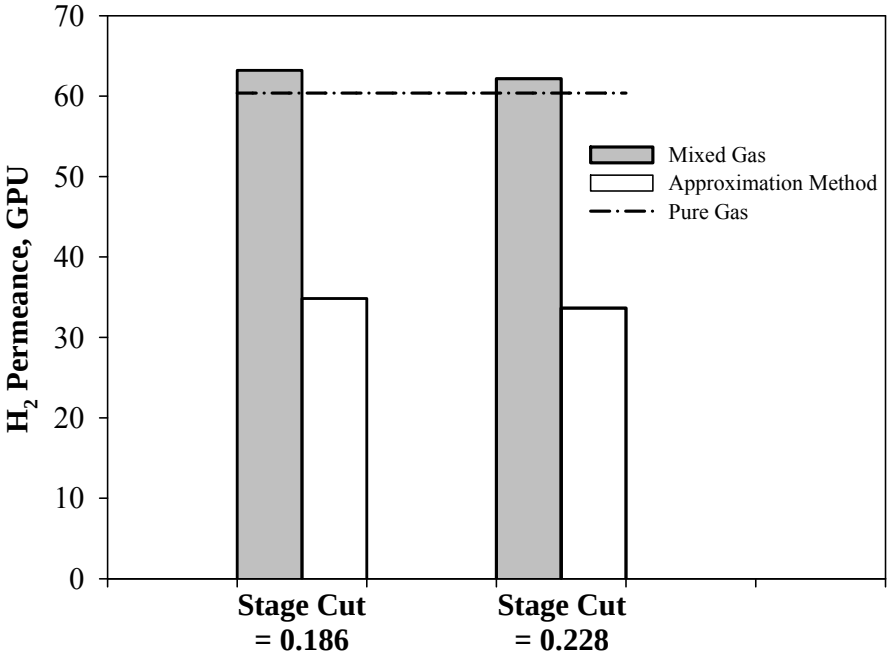

Fig. 5.12: A comparison of H_2 permeance from pure gas experiments, mixed gas experiments and approximation methods as a function of stage cut.

permeance deviated significantly from that of the pure gas intrinsic permeance at higher stage cuts. The reason may be due to concentration polarization and competitive sorption which come into play at higher stage cuts, but are negligible at low stage cuts (Wang et al., 2002). Sample computer programs have been provided in Appendix C for perusal.

Table 5.2: Comparison of H_2 permeance at different methods.

Stage cut	H_2 permeance, GPU		
	Pure gas analysis	Mixed gas analysis	Approximation method
0.186	60.4	63.2	34.8
0.228	60.4	62.8	33.6

5.4 Conclusions

The permeate pressure build-up in fiber lumen plays an important role in characterizing true separation properties of hollow fiber membranes. The deviation

between intrinsic and apparent permeances of H_2 for the long module was found larger at low feed pressures than at high feed pressures, which infers that the effect of pressure build-up maximizes at low feed pressures. On the other hand, the effect of pressure build-up minimizes at high feed pressures as the apparent permeance of H_2 for long fiber tends to approach that of the intrinsic permeance at high feed pressures. It implies that membrane performs close to its intrinsic separation properties if operated at high feed pressures. The observations were also supported by some of the pure gas permeation experiments reported in literature, which were inadvertently overlooked. The average loss and percentage loss in the driving force due to pressure build-up were estimated to support our reasoning. It was found that the percentage loss in the driving force decays at high pressures. Although the average loss in driving force is more at higher pressures, the effect of pressure build-up or equivocally the percentage loss in driving force minimizes at higher pressures. The inside diameter in the Hagen-Poiseuille equation was carefully adjusted to determine the nominal fiber inside diameter, which was otherwise difficult to determine due to inconsistent shape of the fiber. It was also found that intrinsic permeance evaluated here represents true separation performance compared to approximation methods.

Chapter 6

Application of unsteady state cyclic pressure-vacuum swing permeation for CO_2 separation from flue gas[†]

6.1 Introduction

Conventional membrane gas separation is operated in a steady-state fashion where both the feed pressure and the permeate pressure are maintained at constant levels, and the permeation rate and permeate concentration do not change with time, except at the initial start-up stage (Wang et al., 2011). The advantages with steady-state operation include easy start-up and shout-down, simplicity of pressure and flow controls, large throughput of permeation, and low maintenance requirements. Since transmembrane pressure difference is the driving force for permeation, the most efficient way to enhance permeation is to increase the pressure difference across the membrane. The pressure differential across the membrane can be enhanced by feed pressurization or permeate evacuation. Further enhancement is possible if both feed pressurization and permeate evacuation are employed together. However, simultaneous use of a compressor and a vacuum pump to increase the transmembrane pressure difference is normally not considered rewarding, especially with "deep" vacuum on the permeate side to suck the permeate.

Membrane gas separations under transient state conditions are rather unexplored. Enhanced separation as compared to steady-state operation was reported using unsteady state permeation (Beckman et al., 1991; Higuchi and Nakagawa, 1989; Paul, 1971). The solution-diffusion mechanism states that the permeability coefficient can be considered to be equal to the product of solubility coefficient and diffusion coefficient (Baker 2004, Nunes and Peinemann, 2006). Unfortunately, a trade-off relationship between the permeability and selectivity often exists for most membrane materials. An upper bound appears in permeability vs. selectivity plot above which virtually no data exist (Robeson, 1991). This suggests that once the membrane material is fixed, the selectivity characteristics are essentially fixed if a steady-state operation is used. However, transient

[†] Part of Chapter 6 will be submitted shortly for publication

and, in particular, steady cyclic operation of the membrane can be used to alter the selectivity characteristics. The first theoretical study dedicated to a membrane separation process operating in a cyclic transient fashion was performed by Paul in 1971 to improve the separation when the mobility selectivity is significantly greater than permselectivity (Paul, 1971). Transient permeation occurs due to diffusion upon admission of a feed gas to the membrane, and the permeation rate responds to diffusivity and solubility somewhat more independently. The feed is admitted intermittently at appropriate time intervals such that the difference in the desorption fallout rates due to the difference in the permeant diffusivity can be exploited to effect the separation. Corriou et al. (2008) reported that cyclic operation could potentially compete with the most selective polymers available to date, both in terms of selectivity and productivity.

Higuchi and Nakagawa (1989) theoretically studied transient permeation with pulse upstream pressure as suggested by Paul (Paul, 1971) for air separation to illustrate the improvement in selectivity over steady-state operation. Beckman et al. (1991, 1993) carried out a dynamic process with intermittent feed admission on a continuous basis to exemplify the pulse feeding process for He/CO_2 separation. The permeate and residue were removed periodically and they were synchronized with the feed admission sequence. It was reported that since the permeate product is collected for a fraction of the time interval, a significant reduction in the membrane throughput occurs when compared to steady-state permeation. It was estimated that the time interval for the upstream pressure pulse to operate in a transient permeation scheme with the current generation of polymeric membranes (gas diffusivities of the order of 10^{-8} cm^2/s) would be of the order of 10^{-5} to 10^{-3} s, which is clearly not acceptable as the cycle frequency is too fast to be handled by switching valves for any practical applications (Beckman et al., 1991; Higuchi and Nakagawa, 1989; Koros and Chern, 1987; Koros and Fleming, 1993). However, Corriou et al. (2008) optimized Paul's (Paul, 1971) mode of operation and claimed that synchronous operation would offer the best performances.

Kao et al. (1991) reported a pressure swing scheme similar to pressure swing adsorption to carry out transient permeation where the opposite solubility and diffusivity

selectivities were exploited synergistically. LaPack and Dupuis (1994) modified the process to exploit the differences in the rates of either attainment of steady-state permeation or fall-off from steady-state permeation. Ueda et al. (1990) reported a cyclic process comprising of the steps of feed pressurization and permeates evacuation using a compressor and a vacuum pump separately or using a single pump suitable for both pressurization and suction. It was reported that due to limited adsorptive capacity of current polymeric membranes, the transient permeation processes based on solubility or diffusivity difference for gas separation are unlikely to be practical unless suitable membranes with sufficient adsorption capacities comparable to the adsorbent used in pressure swing adsorption are available. Bowser (2004) and Nemser (2005) extended the application of the cyclic process for controlling emissions of volatile organic compounds (VOC) from solvent storage.

Feng et al. (2000) reported a novel process for gas separation called pressure swing permeation, and a bench-scale unit was tested for H_2/N_2 separation to demonstrate the effectiveness of the process. The relatively low permeate pressure was elevated by periodically "pushing" the permeate with the high pressure feed gas, producing a permeate stream at a pressure as high as the feed pressure, which is otherwise impossible to achieve with conventional steady-state permeation. Feng and Lawless (2012) recently filed a patent of unsteady state pressure-vacuum swing process to accomplish feed pressurization and permeate evacuation with a single pump, thereby enhancing the transmembrane driving force for permeation. The pressures of the feed and the permeate stream were elevated and lowered, respectively, using the same pump in a dynamic fashion without the need of operating a compressor and a vacuum pump simultaneously. The separation is still based on selective permeability of the membrane; however, the enhanced separation is due to the increase in the transmembrane pressure differential for permeation and the feed to permeate pressure ratio. In this study, the theoretical aspects of that novel dynamic process (Feng and Lawless, 2012) were considered, and a parametric analysis was conducted to elucidate the working principle. The simulation strategy and solution scheme of such dynamic process were explained too. CO_2 separation for greenhouse gas emission control was used as a model application to exemplify the feasibility and effectiveness of this process.

6.2 Operating cycle of pressure-vacuum swing permeation assisted with a single pump

As illustrated in Figure 6.1, the pressure-vacuum swing permeation undergoes sequential steps of feed pressurization, permeate evacuation, and residue venting. A cycle

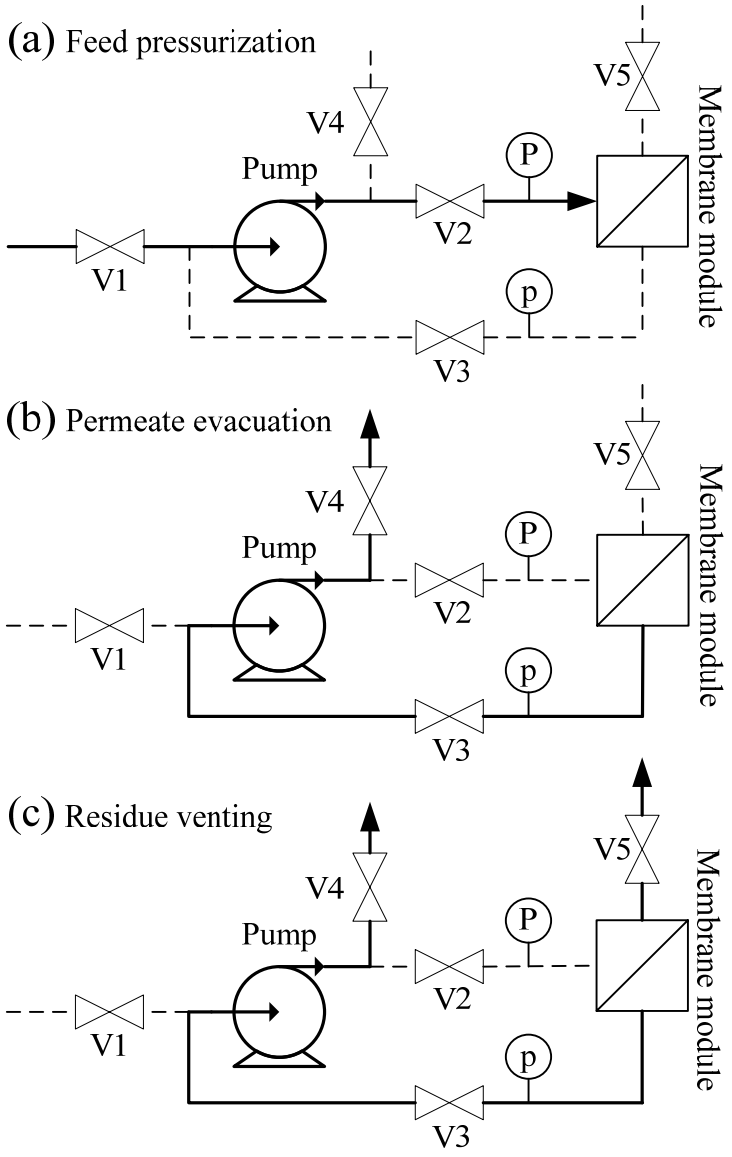

Fig. 6.1: Pressure-vacuum swing permeation assisted by a single pump, $V_{1\sim5}$ switching valves, *P* pressure on feed side, *p* pressure on the permeate side.

can be divided into 5 operating steps, and the schematic of pressure variations (on the feed and permeate sides) with time are shown in Figure 6.2. Step 1 (time t_0 to t_1) is referred to as the "feed pressurization" step. The feed side (volume V_F) is quickly charged with a pressurized gas by using a pump (which functions as a compressor) to reach a pressure of $P_1 = P_h$, and permeation begins to occur under the transmembrane pressure difference. In Step 2 (time t_1 to t_2), the feed is supplied continuously to maintain a constant pressure P_h on the feed side. The pressure on the permeate side gradually increases as soon as the permeation occurs due to accumulation of the permeate. During this step, referred to as the "feed admission/permeation" step (Step 2), the driving force for permeation decreases with time. Step 2 is terminated when the permeate pressure reaches a certain level (preferably 1 atm) at time t_2. Feed admission is stopped as the permeate pressure reaches the prior set level. Step 3 (time t_2 to t_3) is mainly to switch the pump from compression to evacuation,

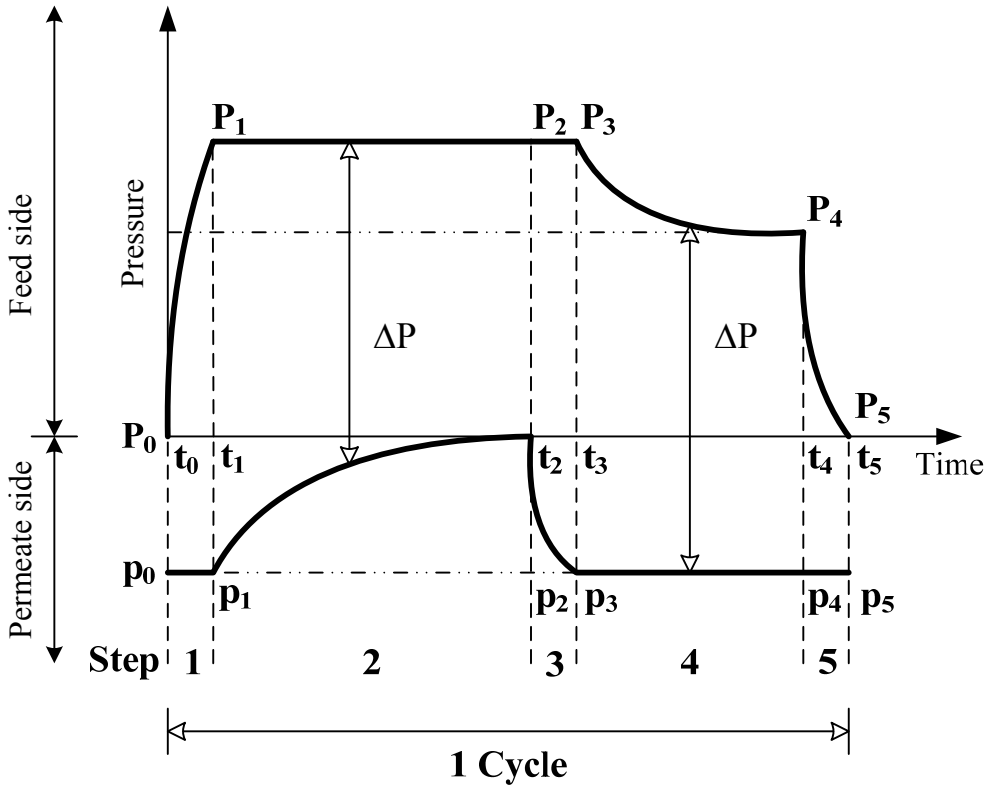

Fig. 6.2: Pressure profile illustrating the pressure variations during various steps of the process.

and to provide a boost to the transmembrane pressure difference. At this time, the pump is switched to function as a vacuum pump to suck the accumulated permeate for withdrawal and collection, and thus the permeate pressure quickly drops to a lower level p_v. It occurs rapidly such that the feed side pressures at the end of Step 2 and at the beginning of Step 3 are comparable i.e., $P_3 \approx P_2$. During Step 4 (time t_3 to t_4), which is called the "permeation/permeate evacuation" step, the permeate evacuation continues while maintaining a low pressure p_v, and the permeate is continuously withdrawn and collected. At this step, the pressure on the feed side begins to decrease because of the permeation. Thus at time t_4 when the pressure on the feed side is sufficiently low that the permeation is no longer effective for gas separation or when the concentration of the residue has reached its target value required for the residue product, the residue is vented off and collected at pressure P_0. This step, from time t_4 to t_5, is called "residue venting" (Step 5). These sequential operating steps, which represent one cycle of the pressure-vacuum swing permeation, are repeated to accomplish gas separation continuously but in a cyclic fashion. Clearly, Steps 2 and 4 (especially Step 4) are primarily responsible for separation. Steps 1, 3 and 5 are assumed to complete very quickly, and for the sake of simplicity the times taken in these steps are neglected in the formulation of mathematical equations and in subsequent parametric studies.

A relatively high transmembrane pressure difference (P - p) can be achieved by exploiting the advantage of feed pressurization and permeate evacuation during the process. The enhanced transmembrane pressure difference, i.e., the relatively high driving force for permeation, leads to an increased productivity. Moreover, the degree of enrichment is also a function of the feed (P) to permeate pressure (p) ratio, and a high (P/p) pressure ratio obtained by using both the permeate evacuation and feed pressurization (which can be accomplished by using a single pump) enhances gas separation. It may be pointed out that in the pressure-vacuum swing permeation assisted with a single pump, diaphragm pumps or other commonly used positive displacement pumps are well equipped to handle both compression and evacuation. The swing permeation process appears to be particularly suitable for low pressure niche applications, i.e., applications that operate

preferably at low to moderate feed pressures as air separation for oxygen enrichment or flue gas separation for CO_2 capture.

6.3 Analysis of the permeation behaviour

The assumptions to formulate the mathematical equations are as follows:

- Ideal gas behaviour.
- Isothermal operation.
- The time lag of permeation due to transient transmission of gas molecules through the membrane is negligible. The permeate is thus assumed to be received on the permeate side as soon as permeation takes place.
- The permselectivity of the membrane is independent of gas composition and pressure.
- The membrane permeability during the cyclic operation is the same as that at steady-state.
- The gas on the feed side is perfectly mixed, that is, the concentration on the membrane surface is the same as the bulk concentration of the teed.
- On the permeate side, there is no back diffusion from the bulk permeate to the membrane surface.

6.3.1 Step 1: Feed pressurization

The feed pressurization step is usually very short, and the permeation can be considered negligible in this step. The feed gas with a known concentration X_F (mole fraction of faster permeating component, i.e., CO_2 in flue gas separation) is quickly admitted to the feed side of the membrane system (with a volume of V_F) to reach a total pressure of P_1. The feed side initially contains a portion of the residue gas (at a pressure of P_0 and with a concentration of X_0) left from the previous cycle of operation. The concentration of the gas mixture on the feed side at time t_1 is calculated from material balance:

$$X_1 = X_F + \frac{P_0}{P_1}(X_0 - X_1) \tag{6.1}$$

Where, $X_0 = X_4$. For flue gas separation, the residue venting occurs conveniently at atmospheric pressure. For flue gas applications, P_0 = 101.3 kPa was used in our study.

6.3.2 Step 2: Feed admission/permeation

Consider a permeation system shown in Figure 6.3a that is relevant to this step (from time t_1 to t_2) of the cyclic pressure-vacuum swing process. The feed gas is continuously supplied to maintain a constant pressure of $P_1 = P_h$ without removing any retentate on the feed side. Permeation takes place in a fashion similar to the "dead end" permeation, and the permeate is accumulated at the permeate side. For the separation of a binary gas mixture, the permeation rate at a given instant can be written as

$$\frac{dQ_A}{dt} = J_A A(PX - pY) \tag{6.2}$$

$$\frac{dQ_B}{dt} = J_B A[P(1-X) - p(1-Y)] \tag{6.3}$$

where Q is the quantity of the permeate, J is the gas permeance of the membrane, and A is the membrane area for permeation. The subscripts A and B represent the fast and slow

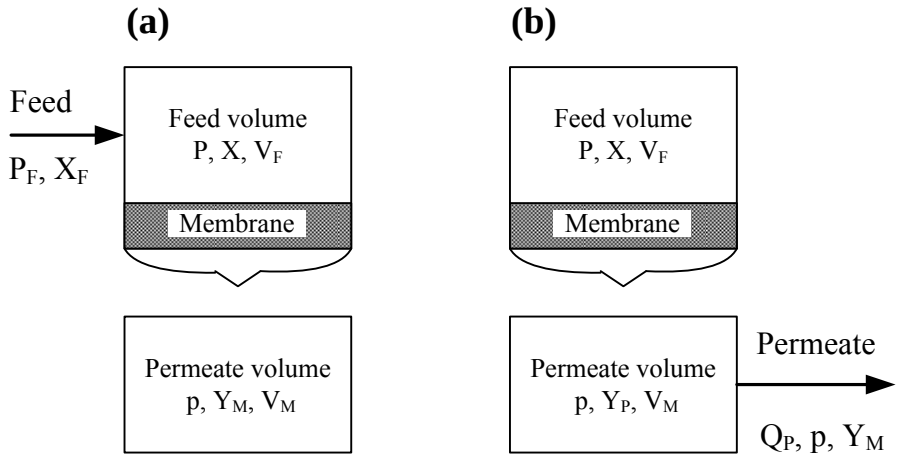

Fig. 6.3: (a) Permeation system with constant feed pressure and varying permeate pressure, (b) Permeation system during permeate evacuation step.

permeating components of a binary gas mixture, respectively. X is the gas concentration on the feed side feed, and Y is the concentration of permeate on the membrane surface; both quantities are expressed in terms of mole fractions of the fast permeating component. The local concentration of permeate leaving the membrane surface is determined by the relative permeation rates of the two permeating components. This is especially the case for asymmetric membranes where the microporous substrate prevents local mixing. Thus, Y can be calculated by

$$Y = \left(\frac{dQ_A}{dt}\right) \Big/ \left(\frac{dQ_A}{dt} + \frac{dQ_B}{dt}\right) \tag{6.4}$$

Since a constant pressure is maintained on the feed side and no residue is withdrawn during permeation, the molar flow rate of gas fed to the feed side of the permeator is equal to the molar permeation rate. On the basis of materials balance, the gas concentration on the feed side X at a given instant is related to X_1 and X_F by

$$X = \frac{(PV_F/RT)X_1 + (Q_A + Q_B)X_F - Q_A}{(PV_F/RT)} \tag{6.5}$$

The bulk concentration of the permeate, Y_M, is determined by the overall quantity of the gases accumulated and is given by

$$Y_M = \frac{Q_A + (P_V V_M Y_{M1}/RT)}{Q_A + Q_B + (P_V V_M/RT)} \tag{6.6}$$

Where V_M is the volume on the permeate side, P_V is the permeate pressure when the permeate side is evacuated, and Y_{M1} is the concentration of the residual permeate retained from previous step ($Y_{M1} = Y_{M0} = Y_{M4}$). When the vacuum level is sufficiently high, the amount of the residual permeate left from the previous step is negligible and Y_M, can thus be simplified as

$$Y_M = \frac{Q_A}{Q_A + Q_B} \tag{6.7}$$

The pressure change with time on the permeate side is related to the permeation rate by

$$\frac{dp}{dt} = \left(\frac{dQ_A}{dt} + \frac{dQ_B}{dt}\right)\frac{RT}{V_M} \tag{6.8}$$

Equations (6.2) to (6.8) constitute an initial value problem. The quantities p, X, Y, Q_A, Q_B and Y_M at any instant can be determined by solving these equations for a given set of initial conditions.

6.3.3 Step 3: Pump function switch from compression to evacuation

The pump mode is switched from feed compression to permeate evacuation so that the pressure on the permeate side drops to p_v rapidly. The time for this step is very short and the permeation is neglected during this period.

6.3.4 Step 4: Permeation and permeate evacuation

During this step (from time t_3 to t_4) the feed admission is stopped, and the permeate is continuously evacuated. As a result, the pressure on the residue side gradually decreases due to gas permeation through the membrane, while the permeate side retains a constant pressure of p_v, considering a permeation system shown in Figure 6.3b, the pressure change on the feed side is related to the permeation rate by

$$\frac{dp}{dt} = -\left(\frac{dQ_A}{dt} + \frac{dQ_B}{dt}\right)\frac{RT}{V_F} \tag{6.9}$$

where the permeation rates dQ_A/dt and dQ_B/dt can be described by Eqns (6.2) and (6.3), respectively. Since no residue is withdrawn and no fresh feed is supplied during permeation, the quantity of an individual gas component on the feed side decreases at the same rate at which it permeates through the membrane. In addition, the removal rate of the permeate from the permeator is the same as the overall permeation rate. Based on materials balance, the following equations can be obtained

$$X = \frac{(P_3 V_F / RT) X_3 - Q_A}{(P_3 V_F / RT)} \tag{6.10}$$

$$\frac{dQ_P}{dt} = \frac{dQ_A}{dt} + \frac{dQ_B}{dt} \tag{6.11}$$

$$Y_P = \frac{Q_{PA}}{Q_P} = \frac{Q_{PA}}{Q_A + Q_B} \tag{6.12}$$

$$\frac{dQ_{PA}}{dt} = \frac{dQ_P}{dt} Y_M \tag{6.13}$$

$$Y_M = \frac{Q_A + (p_V V_M Y_{M3}/RT) - Q_{PA}}{(p_V V_M/RT)} \tag{6.14}$$

where Q_P represents the quantity of permeate withdrawn and collected during this step. The values of X_3 and Y_{M3} are assumed to be equal to X_2 and Y_{M2}, respectively, which have been calculated in Step 2.

6.3.5 Step 5: Residue venting

In this step, the gas on the residue side, which is enriched with slower permeating component, is vented for release, and its pressure quickly decreases.

6.4 Application of pressure-vacuum swing permeation to flue gas separation

The following properties with respect to asymmetric cellulose acetate hollow fiber membranes and operating conditions were chosen for parametric analysis:

CO_2 permeance: $J_A = 63.6\times10^{-10}$ mol/(m^2. s. Pa), or 19.0 GPU

CO_2/N_2 selectivity: $(J_A/J_B) = 20.9$

Membrane area: $A = 100$ m^2

Permeator volume occupied by permeate: $V_M = 0.01$, 0.02, and 0.05 m^3

Target value of CO_2 concentration in permeate: $Y_{M4} = 0.60$

Temperature: $T = 298$ K

The above numerical values of the membrane area and permeate volume were chosen based on the typical membrane areas packing densities of hollow fiber modules. With typical fiber dimensions, the membrane area per module volume is in the range of 6,000-13,000 m^2/m^3. Moreover, the shell side void volume is close to the tube side void volume for standard operation (Feng et al., 2000), that is $V_F = V_M$. However, when hollow fiber modules are used, an additional external vessel may be used on either the feed or permeate side for gas storage in order to slow down depletion of faster permeating component on the

feed side or to slow down the pressure build-up on the permeate side. An equal volume of V_F and V_M are used in the calculations unless otherwise specified.

Figures 6.4-6.7 show the sensitivity analysis of all the associated variables of pressure-vacuum swing permeation process for CO_2 removal from flue gas. A base case configuration (shown as solid lines in the figures 6.4-6.7) has been considered where feed pressure P_1 = 810.6 kPa, membrane area per module volume (A/V) = 5000 m^2/m^3, permeate pressure when the permeate side is evacuated p_v = 1.33 kPa, and feed to permeate volume ratio (V_F/V_M) = 1.0. Figures 6.4a, b and c show the instantaneous permeate pressure, permeate composition and residue composition at different feed pressures (P_1) as a function of time for Step 2. As expected, as permeation proceeds with time, the residue is gradually depleted in CO_2, and the permeate pressure increases. Interestingly, the concentration of CO_2 in the permeate initially increases and then decreases. This is because the space for receiving the permeate is initially filled with residual permeate left from the previous step at a lower concentration. The accumulation of the "freshly" produced permeate, which is at a higher CO_2 concentration, will lead to an increase in the overall permeate CO_2 concentration However, as permeation continues, the transmembrane pressure difference gradually decreases due to build-up of permeate pressure, and the reduction in the driving force for CO_2 permeation will be more significant than the reduction in the driving force for nitrogen permeation. As a result, the concentration of CO_2 in the permeate leaving the membrane surface gradually decreases with time, causing a reduction in the bulk concentration of CO_2 in the permeate. Figures 6.4a, b and c also show that an increase in feed pressure P_1 tends to increase the CO_2 concentration in the permeate, indicating that a higher feed pressure favours CO_2 permeation. Since a fixed feed pressure is maintained, the molar permeation rate equals the feeding rate during the course of permeation. As a result, for a given amount of CO_2-enriched flue gas going to the permeate, an equal number of moles of flue gas is supplied at the feed side. As such, a higher feed pressure, which causes faster permeation, will result in a higher CO_2 concentration in the residue (as shown in Figure 6.4c). In the subsequent studies where the feed pressure is not a controlled variable, feed pressure P_1 = 810.6 kPa is used.

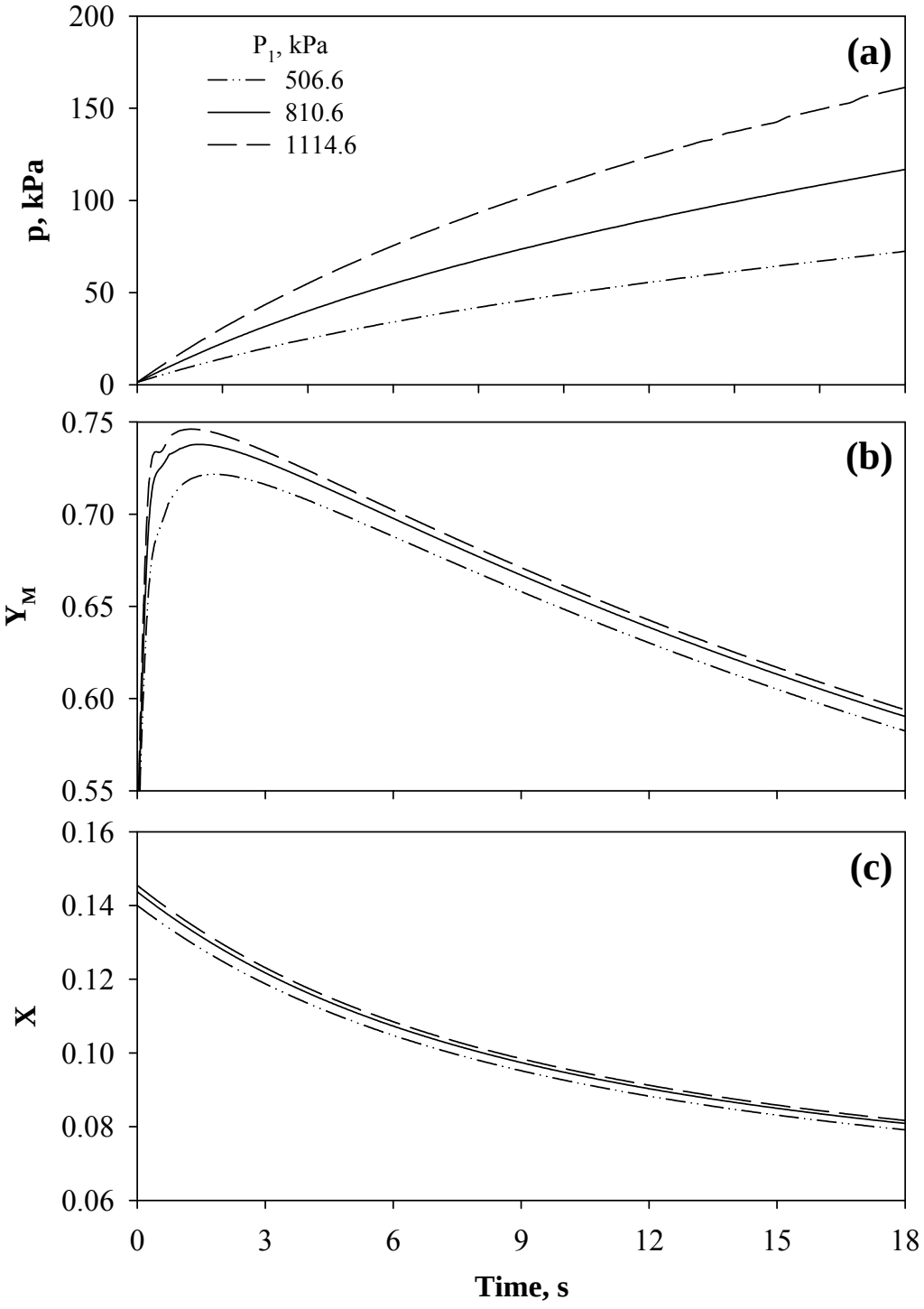

Fig. 6.4: Permeate pressure, permeate CO_2 concentration and residue CO_2 concentration at different pressures P_1 as a function of time for Step 2 of the pressure-vacuum swing permeation process. Other conditions p_V = 1.33 kPa, (V_F/V_M) = 1.0, and (A/V) = 5000 m^2/m^3.

Figures 6.5a, b and c illustrate the influence of the quantity (A/V) on the separation performance as a function of time for Step 2, where A is the membrane area and V is the volume of the permeator for feed or permeate "storage" (assuming V_F and V_M are the same and equal to V). Parameters A and V are independent, and they do not affect the separation behaviour as long as their ratio (A/V) is kept constant. The (A/V) ratio is thus used here as a single variable to show their combined effects on the separation performance. When other operating conditions remain unchanged, an increase in the (A/V) ratio will yield a higher permeate pressure (Figure 6.5a) and lower CO_2 concentration if the permeation time is sufficiently long (Figure 6.5b). However, the permeate concentration initially increases with an increase in (A/V), which is consistent with the earlier observation on the effects of feed pressure P_1. An increase in (A/V) means an increase in the membrane area packing density, which increases the overall permeation rate. It appears that as permeation proceeds, the higher the value of (A/V) is, the sooner the permeate CO_2 concentration reaches its maximum value. Unfortunately, the maximum permeate CO_2 concentration is attained within only a couple of seconds. It will be inappropriate to terminate this step when the maximum permeate concentration is reached; otherwise the cycle frequency of the pressure-vacuum swing process will be too fast for practical application. However, for a given membrane module, when the (A/V) ratio is too high based on the internal space of the permeator, an external gas tank may be used in order to attain a proper (A/V) value.

Figures 6.6a, b and c show that p_v, which is the permeate pressure when the permeate side is evacuated, has little effects on the separation performance during this process step (Step 2) if the permeation is allowed to last for more than 15 s. It suggests that the commonly used diaphragm vacuum/pressure pumps will be adequate for the pressure-vacuum swing permeation process because a moderate vacuum level will be adequate.

Figures 6.7a, b and c show the calculated results for Step 2 with different (V_F/V_M) values as a function of time for permeation over a period of 60 s. The ratio (V_F/V_M) represents the relative volumes occupied by the feed and permeate. During this step, the permeate pressure is set to an upper limit of atmospheric pressure (101.3 kPa), as the

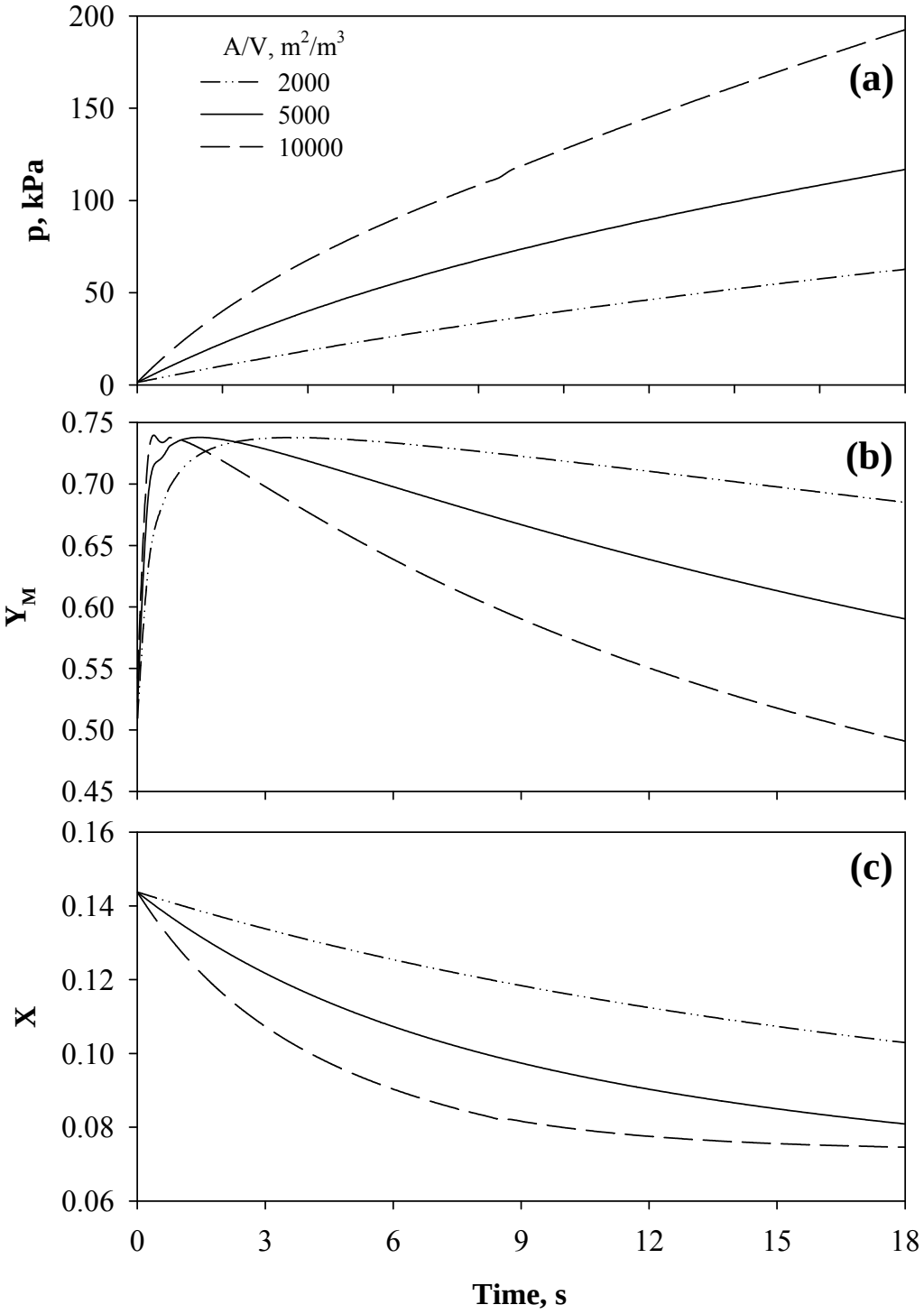

Fig. 6.5: Permeate pressure, permeate CO_2 concentration and residue CO_2 concentration at different (*A/V*) values as a function of time for Step 2 of the pressure-vacuum swing permeation process. Other conditions P_1 = 810.6 kPa, p_V = 1.33 kPa, and (V_F/V_M) = 1.0.

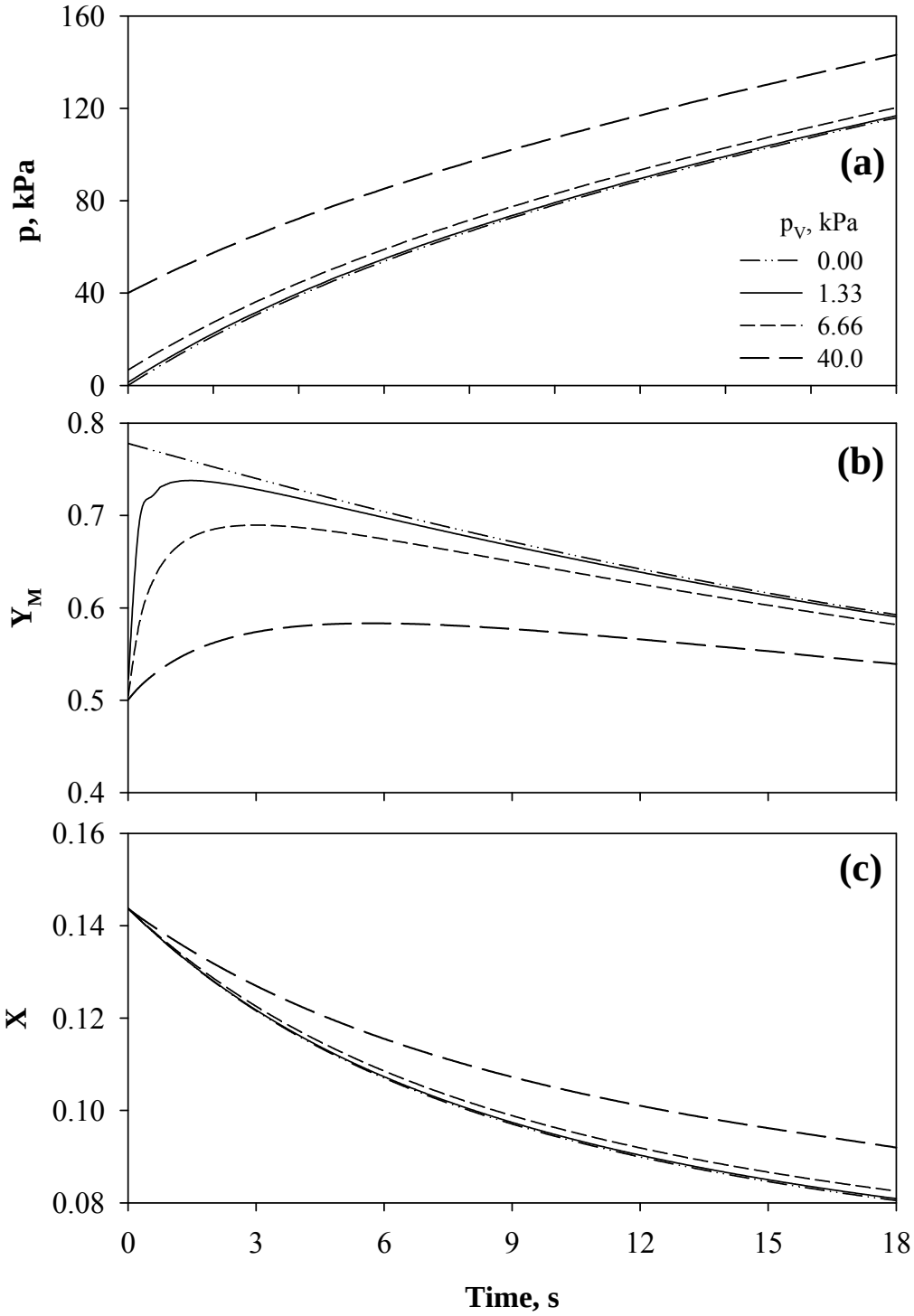

Fig. 6.6: Permeate pressure, permeate CO_2 concentration and residue CO_2 concentration at different p_V values as a function of time for Step 2 of the pressure-vacuum swing permeation process. Other conditions P_1 = 810.6 kPa, (V_F/V_M) = 1.0, and (A/V) = 5000 m^2/m^3.

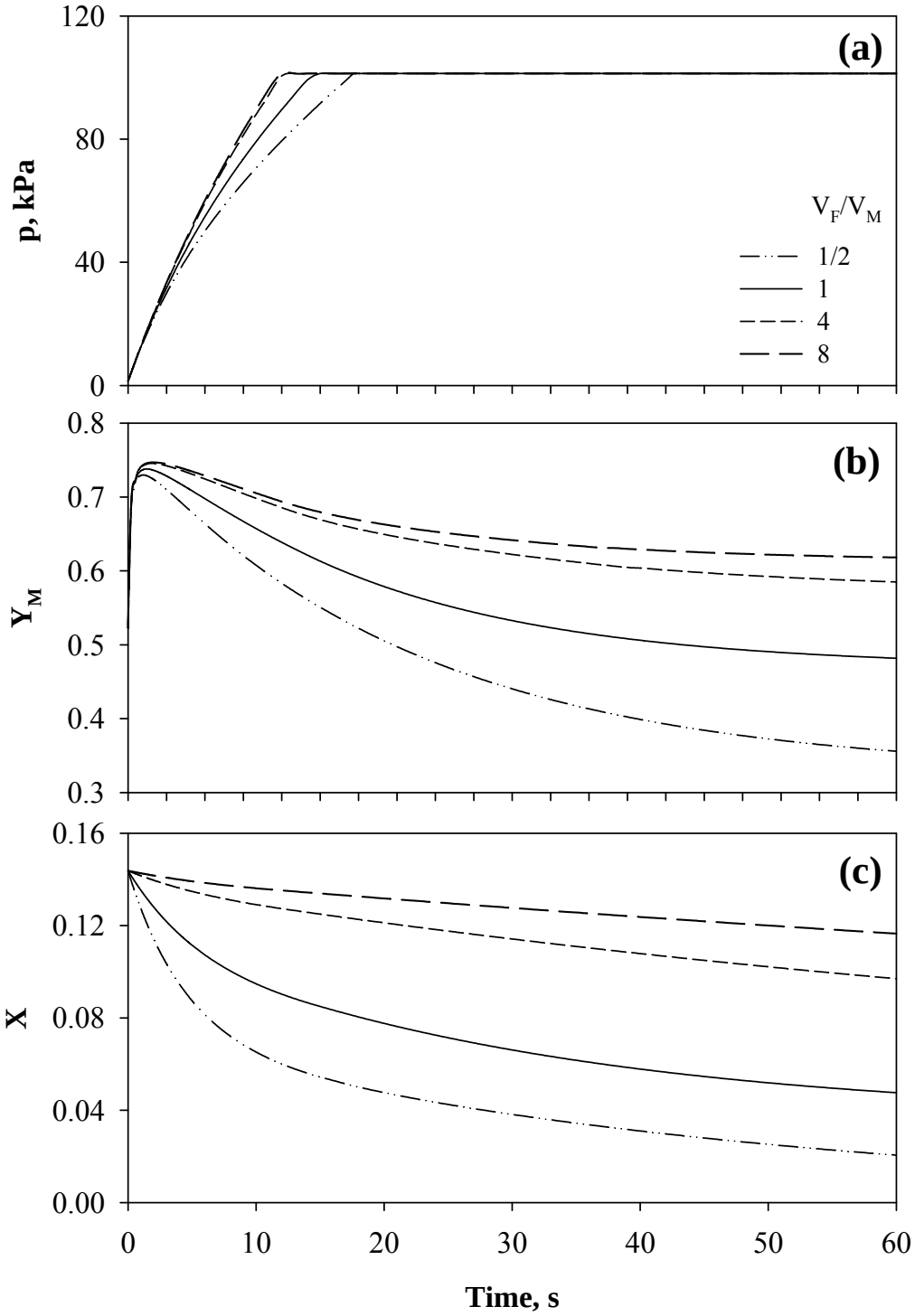

Fig. 6.7: Permeate pressure, permeate CO_2 concentration and residue CO_2 concentration at different (V_F/V_M) values as a function of time for Step 2 of the pressure-vacuum swing permeation process. Other conditions P_1 = 810.6 kPa, p_V = 1.33 kPa, and (A/V) = 5000 m^2/m^3.

permeate at such a pressure can be released readily by venting via a check valve. This will maximize the transmembrane pressure difference. As expected, at a given time, an increase in (V_F/V_M) will increase the concentrations of CO_2 in both the residue and permeate. A relatively large V_F means a large reservoir for the storage of feed gas, and thus the gas composition on the feed side will change less significantly because of the large amount of feed gas relative to the amount of gas permeated through the membrane. Therefore, a relatively high driving force for permeation can be sustained for a longer period of time, which favours the CO_2 concentration in the permeate. The permeate pressure, on the other hand, increases very marginally with an increase in (V_F/V_M), which is also favourable for CO_2 permeation. This can further be demonstrated by Figures 6.8a and b, which show the quantities of CO_2 and N_2 in the permeate as a function of time. With an increase in (V_F/V_M), the quantity of CO_2 increases, whereas the quantity of N_2 decreases.

It may be mentioned that in the calculation the initial values of X_1 and Y_{M1} are supposed to be calculated based on materials balance taking into account of the gases remaining in the permeator from the previous step. The calculation will involve iterations over all the process steps. It was found that the calculated gas compositions on both the residue and permeate sides at the completion of this step (i.e., X_2 and Y_{M2}) varied very little for a wide range of final product concentrations under the operating conditions investigated. It can be inferred from the analysis that the amount of gas left from the previous step is insignificant. Thus, the initial values could be estimated based on the product concentrations without performing the cumbersome iterative calculations.

For the sake of calculation, a time interval of 18 s was chosen for Step 2. The calculated results showed that the general trends for the effects of parameters P_1, (A/V), and p_v on the separation performance were very similar to those shown in Step 2 since these two steps are fundamentally same. It should, however, be emphasized that because a higher pressure differential across the membrane may be achieved in Step 4, the relative volume (V_F/V_M) affects separation performance more significantly. As shown in Figures 6.9a, b and c, a high concentration of CO_2 can be obtained at p_v for a long time when a large V_F is

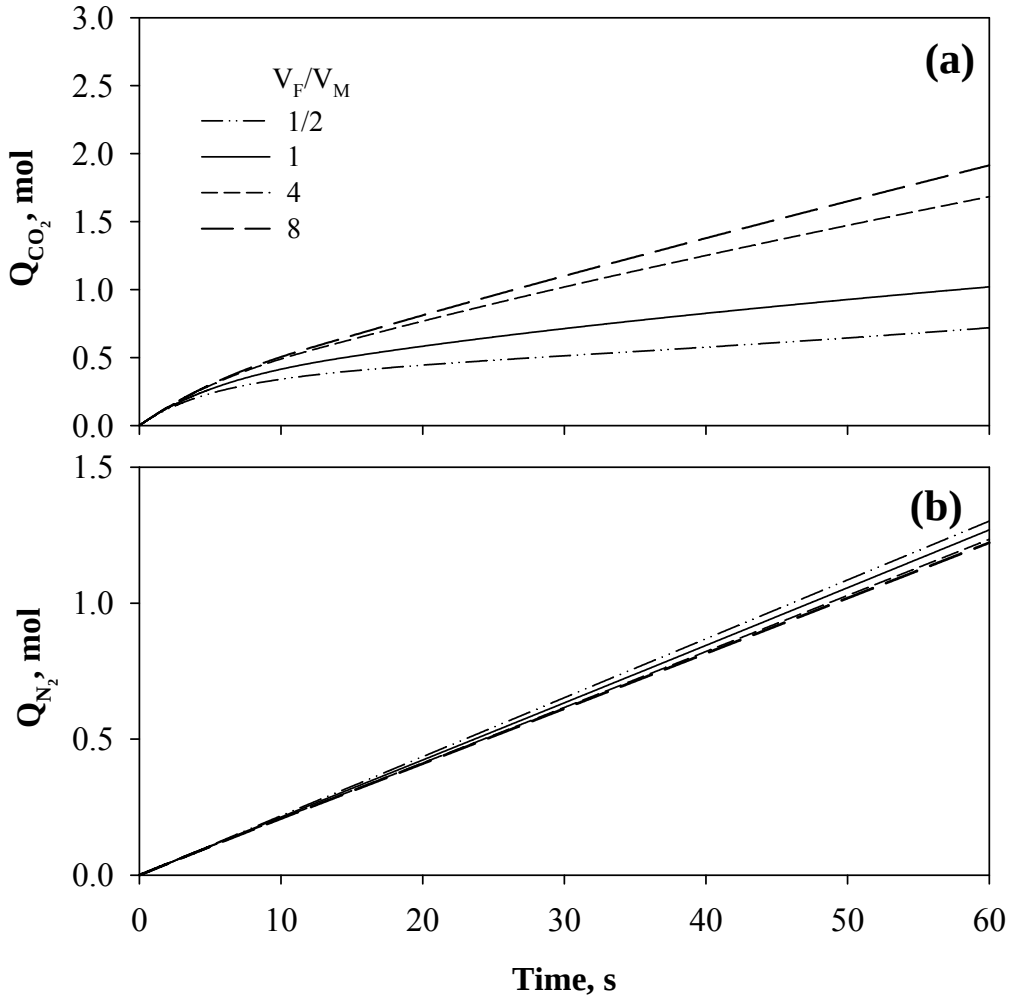

Fig. 6.8: Quantities of CO_2 and nitrogen in permeate at different (V_F/V_M) values vs. time during Step 2. P_1 = 810.6 kPa, p_V = 1.33 kPa, and (A/V) = 5000 m^2/m^3.

used, but this is at the expense of a low recovery since the concentration of CO_2 on the feed remains high. Furthermore, the slow decline in the pressure on the feed side (Figure 6.9a) also helps maintaining a high driving force for a relatively long period of time. An increase in the step time will reduce the pump switching frequencies for alternate compression and evacuation, which are desirable from an application perspective in terms of process control and operation. However, one should also keep in mind that as time proceeds, there is a reduction in the CO_2 permeation rate. That is, the CO_2 productivity will gradually slow

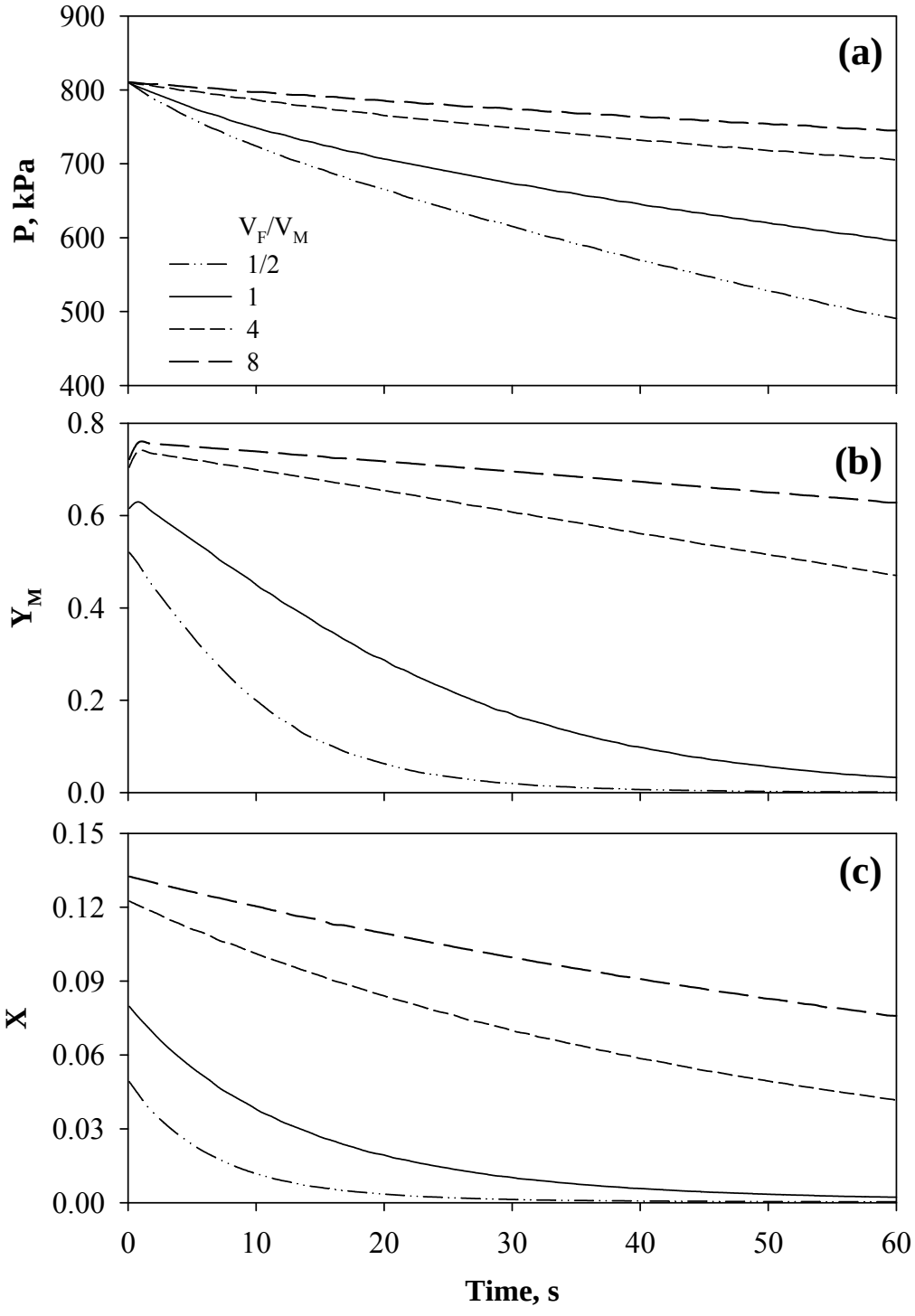

Fig. 6.9: Effects of (V_F/V_M) on residue CO_2 concentration, permeate CO_2 concentration and feed pressure during Step 4. P_1 = 810.6 kPa, p_V = 1.33 kPa, and (A/V) = 5000 m^2/m^3.

down, as illustrated in Figures 6.10a and b. The rate of reduction in the CO_2 productivity becomes more pronounced at lower (V_F/V_M) values. Clearly, the step time should be selected properly considering both the productivity and the purity of the product. A high (V_F/V_M) ratio (> 1) favours CO_2 production in the permeate.

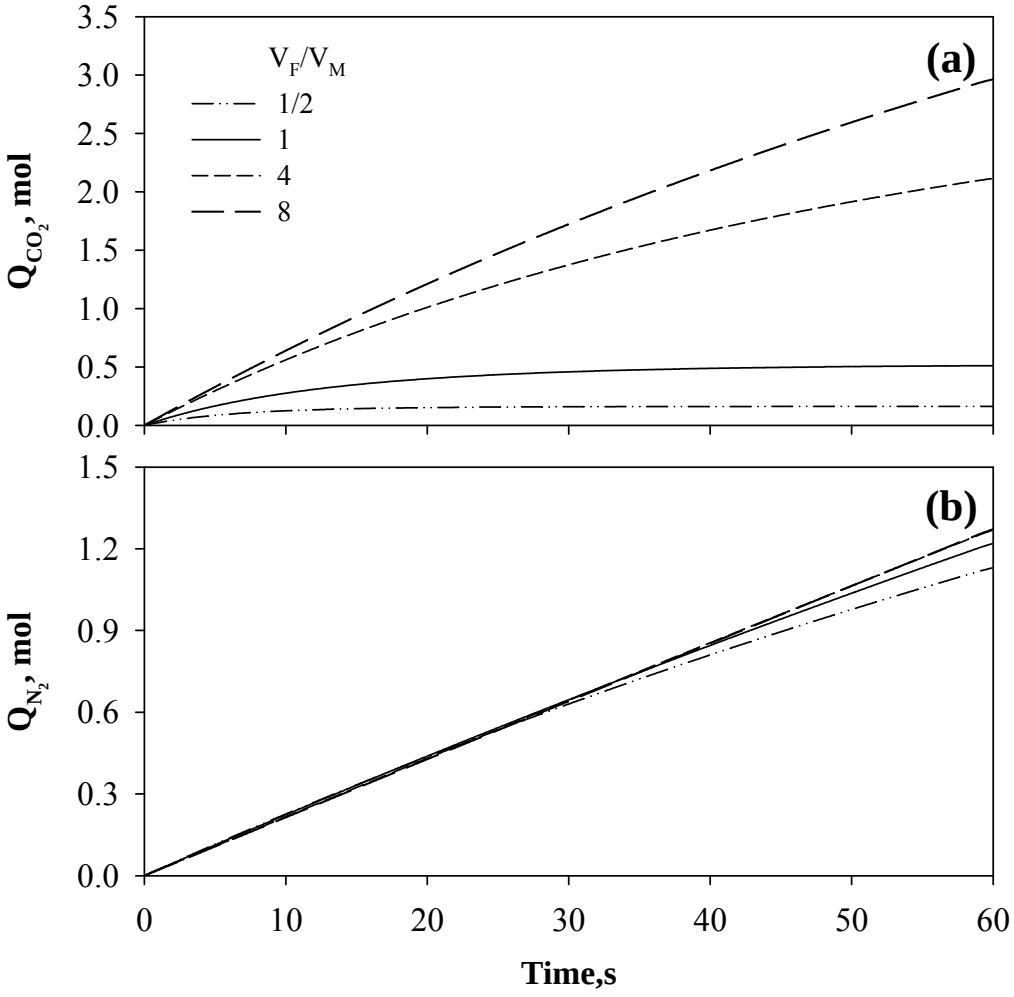

Fig. 6.10: Quantities of CO_2 and nitrogen in permeate at different (V_F/V_M) values vs. time during Step 4. P_1 = 810.6 kPa, p_V = 1.33 kPa, and (A/V) = 5000 m^2/m^3.

6.5 Performance of pressure-vacuum swing permeation and comparison with conventional membrane process

The parametric analysis indicates that the pressure-vacuum swing permeation is feasible at least for the aforementioned applications, where the membrane permselectivity is generally low and that an increase in the transmembrane pressure will have a significant impact on the separation performance. As a case study, the overall separation performance of the pressure-vacuum swing permeation was evaluated for separation of CO_2 from flue gas at 50 and 60 mol% CO_2 using the membrane properties and operating conditions mentioned as the base case for flue gas application (also shown in Table 6.1). Other membrane and operating parameters were selected based on the above calculations for Steps 2 and 4, which are the two primary steps of the cyclic process. The results are summarized in Table 6.1. In the calculation, the time for Step 2 was determined so that at the end of this step the permeate pressure would reach atmospheric pressure, and the time for Step 4 was determined such that the overall concentration of CO_2 in the accumulated permeate product would reach the desired target purity. Unlike the transient permeation processes based on differences in sorption uptake rates or desorption fall off rates, the present process is based on permselectivity of the membrane and a much longer cycle lime can be used. It is obvious that the cycle time can be increased further by prolonging the time of Step 2; however, a substantially extended period will render the permeation similar to the conventional steady-state permeation where the feed and permeate pressures are P_h and P_0, respectively, thereby losing the advantage of using the swing process to enhance the driving force for permeation.

The data in Table 6.1 show that to attain a given CO_2 concentration in the permeate product, an increase in (V_F/V_M) will increase the CO_2 recovery, while the productivity (that is, the mean flow rate of the CO_2 enriched product per membrane area) also increases. In conventional membrane gas separation, a high recovery is often accompanied with a lower productivity for a given product purity (Liu et al., 2005). However, in pressure-vacuum swing mode of permeation, a high (V_F/V_M) ratio favours both the CO_2 recovery and

Chapter 6

Table 6.1: Performance of pressure-vacuum swing permeation for CO_2 separation from flue gas.

Purpose of separation	CO_2 separation							
Volume Ratio (V_F/V_M)	8/1		4/1		1/1		1/2	
Desired CO_2 concentration (mol %)	50	60	50	60	50	60	50	60
Cycle time (s)	129.6	86.4	68.2	46.6	23.0	18.0	18.3	-
Mean flow rate of product (mol/m^2.h)	2.32	2.49	2.16	2.40	1.97	2.02	1.66	-
Recovery of target component (%)	95.23	85.73	81.20	77.46	63.9	59.26	57.54	-
A = 100 m^2; V_M = 0.02 m^3; P_h = 810.6 kPa; p_v = 1.33 kPa								

Table 6.2: Performance of steady-state permeation for CO_2 separation from flue gas.

Purpose of separation	Case 1		Case 2	
Feed and permeate pressures	Feed 810.6 kPa, permeate 101.3 kPa		Feed 101.3 kPa, permeate 1.33 kPa	
Desired CO_2 concentration (mol %)	50	60	50	60
Flow rate of product (mol/m^2.h)	1.49	1.82	0.21	0.26
Recovery of target component (%)	65.04	25.90	96.48	86.21
A = 100 m^2				

productivity in the permeate (Figure 6.11). It is interesting to note that using a larger value of (V_F/V_M) allows a longer cycle time to be used for the pressure-vacuum swing permeation, which is desired from an operating standpoint as less frequent valve switching will be favourable for process control and operation. On the other hand, for a given (V_F/V_M) value, the pressure-vacuum swing process will have a higher productivity for a higher product concentration, but the recovery will be lowered. It should be pointed out that because (V_F/V_M) determines the instantaneous CO_2 concentration on the feed side, there exists a lower limit in (V_F/V_M) below which a target CO_2 concentration in the product cannot be achieved. Improved recovery and productivity in pressure-vacuum swing permeation relative to conventional steady-state permeation can be seen from Figure 6.11. However, when a very small cycle time is used to increase the product purity, the recovery and productivity drastically falls. Permeation does not work well for short cycle times and the pressure-vacuum swing permeation may become unstable. There exists a purity limit for a given (V_F/V_M) and given feed CO_2 beyond which the mean product flow rate falls due to insufficient permeation.

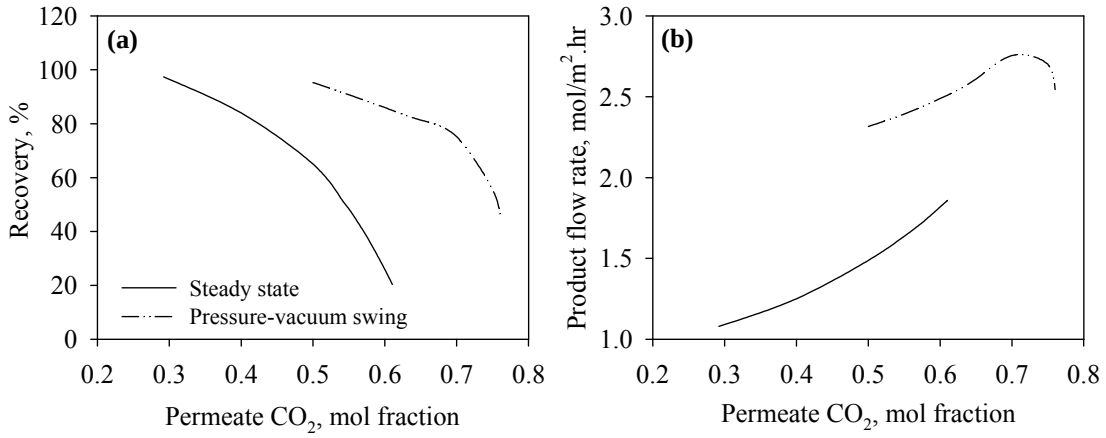

Fig. 6.11: Performance comparison of steady-state permeation and pressure-vacuum swing permeation for flue gas separation application, (a) Recovery vs. permeate CO_2 purity, and (b) Mean product flow rate vs. permeate CO_2 purity.

The advantages of using pressure-vacuum swing permeation can be illustrated by comparing with the separation performance that would be obtained with conventional steady-state operations. Table 6.2 shows the productivity and recovery for the same CO_2 concentration (i.e., 50 and 60% CO_2) at steady-state permeation with a counter-current feed/permeate flow configuration using (1) a single compressor to deliver a constant feed pressure of 810.6 kPa while the permeate is withdrawn at atmospheric pressure, or (2) a single vacuum pump to maintain a constant permeate pressure of 1.33 kPa while the feed flue gas is at atmospheric pressure. The calculation was performed using the same permeability and selectivity while neglecting the permeate pressure build-up on the permeate side. It is shown that for a given product concentration, the productivity in case (2) is much lower than that in case (1), whereas case (2) tends to have a higher recovery. The separation performance in both cases (1) and (2) are inferior to the separation achieved using the pressure-vacuum swing permeation process. To produce 50% CO_2 in the permeate using the pressure-vacuum swing permeation, a high V_F/V_M ($V_F/V_M > 1$) favours both the recovery (81.2 - 95.2%) and productivity (2.16-2.32 mol/m^2.h) as compared with case (1) in Table 6.2 (recovery 65%, and productivity 1.49 mol/m^2.h). Recovery in case (1) is still comparable with that of low V_F/V_M ($V_F/V_M \leq 1$), however, productivity (1.66-1.97 mol/m^2.h) in pressure-vacuum swing permeation process is much more that of the conventional process. The scope for pressure-vacuum swing process appears to be more promising as more and more permselective membranes become available (Hosseini et al., 2007; Li et al., 2008).

6.6 Conclusions

A parametric analysis of operating parameters associated with pressure-vacuum swing permeation for CO_2 separation from flue gas was presented. The novel and innovative unsteady state process mode was carried out in a cyclic fashion by alternately pressurizing the feed and evacuating the permeate with a single pump capable of both pressurization and suction. The cyclic pressure-vacuum swing permeation increases the transmembrane pressure difference and the feed to permeate pressure ratio, resulting in

enhanced separation that is superior to the conventional steady-state operation. The relative volume of the feed and permeate sides of the membrane unit was shown to be an important parameter in the process design. Identifying optimal volume ratio is essential for efficient separation depending on whether the permeate or the retentate is the desired product. The feasibility and effectiveness of such a dynamic process was exemplified using CO_2 separation from flue gas as model application. The pressure-vacuum swing permeation improved CO_2 recovery and productivity by 25% and 45%, respectively, compared to the conventional membrane gas separation processes.

Chapter 7

Effectiveness of membrane processes and feasibility of membrane-amine hybrid systems for post-combustion CO_2 capture[†]

7.1. Introduction

Amine absorption is regarded as a promising method to capture CO_2 from flue gases because of dealing with low concentration, low pressure, and large flow of exhaust gases. However, amine units use more energy when the CO_2 concentration increases. Major R&D efforts are currently going on worldwide to improve this technology. A substantial part of the energy requirement consists of heat duty to regenerate the used solvent at the reboiler. Membranes, on the other hand, use partial pressure as the driving force for separation and are most effective for feed gas at high concentrations of CO_2. Membranes can easily be combined with amine absorption to yield hybrid processes with cost/performance advantages that neither process could achieve individually. The hybrid systems take the advantage of bulk CO_2 removal properties of membranes while the amine is used for the final cleanup to achieve the required specification.

Several membrane amine hybrid systems are currently operating around the world for processing natural gas. Some of the noteworthy EOR projects in Texas employ a combination of membranes and amine technologies to produce pipeline quality natural gas and at the same time recover CO_2 (Chowdhury, 2012; Echt, 2002). The economic viability of membrane-amine hybrid processes for the removal of acid gases (i.e., CO_2, and H_2S) from crude natural gas has been investigated (Bhide et al., 1998; Echt, 2002; McKee et al., 1991). A high CO_2 content in the feed gas generally is a good indicator for the preferential use of membranes and/or hybrid systems. The CO_2 content in EOR plants is as high as 70% or more (Echt, 2002). McKee et al. (1991) reported that hybrid systems can be economical at lower CO_2 concentrations than is normally found in EOR applications using a feed stream of moderate flow rate and no H_2S. Bhide et al. (1998) also conducted a process design and economic assessment study for a hybrid process for sweetening crude natural

[†] Part of Chapter 7 will be submitted shortly for publication

gas. In a two-in-series arrangement, membrane separation was used first for the bulk removal of the acid gases followed by gas absorption/stripping process using diethanolamine (DEA) for final purification to meet pipeline specifications. It was reported that gas absorption process alone is not competitive with either the hybrid process or the membrane process alone under most of the conditions. Echt (2002) conducted a techno-economic analysis of hybrid systems and reported substantial cost benefits for processing large volume of natural gas.

The potential of using a membrane-amine hybrid process for post-combustion CO_2 capture has not been well addressed in the open literature, except in quite few cases (Chowdhury, 2012). Recently, Chowdhury (2012) reported that membrane-amine hybrid systems might not be a good choice for the post-combustion CO_2 capture based on his study for post-combustion CO_2 capture using the two different unit operations arranged in parallel and in series. A varying portion of the feed stream was introduced to the individual unit operations rather than taking advantages of the bulk separation properties of membrane processes. Belaissaoui et al. (2012) studied hybrid membrane-cryogenic processes for post-combustion CO_2 capture and reported that the energy requirement of the hybrid process is lower than the energy required for a standalone cryogenic process, and the overall energy requirement of the hybrid process could possibly be significantly decreased if a less stringent capture constraint is taken. A case study of hybrid process combining oxygen enriched air combustion and membrane separation for post-combustion CO_2 capture was investigated from an energy requirement perspective (Favre et al., 2009a). It was reported that the hybrid process can lead to a 35% decrease in the energy requirement compared to oxycombustion within certain operating conditions and limitations. In this study, a technical analysis of post-combustion CO_2 capture from flue gases with competing technologies such as membranes, amine absorption and their hybrid processes was conducted. Several cascade configurations of hollow fiber membranes, and amine absorption with MEA and DEA as solvents were studied independently for a target recovery and purity, both for the product value of CO_2 (e.g., enhanced oil/coal bed methane recovery) and for environmental reasons (reducing the greenhouse effect). A membrane-amine hybrid process was studied thereafter for the design specifications. The study was

conducted to find the extent of optimal conditions for which the aforementioned technologies are best suited.

7.2. Design basis and process description

7.2.1 Membrane processes

The design of membrane gas separation processes involves the determination of appropriate permeator arrangements/configurations as well as specification of process unit (i.e., module) sizes and operating conditions. A single stage arrangement with feed compression and/or permeate vacuum or both (without any recycle stream) is the most common and simplest design consideration. However, a high purity and recovery of the desired product sometimes may require the use of stream recycle and multi-stage configurations (Koros and Chern, 1987). The modeling and simulation strategy described in Chapters 3 and 4 were used in this Chapter to simulate single stage and multi-stage configurations. The model described earlier could be implemented in Aspen Plus® as a membrane unit (custom unit operation model for hollow fiber membrane module, which is not available in the standard version of Aspen Plus®) to design, simulation and optimization of the overall membrane and hybrid processes. The procedures and modifications required are reported by Chowdhury (2012). However, a multi-stage permeator design involves a complex set of differential and algebraic equations, and the computation complexity increases when some of the streams are recycled. Moreover, since the convergence of the process flowsheet in amine scrubbing is a nontrivial exercise due to the highly nonlinear nature of the process and the large recycle stream involved, we opted not to study the hybrid process in Aspen Plus® for simplicity.

It is generally agreed that the membrane area and energy consumption are the key factors determining the cost of membrane processes. Flue gas from coal-fired power plants and cement plants were taken as the basis to investigate effectiveness of membrane processes. Details of the flue gas characteristics of a 500 MW coal-fired power plant and St. Marys cement Inc. can be found in Chowdhury (2012) and Hassan (2005), respectively.

Chowdhury (2012) studied the simulation, design and optimization of membrane gas separation, chemical absorption and combinations of both for post combustion CO_2 capture from flue gases. The amine absorption was simulated for different reaction chemistry (equilibrium and rate-based), tray sizing, tray rating, flooding, and foaming factors. However, in our study, the amine absorption process was simulated in equilibrium mode only to find the minimum reboiler heat duty for the design specifications. Hassan (2005) studied amine absorption for post combustion CO_2 capture in RateFrac™ (rate-based non-equilibrium model) and reported an economic evaluation of the process. Since certain gas separation membranes can not handle the moisture content, the feed gas characteristics reported by Hassan (2005) was calculated accordingly on a dry basis. As membrane replacement is a critical operating cost, pre-treatment of feed stream is necessary to extend the membrane life. The feed stream was assumed to be free of such minor components as SO_X, NO_X, CO, Ar, H_2O and ash by pre-treatment before entering the membrane unit. The flue gas flow rate, composition, temperature and pressure after the pre-treatment are presented in Table 7.1. A capture requirement of CO_2 purity equal to 98% with a recovery of 85% from standalone membrane processes was targeted for enhanced oil recovery (EOR) and/or enhanced coal bed methane (ECMB) recovery applications. It is reported that the purity of captured CO_2 needs to be equal or more than 98% for EOR application (Alie et al., 2005; Zhao et al., 2008). However, the recovery is somewhat arbitrary, which reflects how aggressively we want to reduce the CO_2 emissions. Permeances of Polaris™

Table 7.1: Flue gas characteristics (after treatment, and before entering the membrane unit).

Feed Gas Conditions	**Coal-fired Power Plant**	**Cement Plant**
Flow rate, kmol/s	20.95	2.10
Temperature, ^oC	40	40
Pressure, kPa	101	101.325
Composition, mol%		
CO_2	15.0	24.1
N_2	81.0	73.4
O_2	4.0	2.5

membrane developed by MTR (Membrane Technology and Research, Inc.) were taken in the calculations for the study. The permeances of Polaris™ membrane are 1000, 50 and 20 GPU for CO_2, O_2 and N_2, respectively, with CO_2/N_2 selectivity of 50 (Lin et al., 2007). These values will be used throughout the study if not stated otherwise. The extent of separation that can be achieved by a single stage membrane process with current and future generation membranes was also evaluated.

7.2.2 Amine absorption processes

The amine absorption process was modeled in Aspen Plus® and targeted to capture 85% of the CO_2 with a purity requirement of 98% for a comparison with standalone membrane processes. The case study includes simulating the amine process for two solvents, i.e., monoethanolamine (MEA) and diethanolamine (DEA) for acid gas removal from flue gas. A comparison of popular solvents in chemical solvent based separations and strategies to reduce energy consumption through engineered and formulated solvents could be found elsewhere (Chakma, 1997; Chakma, 1999; Mofarahi et al., 2008). The conventional MEA process flowsheet is shown in Figure 7.1. The flue gas containing CO_2 enters the absorber and contacts the aqueous solution of MEA flowing countercurrently to the flue gas stream. CO_2, a weak base, reacts exothermically with MEA, a weak acid, to form a water soluble salt. The 'rich' MEA stream exits the absorber at the bottom of the column. It is then preheated in a heat exchanger by the lean MEA stream leaving from the bottom of the stripper and enters the stripper where, with further addition of heat, the reaction is reversed. The CO_2, having been stripped off from the MEA, leaves through the top of the stripper column. The 'lean' MEA is then recycled back to the absorber. A detailed description of conventional amine processes could be found elsewhere (Abu-Zahra et al., 2007; Alie et al., 2005; Aroonwilas and Veawab, 2009; Chowdhury, 2012; Desideri and Paolucci, 1999; Geuzebroek et al., 2004; Hassan, 2005; Hassan et al., 2007; Lee et al., 2009; Mofarahi et al., 2008; Romeo et al., 2008; Singh et al., 2003).

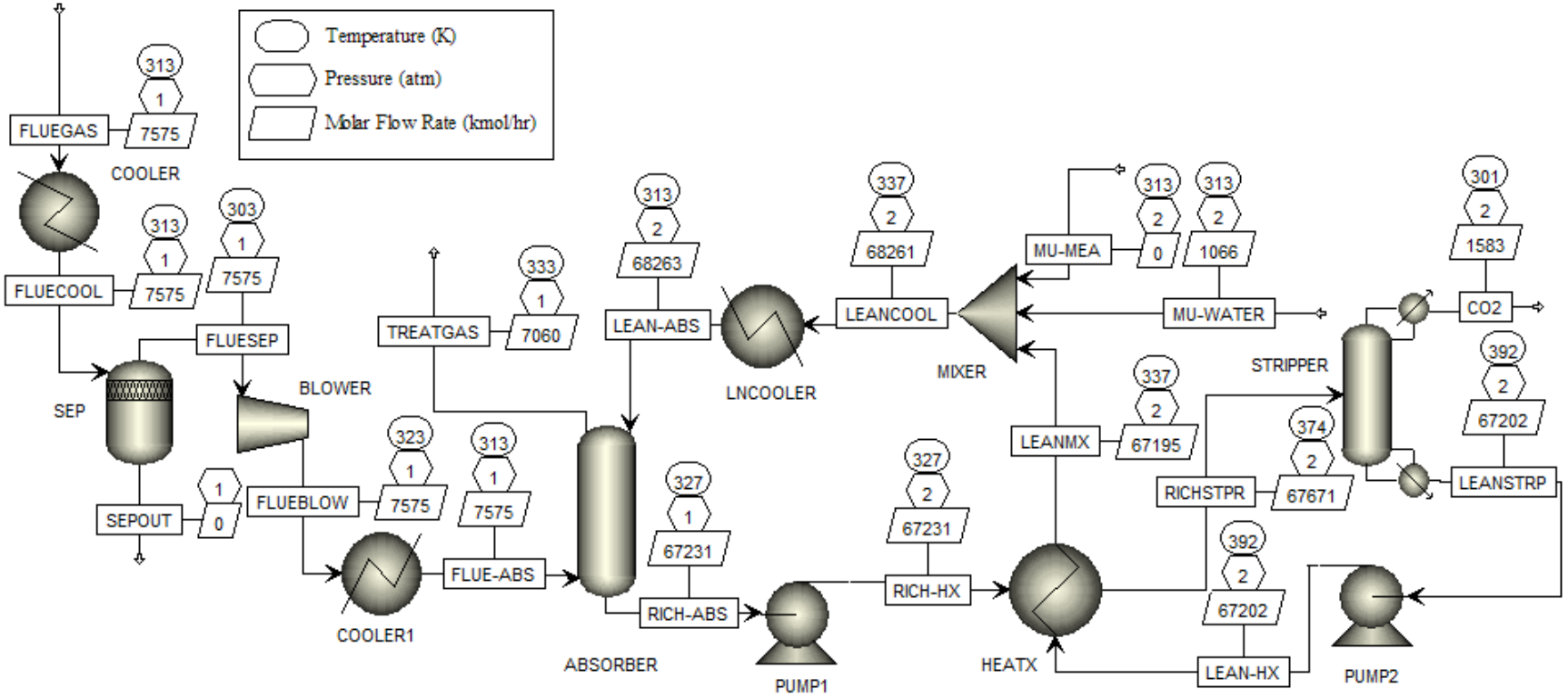

Fig. 7.1: Aspen Plus® process flow sheet for MEA process (cement plant).

There are several electrolyte-based physical property models in Aspen Plus® such as *emea*, *kemea*, *mea* and *kmea* that specify the property method and solution chemistry for processes containing CO_2, H_2O and MEA. These property package inserts use the electrolyte-NRTL method to calculate the fluid transport and thermodynamic properties. Electrolyte-NRTL is an activity coefficient model-based property method that uses the electrolyte-NRTL model for the liquid phase and Redlich-Kwong equation of state for the vapour phase (Harun, 2012). In this work, *emea* property insert was selected in modeling the MEA absorption process in Aspen Plus®. The *emea* package was inserted in the Aspen Plus® property set prior to the development of the entire flowsheet. It is applicable for the systems containing CO_2-H_2S-H_2O-MEA with a temperature up to 120^oC and a MEA concentration up to 50%. Since N_2 and O_2 are not included in the *emea* insert package, they were added as individual components. CO_2, N_2 and O_2 were defined in the system to obey Henry's law. The *emea* property package assumes that the reaction is at equilibrium. For simulations involving DEA, the property package *edea* was selected. The *edea* property insert is applicable for the systems containing CO_2-H_2S-H_2O-DEA at temperatures up to 140^oC and DEA concentrations up to 30%. The accepted range of process conditions and parameters for each amine (i.e., amine degradation temperature, lean loadings) were cautiously monitored during the simulation.

An Aspen Plus® design specification was imposed which adjusted the lean solvent (i.e., MEA) flow rate in a standalone absorber to achieve a CO_2 recovery of 85% (i.e., 15% CO_2 in the treated gas). Inside the stripper, there were two design specifications. The first one was to achieve a desired mass flow of CO_2 in the distillate (commonly 85% of the CO_2 in the flue gas, calculated from the absorber design specification) by varying the bottom to feed ratio at the bottom of the stripper. The other specification was to achieve a carbon dioxide purity (typically 98% CO_2) in the product stream by varying the molar reflux ratio at the top of the stripper. These specifications, once met, would render the desired loading in Lean MEA (LEANSTRP or LEAN-ABS) stream. Calculator blocks were added where necessary to check the loadings. In particular, the energy required by the stripper reboiler overshadows the annualized capital costs of the capture plant (Alie et al., 2005; Desideri and Paolucci, 1999; Singh et al., 2003). Therefore, minimizing the reboiler heat duty is

important in this process. The number of stages, lean loadings and reboiler temperature were varied to find the minimum reboiler heat duty.

Several factors contribute to the simulation difficulties in a MEA process. Firstly, we used the Aspen Radfrac model in equilibrium mode for the absorber and the stripper. Though Radfrac assumes equilibrium stages in equilibrium mode, it is a rigorous model that behaves in a nonlinear fashion. Thus, the absorber and stripper models are sensitive to changes in their respective input streams. Moreover, because of the recycle structure of the flowsheet, it is extremely difficult to converge the MEA flowsheet with a closed recycle stream. Since most of the MEA solution entering the stripper is being recycled, a large number of iterations is necessary to converge the large tear streams. A very good initial estimate of the lean MEA flow and composition is desired since an excess of solvent in the absorber can cause divergence. It is difficult to obtain an initial estimate to initialize the stripper, and reasonable ranges for the design specifications in the stripper are also required for ease of convergence. To overcome the difficulties in converging the flowsheet, the flowsheet decomposition method by Alie et al. (2005) was adopted. Initially, the standalone absorber model was simulated, followed by absorber and stripper integrated model. Finally, the recycle stream was connected to the absorber and stripper integrated model. This approach determines a very good first initial guess for each step, and the results from the previous step become the initial guesses for the subsequent steps. Decomposing the flowsheet simplifies the modelling effort, provides a good insight into the process and also provides a good starting point for coupling the process.

7.2.3 Hybrid membrane processes

The hybrid process was also targeted to capture 85% of the CO_2 with a purity of 98% for a comparison with the standalone membrane processes and MEA processes. A fraction of the fed CO_2 was recovered from the membrane processes and the residual CO_2 was captured through the MEA processes to count on an overall 85% recovery. The design specifications for the MEA processes were modified accordingly. The total energy required for the hybrid processes was calculated.

7.3. Results and discussion

Separation that can be achieved with a single stage membrane process without recycle was evaluated for different CO_2/N_2 selectivity and feed CO_2 concentration. Figure 7.2 depicts the permeate CO_2 purity versus recovery for a membrane selectivity of 50,100 and 200. The feed concentration of CO_2 was set at 10% (Figure 7.2a), 20% (Figure 7.2b) and 30% (Figure 7.2c). It is clear that a high membrane selectivity is critical to obtain satisfactory permeate CO_2 concentrations and CO_2 recovery rates. Many studies and potential regulations require that both the permeate CO_2 purity and CO_2 recovery surpass 80% for post-combustion carbon capture (Bounaceur et al., 2006). It is evident from Figure 7.2a that this is hard to attain for CO_2 capture from flue gas with the membrane CO_2/N_2 selectivity of 50, where the CO_2 content is less than 10%. If the feed CO_2 content increases to 20~30% (Figure 7.2b and c), a permeate CO_2 purity and recovery above 80% can be achieved at a membrane selectivity of 50. Bounaceur et al. (2006) reported a similar study of purity-recovery achievable with membranes having different selectivities, and concluded that membranes are viable CO_2 capture alternatives only for flue gas containing more than 10% carbon dioxide, if the membrane selectivities are limited in the range of 50 or below.

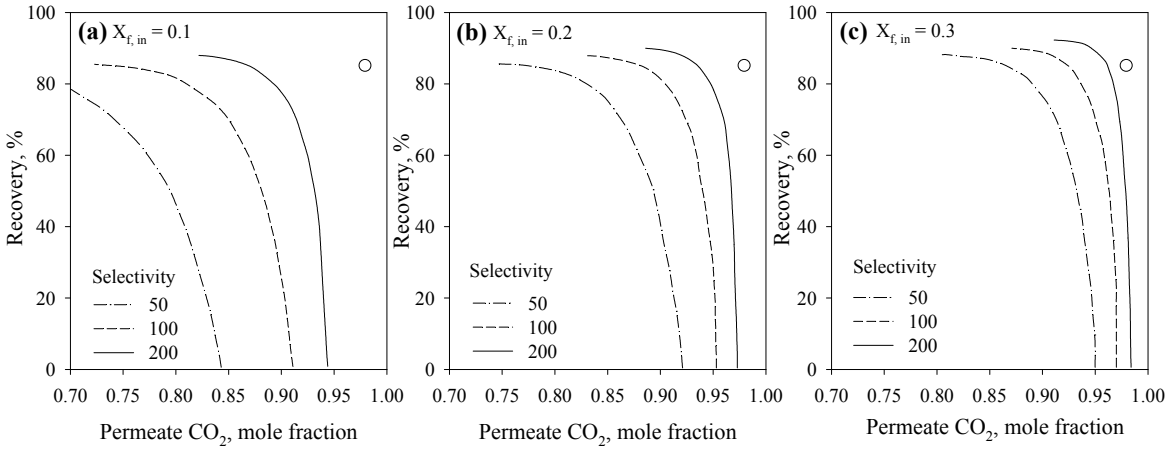

Fig. 7.2: Permeate CO_2 purity versus recovery at different CO_2/N_2 selectivities with a single stage membrane unit, (a) 10% CO_2 in the feed, (b) 20% CO_2 in the feed, and (c) 30% CO_2 in the feed.

However, our study was targeted to recover 85% of the CO_2 with a purity of 98% CO_2 (denoted by the open circle in Figure 7.2). It was found that the target specifications are unattainable with a single stage permeator even with a membrane selectivity of 200. However, when a single-stage design is unsatisfactory in terms of product purity or recovery, multi-staging or cascading is sometimes an attractive approach. It is also to be noted that single-stage membrane units are rarely used in practice for the separations. It is obvious from Figure 7.2 that the success of membranes depends heavily on the membrane selectivity or at least in multi-staging.

Detailed parametric studies of gas separation membrane processes for post-combustion carbon capture are available elsewhere (Bounaceur et al., 2006; Brunetti et al., 2010; Favre, 2007; Ho et al., 2008; Zhao et al., 2008). These studies included a parametric analysis of the effects of CO_2 permeability, CO_2/N_2 selectivity, membrane area, pressure ratio, feed CO_2 concentration on the membrane performance. Chowdhury (2012) studied fifteen single and multi-stage membrane process configurations with and without recycle streams through simulation for an industrial scale post-combustion CO_2 capture. Among the various configurations studied, only two of them (Figures 7.3a and b) were capable to satisfy the design specifications. The configuration shown in Figure 7.3a was developed by Lin et al. (2007) to recover 90% CO_2 with a permeate purity of 88.3% for a CO_2 concentration of 13% in the feed. The configuration shown in Figure 7.3b, which is a modified configuration shown in Figure 7.3a, eliminates a compressor. In our study, these two three-stage configurations were simulated for the aforementioned capture requirements at the operating conditions reported by Chowdhury (2012). Several two-stage configurations were investigated too. However, the two stage configurations were not capable of meeting the CO_2 capture requirements for coal-fired power plants where the feed CO_2 concentration is 15%. They are capable of meeting the capture requirements in case of cement plants with a CO_2 concentration of 24.1% in the feed. As the feed CO_2 concentration increases, the membrane processes offer significant advantages. The two-stage configurations were very simple in design and no vacuum pumps were used. Vacuum operation does not save much power and uses lots more membrane area.

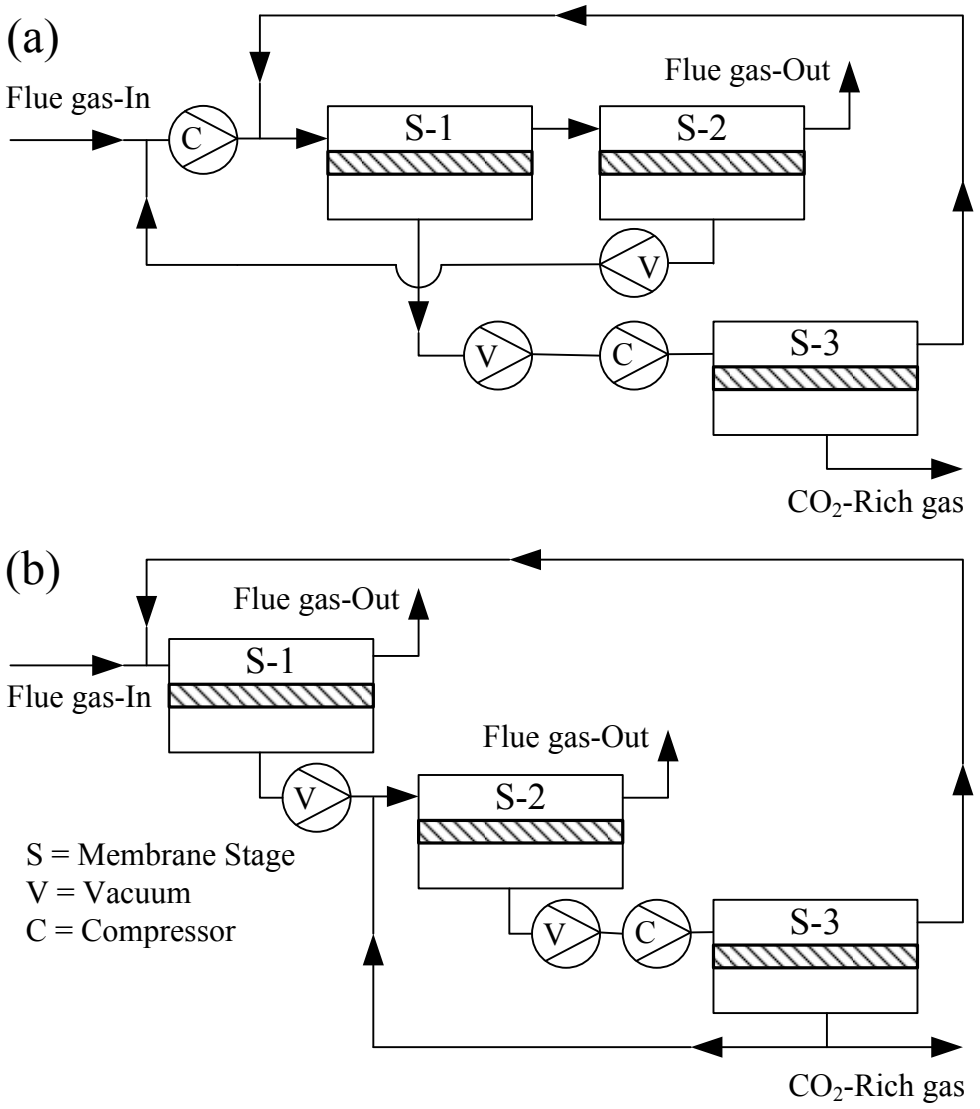

Fig. 7.3: Three-stage configurations investigated for post-combustion CO_2 capture.

The performance of all the process configurations is compared on the basis of membrane area and power requirements. The three-stage configuration shown in Figure 7.3b requires the lowest energy penalty for coal-fired power plant applications, however, it requires larger membrane area (Table 7.2). Configuration in Figure 7.3b consumes 31% less energy but requires 237% more membrane area than the configuration in Figure 7.3a. On the other hand, the energy penalties for the two-stage configurations (Figures 7.4a and

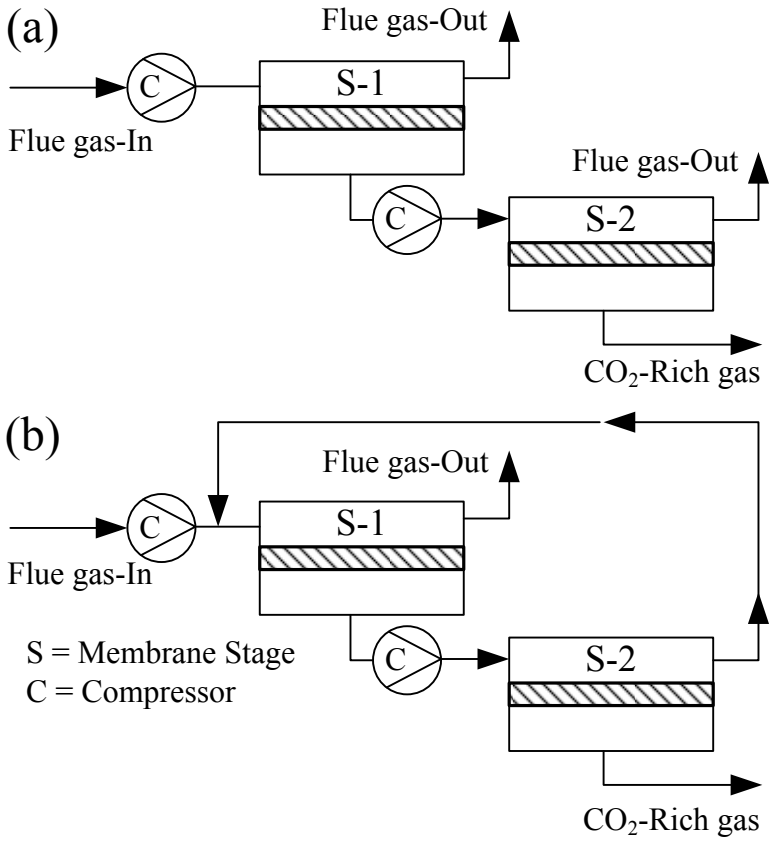

Fig. 7.4: Two-stage configurations investigated for post-combustion CO_2 capture.

b) are comparable for cement plant application (Table 7.3). There should be a room for minimizing the energy penalty and membrane area requirements by conducting an optimization study.

Table 7.4 shows the Aspen Plus® block input data for the cement plant. Initially, the number of stages in the absorber and the stripper was arbitrarily chosen to be 10 and 14, respectively. The reboiler heat duty strongly depends on the number of stages/trays of the absorber and stripper. Simulations were conducted to optimize the number of stages required for both the absorber and the stripper columns to minimize the reboiler heat duty. The effect of number of stripper stages on the reboiler heat duty was studied by varying the

Table 7.2: Multi-stage configurations investigated for post-combustion CO_2 capture (Coal-fired power plant).

Process Variables	Process Configurations		
	Fig. 7.3a	Fig. 7.3b	Fig. 7.4a
Feed CO_2, mol fraction	0.15	0.15	0.15
Total Feed Flow, kmol/s	20.95	20.95	20.95
Temperature, K	313	313	313
Feed Blow/Comp Pressure, kPa	300	-	3000
Permeate Vacuum, kPa	33	10	-
Permeate Compressor Pressure, kPa	2000	2700	4000
CO_2 in CO_2-Rich Stream, mol fraction	0.98	0.98	0.966
CO_2 Capture Rate, %	85	85	85
Membrane Area, m^2	1820000	6150000	109210
Net Power Consumption, MW	255	175	362
Net Energy Required, GJ/ton CO_2 Recovered	2.17	1.49	3.08

Table 7.3: Multi-stage configurations investigated for post-combustion CO_2 capture (Cement plant).

Process Variables	Process Configurations	
	Fig. 7.4a	Fig. 7.4b
Feed CO_2, mol fraction	0.241	0.241
Total Feed Flow, kmol/s	2.1042	2.1042
Temperature, K	313	313
Feed Blow/Comp Pressure, kPa	2000	1750
Permeate Vacuum, kPa	-	-
Permeate Compressor Pressure, kPa	1850	1750
CO_2 in CO_2-Rich Stream, mol fraction	0.98	0.98
CO_2 Capture Rate, %	85	85
Membrane Area, m^2	14820.4	19637.7
Net Power Consumption, MW	32.4	31.7
Net Energy Required, GJ/ton CO_2 Recovered	1.71	1.67

Table 7.4: Block input data for Aspen Plus® process flowsheet (cement plant).

Block Name	Unit Operation Model	Block Specifications	Type/Value
COOLER	HEATER	Temperature, ^{o}C	40
		Pressure, bar	1.013
SEP	FLASH2	Temperature, ^{o}C	30
		Pressure, bar	1.013
BLOWER	COMPR	Pressure, bar	1.2
COOLER1	HEATER	Temperature, ^{o}C	40
		Pressure, bar	1.2
ABSORBER	RADFRAC	Condenser/Reboiler	None/None
		Temperature, ^{o}C	40
		No. of Stages	7
		Top Stage Pressure, bar	1.2
		Column Pressure Drop, bar	0
		Flue-Abs Feed Location	Above Stage 1
		Lean-Abs Feed Location	Above Stage 8
PUMP1/PUMP2	PUMP	Discharge Pressure, bar	2.1
HEATX	HEATX	Cold Stream Outlet Temperature, ^{o}C	101.5
		Pressure, bar	2.1
STRIPPER	RADFRAC	Condenser/Reboiler	Partial vapour /Kettle
		Temperature, ^{o}C	40
		No. of Stages	10
		Top Stage Pressure, bar	1.9
		Column Pressure Drop, bar	0
		Feed Tray Location	Above Stage 6
LNCOOLER	HEATER	Temperature, ^{o}C	40
		Pressure, bar	2.1

stripper stages from 4 to 14 while keeping the absorber stages fixed. It was observed that the reboiler heat duty can be reduced by increasing the stripper number of stages. However, after a certain number of stages, a further increase in the number of stages in the stripper increases the reboiler heat duty only marginally. An increase in the number of trays in the stripper requires a lower reflux ratio for a given carbon dioxide recovery thereby helping in the reduction of the reboiler heat duty (Hassan, 2005). Similarly, an increase in the number of stages in the absorber also reduces the reboiler heat duty. The reduction in reboiler heat duty is due to the fact that a greater number of stages in the absorber allows a lower solvent circulation rate in the absorber, and thus reduces the heat required by the reboiler to regenerate the solvent. It was also observed that the required lean solvent flow rate decreases as the number of stages in the absorber increases. However, as the lean solvent flow rate increases, the diameter of the column increases subsequently, thereby increasing the capital cost of the capture process (Hassan, 2005). The number of stages in the absorber and the stripper was finally chosen to be 7 and 10, respectively.

Figure 7.5 represents the LEAN-ABS and RICH-ABS flow rate, respectively, for different lean loadings (mol CO_2/mol MEA). As can be seen from Figure 7.5, the required LEAN-ABS flow rate increased from 680,122 to 1,660,781 Kg/hr for the cement plant when the lean loading was increased from 0.05 to 0.30 mol CO_2/mol MEA. Higher CO_2 loadings require higher flow rate of lean MEA to achieve the target CO_2 recovery. However, the required LEAN-ABS flow rate was much higher when DEA was used as the solvent. The required DEA flow rate was 40-70% more than that of MEA, as shown in Figure 7.5. This is because MEA provides the highest overall forward rate constant for CO_2-amine reactions (7600 mol/L/s), while rate constant of DEA (1500 mol/L/s) is somewhat intermediate among the amines (Chakma, 1997).

Hassan (2005) reported that the rich loading increases with increasing lean loading, but the rich loading increase is not much compared to the value of lean loading increase. The rich loading increase is due to a significant increase in carbon dioxide recirculation through the columns as the lean loading increases. On the contrary, Alie et al. (2005)

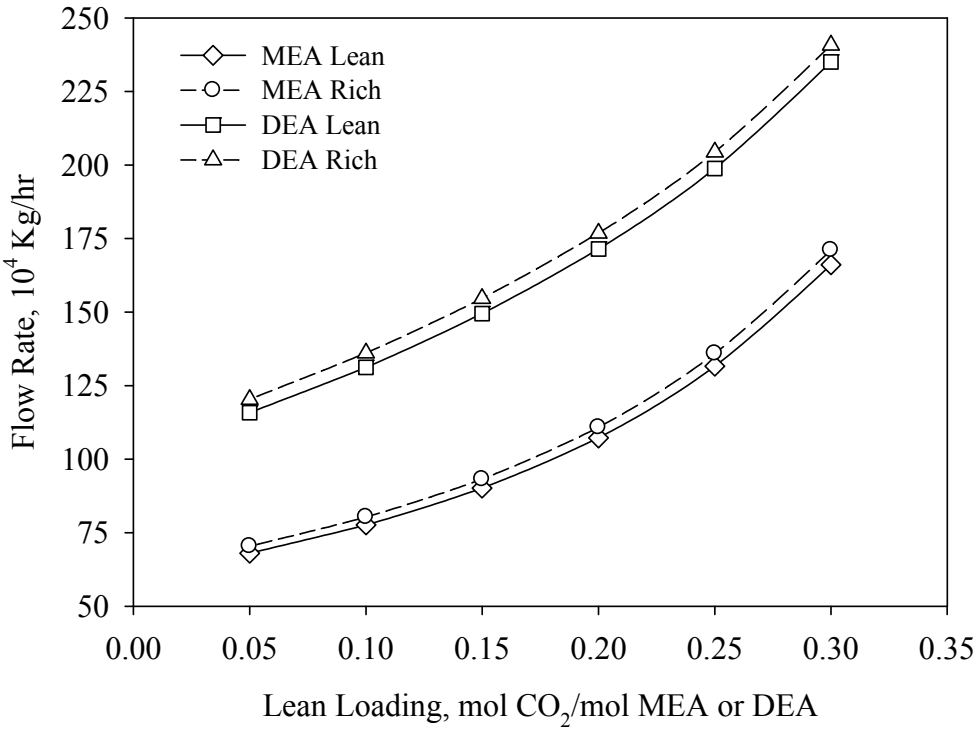

Fig. 7.5: LEAN-ABS and RICH-ABS flow rate for different lean loadings (mol CO_2/mol MEA or DEA) in case of cement plant.

reported that the rich loading is essentially independent of the lean loading for a given CO_2 concentration. The rich loadings (α_{Rich}) profile in the absorber was studied for a variation of lean loadings (α_{Lean}) both for MEA and DEA. The mean rich loadings (α_{Rich}) and standard deviation are shown in Table 7.5. The rich loadings range from 0.503 to 0.52 (mol CO_2/mol MEA) for MEA. However, no direct relationship was established.

Figure 7.6 shows the reboiler duty required for the targeted CO_2 recovery and purity when lean loading varies from 0.05 to 0.30 (mol CO_2/mol MEA) for the cement plant data. The required reboiler heat duty decreases as the lean loading increases. The heat duty reduced by 86% as the lean loading was increased from 0.05 to 0.30 for MEA (as the solvent). It was also observed the reboiler heat duty is relatively independent of the lean loading above a lean loading of 0.25. The required reboiler heat duty was found to be the

Table 7.5: Mean rich loadings (α_{Rich}) and standard deviation for a variation of lean loadings (α_{Lean}) both for MEA and DEA.

α_{Lean}	α_{Rich} (MEA)	α_{Rich} (DEA)
0.0500	0.5199	0.5225
0.1000	0.5161	0.5196
0.1500	0.5119	0.5208
0.2000	0.5072	0.5251
0.2500	0.5033	0.5317
0.3000	0.5027	0.5400
Mean α_{Rich}	**0.5102**	**0.5266**
Standard Deviation α_{Rich}	**0.0069**	**0.0078**

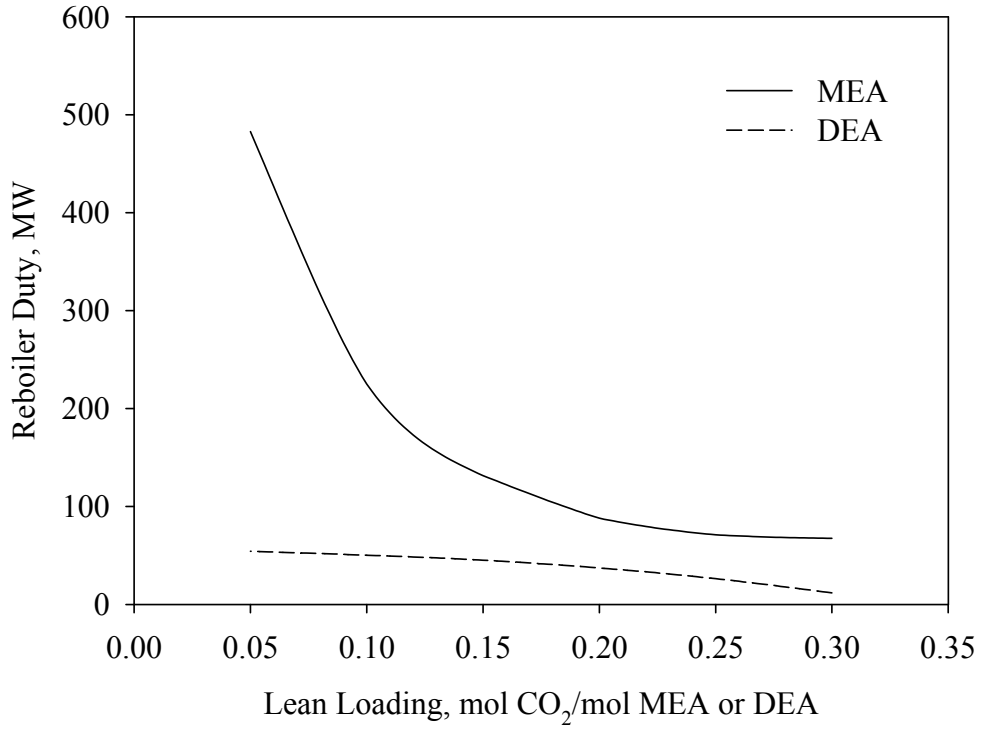

Fig. 7.6: Reboiler duty required for the targeted CO_2 recovery and purity when lean loading varies from 0.05 to 0.30 (mol CO_2/mol MEA) for the cement plant data.

least when the lean loading was 0.30 for MEA. These observations are also true for DEA. The circulation rate of the solvent and the value of the lean loading of the stream leaving the stripper (and subsequently recycled back to the absorber) are two important factors affecting the reboiler heat duty. At a lean loading of 0.05 (mol CO_2/mol MEA), a large amount of heat is required at the reboiler to separate the desired carbon dioxide. Albeit the solvent circulation rate is low, the reboiler would consume a lot of energy to separate the carbon dioxide until the lean solvent reaches that CO_2 loading. That suggests at a low lean CO_2 loading, a significant amount of additional energy is required during the regeneration process. As the lean loading specification is increased, the reboiler duty decreases until it reaches a plateau above a lean loading of 0.25. The amine solution with a higher CO_2 loading can be regenerated more easily and with lower reboiler duty than that of with a lower CO_2 loading. The CO_2 loading of the lean solution needs to be adjusted to a proper level where the energy consumption at the regeneration unit is reduced, while maintaining a satisfactory capture performance. This may result in a reduction in the overall cost of the capture process. However, it is to be noted that due to lower heats of reaction and latent heats of vaporization, DEA offers better energy savings than MEA (Chakma, 1997; Chakma, 1999).

The reboiler duty required to treat the flue gas to the aforementioned design specifications was investigated for other flue gas compositions i.e., CO_2 concentrations of 5%, 15% and 25%. In each case, the flow rate of flue gas was kept constant at that of the cement plant (Table 7.1) and MEA was used as the solvent. Figure 7.7 represents the reboiler duty at the studied concentrations plotted against the lean loading. The reboiler duty decreases and reaches a plateau for a lean loading equal to 0.30. It is also apparent that the MEA process is advantageous when CO_2 content in the flue gas is lower.

Absorption processes use more energy when the CO_2 concentration increases. Membranes, on the other hand, use partial pressure as the driving force for separation and are most effective at high concentrations of CO_2. Hybrid processes can be developed to take the cost/performance advantages that neither process could achieve individually.

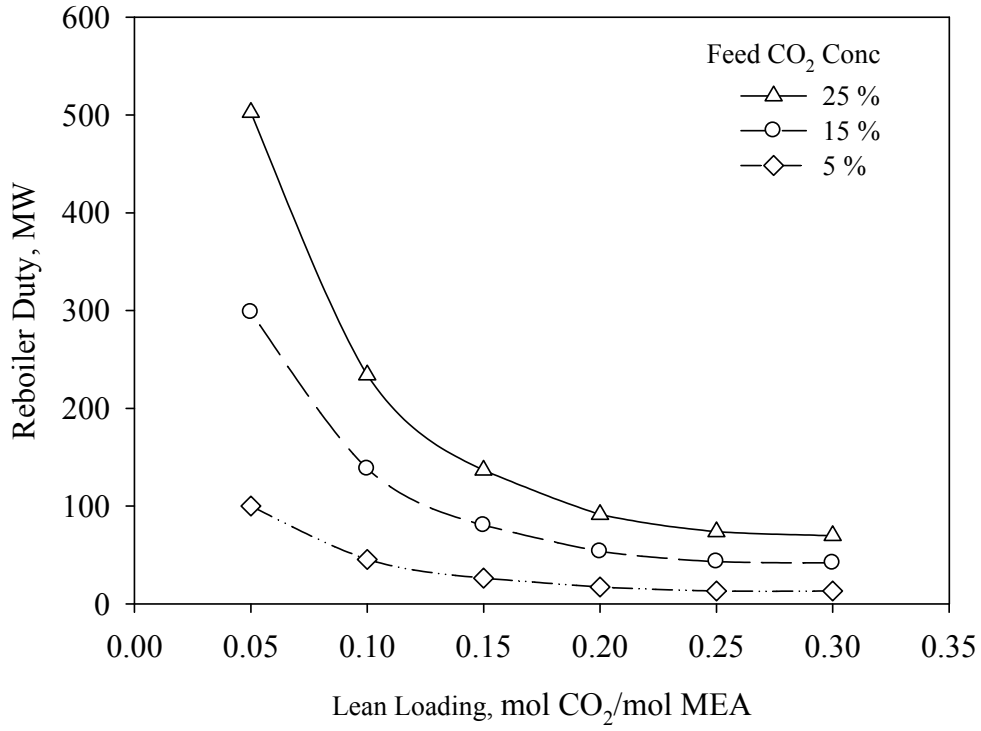

Fig. 7.7: Reboiler heat duties at different CO_2 concentrations with different lean loading.

Chowdhury (2012) studied hybrid membrane processes for post-combustion CO_2 capture as two different unit operations arranged in parallel or in series. In the parallel arrangement, a portion of the flue gas was split and fed to the amine unit while the remaining flue gas enters the membrane unit. In the series arrangement, the flue gas was first concentrated in CO_2 with the membranes, and then the CO_2 concentrated stream was fed to amine unit. It was concluded that the hybrid process combining of membrane and MEA might not be a good choice for the post-combustion CO_2 capture. Chowdhury (2012) also reported that the standalone membrane process utilizes the lowest energy, and neither hybrid process was competitive, the worse being the two-in-series hybrid arrangement. It is comprehensible from Figure 7.7 that as CO_2 concentration increases, so does the required reboiler heat duty. This also implies that the two-in-series arrangement might not be effective from the energy perspectives. Moreover, the parallel arrangement fails to take the advantage of the membrane process which is effective for bulk CO_2 removal.

Considering all these, an alternative hybrid process may be arranged to take advantage of the bulk removal efficiency of membranes. A two stage membrane process (as shown in Figure 7.4b) was combined with the MEA process. Figure 7.8 represents such a hybrid of membrane-amine process investigated in this study. The membrane was designed to yield a permeate stream of desired purity. A fraction of the fed CO_2 was recovered from the membrane process and the residual CO_2 was captured through the MEA process to yield an overall 85% recovery. The retentate stream from the membrane unit (having been depleted of CO_2) was fed to the amine unit to match the desired recovery of the overall hybrid processes. Figure 7.9 represents the energy consumption for the membrane component, amine component and their combined total for the cement plant application. As more of the CO_2 is being removed with membranes, the energy penalty for the amine unit reduces. The total energy penalty of the hybrid process thus decreases as more and more CO_2 is removed by the membrane, as the membrane process is more energy efficient.

Table 7.6 provides a comparison of energy consumption in membrane processes, amine processes and their hybrid combinations. Membrane processes exhibit the lowest

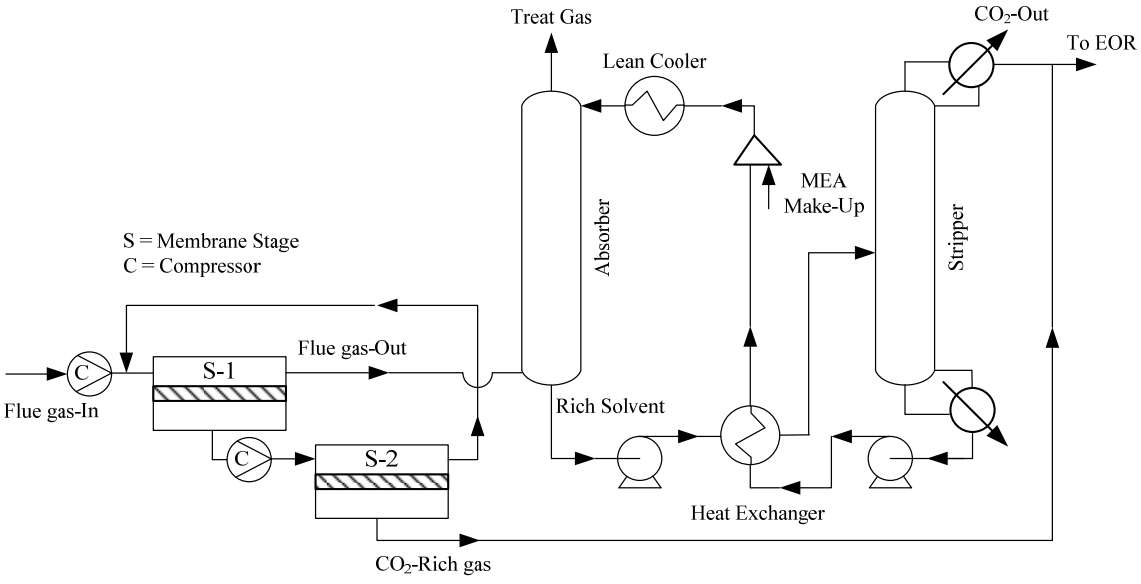

Fig. 7.8: A hybrid of membranes and amine processes to treat flue gas of cement plant.

energy demand and can save up to 20~45% energy compared to the standalone MEA capture processes. An energy consumption of 2 GJ/ton of CO_2 captured is often mentioned as the target for the post-combustion CO_2 capture, which corresponds to the recommendations of the European Union (Favre et al., 2009a). However, it was not achievable by amine processes even if hindered amines or engineered solvents were used. Membrane processes can offer significant advantages over amine processes by limiting the energy demand. The energy demand of the hybrid process is expected to be between the two process components. A detailed techno-economic analysis of the membrane-amine hybrid process is necessary to confirm the merit of the hybrid processes. Nevertheless, the key information reported in this study is useful for a techno-economic analysis. Additional Aspen Plus® input/output data for hybrid membrane systems data have been presented in Appendix D for perusal.

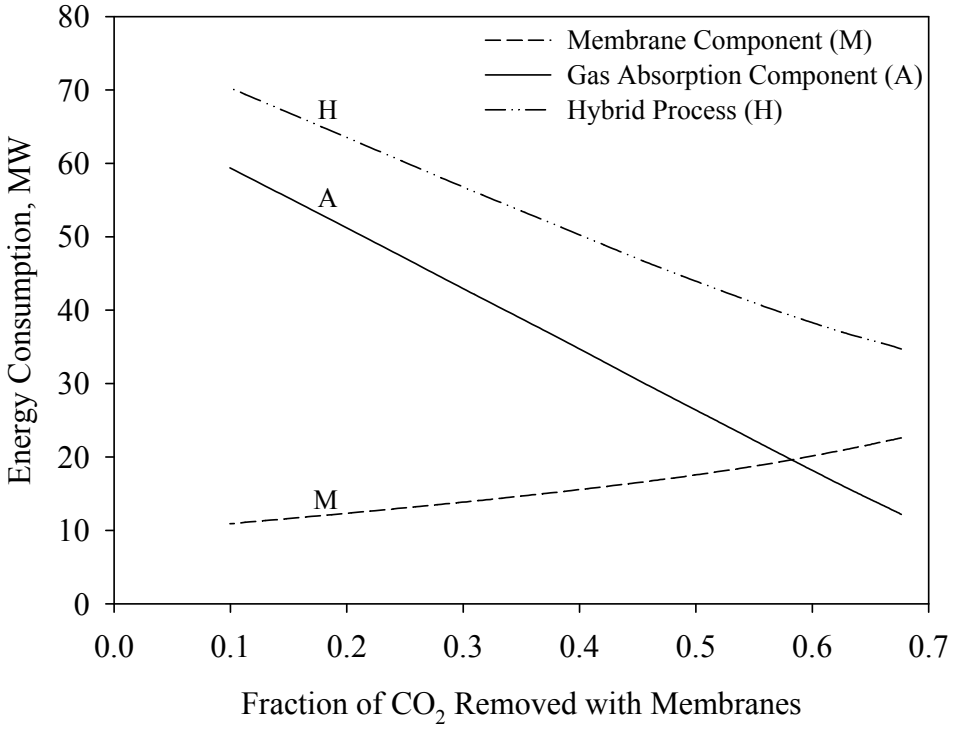

Fig. 7.9: Energy consumption for the membrane fraction, amine fraction and their combined total for the cement plant application.

Table 7.6: A comparison of energy penalty of CO_2 capture by membranes, amines and their hybrid processes.

CO_2 Capture Technology	**Energy, GJ/ton CO_2**	**References**
MEA scrubbing, coal fired power plant	4.0	(Alie et al., 2005)
Fluor Econamine FG^{TM}	4.2	(Chapel et al., 1999)
Fluor Econamine FG Plus^{TM}	3.24	(IEA, 2004)
Sterically hindered amines (SHA)	2.76	(Mimura et al., 1997)
MEA scrubbing, coal fired power plant	3.3-5.1	(Chowdhury, 2012)
MEA scrubbing, fossil fuel powered power plant	3.9	(Abu-Zahra et al., 2007)
Amine absorption	4.0-6.0	(Bounaceur et al., 2006)
MEA scrubbing, cement plant	3.63	(Hassan et al., 2007)
Membrane processes, coal fired power plant	1.27-1.85	(Chowdhury, 2012)
Membrane processes	0.5-1.0	(Bounaceur et al., 2006)
Diglycolamine scrubbing, gas turbine	5.8	(Mofarahi et al., 2008)
MEA scrubbing, coal fired power plant	3.8	(Singh et al., 2003)
Hybrid membrane cryogenic processes	< 3.0	(Belaissaoui et al., 2012)
Membrane processes, coal fired power plant	1.49-2.17	This study
Membrane processes, cement plant	1.67-1.71	This study
MEA scrubbing, coal fired power plant	3.5	This study
MEA scrubbing, cement plant	3.55	This study
Hybrid membrane amine processes, cement plant	1.83-3.7	This study

7.4. Conclusions

Membrane processes offer the lowest energy penalty for post-combustion CO_2 capture and likely to expand as more and more CO_2 selective membranes are synthesized. Membrane processes can save up to 20~45% energy compared to the standalone MEA capture processes. The energy demand of the hybrid process is somewhat between the two process components. The total energy penalty of the hybrid process decreases as more and

more CO_2 is removed by the membranes. The overall energy requirement of the hybrid process needs to be investigated in case a less stringent capture rate constraint is taken. A detailed economic evaluation of the membrane-amine hybrid process is essential to confirm its techno-economic advantage for post-combustion CO_2 capture.

Chapter 8

Conclusions and future recommendations

8.1 General conclusions and contributions

The overall objective of the study is to develop models that can be used to help in the design and operation of CO_2 capture processes. Although the objective of this research is multi-fold, the study provides a process analysis perspective for hollow fiber permeators, pressure-vacuum swing permeation, and membrane-amine hybrid systems for gas separations. From the work completed in this study, a number of important conclusions can be drawn with respect to the design viability and performance of membrane gas separations. Moreover, the unprecedented process concepts discussed here could potentially emerge a new application of membrane gas separation.

8.1.1 Modeling and simulation of hollow fiber membranes

The developed model and solution technique for high flux asymmetric hollow fiber membranes provides reliable examination of pressure and concentration profiles along the permeator length (both residue/permeate streams). The solution technique has merits over other techniques commonly used since it requires minimal computational effort and provides improved solution stability. Moreover, the computational complexity does not multiply as the number of components increases. The solution technique was found very efficient for the solution of binary/multicomponent systems.

8.1.2 Membrane process configurations

The study demonstrates that the new solution technique can conveniently handle the high-flux hollow fibre membrane problems with different flow and process configurations. Membrane area requirement may be reduced through the use of feed gas bypass for applications where oxygen-enriched air with moderate product purity is required. It was shown that two modules in series operation can be used to enhance the overall performance

for nitrogen production, especially when a high concentration of the nitrogen is needed. Recycle ratio plays a crucial role, and optimum recycle ratio vital for the retentate recycle to permeate and permeate recycle to feed operation for methane enrichment from biogas was found. From the concept of two recycle operations, complexities involved in the design and operation of continuous membrane column was simplified. It was shown that with current CO_2-selective membranes, it is difficult for the methane-enriched retentate stream to reach a pipeline quality natural gas primarily due to the presence of a small amount of nitrogen, and an additional separation step to remove nitrogen is needed. Membrane permselectivity required for a targeted separation to produce pipeline quality natural gas by methane-selective or nitrogen-selective membranes was calculated.

8.1.3 Effect of permeate pressure build-up on intrinsic permeances

It was observed that considerable pressure build-up in the fiber lumen can occur, resulting in discrepancy in the predicted membrane performance if this effect is neglected. It was shown that membrane performs close to its intrinsic separation properties if operated at high feed pressures, and at the same time the effect of pressure build-up on the membrane performance is minimized. It was also shown that the average loss in driving force due to pressure build-up increases as feed pressure increases, however, percentage loss in driving force is actually minimized at higher feed pressures.

8.1.4 Novel process of pressure-vacuum swing permeation

A relatively higher transmembrane driving force compare to conventional steady state membrane process can be achieved in unsteady state pressure-vacuum swing permeation process using a single pump, which can also be sustained over a longer period of time. Moreover, a higher feed to permeate pressure ratio can be achieved, which enhances gas separations. The relative volume of the feed and permeate sides of the membrane unit was shown to be an important parameter in the process design. It was shown that the pressure-vacuum swing process using a single pump improves CO_2

recovery and productivity by 25% and 45% (for CO_2 separation from flue gas), respectively, compared to the conventional steady state permeation process.

8.1.5 Membrane-amine hybrid systems for post-combustion CO_2 capture

It was found that the target specifications (i.e., 85% recovery with 98% CO_2 purity) for application in EOR were unattainable with current generation membranes in single stage permeator even with a CO_2/N_2 selectivity of 200. However, multi-stage configurations can satisfy the design specifications. It was shown that membrane processes offer the lowest energy penalty for post-combustion CO_2 capture and likely to expand as more and more CO_2 selective membranes are synthesized. It was estimated that membrane processes can save up to 20~45% energy compared to the stand-alone MEA capture processes. It was also shown that the total energy penalty of the hybrid process decreases as more and more CO_2 is removed by the membranes.

8.2 Future recommendations

Membrane-based gas separation is one of the most exciting and significant new unit processes that have appeared in recent years. A substantial amount of research works have been conducted in membrane gas separation industry, which helped the membrane technology to widely penetrate across various end-use markets. The future of membrane technology promises to be equally exciting as new membrane materials, processes and innovations make their way to the marketplace. The opportunities to extend the technology to new applications (and/or, cost/energy saving improvement of existing membrane processes) are limitless. The research works based on the thesis context can be extended to cope with the following recommendations:

8.2.1 Gas permeation membrane networks

The gas permeation model can be extended to develop a comprehensive gas permeation membrane network representation in the form of superstructures that capture all

possible conventional and novel combinations of cocurrent, countercurrent, and crossflow gas permeation membrane units. The superstructures can be optimized thereafter to extract those designs that exhibit the best economic performances. The approach might help membrane professionals to systematically and quickly determine the most economical membrane network structures for a specific design.

8.2.2 Experimental investigation of pressure-vacuum swing permeation process

An experimental investigation of pressure-vacuum swing permeation process is required at this stage to materialize the concept to proof of concept.

8.2.3 Economic evaluation of membrane-amine hybrid systems

The energy demand of the hybrid process is somewhat intermediate of membrane processes being the lowest and amine processes being the highest. The decisive factor of hybrid processes over amine processes lying in analyzing if the amine processes (in hybrid configurations) can actually be downsized. Moreover, the membrane area savings (if any) should be taken into consideration. A detailed techno-economic analysis of the hybrid membrane amine processes is deemed necessary at this point to confirm the merit of the hybrid processes. Nevertheless, it is hoped that the key data reported in this study can aid the possibility to undertake techno-economic analysis. However, apple to apple comparisons are required between competitive capture technologies to make the economic evaluation more credible.

Copyright Permissions

JOHN WILEY AND SONS LICENSE

This is a License Agreement between Prodip K Kundu ("You") and John Wiley and Sons ("John Wiley and Sons") provided by Copyright Clearance Center ("CCC"). The license consists of your order details, the terms and conditions provided by John Wiley and Sons, and the payment terms and conditions.

License Details:

License Number	3131071161968
License date	Apr 16, 2013
Licensed content publisher	John Wiley and Sons
Licensed content publication	Canadian Journal of Chemical Engineering
Licensed content title	Simulation of binary gas separation with asymmetric hollow fibre membranes and case studies of air separation
Licensed copyright line	Copyright © 2011 Canadian Society for Chemical Engineering
Licensed content author	Prodip K. Kundu,Amit Chakma,Xianshe Feng
Licensed content date	Aug 18, 2011
Start page	1253
End page	1268
Type of use	Dissertation/Thesis
Requestor type	Author of this Wiley article
Format	Print and electronic
Portion	Full article
Will you be translating?	No
Total	0.00 USD

TERMS AND CONDITIONS

This copyrighted material is owned by or exclusively licensed to John Wiley & Sons, Inc. or one of its group companies (each a "Wiley Company") or a society for whom a Wiley Company has exclusive publishing rights in relation to a particular journal (collectively "WILEY"). By clicking "accept" in connection with completing this licensing transaction, you agree that the following terms and conditions apply to this transaction (along with the billing and payment terms and conditions established by the Copyright Clearance Center Inc., ("CCC's Billing and Payment terms and conditions"), at the time that you opened your RightsLink account (these are available at any time at http://myaccount.copyright.com).

Copyright Permissions

JOHN WILEY AND SONS LICENSE

This is a License Agreement between Prodip K Kundu ("You") and John Wiley and Sons ("John Wiley and Sons") provided by Copyright Clearance Center ("CCC"). The license consists of your order details, the terms and conditions provided by John Wiley and Sons, and the payment terms and conditions.

License Details:

License Number	3131070854227
License date	Apr 16, 2013
Licensed content publisher	John Wiley and Sons
Licensed content publication	Canadian Journal of Chemical Engineering
Licensed content title	Modelling of multicomponent gas separation with asymmetric hollow fibre membranes—methane enrichment from biogas
Licensed copyright line	Copyright © 2012 Canadian Society for Chemical Engineering
Licensed content author	Prodip K. Kundu,Amit Chakma,Xianshe Feng
Licensed content date	Aug 7, 2012
Start page	n/a
End page	n/a
Type of use	Dissertation/Thesis
Requestor type	Author of this Wiley article
Format	Print and electronic
Portion	Full article
Will you be translating?	No
Total	0.00 USD

TERMS AND CONDITIONS

This copyrighted material is owned by or exclusively licensed to John Wiley & Sons, Inc. or one of its group companies (each a "Wiley Company") or a society for whom a Wiley Company has exclusive publishing rights in relation to a particular journal (collectively "WILEY"). By clicking "accept" in connection with completing this licensing transaction, you agree that the following terms and conditions apply to this transaction (along with the billing and payment terms and conditions established by the Copyright Clearance Center Inc., ("CCC's Billing and Payment terms and conditions"), at the time that you opened your RightsLink account (these are available at any time at http://myaccount.copyright.com).

References

Abboud, S., Aschim, K., Bagdan, B., Sarkar, P., Yuan, H., Scorfield, B., Felske, C., Rahbar, S. and Marmen, L., "Potential for producing renewable natural gas from Canadian wastes," Report prepared jointly by Alberta Research Council and Canadian Gas Association (2010).

Abu-Zahra, M.R.M., Schneiders, L.H.J., Niederer, J.P.M., Feron, P.H.M. and Versteeg, G.F., "CO_2 capture from power plants. Part I. A parametric study of the technical performance based on monoethanolamine," Int. J. Greenhouse Gas Control **1**, 37-46 (2007).

Agrawal, R. and Xu, J., "Gas separation membrane cascades II. Two-compressor cascades," J. Membr. Sci. **112**, 129-146 (1996).

Agrawal, R., "Simplified method for the synthesis of gas separation membrane cascades with limited numbers of compressors," Chem. Eng. Sci. **52**, 1029-1044 (1997).

Alefeld, G. and Voelkl, J., "Hydrogen in metals I: basic properties," Springer-Verlag, Berlin (1978).

Alie, C., Backham, L., Croiset, E. and Douglas, P.L., "Simulation of CO_2 capture using MEA scrubbing: a flowsheet decomposition method," Energy Convers. Manage. **46**, 475-487 (2005).

Aroonwilas, A. and Veawab, A., "Integration of CO_2 capture unit using blended MEA–AMP solution into coal-fired power plants," Energy Procedia **1**, 4315-4321 (2009).

Baker, R.W., "Future directions of membrane gas separation technology," Ind. Eng. Chem. Res. **41**, 1393-1411 (2002).

Baker, R.W., "Membrane technology and applications," 2nd ed., John Wiley & Sons., Chichester, England (2004).

Baker, R.W. and Lokhandwala, K., "Natural gas processing with membranes: an overview," Ind. Eng. Chem. Res. **47**, 2109-2121 (2008).

Barchas, R. and Davis, R., "The Kerr-McGee/ABB Lummus Crest technology for the recovery of CO_2 from stack gases," Energy Convers. Manage. **33**, 333-340 (1992).

Basaran, O.A. and Auvil, S.R., "Asymptotic analysis of gas separation by a membrane module," AICHE J. **34**, 1726-1731 (1988).

Basu, A., Akhtar, J., Rahman, M.H. and Islam, M.R., "A review of separation of gases using membrane systems," Pet. Sci. Technol. **22**, 1343-1368 (2004).

References

Beckman, I.N., Shelekhin, A.B. and Teplyakov, V.V., "Separation of gas mixtures in unsteady-state conditions," J. Membr. Sci. **55**, 283-297 (1991).

Beckman, I.N., Bessarabov, D.G. and Teplyakov, V.V., "Selective membrane valve for ternary gas mixture separation: model of mass transfer and experimental test," Ind. Eng. Chem. Res. **32**, 2017-2022 (1993).

Belaissaoui, B., Le Moullec, Y., Willson, D. and Favre, E., "Hybrid membrane cryogenic process for post-combustion CO_2 capture," J. Membr. Sci. **415–416**, 424-434 (2012).

Berman, A.S., "Laminar flow in channels with porous walls," J. Appl. Phys. **24**, 1232-1235 (1953).

Bernardo, P., Drioli, E. and Golemme, G., "Membrane gas separation: A review/state of the art," Ind. Eng. Chem. Res. **48**, 4638-4663 (2009).

Bhide, B.D. and Stern, S.A., "A new evaluation of membrane processes for the oxygen-enrichment of air. I. Identification of optimum operating conditions and process configuration," J. Membr. Sci. **62**, 13-35 (1991a).

Bhide, B.D. and Stern, S.A., "A new evaluation of membrane processes for the oxygen-enrichment of air. II. Effects of economic parameters and membrane properties," J. Membr. Sci. **62**, 37-58 (1991b).

Bhide, B.D., Voskericyan, A. and Stern, S.A., "Hybrid processes for the removal of acid gases from natural gas," J. Membr. Sci. **140**, 27-49 (1998).

Blaisdell, C.T. and Kammermeyer, K., "Counter-current and co-current gas separation," Chem. Eng. Sci. **28**, 1249-1255 (1973).

Blizzard, G., Parro, D. and Hornback, K., "Mallet gas processing facility uses membranes to efficiently separate CO_2," Oil Gas J. **103**, 48-53 (2005).

Boucif, N., Majumdar, S. and Sirkar, K.K., "Series solutions for a gas permeator with countercurrent and cocurrent flow," Ind. Eng. Chem. Fundam. **23**, 470-480 (1984).

Boucif, N., Sengupta, A. and Sirkar, K.K., "Hollow fiber gas permeator with countercurrent or cocurrent flow: series solutions," Ind. Eng. Chem. Fundam. **25**, 217-228 (1986).

Bounaceur, R., Lape, N., Roizard, D., Vallieres, C. and Favre, E., "Membrane processes for post-combustion carbon dioxide capture: A parametric study," Energy. **31**, 2220-2234 (2006).

Bowser, J., "Cyclic membrane separation process," US Patent 6,719,824 (2004).

References

Brubaker, D.W. and Kammermeyer, K., "Separation of gases by plastic membranes-Permeation rates and extent of separation," Ind. Eng. Chem. Res. **46**, 733-739 (1954).

Brunetti, A., Scura, F., Barbieri, G. and Drioli, E., "Membrane technologies for CO_2 separation," J. Membr. Sci. **359**, 115-125 (2010).

Cavenati, S., Grande, C.A. and Rodrigues, A.E., "Upgrade of methane from landfill gas by pressure swing adsorption," Energy Fuels **19**, 2545-2555 (2005).

Chakma, A., "CO_2 capture processes — Opportunities for improved energy efficiencies," Energy Convers. Manage. **38**, S51-S56 (1997).

Chakma, A., "Formulated solvents: New opportunities for energy efficient separation of acid gases," Energy Sources **21**, 51-62 (1999).

Chapel, D.G., Mariz, C.L. and Ernest, J., "Recovery of CO_2 from Flue Gases: Commercial Trends," Presented at the Canadian Society of Chemical Engineers Annual Meeting, Saskatoon, Saskatchewan, Canada, October 4-6, 1999.

Chenar, M.P., Soltanieh, M., Matsuura, T., Tabe-Mohammadi, A. and Feng, C., "Gas permeation properties of commercial polyphenylene oxide and Cardo-type polyimide hollow fiber membranes," Sep. Purif. Technol. **51**, 359-366 (2006).

Chern, R.T., Koros, W.J. and Fedkiw, P.S., "Simulation of a hollow-fiber gas separator: the effects of process and design variables," Ind. Eng. Chem. Process Des. Dev. **24**, 1015-1022 (1985).

Chowdhury, M.H.M., Feng, X., Douglas, P. and Croiset, E., "A new numerical approach for a detailed multicomponent gas separation membrane model and AspenPlus simulation," Chem. Eng. Technol. **28**, 773-782 (2005).

Chowdhury, M.H.M., "Simulation, design and optimization of membrane gas separation, chemical absorption and hybrid processes for CO_2 capture," PhD Dissertation, Chemical Engineering, University of Waterloo, ON, Canada (2012).

Coker, D.T., Freeman, B.D. and Fleming, G.K., "Modeling multicomponent gas separation using hollow-fiber membrane contactors," AICHE J. **44**, 1289-1302 (1998).

Coker, D.T., Allen, T., Freeman, B.D. and Fleming, G.K., "Nonisothermal model for gas separation hollow-fiber membranes," AICHE J. **45**, 1451-1468 (1999).

Corriou, J., Fonteix, C. and Favre, E., "Optimization of a pulsed operation of gas separation by membrane," AICHE J. **54**, 1224-1234 (2008).

References

Crowder, R.O. and Cussler, E.L., "Mass transfer in hollow-fiber modules with non-uniform hollow fibers," J. Membr. Sci. **134**, 235-244 (1997).

Cruz, P., Santos, J.C., Magalhaes, F.D. and Mendes, A., "Simulation of separation processes using finite volume method," Comput. Chem. Eng. **30**, 83-98 (2005).

Dautzenberg, F.M. and Mukherjee, M., "Process intensification using multifunctional reactors," Chem. Eng. Sci. **56**, 251-267 (2001).

Davis, J.C., Valus, R.J., Eshraghi, R. and Velikoff, A.E., "Facilitated transport membrane hybrid systems for olefin purification," Sep. Sci. Technol. **28**, 463-476 (1993).

Demirbas, M.F., Balat, M. and Balat, H., "Biowastes-to-biofuels," Energy Convers. Manag. **52**, 1815-1828 (2011).

Desideri, U. and Paolucci, A., "Performance modelling of a carbon dioxide removal system for power plants," Energy Convers. Manage. **40**, 1899-1915 (1999).

Doshi, K.J., Werner, R.G., Mitariten, M.J. and UOP, "Integrated membrane/PSA process and system," US Patent 4,863,492 (1989).

Du, R., Chakma, A. and Feng, X., "Interfacially formed poly(N,N-dimethylaminoethyl methacrylate)/polysulfone composite membranes for CO_2/N_2 separation," J. Membr. Sci. **290**, 19-28 (2007).

Echt, W., "Hybrid systems: Combining technologies leads to more efficient gas conditioning," 52nd Laurance Reid Gas Conditioning Conference, Oklahoma, 2002.

Environment Canada, "An inventory of landfill gas recovery and utilization in Canada-2005," Report prepared by the Greenhouse Gas Division of Environment Canada with the support of the University of Manitoba, Winnipeg (2007).

Environment Canada, “National inventory report 1990–2008: Greenhouse gas sources and sinks in Canada,” Catalogue No.: En81-4/2008E-PDF (2010), <http://www.ec.gc.ca/> [accessed: April 2012].

Esteves, I.A.A.C. and Mota, J.P.B., "Gas separation by a novel hybrid membrane/pressure swing adsorption process," Ind. Eng. Chem. Res. **46**, 5723-5733 (2007).

Ettouney, H.M. and Majeed, U., "Permeability functions for pure and mixture gases in silicone rubber and polysulfone membranes: Dependence on pressure and composition," J. Membr. Sci. **135**, 251-261 (1997).

Ettouney, H.M., El-Dessouky, H.T. and Abou Waar, W., "Separation characteristics of air by polysulfone hollow fiber membranes in series," J. Membr. Sci. **148**, 105-117 (1998).

References

Favre, E., "Carbon dioxide recovery from post-combustion processes: Can gas permeation membranes compete with absorption?" J. Membr. Sci. **294**, 50-59 (2007).

Favre, E., Bounaceur, R. and Roizard, D., "A hybrid process combining oxygen enriched air combustion and membrane separation for post-combustion carbon dioxide capture," Sep. Purif. Technol. **68**, 30-36 (2009a).

Favre, E., Bounaceur, R. and Roizard, D., "Biogas, membranes and carbon dioxide capture," J. Membr. Sci. **328**, 11-14 (2009b).

Feng, X., Pan, C.Y., Ivory, J. and Ghosh, D., "Integrated membrane/adsorption process for gas separation," Chem.Eng. Sci. **53**, 1689-1698 (1998a).

Feng, X., Pan, C.Y., McMinis, C.W., Ivory, J. and Ghosh, D., "Hollow-fiber-based adsorbers for gas separation by pressure-swing adsorption," AICHE J. **44**, 1555-1562 (1998b).

Feng, X., Ivory, J. and Rajan, V.S.V., "Air separation by integrally asymmetric hollow-fiber membranes," AIChE J. **45**, 2142-2152 (1999).

Feng, X., Pan, C.Y. and Ivory, J., "Pressure swing permeation: Novel process for gas separation by membranes," AIChE J. **46**, 724-733 (2000).

Feng, X., Shao, P., Huang, R.Y.M., Jiang, G. and Xu, R., "A study of silicone rubber/polysulfone composite membranes: Correlating H_2/N_2 and O_2/N_2 permselectivities," Sep. Purif. Technol. **27**, 211-223 (2002).

Feng, X. and Lawless, D. “Unsteady state gas permeation process” US Patent 13,402,425 (filed Feb 22, 2012).

Freeman, B.D., "Basis of permeability/selectivity tradeoff relations in polymeric gas separation membranes," Macromolecules **32**, 375-380 (1999).

Gardner, N., Manley, B.J.W. and Pearson, J.M., "Gas emissions from landfills and their contributions to global warming," Appl. Energy. **44**, 165-174 (1993).

Geuzebroek, F.H., Schneiders, L.H.J.M., Kraaijveld, G.J.C. and Feron, P.H.M., "Exergy analysis of alkanolamine-based CO_2 removal unit with AspenPlus," Energy **29**, 1241-1248 (2004).

Giglia, S., Bikson, B., Perrin, J.E. and Donatelli, A.A., "Mathematical and experimental analysis of gas separation by hollow fiber membranes," Ind. Eng. Chem. Res. **30**, 1239-1248 (1991).

References

Global Industry Analysts Inc., "Membrane separation technologies: A global strategic business report," (2011), <www.prweb.com/releases/prwebmembrane_separation/ technologies/prweb8953901.htm> [accessed: September 2012].

Gottschlich, D.E., Roberts, D.L., Wijmans, J.G., Bell, C. and Baker, R.W., "Economic comparison of several membrane configurations for H_2/N_2 separation," Gas Sep. Purif. **3**, 170-179 (1989).

Gowing, A.L., "Measuring and modelling of landfill gas emissions," PhD Dissertation, Civil Engineering, University of Waterloo, ON, Canada (2001).

Graham, T., "On the absorption and dialytic separation of gases by colloid septa," Phil. Trans. R. Soc. Lond. **32**, 399-439 (1866).

Haraya, K., Obata, K., Itoh, N., Shndo, Y., Hakuta, T. and Yoshitome, H., "Gas permeation and separation by an asymmetric polyimide hollow fiber membrane," J. Membr. Sci. **41**, 23-35 (1989).

Haraya, K. and Hwang, S., "Permeation of oxygen, argon and nitrogen through polymer membranes," J. Membr. Sci. **71**, 13-27 (1992).

Harun, N., "Dynamic simulation of MEA absorption process for CO_2 capture from power plants," PhD Dissertation, Chemical Engineering, University of Waterloo, ON, Canada (2012).

Hassan, M.H., Douglas Way, J., Thoen, P.M. and Dillon, A.C., "Single component and mixed gas transport in a silica hollow fiber membrane," J. Membr. Sci. **104**, 27-42 (1995).

Hassan, S.M.N., "Techno-economic study of CO_2 capture process for cement plants," MASc Dissertation, Chemical Engineering, University of Waterloo, ON, Canada (2005).

Hassan, S.M.N., Douglas, P. and Croiset, E., "Techno-economic study of CO_2 capture from an existing cement plant using MEA scrubbing," Int. J. Green Energy **4**, 197-220 (2007).

Helmut, B., "Liquid ring vacuum pumps, compressors and systems: Conventional and hermetic design," Wiley-VCH, Weinheim, Germany (2005), pp. 101-104.

Higuchi, A. and Nakagawa, T., "Permselectivities through artificial membranes at a non-steady state," J. Appl. Polym. Sci. **37**, 2181-2190 (1989).

Ho, M.T., Allinson, G.W. and Wiley, D.E., "Reducing the cost of CO_2 capture from flue gases using membrane technology," Ind. Eng. Chem. Res. **47**, 1562-1568 (2008).

References

Hosseini, S.S., Li, Y., Chung, T. and Liu, Y., "Enhanced gas separation performance of nanocomposite membranes using MgO nanoparticles," J. Membr. Sci. **302**, 207-217 (2007).

Hughes, R. and Jiang, B., "Permeabilities of carbon dioxide, nitrous oxide and oxygen and their mixtures through silicone rubber and cellulose acetate membranes," Gas Sep. Purif. **9**, 27-30 (1995).

IEA Greenhouse Gas R&D Programme, "Improvement in power generation with post-combustion capture of CO_2," Report No. PH4/33 (2004).

Ilconich, J.B., Xu, X., Coleman, M. and Simpson, P.J., "Impact of ion beam irradiation on microstructure and gas permeance of polysulfone asymmetric membranes," J. Membr. Sci. **214**, 143-156 (2003).

Jiang, X. and Kumar, A., "Modelling and process development for gaseous separation with silicone-coated polymeric membranes," Can. J. Chem. Eng. **86**, 151-159 (2008).

Kaldis, S.P., Kapantaidakis, G.C., Papadopoulos, T.I. and Sakellaropoulos, G.P., "Simulation of binary gas separation in hollow fiber asymmetric membranes by orthogonal collocation," J. Membr. Sci. **142**, 43-59 (1998).

Kaldis, S.P., Kapantaidakis, G.C. and Sakellaropoulos, G.P., "Simulation of multicomponent gas separation in a hollow fiber membrane by orthogonal collocation - hydrogen recovery from refinery gases," J. Membr. Sci. **173**, 61-71 (2000).

Kao, Y.K., Yan, Z., Li, L. and Fan, H., "A pressure swing membrane separation process," Gas Sep. Purif. **5**, 151-160 (1991).

Katoh, T., Tokumura, M., Yoshikawa, H. and Kawase, Y., "Dynamic simulation of multicomponent gas separation by hollow-fiber membrane module: nonideal mixing flows in permeate and residue sides using the tanks-in-series model," Sep. Purif. Technol. **76**, 362-372 (2011).

Kesting, R.E. and Fritzsche, A.K., "Polymeric gas separation membranes," John Wiley & Sons., New York (1993).

Khan, M.M. and Islam, M.R., "Zero waste lifestyle with inherently sustainable technologies," in: "Zero waste engineering," John Wiley & Sons, Hoboken, NJ, USA (2012), pp. 185-216.

Kimura, S.G. and Browall, W.R., "Membrane oxygen enrichment," J. Membr. Sci. **29**, 69-77 (1986).

References

Knaebel, K.S. and Reinhold, H.E., "Landfill gas: from rubbish to resource," Adsorption. **9**, 87-94 (2003).

Koros, B., "Three hundred volumes," J. Membr. Sci. **300**, 1-1 (2007).

Koros, W.J. and Chern, R.T., "Separation of gaseous mixtures using polymer membranes," in: Rousseau, R.W., Eds., "Handbook of Separation Process Technology," Wiley, New York (1987), pp. 862-953.

Koros, W.J. and Fleming, G.K., "Membrane-based gas separation," J. Membr. Sci. **83**, 1-80 (1993).

Kovvali, A.S., Vemury, S. and Admassu, W., "Modeling of multicomponent countercurrent gas permeators," Ind. Eng. Chem. Res. **33**, 896-903 (1994).

Krovvidi, K.R., Kovvali, A.S., Vemury, S. and Khan, A.A., "Approximate solutions for gas permeators separating binary mixtures," J. Membr. Sci. **66**, 103-118 (1992).

Kumazawa, H., Sada, E., Nakata, K., Kawashima, N., Kataoka, S. and Tada, K., "Enrichment of helium by asymmetric hollow-fiber membrane of cellulose triacetate," J. Appl. Polym. Sci. **53**, 113-119 (1994).

Kundu, P.K., Chakma, A. and Feng, X., "Simulation of binary gas separation with asymmetric hollow fibre membranes and case studies of air separation," Can. J. Chem. Eng. **90**, 1253-1268 (2012a).

Kundu, P. K., Chakma, A. and Feng, X., "Modelling of multicomponent gas separation with asymmetric hollow fibre membranes—methane enrichment from biogas," Can. J. Chem. Eng. (2012b). DOI: 10.1002/cjce.21721.

Lababidi, H., Al-Enezi, G. and Ettouney, H.M., "Optimization of module configuration in membrane gas separation," J. Membr. Sci. **112**, 185-197 (1996).

Laguntsov, N.I., Gruzdev, E.B., Kosykh, E.V. and Kozhevnickov, V.Y., "The use of recycle permeator systems for gas mixture separation," J. Membr. Sci. **67**, 15-28 (1992).

LaPack, M.A. and Dupuis, F., "Dynamic membrane separation process for improved selectivity," US Patent 5,354,474 (1994).

Lee, B.D., Kim, D.M., Cho, J. and Park, S.W., "A comparative study on the carbon dioxide capture power between 30 wt% 2-amino-2-methyl-1-propanol and 30 wt% methyldiethanol amine aqueous solutions," Korean J. Chem. Eng. **26**, 818-823 (2009).

References

Lee, S.Y., Minhas, B.S. and Donohue, M.D., "Effect of gas composition and pressure on permeation through cellulose acetate membranes," in: Sirkar, K.K. and Lloyd, D.R., Eds., AIChE Symp. Ser. **261**, (1988), pp. 93-101.

Lee, W., Kim, D. and Kim, J., "Preparation and gas separation properties of asymmetric polysulfone membranes by a dual bath method," Korean J. Chem. Eng. **17**, 143-148 (2000).

Lemanski, J. and Lipscomb, G.G., "Effect of fiber variation on the performance of countercurrent hollow fiber gas separation modules," J. Membr. Sci. **167**, 241-252 (2000).

Li, K., Acharya, D.R. and Hughes, R., "Mathematical modelling of multicomponent membrane permeators," J. Membr. Sci. **52**, 205-219 (1990).

Li, Y., Chung, T. and Xiao, Y., "Superior gas separation performance of dual-layer hollow fiber membranes with an ultrathin dense-selective layer," J. Membr. Sci. **325**, 23-27 (2008).

Lim, S.P., Tan, X. and Li, K., "Gas/vapour separation using membranes: Effect of pressure drop in lumen of hollow fibres," Chem. Eng. Sci. **55**, 2641-2652 (2000).

Lin, H., Merkel, T. and Baker, R., "The membrane solution to global warming," 6th Annual Conference on Carbon Capture & Sequestration, Pittsburgh, Pennsylvania, May, 2007.

Liu, L., Chakma, A. and Feng, X., "CO_2/N_2 Separation by poly(ether block amide) thin film hollow fiber composite membranes," Ind. Eng. Chem. Res. **44**, 6874-6882 (2005).

Lokhandwala, K.A., Pinnau, I., He, Z., Amo, K.D., Da Costa, A.R., Wijmans, J.G. and Baker, R.W., "Membrane separation of nitrogen from natural gas: a case study from membrane synthesis to commercial deployment," J. Membr. Sci. **346**, 270-279 (2010).

Lyons, P.C., "Coalbed methane potential in the appalachian states of Pennsylvania,West Virginia, Maryland, Ohio, Virginia, Kentucky, and Tennessee-An overview," Report: 96-735 (1996), <http://pubs.usgs.gov/of/1996/of96-735/cbm_comp.htm> [accessed: April 2012].

Maier, G., "Gas separation with polymer membranes," Angew. Chem. Int. Ed. **37**, 2960-2974 (1998).

Majumdar, S., Heit, L.B., Sengupta, A. and Sirkar, K.K., "Experimental investigation of oxygen enrichment in a silicone capillary permeator with permeate recycle," Ind. Eng. Chem. Res. **26**, 1434-1441 (1987).

Makaruk, A. and Harasek, M., "Numerical algorithm for modelling multicomponent multipermeator systems," J. Membr. Sci. **344**, 258-265 (2009).

References

Marriott, J.I., Sørensen, E. and Bogle, I.D.L., "Detailed mathematical modelling of membrane modules," Comput. Chem. Eng. **25**, 693-700 (2001).

Marriott, J. and Sørensen, E., "A general approach to modelling membrane modules," Chem. Eng. Sci. **58**, 4975-4990 (2003).

Matsuura, T., "Synthetic membranes and membrane separation processes," CRC Press Inc., Boca Raton (1994).

Matteucci, Y., Yampolskii, Y., Freeman, B.D. and Pinnau, I., "Transport of gases and vapors in glassy and rubbery polymers," in: Yampolskii, Y., Pinnau, I. and Freeman, B.D., Eds., "Materials science of membranes for gas and vapor separation," John Wiley and Sons Ltd., England (2006), pp. 1-47.

McCandless, F.P., "A comparison of some recycle permeators for gas separations," J. Membr. Sci. **24**, 15-28 (1985).

McCandless, F.P., "Iterative solution of multicomponent permeator model equations," J. Membr. Sci. **48**, 115-122 (1990).

McKee, R.L., Changela, M.K. and Reading, G.J., "CO_2 removal: membrane plus amine," Hydrocarbon Process. **70**, 63-65 (1991).

Membrane Technology, "US membrane market grows 6.6% per year," Membr. Technol. **4** (2005).

Membrane Technology, "Liquid and gas separation membranes market set for solid growth," Membr. Technol. **3-4** (2009).

Membrane Technology and Research, "New project explores membrane process to convert landfill gas into useful fuel; multiple test sites sought (January 2012)," (2012), <http://www.mtrinc.com/news.html> [accessed: September 2012].

Mimura, T., Simayoshi, H., Suda, T., Iijima, M. and Mituoka, S., "Development of energy saving technology for flue gas carbon dioxide recovery in power plant by chemical absorption method and steam system," Energy Convers. Manage. **38**, S57-S62 (1997).

Mofarahi, M., Khojasteh, Y., Khaledi, H. and Farahnak, A., "Design of CO_2 absorption plant for recovery of CO_2 from flue gases of gas turbine," Energy **33**, 1311-1319 (2008).

Mulder, M., "Basic principles of membrane technology," 2nd ed., Kluwer Academic Publishers, Dordrecht, Netherlands (1996).

Narinsky, A.G., "Applicability conditions of idealized flow models for gas separation by asymmetric membrane," J. Membr. Sci. **55**, 333-347 (1991).

References

Naylor, R.W. and Backer, P.O., "Enrichment calculations in gaseous diffusion: large separation factor," Chem. Eng. Prog. **1**, 95-99 (1955).

Nemser, S.M., "Cyclic membrane separation process," US Patent 6,887,300 (2005).

Noble, R.D. and Stern, S.A., Eds., "Membrane separations technology: Principles and applications," Elsevier Science, Amsterdam, The Netherlands (1995).

Nunes, S. and Peinemann, K., "Membrane materials and membrane preparation," in: Nunes, S. and Peinemann, K., Eds., "Membrane technology in the chemical industry," Wiley-VCH, Weinhim (2006), pp. 3-92.

Omole, I.C., Adams, R.T., Miller, S.J. and Koros, W.J., "Effects of CO_2 on a high performance hollow-fiber membrane for natural gas purification," Ind. Eng. Chem. Res. **49**, 4887-4896 (2010).

Ostrem, K., "Greening Waste: Anaerobic digestion for treating the organic fraction of municipal solid wastes," MSc Dissertation, Earth and Environmental Engineering, Columbia University, New York (2004).

Pan, C.Y. and Habgood, H.W., "An analysis of the single-stage gaseous permeation process," Ind. Eng. Chem. Fundam. **13**, 323-331 (1974).

Pan, C.Y. and Habgood, H.W., "Gas separation by permeation I. Calculation methods and parametric analysis," Can. J. Chem. Eng. **56**, 197-209 (1978a).

Pan, C.Y. and Habgood, H.W., "Gas separation by permeation. II. Effect of permeate pressure drop and choice of permeate pressure," Can. J. Chem. Eng. **56**, 210-217(1978b).

Pan, C.Y., "Gas separation by permeators with high-flux asymmetric membranes," AICHE J. **29**, 545-552 (1983).

Pan, C.Y., "Gas separation by high-flux, asymmetric hollow-fiber membrane," AICHE J. **32**, 2020-2027 (1986).

Pandey, P. and Chauhan, R.S., "Membranes for gas separation," Prog. Polym. Sci. **26**, 853-893 (2001).

Paul, D., "Membrane separation of gases using steady cyclic operation," Ind. Eng. Chem. Proc. Des. Dev. **10**, 375-379 (1971).

Peer, M., Mahdyarfar, M. and Mohammadi, T., "Evaluation of a mathematical model using experimental data and artificial neural network for prediction of gas separation," J. Nat. Gas Chem. **17**, 135-141 (2008).

References

Peer, M., Mahdeyarfar, M. and Mohammadi, T., "Investigation of syngas ratio adjustment using a polyimide membrane," Chem. Eng. Process. **48**, 755-761 (2009).

Perry, R.H. and Green, D.W., "Perry's chemical engineers' handbook," 7th ed., McGraw-Hill, New York (1997).

Pettersen, T. and Lien, K.M., "A new robust design model for gas separating membrane modules, based on analogy with counter-current heat exchangers," Comput. Chem. Eng. **18**, 427-439 (1994a).

Pettersen, T. and Lien, K.M., "Insights into the design of optimal separation systems using membrane permeators," Comput. Chem. Eng. **18**, S319-S324 (1994b).

Pfromm, P.H., Pinnau, I. and Koros, W.J., "Gas transport through integral-asymmetric membranes: A comparison to isotropic film transport properties," J. Appl. Polym. Sci. **48**, 2161-2171 (1993).

Pinnau, I. and Freeman, B.D., "Membrane formation and modification overview," in: Pinnau, I. and Freeman, B.D., Eds., ACS Symp. Ser. **744**, American Chemical Society, Washington, DC (2000), pp. 1-12.

Rao, A.B. and Rubin, E.S., "A technical, economic, and environmental assessment of amine-based CO_2 capture technology for power plant greenhouse gas control," Environ. Sci. Technol. **36**, 4467-4475 (2002).

Rasi, S., Läntelä, J. and Rintala, J., "Trace compounds affecting biogas energy utilisation – A review," Energy Convers. Manag. 52, 3369-3375 (2011).

Rautenbach, R. and Dahm, W., "The separation of multicomponent mixtures by gas permeation," Chem. Eng. Process. **19**, 211-19 (1985).

Rautenbach, R. and Welsch, K., "Treatment of landfill gas by gas permeation-pilot plant results and comparison to alternatives," Desalination **90**, 193-207 (1993).

Rice, L.H., “Membrane separation processes and systems for enhanced permeant recovery,” US Patent 7,812,207 (2007).

Robeson, L.M., "Correlation of separation factor versus permeability for polymeric membranes," J. Membr. Sci. **62**, 165-185 (1991).

Romeo, L.M., Bolea, I. and Escosa, J.M., "Integration of power plant and amine scrubbing to reduce CO_2 capture costs," Appl. Therm. Eng. **28**, 1039-1046 (2008).

References

Sada, E., Kumazawa, H., Wang, J. and Koizumi, M., "Separation of carbon dioxide by asymmetric hollow fiber membrane of cellulose triacetate," J. Appl. Polym. Sci. **45**, 2181-2186 (1992).

Schulz, G., "Gas separation in one- or two-step membrane processes," Chem. Eng. Process. **19**, 235-241 (1985).

Sengupta, A. and Sirkar, K.K., "Multicomponent gas separation by an asymmetric permeator containing two different membranes," J. Membr. Sci. **21**, 73-109 (1983).

Sengupta, A. and Sirkar, K.K., "Ternary gas mixture separation in two-membrane permeators," AICHE J. **33**, 529-539 (1987).

Sengupta, A. and Sirkar, K.K., "Ternary gas separation using two different membranes," J. Membr. Sci. **39**, 61-77 (1988).

Sengupta, A. and Sirkar, K.K., "Analysis and design of membrane permeators for gas separation," in: Noble, R.D. and Stern, S.A., Eds., "Membrane separations technology: principles and applications," Elsevier Science, Amsterdam, The Netherlands (1995), pp. 499-552.

Singh, D., Croiset, E., Douglas, P.L. and Douglas, M.A., "Techno-economic study of CO_2 capture from an existing coal-fired power plant: MEA scrubbing vs. O_2/CO_2 recycle combustion," Energy Convers. Manage. **44**, 3073-3091 (2003).

Singh, V., Rhinehart, R.R., Narayan, R.S. and Tock, R.W., "Transport analysis of hollow fiber gas separation membranes," Ind. Eng. Chem. Res. **34**, 4472-4478 (1995).

Shampine, L.F., Gladwell, I. and Thompson, S., "Solving ODEs with MATLAB," 1st ed., Cambridge University Press, Cambridge (2003).

Shao, P. and Huang, R.Y.M., "An analytical approach to the gas pressure drop in hollow fiber membranes," J. Membr. Sci. **271**, 69-76 (2006).

Sidhoum, M., Sengupta, A. and Sirkar, K.K., "Asymmetric cellulose acetate hollow fibers: Studies in gas permeation," AICHE J. **34**, 417-425 (1988).

Sidhoum, M., Majumdar, S. and Sirkar, K.K., "Internally staged hollow-fiber permeator for gas separation," AICHE J. **35**, 764-774 (1989).

Sirkar, K.K., "Separation of gaseous mixtures with asymmetric dense polymeric membranes," Chem. Eng. Sci. **32**, 1137-1145 (1977).

Skoulidas, A.I. and Sholl, D.S., "Multiscale models of sweep gas and porous support effects on zeolite membranes," AICHE J. **51**, 867-877 (2005).

References

Spillman, R.W., "Economics of gas separation membranes," Chem. Eng. Prog. **85**, 41-62 (1989).

Statistics Canada, "Human activity and the environment," Catalogue no. 16-201-XIE (2005), <http://www.statcan.gc.ca/> [accessed: April 2012].

Statistics Canada, "Waste management industry survey: Business and government sectors," Catalogue no. 16F0023X (2008), <http://www.statcan.gc.ca/> [accessed: April 2012].

Stern, S.A., Sinclair, T.F., Gareis, P.J., Vahldieck, N.P. and Mohr, P.H., "Helium recovery by permeation," Ind. Eng. Chem. Res. **57**, 49-60 (1965).

Stern, S.A., Perrin, J.E. and Naimon, E.J., "Recycle and multimembrane permeators for gas separations," J. Membr. Sci. **20**, 25-43 (1984).

Tchobanoglous, G. and Kreith, F., "Handbook of solid waste management," 2nd ed., McGraw-Hill, New York (2002).

Thompson, S., Sawyer, J., Boman, R. and Smith, S., "Recommendations for improving the Canadian methane generation model for landfills," Report prepared for Environment Canada on contract in association with Environment Canada and University of Manitoba, Winnipeg (2006).

Thompson, S., Sawyer, J., Bonam, R. and Valdivia, J.E., "Building a better methane generation model: Validating models with methane recovery rates from 35 Canadian landfills," Waste Manage. **29**, 2085-2091 (2009).

Thorman, J.M. and Hwang, S.T., "Compressible flow in permeable capillaries under deformation," Chem. Eng. Sci. **33**, 15-20 (1978).

Thundyil, M.J. and Koros, W.J., "Mathematical modeling of gas separation permeators - for radial crossflow, countercurrent, and cocurrent hollow fiber membrane modules," J. Membr. Sci. **125**, 275-291 (1997).

Tsuru, T. and Hwang, S., "Evaluation of retentate recycle effect on enrichment of less permeable gas component in a membrane permeator," J. Membr. Sci. **94**, 213-224 (1994).

Ueda, K., Haruna, K. and Inoue, M., "Process for separating gas," US Patent 4,955,998 (1990).

Vallieres, C. and Favre, E., "Vacuum versus sweeping gas operation for binary mixtures separation by dense membrane processes," J. Membr. Sci. **244**, 17-23 (2004).

References

Visser, T., Koops, G.H. and Wessling, M., "On the subtle balance between competitive sorption and plasticization effects in asymmetric hollow fiber gas separation membranes," J. Membr. Sci. **252**, 265-277 (2005).

Walawender, W.P. and Stern, S.A., "Analysis of membrane separation parameters. II. counter-current and cocurrent flow in a single permeation stage," Sep. Sci. Technol. **7**, 553-584 (1972).

Wang, D., Li, K. and Teo, W.K., "Effects of temperature and pressure on gas permselection properties in asymmetric membranes," J. Membr. Sci. **105**, 89-101 (1995).

Wang, L., Corriou, J., Castel, C. and Favre, E., "A critical review of cyclic transient membrane gas separation processes: State of the art, opportunities and limitations," J. Membr. Sci. **383**, 170-188 (2011).

Wang, R., Liu, S.L., Lin, T.T. and Chung, T.S., "Characterization of hollow fiber membranes in a permeator using binary gas mixtures," Chem. Eng. Sci. **57**, 967-976 (2002).

Weller, S. and Steiner, W.A., "Separation of gases by fractional permeation through membranes," J. Appl. Phys. **21**, 279-283 (1950).

Wijmans, J.G. and Baker, R.W., "The solution-diffusion model: A review," J. Membr. Sci. **107**, 1-21 (1995).

Williams, P.T., "Waste treatment and disposal," 2nd ed., John Wiley & Sons., Chichester, England (2005).

Xie, Z., Duong, T., Hoang, M., Nguyen, C. and Bolto, B., "Ammonia removal by sweep gas membrane distillation," Water Res. **43**, 1693-1699 (2009).

Xu, J., Furuswa, M. and Ito, A., "Air-sweep vacuum membrane distillation using fine silicone, rubber, hollow-fiber membranes," Desalination **191**, 223-231 (2006).

Yampolskii, Y., "Polymeric gas separation membranes," Macromolecules. **45**, 3298-3311 (2012).

Zakaria, R., "Hydrogen separation using asymmetric cellulose acetate hollow fiber membranes," MASc Dissertation, University of Waterloo, Canada (2006).

Zhao, L., Riensche, E., Menzer, R., Blum, L. and Stolten, D., "A parametric study of CO_2/N_2 gas separation membrane processes for post-combustion capture," J. Membr. Sci. **325**, 284-294 (2008).

Appendix A

Extent of separation at permeate vacuum operation

Figures A.1 and A.2 represent the extent of separation achieved for feed compression and permeate vacuum operation (fibers are exposed to air), respectively. Details of membrane properties and module dimensions are provided in Chapter 3.

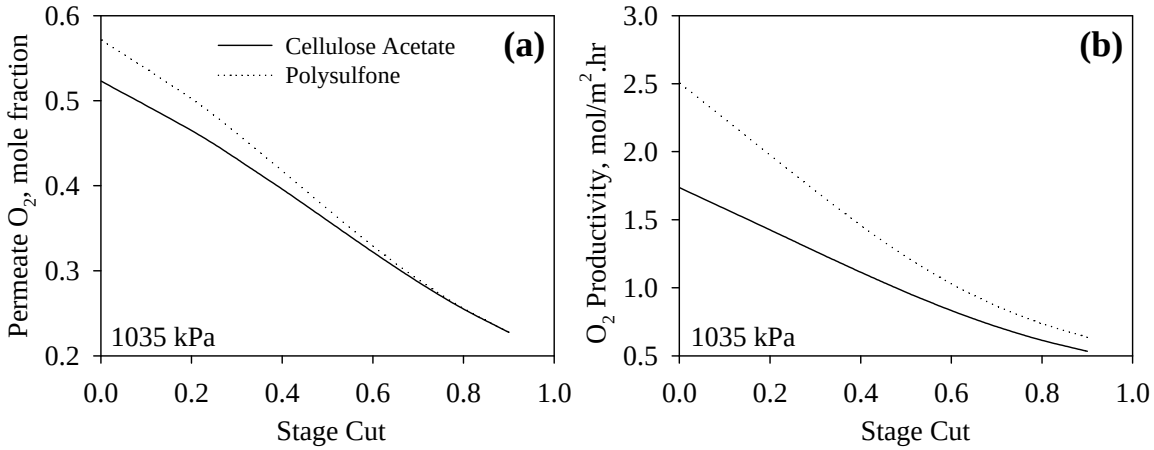

Fig. A.1: (a) permeate O_2 purity vs. stage cut, and (b) O_2 productivity vs. stage cut, for feed compression operation.

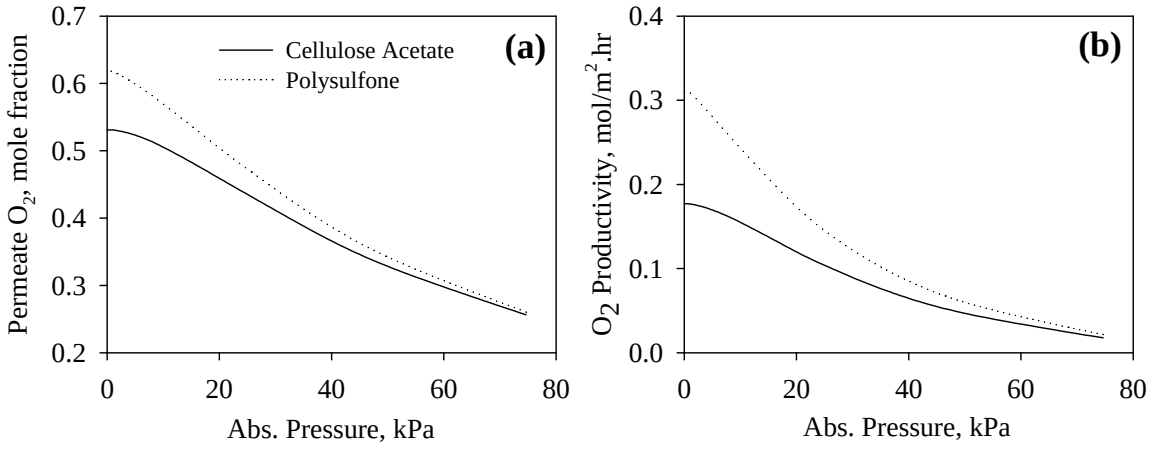

Fig. A.2: (a) permeate O_2 purity vs. absolute pressure, and (b) O_2 productivity vs. absolute pressure, for permeate vacuum operation.

Appendix B

Methane production from Canadian municipal solid wastes

In 2008, Canadians produced over 1 ton of waste per person, and about 76% of the waste was disposed of in landfills or was incinerated (Statistics Canada, 2008). Landfills have been the traditional repositories for solid wastes in Canada. Since Canada does not rely much on incineration for volume reduction, 95% of the waste disposed ends up in landfills (Statistics Canada, 2005). Table B.1 shows the amount of methane generated from anaerobic digestion and landfills in Canada. The data also shows the amount of methane captured and the amount emitted to the atmosphere. As expected, Ontario and Quebec, which have the largest populations in Canada, are the largest producers of landfill methane, followed by British Columbia and Alberta. In Ontario, 27.1% of the methane generated in landfills is captured, and 30.7% of the methane generated is captured in Quebec. The overall methane generation from Canadian landfills is about 1.45 Mt/yr, with only 21.3% being captured. The total potential renewable methane production from Canadian municipal wastes was estimated to be 3.2 Mt/yr, which represents a significant potential addition to the natural gas supply (Abboud et. al, 2010). In 2008, the Canadian waste sector, including municipal and industrial landfills, emitted a total of 22 Mt of carbon dioxide equivalent. Remarkably, the national greenhouse gas emissions from the waste sector decreased from 3.19% in 1990 to 2.59% in 2008. The decrease in the national emission was reported to be mainly due to the introduction of landfill gas collection and utilization (Environment Canada, 2010). There is still an enormous potential to increase methane capture from biogases, making a good use of CH_4 and CO_2 for various applications.

Abboud et al. (2010) analyzed the economic aspects of four different scenarios involving the production of biogas in Canada: an industrial scale anaerobic biogas plant processing feedlot manure and producing pipeline grade natural gas, the same plant producing power only without upgrading the gas, a gasification plant processing forest biomass to produce power and heat for an adjacent pulp mill, and a large landfill producing

Appendix B

Table B.1: Estimated methane generation from anaerobic digestion and landfills in Canada (2005).

Province	Aanaerobic Digestion	Landfills		
	Methane Generation[a] (kt CH_4/yr)	Methane Generation[b] (kt CH4/yr)	Methane Capture[c] (kt CH_4/yr)	Methane Emitted (kt CH_4/yr)
NL	2.21	38.57	0.00	38.57
PE	0.00	6.69	0.00	6.69
NS	1.74	39.66	5.39	34.27
NB	2.08	43.34	0.00	43.34
QC	29.43	469.46	143.97	325.49
ON	35.19	465.17	126.09	339.08
MB	4.22	44.10	0.00	44.10
SK	2.85	43.71	0.00	43.71
AB	8.87	103.55	5.39	98.16
BC	9.59	189.60	27.89	161.71
NT	0.00	2.34	0.00	2.34
NU	0.00	0.00	0.00	0.00
YK	0.00	1.15	0.00	1.15
Canada	96.18	1,447.34	308.73	1,138.61

[a] Abboud et al., 2010; Ostrem, 2004; [b] Thompson et al., 2006; Thompson et al., 2009; [c] Environment Canada, 2007

biogas for power generation. After analyzing all associated costs and expected revenues, the landfill gas project was found to be economically viable among all. The economics of energy recovery from landfill gas associated with CO_2 reductions were reported to be significantly better than other alternative energy forms (e.g., nuclear, onshore wind power, tidal power, and gas turbines). In economic terms, of all renewable options, landfill gas performs the best, even though its actual contribution to CO_2 reductions is inherently small

(Gardner et al., 1993). Harnessing biogas for energy production and/or fuel power is one of the most promising options that encourages more efficient gas collection systems. This will reduce global methane emissions into the atmosphere and generate additional revenues for landfill operators via commercialization of green power and carbon credits for emission reductions. However, separating methane from biogas for energy production is not always perceived as an attractive option because of the lack of efficient separation techniques. It is thus necessary to develop energy-efficient membrane technology for methane separation from biogas from a techno-economic perspective and to motivate utilization of biogases as an energy source.

Appendix C

SAMPLE COMPUTER PROGRAMS

COUNTER-CURRENT FLOW WITH SHELL SIDE FEED WITH BINARY

```
PROGRAM FNL
INCLUDE 'LINK_FNL_SHARED.H'          ! IMSL LIBRARY
USE UMACH_INT
USE DIVPAG_INT
USE SSET_INT
IMPLICIT NONE
INTEGER MXPARAM, N, NT, NOUT       ! N= NUMBER OF DIFFERENTIAL EQUATIONS
PARAMETER (MXPARAM=50, N=5)
! SPECIFICATION FOR PARAMETERS
INTEGER MABSE, MBDF, MSOLVE
PARAMETER (MABSE=1, MBDF=2, MSOLVE=2)
! SPECIFICATION FOR LOCAL VARIABLES
INTEGER IDO, ISTEP
DOUBLE PRECISION A(1,1), PARAM(MXPARAM), Z, TEND, TOL, F(N)
DOUBLE PRECISION DOD, DID
DOUBLE PRECISION MIU1, MIU2, MIU
DOUBLE PRECISION LE, LF
DOUBLE PRECISION K1, K2
DOUBLE PRECISION TG, RG
DOUBLE PRECISION L, V
DOUBLE PRECISION PP, PF, Q2, ALPHA
DOUBLE PRECISION YP
COMMON /DA1/ YP, ALPHA, K1, K2

! SPECIFICATION FOR SUBROUTINES
! SPECIFICATION FOR FUNCTION

EXTERNAL FCN, FCNJ
OPEN (UNIT=300, FILE='COUNTERCURRENT.TXT')
WRITE (300, *)
WRITE (300, 99900)
99900 FORMAT (4X, 'ISTEP', 5X, 'F(1)', 7X, 'F(2)', 9X, 'F(3)', 10X, 'F(4)', 7X, 'F(5)', 10X, 'L', 11X, 'V', 11X, 'PP', 13X, 'YP', 13X, 'K1',
10X, 'K2', 10X, 'MIU')

! DETAILING OF VARIABLES
! READ INPUT VARIABLES FROM TEXT FILE
CALL UMACH(2, NOUT)
! SET INITAIL CONDITIONS
Z=0.0

! SET ERROR TOLERANCE
TOL=0.00001
! SET PARAM TO DEFAULT
CALL SSET(MXPARAM, 0.0, PARAM, 1)
! SET PARAM VALUE
PARAM(4)=100000000  ! MAXIMUM NO OF STEPS ALLOWED
PARAM(10)=MABSE    ! SWITCH DETERMINING ERROR NORM
PARAM(12)=MBDF      ! INTEGRATION METHOD INDICATOR
! END PARAM VALUE

! DETAILING OF VARIABLES
! START OF DIVPAG
IDO=1
ISTEP=1
DO 600 WHILE (ISTEP .LE. 1000)
YP=(1+(ALPHA-1)*(F(1)+F(5))-((1+(ALPHA-1)*(F(1)+F(5)))**2-4.0*ALPHA*(ALPHA-1)*F(5)*F(1))**0.5)/(2.0*(ALPHA-
1)*F(5))   ! EQ 3.10
MIU=MIU1*F(2)+MIU2*(1-F(2))
K2=128*MIU*RG*TG*LE*LF/(3.1415*(DID**4)*NT*(PF**2))
L=F(4)*LF     ! LP=F(4)
V=F(3)*LF     ! VP=F(3)
PP=F(5)*PF    ! GAMMA=F(5)
PRINT 99997, ISTEP, F(1), F(2), F(3), F(4), F(5), L, V, PP, YP
WRITE (300, 99997) ISTEP, F(1), F(2), F(3), F(4), F(5), L, V, PP, YP, K1, K2, MIU
```

Appendix C

```
IF (ISTEP .EQ. 1000) IDO=3
ISTEP=ISTEP+1
TEND=(DOUBLE PRECISION (ISTEP)/1000)
CALL DIVPAG (IDO, FCN, FCNJ, Z, TEND, F, TOL=TOL)
PRINT 99997, ISTEP, F(1), F(2), F(3), F(4), F(5), L, V, PP, YP
! PRINT*, PARAM(35)
600 CONTINUE
99997 FORMAT(1X, I6, 2X, 2F11.6, 2X, F12.6, 2X, 2F11.6, 2X, 2E12.3, 2X, E12.5, 2X, F11.6, 4X, 3F12.8)
! PRINT*,YPRIME(1), YPRIME(2), YPRIME(3), YPRIME(4), YPRIME(5)
! WRITE(NOUT, 99999) PARAM(35)
! 99999 FORMAT(4X, 'NUMBER OF FCN CALLS WITH DIVPAG=', F6.0)
END

SUBROUTINE FCN(N, Z, F, YPRIME)    ! USER SUPPLIED SUBROUTINE TO EVALUATE FUNCTIONS
INTEGER N
DOUBLE PRECISION Z, F(N), YPRIME(N)
DOUBLE PRECISION YP, ALPHA, K1, K2
COMMON /DA1/ YP, ALPHA, K1, K2
YPRIME(4)=-K1*(ALPHA*(F(1)-F(5)*YP)+((1-F(1))-F(5)*(1-YP)))   ! EQ 3.11
YPRIME(3)=-K1*(ALPHA*(F(1)-F(5)*YP)+((1-F(1))-F(5)*(1-YP)))   ! EQ 3.12
YPRIME(1)=-K1*(ALPHA*(1-F(1))*(F(1)-F(5)*YP)-F(1)*((1-F(1))-F(5)*(1-YP)))/F(4)   ! EQ 3.13
YPRIME(5)=K2*F(3)/F(5)   ! EQ 3.14
YPRIME(2)=-K1*(ALPHA*(1-F(2))*(F(1)-F(5)*YP)-F(2)*((1-F(1))-F(5)*(1-YP)))/F(3)   ! EQ 3.16
RETURN
END

SUBROUTINE FCNJ(N, Z, F, DYPDY)    ! USER SUPPLIED SUBROUTINE TO COMPUTE THE JACOBIAN
INTEGER N
DOUBLE PRECISION Z, F(N), DYPDY(N,*)
RETURN
END

CALCULATE ALL THE SOLUTION FOR SINGLE STAGE PERMEATOR

! THIS SECTION CALCULATES ALL POSSIBLE SOLUTION
CALL NSGA2 (ALOW, AHIGH, LSUBSTR, FACTOR)

! THIS SUBROUTINE DEFINES THE OBJECTIVES
SUBROUTINE SIMUL(NPARAM,X,SIMULOUT, PUR, SEL)
IMPLICIT DOUBLE PRECISION (A-H,O-Z)
PARAMETER (NDATAS=10)     ! ONLY NDATA HERE
INTEGER IPOPSIZE, LCHROM, MAXGEN, NCROSS, NMUTE, NPARAMM, IGEN, NOBJFN, I, J
DOUBLE PRECISION X(NPARAM), SIMULOUT(NDATAS), PEN, PCROSS, PMUTE, PJUMP
DOUBLE PRECISION PUR, SEL
COMMON/SGAPARAM/IPOPSIZE, LCHROM, MAXGEN, NCROSS, NMUTE, NPARAMM
COMMON/SGAPARAM1/PCROSS, PMUTE, PJUMP
COMMON/STATIST/IGEN, AVG, AMAX, MEMSP, SUMFITNESS
EXTERNAL MEMBR2
! CALL EXTERNAL FILE FOR SIMULATION

! COUNTER-CURRENT FLOW WITH SHELL SIDE FEED WITH MULTICOMPONENT

PROGRAM FNL
INCLUDE 'LINK_FNL_SHARED.H'
USE UMACH_INT
USE NEQNF_INT
USE DIVPAG_INT
USE SSET_INT
INTEGER MXPARAM, N, NT, NE, ITMAX, NOUT    ! N= NUMBER OF DIFFERENTIAL EQUATIONS
PARAMETER (MXPARAM=50, N=7, NE=2)

! SPECIFICATION FOR PARAMETERS
INTEGER MABSE, MBDF, MSOLVE
PARAMETER (MABSE=1, MBDF=2, MSOLVE=2)
! SPECIFICATION FOR LOCAL VARIABLES
INTEGER IDO, ISTEP
DOUBLE PRECISION A(1,1), PARAM(MXPARAM), Z, TEND, TOL, F(N)
DOUBLE PRECISION DOD, DID
DOUBLE PRECISION MIU1, MIU2, MIU3, MIU
```

Appendix C

```
DOUBLE PRECISION LE, LF
DOUBLE PRECISION K1, K2
DOUBLE PRECISION T, R
DOUBLE PRECISION L, V
DOUBLE PRECISION PP, PF, Q3, ALPHA1, ALPHA2, ALPHA3
DOUBLE PRECISION ERRREL, FNORM, YP(NE), YPGUESS(NE)
COMMON /DA1/ ALPHA1, ALPHA2, ALPHA3, K1, K2
COMMON /DA2/ F
COMMON /DA3/ YP

! SPECIFICATION FOR SUBROUTINES
EXTERNAL FCN, FCNJ, FCN2

! SPECIFICATION FOR FUNCTION
OPEN (UNIT=305, FILE='COUNTERCURRENT.TXT')
WRITE (305, *)
WRITE (305, 99905)
99905 FORMAT (4X, 'ISTEP', 5X, 'F(1)', 7X, 'F(2)', 9X, 'F(3)', 10X, 'F(4)', 7X, 'F(5)', 7X, 'F(6)', 7X, 'F(7)', 10X, 'L', 11X, 'V', 11X, 'PP',
13X, 'YP(1)', 6X, 'YP(2)', 10X, 'K1', 10X, 'K2', 12X, 'MIU')
DATA YPGUESS / 0.54, 0.6/
ERRREL=0.0001
ITMAX=200

! DETAILING OF VARIABLES
CALL UMACH(2, NOUT)
! SET INITAIL CONDITIONS
Z=0.0

! SET ERROR TOLERANCE
TOL=0.0000001
! SET PARAM TO DEFAULT
CALL SSET(MXPARAM, 0.0, PARAM, 1)
! SET PARAM VALUE
PARAM(4)=100000000
PARAM(10)=MABSE
PARAM(12)=MBDF
PARAM(13)=MSOLVE
! END PARAM VALUE

! START OF DIVPAG
IDO=1
ISTEP=0
DO 605WHILE (ISTEP .LE. 1000)
CALL NEQNF (FCN2, YP, XGUESS=YPGUESS, FNORM=FNORM)
YPGUESS(1)=YP(1)
YPGUESS(2)=YP(2)
MIU=MIU1*F(5)+MIU2*F(6)+MIU3*(1-F(5)-F(6))
K2=128.0*MIU*R*T*LE*LF/(3.1415*(DID**4)*NT*(PF**2))
L=F(1)*LF     ! LP=F(1)
V=F(2)*LF     ! VP=F(2)
PP=F(7)*PF    ! GAMMA=F(7)
PRINT 99997, ISTEP, F(1), F(2), F(3), F(4), F(5), F(6), F(7), L, V, PP, YP(1), YP(2)
WRITE (300, 99997) ISTEP, F(1), F(2), F(3), F(4), F(5), F(6), F(7), L, V, PP, YP(1), YP(2), K1, K2, MIU
IF (ISTEP .EQ. 1000) IDO=3
ISTEP=ISTEP+1
TEND=DOUBLE PRECISION(ISTEP)/1000.0
CALL DIVPAG (IDO, FCN, FCNJ, Z, TEND, F, TOL=TOL)
! PRINT*, PARAM(35)
605 CONTINUE
99997 FORMAT(1X, I6, 2X, 2F11.6, 2X, F12.6, 2X, 4F11.6, 2X, 2E12.3, 2X, E12.5, 2X, 2F11.6, 4X, 3F12.8)
! PRINT*,YPRIME(1), YPRIME(2), YPRIME(3), YPRIME(4), YPRIME(5)
! WRITE(NOUT, 99999) PARAM(35)
!  99999 FORMAT(4X, 'NUMBER OF FCN CALLS WITH DIVPAG=', F6.0)
END

SUBROUTINE FCN(N, Z, F, YPRIME)
INTEGER N
DOUBLE PRECISION Z, F(N), YPRIME(N)
DOUBLE PRECISION ALPHA1, ALPHA2, ALPHA3, K1, K2, YP(2)
```

Appendix C

```
COMMON /DA1/ ALPHA1, ALPHA2, ALPHA3, K1, K2
COMMON /DA3/ YP
YPRIME(1)=-K1*((ALPHA1*F(3)+ALPHA2*F(4)+ALPHA3*(1-F(3)-F(4)))-(F(7)*(ALPHA1*YP(1)+ALPHA2*YP(2)+ALPHA3*(1-
YP(1)-YP(2)))))   ! EQ 4.2
YPRIME(2)=-K1*((ALPHA1*F(3)+ALPHA2*F(4)+ALPHA3*(1-F(3)-F(4)))-(F(7)*(ALPHA1*YP(1)+ALPHA2*YP(2)+ALPHA3*(1-
YP(1)-YP(2)))))   ! EQ 4.2
YPRIME(3)=-K1*((ALPHA1*(F(3)-F(7)*YP(1)))-F(3)*((ALPHA1*F(3)+ALPHA2*F(4)+ALPHA3*(1-F(3)-F(4)))
F(7)*(ALPHA1*YP(1)+ALPHA2*YP(2)+ALPHA3*(1-YP(1)-YP(2)))))/F(1)   ! EQ 4.7
YPRIME(4)=-K1*((ALPHA2*(F(4)-F(7)*YP(2)))-F(4)*((ALPHA1*F(3)+ALPHA2*F(4)+ALPHA3*(1-F(3)-F(4)))-
F(7)*(ALPHA1*YP(1)+ALPHA2*YP(2)+ALPHA3*(1-YP(1)-YP(2)))))/F(1)   ! EQ 4.7
%YPRIME(5)=-K1*((ALPHA1*(F(3)-F(7)*YP(1)))-F(5)*((ALPHA1*F(3)+ALPHA2*F(4)+ALPHA3*(1-F(3)-F(4)))-
F(7)*(ALPHA1*YP(1)+ALPHA2*YP(2)+ALPHA3*(1-YP(1)-YP(2)))))/F(2)
%YPRIME(6)=-K1*((ALPHA2*(F(4)-F(7)*YP(2)))-F(6)*((ALPHA1*F(3)+ALPHA2*F(4)+ALPHA3*(1-F(3)-F(4)))-
F(7)*(ALPHA1*YP(1)+ALPHA2*YP(2)+ALPHA3*(1-YP(1)-YP(2)))))/F(2)
YPRIME(7)=K2*F(2)/F(7)
RETURN
END

SUBROUTINE FCNJ(N, Z, F, DYPDY)
INTEGER N
DOUBLE PRECISION Z, F(N), DYPDY(N,*)
RETURN
END

SUBROUTINE FCN2(YP, R, NE)
INTEGER NE
DOUBLE PRECISION YP(NE), R(NE)
DOUBLE PRECISION ALPHA1, ALPHA2, ALPHA3, K1, K2, F(7)
COMMON /DA1/ ALPHA1, ALPHA2, ALPHA3, K1, K2
COMMON /DA2/ F
R(1)=YP(1)-((ALPHA1*(F(3)-F(7)*YP(1)))/((ALPHA1*F(3)+ALPHA2*F(4)+ALPHA3*(1-F(3)-F(4)))-
(F(7)*(ALPHA1*YP(1)+ALPHA2*YP(2)+ALPHA3*(1-YP(1)-YP(2))))))   ! EQ 4.5
R(2)=YP(2)-((ALPHA2*(F(4)-F(7)*YP(2)))/((ALPHA1*F(3)+ALPHA2*F(4)+ALPHA3*(1-F(3)-F(4)))-
(F(7)*(ALPHA1*YP(1)+ALPHA2*YP(2)+ALPHA3*(1-YP(1)-YP(2))))))   ! EQ 4.5
RETURN
END

! PRESSURE SWING PERMEATION FOR FLUE GAS (BINARY COMPONENT): STEP 2

PROGRAM FNL
INCLUDE 'LINK_FNL_SHARED.H'
USE UMACH_INT
USE DIVPAG_INT
USE SSET_INT
USE LINEAR_OPERATORS
IMPLICIT NONE
INTEGER MXPARAM, N2, N4, NOUT
PARAMETER (MXPARAM=50, N2=3, N4=5)
! INTRINSIC MOD
! SPECIFICATION FOR PARAMETERS
INTEGER MABSE, MBDF, MSOLVE
PARAMETER (MABSE=1, MBDF=2, MSOLVE=2)
! SPECIFICATION FOR LOCAL VARIABLES
INTEGER IDO2
DOUBLE PRECISION A(1,1), PARAM(MXPARAM), TS2, TS4, TEND2, TEND4, TOL, F(N2), YPRIME(N2)
DOUBLE PRECISION JA, JB
DOUBLE PRECISION AR
DOUBLE PRECISION T, R
DOUBLE PRECISION VM, VF
DOUBLE PRECISION X, Y, YM, YM1
DOUBLE PRECISION XF, XO, X1
DOUBLE PRECISION PO, P1, PV, ISTEP
DOUBLE PRECISION QA, QB, QC
COMMON /DA1/ JA, JB, AR, P1, PV, VF, VM, R, T
COMMON /DA2/ XF, X1, XO
COMMON /DA3/ X, Y, YM, YM1
COMMON /DA4/ QA, QB, QC
! SPECIFICATION FOR SUB ROUTINES
! SPECIFICATION FOR FUNCTION
```

Appendix C

```
EXTERNAL FCN2, FCNJ2
OPEN (UNIT=310, FILE='PRESSURE SWING PERMEATION.TXT')
WRITE (310, *)
WRITE (310, 99910)
99910 FORMAT (4X, 'ISTEP', 5X, 'F(1)', 7X, 'F(2)', 9X, 'F(3)', 12X, 'X2', 5X, 'Y2', 10X, 'YM2')

! DETAILING OF VARIABLES
CALL UMACH(2, NOUT)
! SET INITAIL CONDITIONS FOR STEP # 2
TS2=0.0
F(1)=0.0
F(2)=0.0
F(3)=PV

! SET ERROR TOLERANCE
TOL=0.000001
! SET PARAM TO DEFAULT
CALL SSET(MXPARAM, 0.0, PARAM, 1)
! SET PARAM VALUE
PARAM = 0.0E0
PARAM(4)=100000000
PARAM(10)=MABSE
PARAM(12)=MBDF
PARAM(13)=MSOLVE
! END PARAM VALUE

! START OF EQUATIONS
! STEP # 1
X1=XF+(PO/P1)*(XO-XF)   ! EQ 6.1
X=(((P1*VF)/(R*T))*X1+(F(1)+F(2))*XF-F(1))/((P1*VF)/(R*T))   ! EQ 6.5
QA=0.0
QB=0.0

! STEP # 2
! START OF DIVPAG
IDO2=1
ISTEP=1
DO 610 WHILE (ISTEP .LE. 3000)
IF (ISTEP .EQ. 3000) IDO2=3
TEND2=(DOUBLE PRECISION(ISTEP)/100)
CALL DIVPAG (IDO2, FCN2, FCNJ2, TS2, TEND2, F, TOL=TOL)
X=(((P1*VF)/(R*T))*X1+(F(1)+F(2))*XF-F(1))/((P1*VF)/(R*T))   ! EQ 6.5
Y=QA/(QA+QB)   ! EQ 6.4
YM=(F(1)+((PV*VM*YM1)/(R*T)))/(F(1)+F(2)+((PV*VM)/(R*T)))   ! EQ 6.6

! PRINT*, PARAM(35)
! PAUSE

PRINT 99997, (ISTEP/100), F(1), F(2), (F(3)*760/101325.0), X, Y, YM
IF(ISTEP .EQ. 1 .OR. MOD(ISTEP,20.0) .EQ. 0) THEN
WRITE (300, 99997) (ISTEP/100), F(1), F(2), (F(3)*760.0/101325.0), X, Y, YM, QA, QB, QC
END IF
ISTEP=ISTEP+1
610 CONTINUE
99997 FORMAT(1X, F6.2, 2X, 2F11.6, 2X, E12.6, 2X, 2F11.6, 2X, 3F12.6, 6X, F12.6)
END

SUBROUTINE FCN2(N2, TS2, F, YPRIME)
INTEGER N2
DOUBLE PRECISION TS2, F(N2), YPRIME(N2)
DOUBLE PRECISION JA, JB, AR, P1, PV, VF, VM, R, T
DOUBLE PRECISION XF, X1, XO
DOUBLE PRECISION X, Y, YM, YM1
COMMON /DA1/ JA, JB, AR, P1, PV, VF, VM, R, T
COMMON /DA2/ XF, X1, XO
COMMON /DA3/ X, Y, YM, YM1
COMMON /DA4/ QA, QB, QC
! PRINT*, JA, JB, AR, P1, PV, VF, VM, R, T
! PRINT*, XF, X1, XO
```

```
! PRINT*, X, Y, YM
! PAUSE
! PAUSE
IF (F(3) .GE. 101325.0) THEN
F(3)=101325.0
END IF
YPRIME(1)=JA*AR*(P1*X-F(3)*Y)   ! EQ 6.2
YPRIME(2)=JB*AR*(P1*(1-X)-F(3)*(1-Y))   ! EQ 6.3
YPRIME(3)=(YPRIME(1)+YPRIME(2))*(R*T/VM)   ! EQ 6.8
QA=YPRIME(1)
QB=YPRIME(2)
QC=YPRIME(3)
! YM=F(1)/(F(1)+F(2))   ! EQ 6.7
! YM=(F(1)+((PV*VM*YM1)/(R*T)))/(F(1)+F(2)+((PV*VM)/(R*T)))   ! EQ 6.6
RETURN
END

SUBROUTINE FCNJ2(N2, TS2, F, DYPDY2)
INTEGER N2
DOUBLE PRECISION TS2, F(N2), DYPDY2(N2,*)
RETURN
END

! PRESSURE SWING PERMEATION (BINARY COMPONENT): STEP 4

! PROGRAM FNL
INCLUDE 'LINK_FNL_SHARED.H'
USE UMACH_INT
USE DIVPAG_INT
USE SSET_INT
USE LINEAR_OPERATORS
IMPLICIT NONE
INTEGER  MXPARAM, N2, N4, NOUT
PARAMETER (MXPARAM=50, N4=5)

! SPECIFICATION FOR PARAMETERS
INTEGER MABSE, MBDF, MSOLVE
PARAMETER (MABSE=1, MBDF=2, MSOLVE=2)

! SPECIFICATION FOR LOCAL VARIABLES
INTEGER  IDO4
DOUBLE PRECISION A(1,1),  PARAM(MXPARAM), TS4,  TEND4, TOL4,  FF(N4)
DOUBLE PRECISION JA, JB, AR, VF, VM, R, T
DOUBLE PRECISION PO, P1, P3, PV
DOUBLE PRECISION X2, Y2, YM2
DOUBLE PRECISION X4, Y4, YM4
DOUBLE PRECISION X3, YM3
DOUBLE PRECISION XF
DOUBLE PRECISION ISTEP4
COMMON /DA1/ JA, JB, AR, VF, VM, R, T
COMMON /DA3/ X2, Y2, YM2
COMMON /DA5/ X4, Y4, YM4
COMMON /DA6/ X3, YM3

! SPECIFICATION FOR SUB ROUTINES
! SPECIFICATION FOR FUNCTION
EXTERNAL FCN4, FCNJ4
! OPENING FILE TO SAVE DATA FOR STEP # 4
OPEN (UNIT=315, FILE='PRESSURESWINGPERMEATIONSTEP4.TXT')
WRITE (315, *)
WRITE (315, 44444)
44444 FORMAT (4X, 'ISTEP4', 5X, 'FF(1)', 7X, 'FF(2)', 7X, 'FF(3)', 7X, 'FF(4)',7X, 'FF(5)', 7X, 'X4', 7X, 'Y4', 7X, 'YM4')

! DETAILING OF VARIABLES
CALL UMACH(2, NOUT)
! SET ERROR TOLERANCE
TOL4=0.000001

! SET PARAM TO DEFAULT
```

Appendix C

```
CALL SSET(MXPARAM, 0.0, PARAM, 1)

! SET PARAM VALUE
PARAM(4)=100000000
PARAM(10)=MABSE
PARAM(12)=MBDF
PARAM(13)=MSOLVE
! END PARAM VALUE

! START OF EQUATIONS
! SET INITAIL CONDITIONS FOR STEP # 4
TS4=0.0
FF(1)=0.0
FF(2)=0.0
FF(3)=P1
FF(4)=0.0
FF(5)=0.0
P3=P1
X3=X2
YM3=YM2

! STEP # 4
! START OF DIVPAG
IDO4=1
ISTEP4=1
DO 44 WHILE (ISTEP4 .LE. 600)
IF (ISTEP4 .EQ. 600) IDO4=3
TEND4=(DOUBLE PRECISION(ISTEP4)/10)
! PRINT*, F(1), F(2), F(3), X2, Y2, YM2
! PAUSE
CALL DIVPAG (IDO4, FCN4, FCNJ4, TS4, TEND4, FF, TOL=TOL4)
! PRINT*, PARAM(35)
PRINT 44447, (ISTEP4/10), FF(1), FF(2), (FF(3)*760/101325), FF(4), FF(5), X4, Y4, YM4
IF(ISTEP4 .EQ. 1 .OR. MOD(ISTEP4,1.0) .EQ. 0) THEN
WRITE (400, 44447) (ISTEP4/10), FF(1), FF(2), (FF(3)*760/101325), FF(4), FF(5), X4, Y4, YM4
END IF
ISTEP4=ISTEP4+1
44 CONTINUE
44447 FORMAT(1X, F6.2, 2X, 2F11.6, 2X, E12.3, 2X, 5F11.6)
END

SUBROUTINE FCN4(N4, TS4, FF, YYPRIME)
INTEGER N4
DOUBLE PRECISION TS4, FF(N4), YYPRIME(N4)
DOUBLE PRECISION JA, JB, AR, VF, VM, R, T
DOUBLE PRECISION PO, P1, P3, PV
DOUBLE PRECISION X4, Y4, YM4
DOUBLE PRECISION X3, YM3
COMMON /DA1/ JA, JB, AR, VF, VM, R, T
COMMON /DA2/ PO, P1, P3, PV
COMMON /DA5/ X4, Y4, YM4
COMMON /DA6/ X3, YM3
YYPRIME(1)=JA*AR*(FF(3)*X4-PV*Y4)   ! EQ 6.2
YYPRIME(2)=JB*AR*(FF(3)*(1-X4)-PV*(1-Y4))   ! EQ 6.3
YYPRIME(3)=-(YYPRIME(1)+YYPRIME(2))*(R*T/VF)   ! EQ 6.9
X4=(((P3*VF)/(R*T))*X3-FF(1))/((P3*VF)/(R*T))   ! EQ 6.10
YYPRIME(4)=YYPRIME(1)+YYPRIME(2)   ! EQ 6.11
Y4=FF(5)/(FF(1)+FF(2))   ! EQ 6.12
YYPRIME(5)=YM4*YYPRIME(4)   ! EQ 6.13
YM4=(FF(1)+((PV*VM*YM3)/(R*T))-FF(5))/((PV*VM)/(R*T))   ! EQ 6.14
RETURN
END

SUBROUTINE FCNJ4(N4, TS4, FF, DYPDY4)
INTEGER N4
DOUBLE PRECISION TS4, FF(N4), DYPDY4(N4,*)
RETURN
END
```

Appendix C

```
! INTRINSIC PERMEANCE-MATLAB BVP

FUNCTION EXBVPX
CLEAR ALL
CLC
GLOBAL PF PP NT MIU1 MIU2 MIU3 DOD DID ALPHA1 ALPHA2 ALPHA3 Q3 LE LF T R;
YP=NLAE1(YPO);
% FSOLVE TO MATCH THE MOLE FRACTION EQUALITY
%WHILE (YP(1)+YP(2)+YP(3))~=1.0;
%YP=NLAE1(YP);
%END

FUNCTION YP=NLAE1(YP)
% GLOBAL PF PP NT MIU1 MIU2 MIU3 DOD DID ALPHA1 ALPHA2 ALPHA3 Q3 LE LF T R;
YP=[((ALPHA1*(F(3)-F(7)*YP(1)))/((ALPHA1*F(3)+ALPHA2*F(4)+ALPHA3*(1-F(3)-F(4)))-
(F(7)*(ALPHA1*YP(1)+ALPHA2*YP(2)+ALPHA3*YP(3)))))
 ((ALPHA2*(F(4)-F(7)*YP(2)))/((ALPHA1*F(3)+ALPHA2*F(4)+ALPHA3*(1-F(3)-F(4)))-
(F(7)*(ALPHA1*YP(1)+ALPHA2*YP(2)+ALPHA3*YP(3)))))
 ((ALPHA3*((1-F(3)-F(4))-F(7)*YP(3)))/((ALPHA1*F(3)+ALPHA2*F(4)+ALPHA3*(1-F(3)-F(4)))-
(F(7)*(ALPHA1*YP(1)+ALPHA2*YP(2)+ALPHA3*YP(3)))))];
END
[YP];
[F(1) F(2) F(3) F(4) F(5) F(6) F(7)];
SOLINIT=BVPINIT(LINSPACE(0,1,10),F);
OPTIONS=BVPSET('RELTOL', 1E-5); % DEFAULT TOLERANCE IS 1E-3, TOLERANCE IS USER DEFINED HERE.
SOL=BVP4C(@ODEFUNX, @BCFUNX, SOLINIT,OPTIONS);
XINT = LINSPACE(0,1);
SXINT = DEVAL(SOL,XINT);
SUBPLOT(4,2,1)
PLOT(XINT,SXINT(1,:))
SUBPLOT(4,2,2)
PLOT(XINT,SXINT(2,:))
SUBPLOT(4,2,3)
PLOT(XINT,SXINT(3,:))
SUBPLOT(4,2,4)
PLOT(XINT,SXINT(4,:))
SUBPLOT(4,2,5)
PLOT(XINT,SXINT(5,:))
SUBPLOT(4,2,6)
PLOT(XINT,SXINT(6,:))
SUBPLOT(4,2,7)
PLOT(XINT,SXINT(7,:))

% DETAILING OF VARIABLES
FUNCTION DFDZ=ODEFUNX(Z,F)
% GLOBAL PF PP NT MIU1 MIU2 MIU3 DOD DID ALPHA1 ALPHA2 ALPHA3 Q3 LE LF T R;
MIU=MIU1*F(5)+MIU2*F(6)+MIU3*(1-F(5)-F(6));

K1=3.1415*DOD*LE*NT*PF*Q3/LF;
K2=128.0*MIU*R*T*LE*LF/(3.1415*(DID^4)*NT*(PF^2));
[YP];
F(1) F(2) F(3) F(4) F(5) F(6) F(7)];
DFDZ=[-K1*((ALPHA1*F(3)+ALPHA2*F(4)+ALPHA3*(1-F(3)-F(4)))-(F(7)*(ALPHA1*YP(1)+ALPHA2*YP(2)+ALPHA3*YP(3))))
       -K1*((ALPHA1*F(3)+ALPHA2*F(4)+ALPHA3*(1-F(3)-F(4)))-(F(7)*(ALPHA1*YP(1)+ALPHA2*YP(2)+ALPHA3*YP(3))))
       -K1*((ALPHA1*(F(3)-F(7)*YP(1)))-F(3)*((ALPHA1*F(3)+ALPHA2*F(4)+ALPHA3*(1-F(3)-F(4)))-
F(7)*(ALPHA1*YP(1)+ALPHA2*YP(2)+ALPHA3*YP(3))))/F(1)
       -K1*((ALPHA2*(F(4)-F(7)*YP(2)))-F(4)*((ALPHA1*F(3)+ALPHA2*F(4)+ALPHA3*(1-F(3)-F(4)))-
F(7)*(ALPHA1*YP(1)+ALPHA2*YP(2)+ALPHA3*YP(3))))/F(1)
       -K1*((ALPHA1*(F(3)-F(7)*YP(1)))-F(5)*((ALPHA1*F(3)+ALPHA2*F(4)+ALPHA3*(1-F(3)-F(4)))-
F(7)*(ALPHA1*YP(1)+ALPHA2*YP(2)+ALPHA3*YP(3))))/F(2)
       -K1*((ALPHA2*(F(4)-F(7)*YP(2)))-F(6)*((ALPHA1*F(3)+ALPHA2*F(4)+ALPHA3*(1-F(3)-F(4)))-
F(7)*(ALPHA1*YP(1)+ALPHA2*YP(2)+ALPHA3*YP(3))))/F(2)
       K2*F(2)/F(7)];
% F(1)=L   [FEED FLOW RATE];
% F(2)=V   [PERMEATE FLOW RATE];
% F(3)=X1 [FEED MOLE FRACTION (1ST PERMEATING COMPONENT)];
% F(4)=X2 [FEED MOLE FRACTION (2ND PERMEATING COMPONENT)];
% F(5)=Y1 [PERMEATE OUTLET MOL FRACTION (1ST PERMEATING COMPONENT)];
% F(6)=Y2 [PERMEATE OUTLET MOL FRACTION (2ND PERMEATING COMPONENT)];
```

Appendix C

```
% F(7)=GAMMA [PRESSURE RATIO];
% YP=LOCAL PERMEATE]
[YP];
[F(1) F(2) F(3) F(4) F(5) F(6) F(7)];
% FSOLVE TO MATCH THE MOLE FRACTION EQUALITY
WHILE (YP(1)+YP(2)+YP(3))~=1.0;
YP=NLAE2(YP);
END
FUNCTION YP=NLAE2(YP)
% GLOBAL PF PP NT MIU1 MIU2 MIU3 DOD DID ALPHA1 ALPHA2 ALPHA3 Q3 LE LF T R;
[YP];
[F(1) F(2) F(3) F(4) F(5) F(6) F(7)];
YP=[((ALPHA1*(F(3)-F(7)*YP(1)))/((ALPHA1*F(3)+ALPHA2*F(4)+ALPHA3*(1-F(3)-F(4)))-
(F(7)*(ALPHA1*YP(1)+ALPHA2*YP(2)+ALPHA3*YP(3)))))
 ((ALPHA2*(F(4)-F(7)*YP(2)))/((ALPHA1*F(3)+ALPHA2*F(4)+ALPHA3*(1-F(3)-F(4)))-
(F(7)*(ALPHA1*YP(1)+ALPHA2*YP(2)+ALPHA3*YP(3)))))
 ((ALPHA3*((1-F(3)-F(4))-F(7)*YP(3)))/((ALPHA1*F(3)+ALPHA2*F(4)+ALPHA3*(1-F(3)-F(4)))-
(F(7)*(ALPHA1*YP(1)+ALPHA2*YP(2)+ALPHA3*YP(3)))))];
END
[YP];
[F(1) F(2) F(3) F(4) F(5) F(6) F(7)];
END

FUNCTION RES=BCFUNX(FR,FL)
% GLOBAL PF PP NT MIU1 MIU2 MIU3 DOD DID ALPHA1 ALPHA2 ALPHA3 Q3 LE LF T R;
YPL=BCNLAE(YP);
% WHILE (YPL(1)+YPL(2)+YPL(3))~=1.0;
% YPL=BCNLAE(YPL);
% END

FUNCTION YPL=BCNLAE(YPL)
YPL=[((ALPHA1*(FL(3)-FL(7)*YPL(1)))/((ALPHA1*FL(3)+ALPHA2*FL(4)+ALPHA3*(1-FL(3)-FL(4)))-
(FL(7)*(ALPHA1*YPL(1)+ALPHA2*YPL(2)+ALPHA3*YPL(3)))))
 ((ALPHA2*(FL(4)-FL(7)*YPL(2)))/((ALPHA1*FL(3)+ALPHA2*FL(4)+ALPHA3*(1-FL(3)-FL(4)))-
(FL(7)*(ALPHA1*YPL(1)+ALPHA2*YPL(2)+ALPHA3*YPL(3)))))
 ((ALPHA3*((1-FL(3)-FL(4))-FL(7)*YPL(3)))/((ALPHA1*FL(3)+ALPHA2*FL(4)+ALPHA3*(1-FL(3)-FL(4)))-
(FL(7)*(ALPHA1*YPL(1)+ALPHA2*YPL(2)+ALPHA3*YPL(3)))))];
END
[YP];
[YPL];
RES=[FR(1)-1.0
    FL(2)
    FR(3)-0.50
    FR(4)-0.03
    FL(5)-YPL(1)
    FL(6)-YPL(2)
    FR(7)-PP/PF];
[FR(1) FR(2) FR(3) FR(4) FR(5) FR(6) FR(7)]
[FL(1) FL(2) FL(3) FL(4) FL(5) FL(6) FL(7)]
END
END

FUNCTION BVP2CINTRINSICMIXED

CLEAR ALL
CLC
ALP(1)=81.96;    % ALP(1)=SELECTIVITY=PERMH2/PERMN2
ALP(2)=0.7;      % ALP(2)=PERMN2
PF=(600+101.325)*1000;
SOLINIT=BVPINIT(LINSPACE(0,1,10),[0.5739 1.0 0.19 (101.325*1000.00/PF)],ALP)
OPTIONS=BVPSET('RELTOL', 1E-3); % DEFAULT TOLERANCE IS 1E-3, TOLERANCE IS USER DEFINED HERE.
SOL=BVP4C(@ODEFUN, @BCFUN, SOLINIT,OPTIONS)
XINT = LINSPACE(0,1);
SXINT = DEVAL(SOL,XINT);
SUBPLOT(3,2,1)
PLOT(XINT,SXINT(1,:))
SUBPLOT(3,2,2)
PLOT(XINT,SXINT(2,:))
SUBPLOT(3,2,3)
```

Appendix C

```
PLOT(XINT,SXINT(3,:))
SUBPLOT(3,2,4)
PLOT(XINT,SXINT(4,:))
% DETAILING OF VARIABLES NOT SHOWN
FUNCTION DFDZ=ODEFUN(Z,F,ALP)
% ALP(2)=0.732;
% Q1=PERM(1)*(3.348E-10);      % H2 PERMEANCE (MOL/PA/M2/S)
Q2=ALP(2)*(3.348E-10);          % N2 PERMEANCE (MOL/PA/M2/S)
% ALP(1)=81.96;                 % PERMH2/PERMN2;
VOLP=0.394;       % VOLUMETRIC FLOW RATE OF PERMEATE (ML/SEC)
VOLR=1.724;       % VOLUMETRIC FLOW RATE OF RESIDUE (ML/SEC)
TG=24.0+273.0;
RG=8.314;
% LF=(((VOLP*101.325)/(RG*TG*1000))+((VOLR*101.325)/(RG*TG*1000)));
% LR=((VOLR*101.325)/(RG*TG*1000));
MIU1=0.09E-4;            % HYDROGEN VISCOSITY (KG/M/S)
MIU2=0.18E-4;            % NITROGEN VISCOSITY (KG/M/S)
MIU=MIU1*F(2)+MIU2*(1-F(2));   % CALCULATED USING MOLE FRACTION BASIS
K1=3.1415*DOD*LE*NT*PF*Q2/LR;
K2=128*MIU*RG*TG*LE*LR/(3.1415*(DID^4)*NT*(PF^2));
YP=(1+(ALP(1)-1)*(F(1)+F(4))-((1+(ALP(1)-1)*(F(1)+F(4)))^2-4.0*ALP(1)*(ALP(1)-1)*F(4)*F(1))^0.5)/(2.0*(ALP(1)-1)*F(4));
DFDZ=[-K1*(ALP(1)*(1-F(1))*(F(1)-F(4)*YP)-F(1)*((1-F(1))-F(4)*(1-YP)))/F(2)
        -K1*(ALP(1)*(F(1)-F(4)*YP)+((1-F(1))-F(4)*(1-YP)))
        -K1*(ALP(1)*(F(1)-F(4)*YP)+((1-F(1))-F(4)*(1-YP)))
         K2*F(3)/F(4)];
% [F(1)=X (RESIDUE MOLE FRACTION);
% F(2)=L (RESIDUE FLOW RATE);
% F(3)=V (PERMEATE FLOW RATE);
% F(4)=GAMMA (PRESSURE RATIO);
% YP=LOCAL PERMEATE]

FUNCTION RES=BCFUN(FL,FR,ALP)
PF=(600+101.325)*1000;
% Q2=PERMN2*(3.348E-10);
% ALP=PERM(1)/PERM(2);
YPL=(1+(ALP(1)-1)*(FL(1)+FL(4))-((1+(ALP(1)-1)*(FL(1)+FL(4)))^2-4.0*ALP(1)*(ALP(1)-1)*FL(4)*FL(1))^0.5)/(2.0*(ALP(1)-
1)*FL(4));
RES=[FR(1)-0.5739
     FL(1)-0.4885
     FL(2)-1.0
     FR(3)-0.19
     FL(3)
     FR(4)-(101.325*1000.00/PF)];
[FR(1) FR(2) FR(3) FR(4) ]
[FL(1) FL(2) FL(3) FL(4) ]
[ALP]
```

Appendix D

Aspen Plus® input/output data for hybrid membrane systems

Table D.1: Reboiler duties at different CO_2 concentrations with different lean loading.

Lean Loading	Reboiler Heat Duty, MW		
	Feed CO_2, 5%	Feed CO_2, 15%	Feed CO_2, 25%
0.30	100.03	298.37	502.50
0.25	45.47	138.14	234.05
0.20	26.28	80.41	136.69
0.15	17.19	53.49	91.35
0.10	13.12	43.13	73.82
0.05	13.09	41.87	69.82

Table D.2: Operating data for membrane amine hybrid systems for post-combustion CO_2 capture (cement plant).

Fraction of CO_2 Removed with Membranes	Membrane Net Work, MW	Stripper Reboiler Duty, MW	Total Energy, MW	Membrane Area, m^2	Feed Pressure, kPa
0.10	10.88	59.39	70.28	43911.80	350
0.21	12.43	50.55	62.98	44769.40	400
0.30	13.88	42.70	56.58	45265.20	450
0.38	15.25	36.04	51.29	45539.90	500
0.45	16.54	30.30	46.84	45667.20	550
0.51	17.77	25.59	43.35	45707.40	600
0.56	18.94	21.59	40.53	45694.00	650
0.60	20.06	18.33	38.40	45630.35	700
0.63	21.13	15.53	36.66	45566.70	750
0.66	22.09	13.35	35.44	44608.60	800
0.68	22.60	12.18	34.71	38792.33	850

Appendix D

Table D.3: Aspen Plus® flow sheet data for MEA process (cement plant).

Substream: MIXED	FLUEGAS	FLUECOOL	FLUESEP	FLUEBLOW	FLUE-ABS	LEAN-ABS	RICH-ABS	TREATGAS
Mole Flow, kmol/hr								
H_2O	0.00	0.00	0.00	0.00	0.00	60535.41	59121.93	1036.27
MEA	0.00	0.00	0.00	0.00	0.00	3094.79	388.58	0.28
CO_2	1825.60	1825.60	1825.60	1825.60	1825.60	0.01	4.23	273.84
HCO3-	0.00	0.00	0.00	0.00	0.00	32.21	421.21	0.00
MEACOO-	0.00	0.00	0.00	0.00	0.00	2229.48	3399.65	0.00
MEA+	0.00	0.00	0.00	0.00	0.00	2334.81	3870.56	0.00
CO3-2	0.00	0.00	0.00	0.00	0.00	36.47	24.84	0.00
H3O+	0.00	0.00	0.00	0.00	0.00	0.00	0.00	0.00
OH-	0.00	0.00	0.00	0.00	0.00	0.17	0.01	0.00
N_2	5560.14	5560.14	5560.14	5560.14	5560.14	0.00	0.19	5559.95
O_2	189.38	189.38	189.38	189.38	189.38	0.00	0.01	189.37
Mole Frac								
H_2O	0.000	0.000	0.000	0.000	0.000	0.887	0.879	0.147
MEA	0.000	0.000	0.000	0.000	0.000	0.045	0.006	0.000
CO_2	0.241	0.241	0.241	0.241	0.241	0.000	0.000	0.039
HCO3-	0.000	0.000	0.000	0.000	0.000	0.000	0.006	0.000
MEACOO-	0.000	0.000	0.000	0.000	0.000	0.033	0.051	0.000
MEA+	0.000	0.000	0.000	0.000	0.000	0.034	0.058	0.000
CO3-2	0.000	0.000	0.000	0.000	0.000	0.001	0.000	0.000
H3O+	0.000	0.000	0.000	0.000	0.000	0.000	0.000	0.000
OH-	0.000	0.000	0.000	0.000	0.000	0.000	0.000	0.000
N_2	0.734	0.734	0.734	0.734	0.734	0.000	0.000	0.788
O_2	0.025	0.025	0.025	0.025	0.025	0.000	0.000	0.027
Mass Flow, kg/hr								
H_2O	0.00	0.00	0.00	0.00	0.00	1090562.40	1065098.21	18668.65
MEA	0.00	0.00	0.00	0.00	0.00	189041.01	23735.82	17.23
CO_2	80344.46	80344.46	80344.46	80344.46	80344.46	0.38	186.11	12051.73
HCO3-	0.00	0.00	0.00	0.00	0.00	1965.61	25701.54	0.00
MEACOO-	0.00	0.00	0.00	0.00	0.00	232049.12	353843.61	0.00
MEA+	0.00	0.00	0.00	0.00	0.00	144963.50	240315.23	0.00
CO3-2	0.00	0.00	0.00	0.00	0.00	2188.82	1490.73	0.00

H3O+	0.00	0.00	0.00	0.00	0.00	0.00	0.00	0.00
OH-	0.00	0.00	0.00	0.00	0.00	2.89	0.21	0.00
N_2	155758.82	155758.82	155758.82	155758.82	155758.82	0.00	5.40	155753.41
O_2	6059.87	6059.87	6059.87	6059.87	6059.87	0.00	0.38	6059.48
Mass Frac								
H_2O	0.000	0.000	0.000	0.000	0.000	0.657	0.623	0.097
MEA	0.000	0.000	0.000	0.000	0.000	0.114	0.014	0.000
CO_2	0.332	0.332	0.332	0.332	0.332	0.000	0.000	0.063
HCO3-	0.000	0.000	0.000	0.000	0.000	0.001	0.015	0.000
MEACOO-	0.000	0.000	0.000	0.000	0.000	0.140	0.207	0.000
MEA+	0.000	0.000	0.000	0.000	0.000	0.087	0.141	0.000
CO3-2	0.000	0.000	0.000	0.000	0.000	0.001	0.001	0.000
H3O+	0.000	0.000	0.000	0.000	0.000	0.000	0.000	0.000
OH-	0.000	0.000	0.000	0.000	0.000	0.000	0.000	0.000
N_2	0.643	0.643	0.643	0.643	0.643	0.000	0.000	0.809
O_2	0.025	0.025	0.025	0.025	0.025	0.000	0.000	0.031
Total Flow, kmol/hr	7.58E+03	7.58E+03	7.58E+03	7.58E+03	7.58E+03	6.83E+04	6.72E+04	7.06E+03
Total Flow, kg/hr	2.42E+05	2.42E+05	2.42E+05	2.42E+05	2.42E+05	1.66E+06	1.71E+06	1.93E+05
Total Flow, l/min	3.24E+06	3.24E+06	3.14E+06	2.82E+06	2.74E+06	2.88E+04	3.03E+04	2.71E+06
Temperature, K	313.15	313.15	303.15	322.55268	313.15	313.15	327.42557	333.44161
Pressure, atm	1.000	1.000	1.000	1.184	1.184	2.073	1.184	1.184
Vapor Frac	1	1	1	1	1	0	0	1
Liquid Frac	0	0	0	0	0	1	1	0

Table D.3: Continued

Substream: MIXED	RICH-HX	RICHSTPR	CO2	LEANSTRP	LEAN-HX	LEANMX	MU-WATER	LEANCOOL
Mole Flow, kmol/hr								
H_2O	59121.89	59294.08	31.46	59434.31	59434.31	59469.33	1066.08	60534.77
MEA	388.65	1113.59	0.00	3173.56	3173.57	3109.66	0.00	3111.04
CO_2	4.24	444.19	1551.78	6.86	6.87	0.08	0.00	0.08
HCO3-	421.27	266.32	0.00	97.50	97.51	47.19	0.00	47.79
MEACOO-	3399.60	3131.86	0.00	2189.21	2189.21	2231.04	0.00	2229.94
MEA+	3870.53	3413.34	0.00	2296.01	2296.01	2318.09	0.00	2318.59
CO3-2	24.83	7.56	0.00	4.57	4.57	19.84	0.00	20.34
H3O+	0.00	0.00	0.00	0.00	0.00	0.00	0.00	0.00
OH-	0.01	0.04	0.00	0.16	0.16	0.18	0.00	0.18
N_2	0.19	0.19	0.19	0.00	0.00	0.00	0.00	0.00
O_2	0.01	0.01	0.01	0.00	0.00	0.00	0.00	0.00
Mole Frac								
H_2O	0.879	0.876	0.020	0.884	0.884	0.885	1.000	0.887
MEA	0.006	0.016	0.000	0.047	0.047	0.046	0.000	0.046
CO_2	0.000	0.007	0.980	0.000	0.000	0.000	0.000	0.000
HCO3-	0.006	0.004	0.000	0.001	0.001	0.001	0.000	0.001
MEACOO-	0.051	0.046	0.000	0.033	0.033	0.033	0.000	0.033
MEA+	0.058	0.050	0.000	0.034	0.034	0.034	0.000	0.034
CO3-2	0.000	0.000	0.000	0.000	0.000	0.000	0.000	0.000
H3O+	0.000	0.000	0.000	0.000	0.000	0.000	0.000	0.000
OH-	0.000	0.000	0.000	0.000	0.000	0.000	0.000	0.000
N_2	0.000	0.000	0.000	0.000	0.000	0.000	0.000	0.000
O_2	0.000	0.000	0.000	0.000	0.000	0.000	0.000	0.000
Mass Flow, kg/hr								
H_2O	1065097.46	1068199.51	566.83	1070725.71	1070725.65	1071356.63	19205.77	1090550.91
MEA	23740.29	68021.98	0.00	193852.93	193853.29	189949.36	0.00	190033.82
CO_2	186.45	19548.89	68293.68	302.10	302.15	3.40	0.00	3.33
HCO3-	25705.05	16250.07	0.00	5949.40	5949.63	2879.63	0.00	2916.21
MEACOO-	353838.48	325971.26	0.00	227858.40	227857.95	232212.12	0.00	232098.00
MEA+	240313.74	211927.57	0.00	142554.85	142554.75	143925.48	0.00	143956.76
CO3-2	1489.76	453.94	0.00	274.31	274.28	1190.50	0.00	1220.41

H3O+	0.00	0.00	0.00	0.00	0.00	0.00	0.00	0.00
OH-	0.21	0.65	0.00	2.66	2.66	3.02	0.00	3.08
N_2	5.40	5.40	5.40	0.00	0.00	0.00	0.00	0.00
O_2	0.38	0.38	0.38	0.00	0.00	0.00	0.00	0.00
Mass Frac								
H_2O	0.623	0.625	0.008	0.652	0.652	0.653	1.000	0.657
MEA	0.014	0.040	0.000	0.118	0.118	0.116	0.000	0.114
CO_2	0.000	0.011	0.992	0.000	0.000	0.000	0.000	0.000
HCO3-	0.015	0.010	0.000	0.004	0.004	0.002	0.000	0.002
MEACOO-	0.207	0.191	0.000	0.139	0.139	0.141	0.000	0.140
MEA+	0.141	0.124	0.000	0.087	0.087	0.088	0.000	0.087
CO3-2	0.001	0.000	0.000	0.000	0.000	0.001	0.000	0.001
H3O+	0.000	0.000	0.000	0.000	0.000	0.000	0.000	0.000
OH-	0.000	0.000	0.000	0.000	0.000	0.000	0.000	0.000
N_2	0.000	0.000	0.000	0.000	0.000	0.000	0.000	0.000
O_2	0.000	0.000	0.000	0.000	0.000	0.000	0.000	0.000
Total Flow, kmol/hr	6.72E+04	6.77E+04	1.58E+03	6.72E+04	6.72E+04	6.72E+04	1.07E+03	6.83E+04
Total Flow, kg/hr	1.71E+06	1.71E+06	6.89E+04	1.64E+06	1.64E+06	1.64E+06	1.92E+04	1.66E+06
Total Flow, l/min	3.03E+04	2.09E+05	3.44E+05	3.02E+04	3.02E+04	2.89E+04	3.23E+02	2.92E+04
Temperature, K	327.446	374.446	300.684	392.099	392.101	337.191	313.150	336.853
Pressure, atm	2.073	2.073	1.875	1.875	2.073	2.073	2.073	2.073
Vapor Frac	0	0.0107762	1	0	0	0	0	0
Liquid Frac	1	0.9892238	0	1	1	1	1	1